



UNIVERSITAT_{DE}
BARCELONA

Building a Scenario of Physics Beyond the Standard Model in the Flavor Sector

Pere Arnau Vendrell



Aquesta tesi doctoral està subjecta a la llicència **Reconeixement 4.0. Espanya de Creative Commons.**

Esta tesis doctoral está sujeta a la licencia **Reconocimiento 4.0. España de Creative Commons.**

This doctoral thesis is licensed under the **Creative Commons Attribution 4.0. Spain License.**

Tesi Doctoral

**Building a Scenario of Physics Beyond the
Standard Model in the Flavor Sector**

Pere Arnan Vendrell

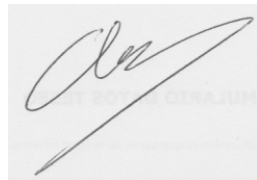


UNIVERSITAT_{DE}
BARCELONA

Building a Scenario of Physics Beyond the Standard Model in the Flavor Sector

Programa de Doctorat en Física

Autor: Pere Arnan Vendrell



Director: Prof. Dr. Federico Mescia

Tutor: Prof. Dr. Domènec Espriu Climent



UNIVERSITAT_{DE}
BARCELONA

Agraïments

Primer de tot, voldria donar les gràcies al Federico, perquè m'ha ajudat molt en l'àmbit acadèmic, professional i també personal. També vull agrair-li al Damir la seva dedicació en mi, fent el paper de segon director de tesi.

Gràcies també a tots els companys físics amb qui he tingut la possibilitat d'interactuar durant aquest temps ja sigui a Barcelona o a fora, incloent tots els postdocs, en especial l'Olcyr i el Marco, i també tots els companys de despatx que m'heu aguantat.

Professionalment, també agraeixo a l'ICCUB i al departament de FQA els serveis oferts per dur a terme amb comoditat la recerca.

Seguidament he d'agrair als meus companys de pis i amics la capacitat de suportar el meu sovintejat mal humor, companys d'esbarjo i de la necessària diversió per la vida.

Per últim, i per això, més important, moltes gràcies de tot cor al Bernat i als meus pares.

Resum

Davant de convincentes observacions experimentals que ens diuen que el model estàndard és incomplet, és just i necessari considerar la manera d'anar més enllà. Dos exemples d'aquestes observacions són la quantitat de matèria fosca i l'asimetria bariònica observades a l'univers, fet que ens permet afirmar que l'univers no pot ser copsat només amb el model estàndard i la relativitat general. Així doncs, poden existir noves partícules que interactuïn amb el model estàndard, tant si tenen fases CP per explicar l'asimetria bariònica, com si reuneixen les condicions suficients per ser candidates a matèria fosca.

Aquestes partícules podrien ser descobertes en futurs experiments, ja sigui a través de la seva producció directa als col·lisionadors a escales d'energia entre 1 i 10 TeV (ATLAS i CMS al LHC), o de forma indirecta a baixes energies per mitjà de processos de sabor (LHCb, Belle II, Bes III i NA62). Els processos de sabor permeten explorar efectes de nova física molt més enllà del límit cinemàtic dels col·lisionadors, però en general no permeten identificar la seva font concreta, encara que ens permeten posar els fonaments per saber per on hem de començar a construir models de nova física.

De fet, estem vivint en temps molt interessants en el camp de la física de sabor perquè recentment s'han observat tensions respecte el model estàndard en tests de universalitat de sabor del leptó als col·lisionadors, proporcionant indicis experimentals a baixes energies de possibles efectes d'una nova teoria a altes energies. Aquestes tensions són conegudes com les anomalies de sabor, i per aquesta raó, en aquesta tesi ens centrem en l'estudi de l'impacte de les anomalies de sabor (o anomalies B) dins del sector de sabor del model estàndard de física de partícules. Després d'una breu introducció sobre els objectius i la motivació d'aquest treball, al Capítol 2 introduïm el model estàndard de física de partícules, tot explicant les tensions rellevants de la teoria amb els experiments tant en els decaïments de $b \rightarrow s\mu^+\mu^-$ com $b \rightarrow c\tau\nu$, comentem breument les possibles solucions que involucren nova física, així com els seus principals avantatges i inconvenients.

Primer de tot ens centrem en un model amb nous escalars i fermions pesats, on només tenim en compte acoblaments tipus esquerra amb les partícules del model estàndard. Considerem dos possibles models: el primer, amb un nou escalar i dos fermions vectorials, mentre que el segon conté dos escalars i un fermió vectorial. L'objectiu d'aquest model és explicar les tensions en les dades de $b \rightarrow s\mu^+\mu^-$ juntament amb el moment magnètic anòmal del muó a_μ , ambdós induïts a nivell d'un bucle en sengles models. Llistem els lligams rellevants i mostrem que els models són capaços de resoldre les anomalies a 2σ , baldament es necessita un acoblament gran dels muons. En el cas de $b \rightarrow s\mu^+\mu^-$, lligams severos provinents de les oscil·lacions $B_s - \bar{B}_s$ poden ser alleujats si els nous fermions són de tipus Majorana. Aquesta part correspon al Capítol 3.

Posteriorment, ja que no es pot explicar a_μ només amb acoblaments tipus esquerra, al Capítol 4 construïm un model amb nous escalars i fermions, permetent la presència de acoblaments tipus dreta, i llistem els coeficients de Wilson rellevants per $b \rightarrow s\mu^+\mu^-$ així com també els observables que actuen com a lligams per qualsevol nombre de noves partícules. Per tal d'il·lustrar aquest model genèric, presentem un model de quarta generació de quarks i leptons del model estàndard, i utilitzem tots els observables calculats de forma genèrica per aquest. Amb aquest model podem explicar les tensions amb l'experiment de $b \rightarrow s\mu^+\mu^-$ i de a_μ , sortejant tots els lligams amb la forçosa presència tant d'acoblaments tipus esquerra com tipus dreta.

El segon tipus de model que explorem al Capítol 5 és una extensió del model estàndard amb leptoquarks escalars. En aquest cas, calculem les contribucions dels decaïments $Z \rightarrow \ell\ell$ and $W \rightarrow \ell\nu$ per cada leptoquark escalar amb l'aproximació més enllà del logaritme, i mostrem que els termes finits suposen un 20% del total de la contribució per masses del leptoquark de $m_\Delta < 1.5 \text{ TeV}$. A més a més mostrem el seu impacte fenomenològic en un model amb un singlet S_1 i un triplet S_3 . A part d'això, també comentem que l'oscil·lació $B_s - \bar{B}_s$ s'ha d'implementar amb cura ja que és un dels lligams més importants, i també ho il·lustrem el seu paper clau en el model amb $S_1 + S_3$. Per acabar construïm tres models diferents amb S_1 i S_3 , i fem un ajust del model a les dades experimentals actuals després de la conferència de Moriond 2019.

Finalment realitzem un escrutini del procés $b \rightarrow s\ell\ell$ en el marc d'un model de dos doblats de Higgs. Calculem tots els coeficients de Wilson rellevants i efectuem una comparació de la teoria a altes energies i a baixes energies, mostrant que és necessari mantenir els moments externs diferents de zero pels operadors escalar i pseudoescalar. Realitzem una anàlisi fenomenològica del model amb $\text{Br}(B_s \rightarrow \mu^+\mu^-)$ i $\text{Br}(B \rightarrow K\mu^+\mu^-)$ a q^2 alt, on tenim controlades les incerteses hadròniques. Aquesta part la desenvolupem al Capítol 6.

Abstract

With compelling experimental evidence that the Standard Model is incomplete, it is necessary to consider how it should be extended. Two examples of such evidences are the amount of dark matter and baryon asymmetry observed in the Universe, which point towards a Universe that cannot be understood solely in terms of the Standard Model and General Relativity. Thus, new particles interacting with the Standard Model ones may exist which carry out CP phases to explain the baryon asymmetry or gather the required conditions to be dark matter candidates.

These new particles could be discovered in future particle experiments, either as directly produced at colliders at the energy scales between 1 to 10 TeV (ATLAS and CMS at LHC), or indirectly observed at low energies via flavor processes (LHCb, Belle II, Bes III, and NA62). Flavor processes can probe new physics effects well beyond the colliders kinematical limit, but typically cannot identify their specific source although they set guide-lines in order to build new physics models.

Actually, we are living interesting times in flavor physics because recently lepton flavor universality tests in colliders have reported tensions with the Standard Model, providing an experimental hint at low energies of the effect of a new high energy theory. These tensions are known as flavor anomalies and that is why in this thesis we focus on the study of the impact of the flavor anomalies (or B -anomalies) on the flavor sector of the Standard Model of particle physics. In Chapter 2 we first introduce the Standard Model of particle physics and list the relevant tensions of the theory with the experiments in the $b \rightarrow s\mu^+\mu^-$ and $b \rightarrow c\tau\nu$ decays, commenting in a brief manner the possible solutions involving new physics, as well as the main advantages and inconveniences of each new physics scenario.

We first focus in a model with new heavy scalars and fermions where we only account for left-handed couplings to the Standard Model particles. We consider two possible models: one with an additional scalar and two vector-like fermions and another with two additional scalars and one vector-like fermion. The purpose of this model is to solve the tensions in $b \rightarrow s\mu^+\mu^-$

data, together with the anomalous magnetic moment of the muon a_μ , which are induced at loop-level in both models. We list the relevant constraints and show that the models are able to solve the anomalies at 2σ level, albeit a relatively large coupling of the muons is required. In the case of $b \rightarrow s\mu^+\mu^-$, stringent constraints arising from $B_s - \bar{B}_s$ mixing can be relaxed if the new fermions are considered Majorana particles. This part is explained in Chapter 3.

Then, since we cannot explain a_μ with only left-handed couplings, in Chapter 4 we construct a model with new scalars and fermions allowing also for right-handed couplings, where we list the relevant Wilson coefficients of $b \rightarrow s\mu^+\mu^-$ as well as the relevant observables acting as constraints for any number of new scalars and fermions. In order to illustrate this generic approach we supplement the Standard Model with a fourth generation of quarks and leptons, using all the computed observables for this concrete model. With this model we can explain $b \rightarrow s\mu^+\mu^-$ data and a_μ avoiding all the constraints if we have the presence of both left- and right-handed couplings.

The second kind of model that we explore is an extension of the Standard Model with scalar leptoquarks, and it can be found in Chapter 5. In this case, we compute the $Z \rightarrow \ell\ell$ and $W \rightarrow \ell\nu$ contributions for each one of the scalar leptoquarks at next-to-leading-logarithm approximation, and show that the finite terms can account for 20% of the total contribution for leptoquark masses of $m_\Delta < 1.5$ TeV. We also show their phenomenological relevance in a model with a singlet S_1 and a triplet S_3 , where our computation pushes the fit towards a better explanation of data. Besides, we comment on the fact that the $B_s - \bar{B}_s$ mixing has to be implemented carefully as it is one of the main constraints that was missing in earlier studies of these kind of models, and we also illustrate its key role in the $S_1 + S_3$ model, since it spoils the pure left-handed scenario with 2018 data. At the end we construct three different models with S_1 and S_3 , and show that it is possible fit them to the present data after Moriond conference 2019, since the new value for $R_{D^{(*)}}$ is closer to the Standard Model.

Finally, we scrutinize the $b \rightarrow s\ell\ell$ process in the framework of a two Higgs doublet model. We compute all the relevant Wilson coefficients performing the matching of the full theory with the low energy theory showing that it is necessary to keep the external momenta for the scalar and pseudo-scalar operators. This is the first time computation of a proper matching including all the relevant operators. We perform a phenomenological analysis of the model with the $\text{Br}(B_s \rightarrow \mu^+\mu^-)$ and $\text{Br}(B \rightarrow K\mu^+\mu^-)$ at high q^2 , where we have control of the hadronic uncertainties. This scenario is developed in Chapter 6.

Contents

Agraiments	iv
Resum	vii
Abstract	ix
1 Introduction: Aim and Motivation	1
2 Standard Model and Flavor Anomalies	5
2.1 Standard Model	6
2.1.1 Gauge Sector and Electroweak Symmetry Breaking	6
2.1.2 Fermion Sector and Flavor Physics	8
2.2 Flavor Anomalies	10
2.2.1 $b \rightarrow s$ Anomalies	10
2.2.2 Effective Theory Description of $b \rightarrow sll$	12
2.2.3 $b \rightarrow c$ Anomalies	14
2.2.4 Effective Theory Description of $b \rightarrow cl\nu_\ell$	15
2.2.5 Simple Models for the Anomalies	16
3 Left-Handed Scalars and Fermions at One Loop	21
3.1 Setup	22
3.2 Observables and Bounds on Wilson Coefficients	25
3.2.1 $b \rightarrow s\mu^+\mu^-$	26
3.2.2 $b \rightarrow s\nu\bar{\nu}$	29
3.2.3 $B_s - \bar{B}_s$ Mixing	31
3.2.4 $b \rightarrow s\gamma$	34

3.2.5	Anomalous Magnetic Moment of the Muon	35
3.2.6	$Z\mu^+\mu^-$ Coupling	37
3.3	Phenomenological Analysis	38
3.3.1	Degenerate Masses: $m_{\Psi(\Phi)} = m_{\Phi_Q(\Psi_Q)} = m_{\Phi_\ell(\Psi_\ell)}$	38
3.3.2	Majorana Case with Non-degenerate Masses	42
4	General Scenario with New Scalars and Fermions at One Loop	45
4.1	Generic Setup and Wilson Coefficients	46
4.1.1	$b \rightarrow s\mu^+\mu^-$ and $b \rightarrow s\gamma$ Transitions	48
4.1.2	$b \rightarrow s\nu\bar{\nu}$	52
4.1.3	$\Delta B = \Delta S = 2$ Processes	52
4.1.4	$D_0 - \bar{D}_0$ Mixing	54
4.1.5	Anomalous Magnetic Moment of the Muon	55
4.1.6	Modified Z Couplings	55
4.2	Experimental Constraints on Wilson Coefficients	58
4.2.1	$b \rightarrow s$ Transitions	58
4.2.2	Neutral Meson Mixing	60
4.2.3	Anomalous Magnetic Moment of the Muon	61
4.2.4	Z Decays	61
4.3	4 th Generation Model	62
4.3.1	Lagrangian	62
4.3.2	Wilson Coefficients	64
4.3.3	Phenomenology	67
5	Two Scalar Leptoquark Model	71
5.1	Scalar Leptoquarks	72
5.2	Addressing Anomalies with a Single Scalar Leptoquark	73
5.3	Leptoquark Contributions to $Z \rightarrow \ell\ell$	75
5.3.1	Effective Field Theory Description	75
5.3.2	One-loop Matching	76
5.3.3	Relevance of the Finite Terms in $Z \rightarrow \ell\ell$	79
5.4	Leptoquark Contributions to $W \rightarrow \ell\bar{\nu}$	82
5.4.1	Effective Field Theory Description	82
5.4.2	One-loop Matching	83

5.4.3	Relevance of the Finite Terms in $W \rightarrow \ell\nu$	85
5.5	Illustration: S_1 & S_3 Explanation of $R_{K^{(*)}}$ and $R_{D^{(*)}}$	85
5.6	On the Importance of $B_s - \bar{B}_s$ Mixing in S_1 & S_3	87
5.7	S_1 & S_3 Status After Moriond 2019	90
6	Two Higgs Doublet Model	93
6.1	General Constraints on 2HDM	94
6.1.1	2HDM	94
6.1.2	General Constraints and Scan of Parameters	96
6.2	Effective Hamiltonian	99
6.3	Wilson coefficients	101
6.3.1	γ -penguins in 2HDM	101
6.3.2	Z -penguins in 2HDM	103
6.3.3	Charged Higgs Boxes in 2HDM	105
6.3.4	Scalar penguins in 2HDM	105
6.4	Comparison with Other Computations	106
6.5	Matching Procedure	107
6.6	$B_s \rightarrow \mu^+\mu^-$ and $B \rightarrow K\mu^+\mu^-$ in 2HDM	110
6.6.1	$B_s \rightarrow \mu^+\mu^-$	111
6.6.2	$B \rightarrow K\mu^+\mu^-$	111
6.7	Phenomenology and Discussion	113
7	Summary and Conclusions	119
A	Matching of a $b \rightarrow s\mu^+\mu^-$ Transition	123
B	Fierz Identities	127
C	New Scalars and Fermions	129
C.1	Loop Functions	129
C.2	Crossed Diagrams	131
C.2.1	$b \rightarrow s\mu^+\mu^-$	132
C.2.2	Meson Mixing	133
C.3	Crossed Diagrams with Complex Scalars	135

D	$\ell_i \rightarrow \ell_j \nu_i \bar{\nu}_j$ with Scalar Leptoquarks	137
E	S_1 & S_3 Observables	141
E.1	$b \rightarrow c \tau \nu$	141
E.2	$b \rightarrow s \mu^+ \mu^-$	142
E.3	$b \rightarrow s \nu \nu$	142
E.4	$b \rightarrow c \ell \nu$ with $\ell = \mu, e$	143
E.5	τ decays	143
E.6	$K \rightarrow \ell \nu_\ell$ with $\ell = e, \mu$ and $\tau \rightarrow K \nu_\tau$	144
E.7	$D_s \rightarrow \ell \nu_\ell$ with $\ell = \mu, \tau$	145
E.8	$B \rightarrow \tau \nu_\tau$	146
E.9	$B \rightarrow K \mu \tau$	146
E.10	χ^2 Tables	147
F	Two Higgs Doublet Model	151
F.1	Hadronic Matrix Elements	151
F.2	Scalar penguins and Auxiliary Functions	151
F.3	Feynman Rules	156
	Bibliography	158

Chapter 1

Introduction: Aim and Motivation

The Standard Model (SM) of particle physics is, without any doubt, one of the greatest theories in science. No other theory has been tested with such a precision, scrutinized so intensely that even the loop corrections have been experimentally verified to unprecedented accuracy, and no other theory has such a predictive power. Among all of the successes the recent Higgs boson discovery by ATLAS [1] and CMS [2] at CERN signified the closure of the SM particle content.

However, the SM is not the final theory of nature. The first clear phenomenon that SM cannot explain is gravity, as it only encompasses electromagnetic, weak and strong interactions. We know for certain that our Universe exhibits gravitational interaction, and the recent observation of gravitational waves implies that there has to be a connection of gravity and quantum physics which goes beyond the scope of the SM.

Another proof that the SM is not complete is that it cannot account for the presence of dark matter and dark energy. During the last century, cosmology and astrophysics, via very different experimental inputs, starting from imprints in the cosmic microwave background radiation to the large scale structures, galaxy clusters, dwarf-spheroidal galaxies and even in our own Milky Way, have shown that approximately 85% of the matter that interacts gravitationally is not predicted by the SM, nor interacts via known strong, weak or electromagnetic interactions. That is why it is called dark matter and its particle nature remains unknown. Moreover, the Universe is in continuous accelerated expansion related to the vacuum energy, the amount of which the SM cannot explain with current observations. The energy needed for the universe to expand is called dark energy, and to explain this phenomena one has to go beyond the SM (BSM).

An additional issue that cannot be explained within the SM is the asymmetry between parti-

cles and anti-particles in the Universe. At some point of the history of the universe, the number of particles became larger than the number of antiparticles in such a way that the universe that we see is made of baryonic matter. This predominance of matter is quantified through the baryon-to-photon ratio $\eta_B \simeq 6 \times 10^{-10}$ via cosmological observations. The SM indeed predicts the CP violating processes that set such an asymmetry via the Cabibbo-Kobayashi-Maskawa (CKM) matrix phase and the quantum chromodynamics (QCD) vacuum angle, but again, the amount of CP violation is too small to reproduce the actual quantity of matter observed in the Universe. Hence, there must exist new sources of CP violation beyond the SM that can explain this asymmetry.

However, the most clear signal that the SM has to be extended in what the particle physics is concerned is that neutrinos have been reported to be massive experimentally. While the SM predicts only left-handed massless neutrinos, the experimental observation of oscillations among different types of neutrinos proves that they should have mass, suggesting that there should be some kind of new physics (NP) related to the existence of right-handed neutrinos, or any kind of physics BSM that provides mass to the neutrinos. Besides, the mechanism that gives mass to neutrinos remains unknown, and the models attempting to solve this problem predict these particles to be of Dirac type or Majorana, as the nature of the neutrino as a Dirac or Majorana fermion is yet to be discovered.

The neutrinos are also a key piece in another theoretical problem of the SM which is often referred to as the flavor puzzle. This issue refers to the pattern of the fermion masses (quarks and leptons) in the SM that have different types of a quantum number called flavor, which rely among very different energy scales. As an example, the top quark has a mass of order 10^5 MeV while the lightest quark, the up quark, is of order of MeV. Something similar occurs in the leptons where the tau lepton is much heavier than the electron or the neutrinos. The origin of the apparent mass hierarchy is unclear and it is not explained by the SM, as it takes the fermion masses (related to the so called Yukawa couplings) as an external input of the theory. Since this fact is quite problematic, many theoretical physicists have struggled to find a model of NP which could explain the masses of the fermions and their values, as well as the mixing among different families of quarks (via CKM matrix) and leptons (via Pontecorvo–Maki–Nakagawa–Sakata (PMNS) matrix). We also do not understand why there are three families of fermions. These flavor puzzles have been studied since many years assuming the principle of so called minimal flavor violation (MFV) [3, 4, 5, 6, 7] which assumes that all of the CP violating effects and mixing comes from the Yukawa terms of the SM. In the past decade, however, a series of

measurements in the flavor sector (including lepton flavor universality (LFU) tests) related to the B -meson decays, carried out in the LHCb [8, 9, 10, 11] and Belle [12, 13] experiments, reported tensions with respect to the SM predictions, setting for the first time a strong hint of lepton flavor universality violation (LFUV), thus questioning the reliability of MFV. This set of observables that do not agree with the SM predictions are known as the flavor anomalies and their possible theoretical explanation via NP models is one of the main goals of this thesis.

In general, the effects of NP can be experimentally explored via direct and/or indirect searches. In direct searches a new particle needs to be produced in an accelerator, and hence it can be detected by a peak or by an excess in various spectra, due to the mass of the new particle. This is how the W and Z have been detected, as well as the Higgs boson in the first run of the LHC in ATLAS and CMS. The indirect searches consist in looking for a deviation of a certain observable in an established theory such as the SM, which predicts a certain value for a given observable, and if a discrepancy between theory and experiment is observed, it can be attributed to the effects of BSM physics. This has already been done in the past with the Fermi theory of weak interactions [14], where in order to explain the observed neutron to proton decay, the W boson was predicted (but not directly observed) to be the mediator of that decay, with a larger mass than the neutron and the proton. Similarly the observation of $B^0 - \bar{B}^0$ mixing at low energy scales ($1 \sim 5$ GeV) was a clear indication of a very large top quark mass ($\Lambda \sim 170$ GeV), long before Tevatron was able to reach the $t\bar{t}$ -production threshold. In order to construct new interactions we perform an operator product expansion (OPE) [15] in powers of the NP scale $1/\Lambda$. For example, if we consider the SM an effective theory we could make an expansion as

$$\mathcal{L}_{\text{eff}} = \mathcal{L}_{\text{SM}} + \sum_i \frac{c_i}{\Lambda^2} \mathcal{O}_i \quad (1.1)$$

where the c_i are the effective coefficients or Wilson coefficients and \mathcal{O}_i are the operators of mass dimension six. The following terms in the expansion are operators of higher dimensions further suppressed by an extra $1/\Lambda^2$ term. The leading NP effects are expected to come from terms proportional to $1/\Lambda^2$. The great advantage of the effective theory is that one can deduce the effective coefficients c_i/Λ^2 from experiment, and then look for a NP model capable of explaining their value. In our case we will make use of a low-energy effective field theory below the electroweak (EW) scale which is formed by 4-fermion operators. This means that the heavier degrees of freedom such as the top quark and the massive gauge bosons will be integrated out. An example of an amplitude of a certain process involving NP contributions

obtained from \mathcal{L}_{eff} in (1.1) would read

$$\mathcal{A} = \frac{c_{\text{SM}}}{v^2} + \frac{c_{\text{NP}}}{\Lambda^2}, \quad (1.2)$$

where the first term encodes the SM contribution from \mathcal{L}_{SM} with $v = 246$ GeV, while the second term accounts for the NP effects at energies $E \ll \Lambda$, where the c_i coefficients are represented with a single NP coupling c_{NP} . It is thus appealing to find observables in the SM which are forbidden at tree-level or CKM-suppressed, ensuring that $c_{\text{SM}} \sim 0$, such as flavor-changing neutral current (FCNC) transitions between quarks and leptons or meson mixing. These low energy observables can then probe, via quantum effects, NP scales up to $v/\sqrt{c_{\text{SM}}}$. As an illustration, the $B_s - \bar{B}_s$ oscillation in the SM is proportional to $\sqrt{c_{\text{SM}}} \sim |V_{ts}|/4\pi \sim 10^{-3}$, which means that assuming the NP contribution with $c_{\text{NP}} \simeq 1$, one could probe up to $\Lambda \sim 10^3$ TeV. That strategy is the one followed in this thesis to describe the flavor anomalies.

This work is structured as follows: We first remind the reader of the general aspects of the SM and explain the flavor anomalies in both the $b \rightarrow s$ and in $b \rightarrow c$ transitions. Interpreting flavor anomalies in terms of NP is discussed in the next chapters. The possible explanation of some of them via the addition of new heavy scalars and vector-like fermions is elaborated in Chapters 3 and 4, and in terms of scalar leptoquarks (LQs) in Chapter 5. Chapter 6 is related to the study of $b \rightarrow s\mu^+\mu^-$ decays in one of the most famous extensions of the SM, the so called two Higgs doublet model (2HDM).

Chapter 2

Standard Model and Flavor Anomalies

As mentioned in the introduction, from 2013 to this day, the measurements of the exclusive $b \rightarrow s\mu^+\mu^-$ processes at LHCb and Belle revealed tensions by several standard deviations between the SM predictions and the experimental results. Angular analyses of $B \rightarrow K^{(*)}\mu^+\mu^-$ and $B_s \rightarrow \phi\mu^+\mu^-$ [16, 17], as well as the LFU tests $R_{K^{(*)}} = \text{Br}(B \rightarrow K^{(*)}\mu^+\mu^-)/\text{Br}(B \rightarrow K^{(*)}e^+e^-)$, indicated important departures from the SM [8, 10, 11, 18]. Combined global fits to the available $b \rightarrow s\mu^+\mu^-$ data [19, 20, 21, 22, 23, 24, 25, 26, 27, 28, 29, 30, 31, 32] suggest that these tensions might have their common origin in NP. i.e. physics BSM. Furthermore, from 2012, in the exclusive $b \rightarrow c\tau\nu$ channels, the measured observables $R_{D^{(*)}} = \text{Br}(B \rightarrow D^{(*)}\tau\nu)/\text{Br}(B \rightarrow D^{(*)}\ell\nu)$ have been reported to be larger than predicted in the SM [33, 12, 34, 35, 36]. These measurements are in tension with the SM and are often referred to as the Flavor Anomalies or B -anomalies, since the b quark decays are involved in all of them.

These anomalies can be classified in two groups: the $b \rightarrow s$ anomalies, which are mediated by the FCNC and loop suppressed in the SM, and the $b \rightarrow c$ anomalies, which are revealed in the charged current processes and occur at tree-level in the SM. The aim of this chapter is to introduce the SM of particle physics and summarize its features, taking special attention in the flavor sector. In the second part we explain the two types of flavor anomalies, and discuss their theoretical impact.

2.1 Standard Model

The SM of particle physics is a gauge theory based in the interactions generated by the SM gauge symmetry group

$$\mathcal{G}_{SM} = SU(3)_c \times SU(2)_L \times U(1)_Y, \quad (2.1)$$

where the $SU(3)_c$ group accounts for strong interactions and the c stands for color, the $SU(2)_L \times U(1)_Y$ accounts for EW interactions, with the L standing for left-handedness and the Y for hypercharge. At lower energies, the $SU(2)_L \times U(1)_Y$ symmetry is broken to $U(1)_{em}$ which is the abelian group that describes the electromagnetic interaction.

2.1.1 Gauge Sector and Electroweak Symmetry Breaking

In the SM each interaction requires the existence of a spin-1 gauge field, which is often referred to as the interaction carrier or the gauge boson mediator. For $SU(3)_c$ there are 8 gauge bosons called gluons which account for the strong interactions and are massless, while the strength of this interaction is encoded in the gauge coupling g_s . The $SU(2)_L \times U(1)_Y$ requires 4 massless gauge bosons, with the couplings g and g' respectively. Since this group is broken due to the Higgs mechanism [37] (also known as Brout-Englert-Higgs Mechanism), we end up with three massive gauge bosons W^\pm and Z , mediating the weak interactions, and the massless gauge boson mediating the electromagnetic interaction, the photon.

The physical process that gives mass to some gauge bosons is called the EW symmetry breaking and the key piece for that to occur is the spin 0 scalar particle Higgs boson. The Higgs boson is a colorless $SU(2)_L$ doublet and has a hypercharge of $Y = 1/2$.

The Lagrangian of the SM gauge sector is written as

$$\mathcal{L}_{\text{gauge}} = -\frac{1}{4} \text{Tr}(F_{\mu\nu}^i F^{i,\mu\nu}), \quad (2.2)$$

and encodes the kinetic term as well as the self-interactions of the gauge bosons where $F_{\mu\nu}^i$ stands for the field strength tensor. The interactions of the gauge bosons are defined with the covariant derivative

$$D_\mu = \partial_\mu + ig_s \frac{\lambda_a}{2} G_\mu^a + ig \frac{\sigma_i}{2} W_\mu^i + ig' Y B_\mu, \quad (2.3)$$

where the first term accounts for the kinetic term, the second term accounts for $SU(3)_c$ interactions, with G_μ^a denoting the 8 gluon fields ($a = 1, \dots, 8$) and λ_a are the Gell-Mann matrices

acting in the color space. The last two terms stem for the EW interactions with the W_μ^i being the three gauge bosons of $SU(2)_L$ and σ_i the Pauli matrices ($i = 1, 2, 3$), while the B_μ is the $U(1)_Y$ gauge boson with Y being the hypercharge of the field in which the covariant derivative is applied. The field strength tensor $F_{\mu\nu}^i$ in Eq.2.2 can be defined then through the covariant derivative

$$F_{\mu\nu}^i = \frac{i}{g_i} [D_\mu, D_\nu], \quad (2.4)$$

with $g_i = \{g_s, g, g'\}$. In particular, for each interaction this tensor reads

$$B_{\mu\nu} = \partial_\mu B_\nu - \partial_\nu B_\mu \quad \text{for } U(1)_Y, \quad (2.5)$$

$$W_{\mu\nu}^i = \partial_\mu W_\nu^i - \partial_\nu W_\mu^i + g\epsilon_{ij} W_\mu^j W_\nu^k \quad \text{for } SU(2)_L \quad \text{and} \quad (2.6)$$

$$G_{\mu\nu}^i = \partial_\mu G_\nu^i - \partial_\nu G_\mu^i + g_s f_{abc} G_\mu^b G_\nu^c \quad \text{for } SU(3)_c. \quad (2.7)$$

In order to define the massive gauge boson Z_μ and the massless photon A_μ after EW symmetry breaking, we implement the rotation

$$\begin{aligned} A_\mu &= \sin\theta_W W_\mu^3 + \cos\theta_W B_\mu \\ Z_\mu &= \cos\theta_W W_\mu^3 - \sin\theta_W B_\mu, \end{aligned} \quad (2.8)$$

with the Weinberg angle defined as $\tan\theta_W = g'/g$, and we also redefine the W boson to its mass basis $W_\mu^\pm = (W_\mu^1 \mp W_\mu^2)/\sqrt{2}$. This simple rotations do not give mass to the gauge fields, thus in order for the Z and the W to acquire mass, let us define the Higgs Lagrangian with the complex scalar field ϕ

$$\mathcal{L}_{\text{Higgs}} = (D_\mu \phi)^\dagger (D^\mu \phi) + \mu^2 \phi^\dagger \phi - \frac{\lambda}{4} (\phi^\dagger \phi)^2 \quad (2.9)$$

with $\phi = (\phi^+, \phi^0)$ being the components under $SU(2)_L$. Since μ and λ are defined positive the Higgs acquires a vacuum expectation value (vev) that can be parametrized as

$$\langle \phi \rangle = (0, v/\sqrt{2}) \quad (2.10)$$

where $v = 246$ GeV sets the EW scale. This parametrization of the vev allows to redefine the Higgs field as

$$\phi = (\phi^+, v/\sqrt{2} + h) \quad (2.11)$$

with $\langle \phi^+ \rangle = \langle h \rangle = 0$. The vev is the responsible for the gauge bosons to acquire mass. Indeed after an appropriate rotation of the gauge fields defined in (2.8), the mass terms for the gauge bosons read

$$\mathcal{L}_{\text{gauge mass}} = \frac{1}{4}v^2 g^2 W_\mu^+ W^{-\mu} + \frac{1}{2}v^2 (g^2 + g'^2) Z_\mu Z^\mu + h.c., \quad (2.12)$$

where the mass terms of the Lagrangian are $m_W = gv/2$ and $m_Z = \sqrt{g^2 + g'^2} v/2$, whereas photon field A_μ does not acquire mass.

2.1.2 Fermion Sector and Flavor Physics

The fermion content of the SM consists of three types of quarks of spin 1/2

$$Q_L^i = (u_L, d_L)^i = (3, 2, 1/6) \quad d_R^i = (3, 1, -1/3) \quad u_R^i = (3, 1, 2/3), \quad (2.13)$$

and also three types of leptons of spin 1/2 (considering non-interacting right-handed neutrinos)

$$L_L^i = (\nu_L, e_L)^i = (1, 2, -1/2) \quad e_R^i = (1, 1, -1), \quad (2.14)$$

where the numbers in the parenthesis stem for the representation of the field under $(SU(3)_c, SU(2)_L, U(1)_Y)$, while the i label is the family or generation index (often referred to as flavor index), and in the SM $i = 1, 2, 3$ ¹. Before the EW symmetry breaking, the fermions of the SM are massless and the Lagrangian encoding the kinetic terms and interactions reads

$$\mathcal{L}_{\text{fermion}} = i \sum_{\text{fermions}} \bar{\psi}_i \not{D} \psi^i, \quad (2.15)$$

where the sum includes all the quarks and leptons with flavor " i " and $\not{D} = D_\mu \gamma^\mu$, with γ^μ being the Dirac matrices. From this Lagrangian we can define a global symmetry such as

$$\mathcal{G}_F = U(3)_{Q_L} \times U(3)_{u_L} \times U(3)_{d_R} \times U(3)_{L_L} \times U(3)_{e_R} \quad (2.16)$$

since we have 3 identical copies of each fermion. This is the flavor symmetry of the SM, which we know that it is broken since the experiments have measured remarkable differences among fermion masses. This breaking is induced by the Yukawa terms arising from the interaction of

¹The flavor quantum number gives also names for the quarks or leptons in different generations: $d^i = \{d, s, b\}$, $u^i = \{u, c, t\}$ and $e^i = \{e, \mu, \tau\}$

the fermions with the Higgs field

$$\mathcal{L}_{\text{Yukawa}} = (Y_d)_{ij} \bar{Q}_L^i \phi d_R^j + (Y_u)_{ij} \bar{Q}_L^i \phi u_R^j + (Y_e)_{ij} \bar{L}_L^i \phi e_R^j + \text{h.c.}, \quad (2.17)$$

where the $Y_{u,d,e}$ Yukawa couplings are matrices 3x3 in the flavor space. Here we can rotate all the fields in order to diagonalize the Yukawas using unitary transformations U such as

$$\psi_L \rightarrow U_{\psi_L} \psi_L \quad \psi_R \rightarrow U_{\psi_R} \psi_R, \quad (2.18)$$

and for each yukawa matrix

$$Y_d \rightarrow U_{d_L} y_d U_{d_R}^\dagger \quad Y_u \rightarrow U_{u_L} y_u U_{u_R}^\dagger \quad Y_e \rightarrow U_{e_L} y_e U_{e_R}^\dagger \quad (2.19)$$

where each y is a diagonal matrix. Introducing these rotations to the Yukawa Lagrangian and setting, without loss of generality, $U_{Q_L} = U_{d_L}$ and $U_{L_L} = U_{\nu_L}$ we have

$$\mathcal{L}_{\text{Yukawa}} = (y_d)_{ij} \bar{Q}_L^i \phi d_R^j + (U_{d_L}^\dagger U_{u_L} y_u)_{ij} \bar{Q}_L^i \phi u_R^j + (U_{\nu_L}^\dagger U_{e_L} y_e)_{ij} \bar{L}_L^i \phi e_R^j + \text{h.c.}, \quad (2.20)$$

where we can define $V_{\text{CKM}}^\dagger \equiv U_{d_L}^\dagger U_{u_L}$ which is the Cabbibo-Kobayashi-Maskawa matrix². Then, after the Higgs acquires its vev, the mass terms of the fermions are generated after one single rotation of the upper $SU(2)_L$ component of quarks $u_L \rightarrow V_{\text{CKM}}^\dagger u_L$ ³

$$\mathcal{L}_{\text{Yukawa}}^{\text{EWSB}} = \frac{y_d}{\sqrt{2}} \bar{d}_L d_R + \frac{y_u}{\sqrt{2}} \bar{u}_L u_R + \frac{y_e}{\sqrt{2}} \bar{e}_L e_R + \text{h.c.}, \quad (2.21)$$

where the masses are now diagonal matrices defined as $m_{\{u,d,e\}} = y_{\{u,d,e\}} v / \sqrt{2}$. The rotation implemented in Eq. 2.21 has a physical impact in the gauge part only in the W interaction with the fermions also known as charged currents (CC)

$$\mathcal{L}_{\text{CC}} = \frac{ig}{\sqrt{2}} V_{\text{CKM}} W^\mu \bar{u}_L \gamma_\mu d_L + \text{h.c.} \quad (2.22)$$

whereas the interaction of fermions with the Z boson or neutral currents remains flavor diagonal. All in all, the SM flavor sector is completely unconstrained and is described by 6 quark + 3

²If we were considering right-handed neutrinos we would also have an analogous matrix $U_{\text{PMNS}} \equiv U_{\nu_L}^\dagger U_{e_L}$, which is the Pontecorvo–Maki–Nakagawa–Sakata matrix.

³The same rotation applies in the up component of the lepton doublets if we have right-handed neutrinos.

lepton masses + 4 CKM parameters = 13 parameters without PMNS and neutrino masses. The goal of flavor physicists is to find a symmetry realized at high scale that make us understand the structure of the flavor sector. We can summarize the SM fermion content in the following table

	$SU(3)$	$SU(2)_L$	$U(1)_Y$
Q_L	3	2	1/6
u_R	3	1	2/3
d_R	3	1	-1/3
L_L	1	2	-1/2
e_R	1	1	-1

(2.23)

2.2 Flavor Anomalies

As we stated in the introduction of this Chapter, some tensions in flavor observables have been reported by many experiments referred as flavor anomalies or B -anomalies. Our purpose in this section is to describe these anomalies by dividing them in two types $b \rightarrow s$ and $b \rightarrow c$ anomalies. We explore their scope and define proper effective Hamiltonians in order to account for possible NP scenarios.

2.2.1 $b \rightarrow s$ Anomalies

$b \rightarrow s$ transitions can only be generated through loop diagrams in the SM. The corresponding loop suppression makes all the related observables very useful in order to probe for new particles exchanged in the loops therefore to test for possible presence of NP. With the purpose of testing LFU, the community proposed to measure $R_{K^{(*)}}$ [38]

$$R_{K^{(*)}}^{[q_1^2, q_2^2]} \equiv \frac{\text{Br}(B \rightarrow K^{(*)} \mu^+ \mu^-)}{\text{Br}(B \rightarrow K^{(*)} e^+ e^-)} \quad (2.24)$$

where the two partial branching ratios are integrated between the dilepton invariant masses q_1^2 and q_2^2 , with $q^2 = (p_B - p_{K^{(*)}})^2$. In the SM, $R_{K^{(*)}}$ is very close to one, and since it is constructed as a ratio of branching fractions in the low q^2 -region, the theoretical error due to non-perturbative QCD is very reduced because of the cancelation of hadronic form factors. LHCb measured R_K in Run 1 [8] and in Run 2 combined with more Run 1 data [11] obtaining

on average

$$R_K^{[1,6]} = 0.846_{-0.054}^{+0.060}(\text{stat})_{-0.014}^{+0.016}(\text{syst}), \quad (2.25)$$

where the first uncertainty accounts for the statistics and the second refers to systematic error and the invariant dilepton mass is in GeV^2 . This is to be compared with the theoretical estimate $R_K^{\text{SM}} = 1.000(1)$ [38, 39] where most of the error bar stems from the QED corrections. This measurement has therefore a 2.5σ discrepancy with respect to the SM, starting an intriguing tension on $b \rightarrow s$ LFU tests.

LHCb also measured R_{K^*} in two different bins in Run 1 [10]

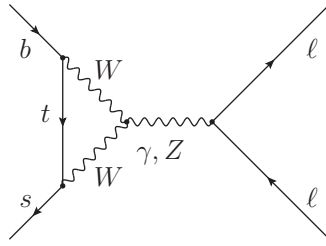
$$\begin{aligned} R_{K^*}^{[0.045,1.1]} &= 0.660_{-0.070}^{+0.110}(\text{stat}) \pm 0.024(\text{syst}), \\ R_{K^*}^{[1.1,6.0]} &= 0.685_{-0.069}^{+0.113}(\text{stat}) \pm 0.047(\text{syst}), \end{aligned} \quad (2.26)$$

which amounts to an average tension of above 2.4σ and 2.5σ with respect to the SM, respectively. On the other hand, Belle collaboration [40, 41] reported other measurements of R_{K^*} where the central value is closer to the SM, but with considerably larger error bars that do not affect the tension observed by LHCb.

Interestingly, there are some observables such as $\text{Br}(B \rightarrow K^* \mu^+ \mu^-)$ and $\text{Br}(B \rightarrow \phi \mu^+ \mu^-)$ which also have been reported to have a tension of $\sim 2\sigma$ with respect to the SM [16, 17]. These observables are more difficult and involved to compute in the SM because one has to take care of non-perturbative QCD effects and a careful treatment of the hadronic form factors is required. In processes such as $B \rightarrow K^* \mu^+ \mu^-$, the K^* meson usually also decays to $K\pi$ mesons, becoming a 4-body decay. This fact allows for scrutinizing $B \rightarrow K^* \mu^+ \mu^-$ decay with not only its branching fraction but also the full angular distribution, allowing to define new observables such as P_1, P_2, P_3 or P_5' which have mild hadronic uncertainties [42, 43, 44], making them very useful to probe for NP. Concretely, the angular observable P_5' has also been measured [9, 40] with a discrepancy of $\sim 3\sigma$ with respect to the SM.

There is also the parity conserving process $B_s \rightarrow \mu^+ \mu^-$ for which the branching fraction is also very clean from theoretical error and because of that it becomes a key observable when performing experimental fits. The world average of the branching fraction is [45]

$$\text{Br}(B_s \rightarrow \mu^+ \mu^-)^{\text{exp}} = (3.1 \pm 0.6)10^{-9}, \quad (2.27)$$


 Figure 2.1: Standard Model contribution to $b \rightarrow s\ell\ell$ via loop level.

while the current SM averaged branching fraction is [46]

$$\text{Br}(B_s \rightarrow \mu^+\mu^-)^{\text{SM}} = (3.57 \pm 0.17)10^{-9}. \quad (2.28)$$

Also very recently, LHCb collaboration was able to perform the analysis of the baryonic decay $\Lambda_b^0 \rightarrow pK^-\ell\ell$ which also involves a $b \rightarrow s\mu^+\mu^-$ transition [47], with the difference that the process involves Λ_b -baryons instead of B -mesons. They reported

$$R_{pK}^{-1} = \frac{\text{Br}(\Lambda_b^0 \rightarrow pK^-e^+e^-)}{\text{Br}(\Lambda_b^0 \rightarrow pK^-\mu^+\mu^-)} \quad (2.29)$$

measured in the $q^2 = [0.1, 6]$ GeV² bin. The prediction in the SM for this observable is $R_{pK}^{-1} \sim 1$, while they find the ratio to be $R_{pK}^{-1} = 1.17_{-0.16}^{+0.18} \pm 0.07$, which is compatible with the SM, although the central value points towards the same direction of the other $b \rightarrow s\mu^+\mu^-$ anomalies. Nonetheless, the theoretical error is huge due to the lack of knowledge of the Λ^* baryon resonances entering in the invariant mass $m(pK)$.

2.2.2 Effective Theory Description of $b \rightarrow s\ell\ell$

With all the experimental results one may interpret data as a hint of the presence of BSM physics. To that effect, it is very useful to construct an effective theory in a model independent way, using 4-fermion vertices as depicted in Fig. 2.1 which encode all the relevant information on the $b \rightarrow s\ell\ell$ transitions. The most general Hamiltonian containing the 4-fermion dimension 6 operators reads

$$\mathcal{H}_{\text{eff}}^{\ell\ell} = -\frac{4G_F}{\sqrt{2}}V_{tb}V_{ts}^* \sum_i \left(C_i \mathcal{O}_i + C'_i \mathcal{O}'_i \right) + \text{h.c.}, \quad (2.30)$$

where G_F is the Fermi constant that sets the strength of weak interactions, $V_{tb}V_{ts}^*$ being the CKM matrix factor that appears in the SM contribution, with

$$\begin{aligned}
 \mathcal{O}_9 &= \frac{\alpha_{\text{EM}}}{4\pi} (\bar{s}\gamma_\mu P_L b)(\bar{\ell}\gamma^\mu \ell), & \mathcal{O}_{10} &= \frac{\alpha_{\text{EM}}}{4\pi} (\bar{s}\gamma_\mu P_L b)(\bar{\ell}\gamma^\mu \gamma_5 \ell), \\
 \mathcal{O}_S &= \frac{\alpha_{\text{EM}}}{4\pi} (\bar{s}P_R b)(\bar{\ell}\ell), & \mathcal{O}_P &= \frac{\alpha_{\text{EM}}}{4\pi} (\bar{s}P_R b)(\bar{\ell}\gamma_5 \ell), \\
 \mathcal{O}_T &= \frac{\alpha_{\text{EM}}}{4\pi} (\bar{s}\sigma_{\mu\nu} b)(\bar{\ell}\sigma^{\mu\nu} P_R \ell), & &
 \end{aligned} \tag{2.31}$$

where $\ell = e, \mu, \tau$ are the three lepton flavors and α_{EM} the fine structure constant. Besides, one has to take into account the electromagnetic and the gluonic penguin operators

$$\mathcal{O}_7 = \frac{e}{16\pi^2} m_b \bar{s} \sigma^{\mu\nu} P_R b F_{\mu\nu}, \quad \mathcal{O}_8 = \frac{g_s}{16\pi^2} m_b \bar{s} \sigma^{\mu\nu} P_R T_{\alpha\beta}^a b_\beta G_{\mu\nu}^a. \tag{2.32}$$

Here, $F_{\mu\nu}$ and $G_{\mu\nu}^a$ are the field strength tensors of the photon and the gluon field, respectively, and m_b is the mass of the bottom quark. The primed operators are obtained by interchanging L and R . The C_i effective vertices are known as Wilson coefficients and encode all the short distance (high energy) information about the 4-fermion interaction. To consider NP scenarios, it is very useful to define

$$C_i = C_i^{\text{SM}} + C_i^{\text{NP}} \tag{2.33}$$

with the exception of the coefficients that are already zero in the SM, for which we omit the NP label. Fitting all of the $b \rightarrow s\ell\ell$ data results in constraining the Wilson coefficients and gives a theoretical direction on which kind of NP scenario we need to consider. In that respect, the one dimensional fits (fits to one parameter) are the most stringent for considering different NP scenarios. Fits in [19, 20, 21, 22, 23, 24, 25, 26, 27, 28, 29, 30, 31, 32] contain more than 40 such observables, and their results provide useful hints to possible NP scenarios. Currently a combined discrepancy of more than 4σ with respect to the SM is reported by all groups. The 1-dimensional fits of Ref. [28] prefer the following two scenarios

1. $C_9^{\mu\text{NP}} = -1.03 \pm 0.16$,
2. $C_9^{\mu\text{NP}} = -C_{10}^{\mu\text{NP}} = -0.50 \pm 0.09$

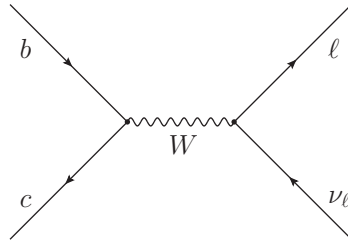


Figure 2.2: Standard Model contribution to $b \rightarrow c \tau \nu_\tau$ via tree level.

The best fit is achieved when NP is coupled to the muon sector^{4,5}, although some LFU contribution to NP is also allowed. The second scenario is very attractive under the theoretical point of view because it is generated by left handed vector currents, which usually relates to a simpler and more elegant explanation than other scenarios involving right and left handed currents. Note, however, that the multi-dimensional fits suggest the presence of a little vector right-handed contribution $(C_9^{\prime\mu\text{NP}}, C_{10}^{\prime\mu\text{NP}})$, specially if one takes all the observables. In the models presented in this thesis, we will work assuming the second scenario $C_9^{\mu\text{NP}} = -C_{10}^{\mu\text{NP}}$, although we allow for small right-handed couplings in Chap.4.

2.2.3 $b \rightarrow c$ Anomalies

In 2012 BaBar experiment reported on a deviation with respect to the SM in the charged current processes $b \rightarrow c \tau \nu$ [33], following on the observables R_D and R_{D^*}

$$R_{D^{(*)}} \equiv \frac{\text{Br}(B \rightarrow D^{(*)} \tau^- \bar{\nu}_\tau)}{\text{Br}(B \rightarrow D^{(*)} l^- \bar{\nu}_l)} \quad , \quad (l = e, \mu) . \quad (2.34)$$

In the same way as $R_{K^{(*)}}$, these observables have little theoretical uncertainties from the fact that they are constructed with ratios. They are build to test LFU in charged currents which occur at tree-level in the SM as we can see in the diagram in Fig. 2.2. The values found by BaBar were respectively [33]

$$\begin{aligned} R_D &= 0.440 \pm 0.058(\text{stat}) \pm 0.042(\text{syst}) , \\ R_{D^*} &= 0.332 \pm 0.024(\text{stat}) \pm 0.018(\text{syst}) . \end{aligned} \quad (2.35)$$

⁴We will refer to $C_{9(10)}^{\mu\text{NP}}$ as $C_{9(10)}^{\text{NP}}$ or simply $C_{9(10)}$ in some chapters in order to ease the notation, as we will only generate effects to the muon in general. In any other case it will be specified.

⁵In Refs. [27] and [28], they also suggest the interesting possibility for LFU NP affecting all the leptons plus a LFUV part affecting the muons. In this thesis we only consider LFUV NP.

Intriguingly, in 2016 the Belle Collaboration [12] also found some discrepancy in these observables with respect to their SM value. In 2019 Belle presented another measurement which was still in tension with the SM [13], although the world average discrepancy was a bit reduced. All in all, combining all of the currently available experimental results for $R_{D^{(*)}}$ we obtain

$$\begin{aligned} R_D &= 0.340 \pm 0.027(\text{stat}) \pm 0.013(\text{syst}), \\ R_{D^*} &= 0.295 \pm 0.011(\text{stat}) \pm 0.008(\text{syst}). \end{aligned} \quad (2.36)$$

In the SM, these processes are carried out via a W boson exchange. Contrary to $R_{K^{(*)}}$, the value of $R_{D^{(*)}}$ is not 1 in the SM because the tau lepton is much heavier than the electron or the muon. The results in the SM are [48]

$$\begin{aligned} R_D^{\text{SM}} &= 0.299 \pm 0.003, \\ R_{D^*}^{\text{SM}} &= 0.258 \pm 0.005. \end{aligned} \quad (2.37)$$

After comparing these numbers with the ones given in Eq. (2.36), we see that these observables present a tension with the SM of 3.1σ ⁶. Moreover, LHCb reported a new measurement related to $b \rightarrow c\ell\nu$ decays which is [49]

$$R_{J/\psi} \equiv \frac{\text{Br}(B_c \rightarrow J/\psi\tau^-\bar{\nu}_\tau)}{\text{Br}(B_c \rightarrow J/\psi\mu^-\bar{\nu}_\mu)} = 0.71 \pm 0.17 \pm 0.18, \quad (2.38)$$

which is also larger than predicted in the SM $R_{J/\psi} = 0.283 \pm 0.048$ computed in Ref [50].

This set of deviations motivates phenomenologists to construct an effective theory for $b \rightarrow c\tau\nu$ in order to assess the amount of the possible NP contribution to these channels.

2.2.4 Effective Theory Description of $b \rightarrow c\ell\nu_\ell$

With the same spirit as in the $b \rightarrow s\ell\ell$ effective theory, one may construct an effective theory involving $b \rightarrow c\ell\bar{\nu}_\ell$ decays. The most general Lorentz invariant parity-conserving effective Hamiltonian for these transitions reads at the bottom scale

$$\mathcal{H}_{\text{eff}}^{\ell\nu_\ell} = \frac{4G_F}{\sqrt{2}} V_{cb} \left[(1 + g_{V_L})\mathcal{O}_{V_L} + g_{V_R}\mathcal{O}_{V_R} + g_{S_L}\mathcal{O}_{S_L} + g_{S_R}\mathcal{O}_{S_R} + g_T\mathcal{O}_T \right] + \text{h.c.}, \quad (2.39)$$

⁶The discrepancy before the last Belle update in 2019 was of 3.8σ .

where V_{cb} is the CKM factor and the 4-fermion operators governing these transitions are given by

$$\begin{aligned}
 \mathcal{O}_{V_L} &= (\bar{c}\gamma_\mu P_L b)(\bar{\ell}\gamma^\mu P_L \nu_\ell), & \mathcal{O}_{V_R} &= (\bar{c}\gamma_\mu P_R b)(\bar{\ell}\gamma^\mu P_L \nu_\ell), \\
 \mathcal{O}_{S_L} &= (\bar{c}P_L b)(\bar{\ell}P_L \nu_\ell), & \mathcal{O}_{S_R} &= (\bar{c}P_R b)(\bar{\ell}P_L \nu_\ell), \\
 \mathcal{O}_T &= (\bar{c}\sigma_{\mu\nu} b)(\bar{\ell}\sigma^{\mu\nu} P_L \nu_\ell), & &
 \end{aligned} \tag{2.40}$$

The couplings g_i are Wilson coefficients which encode the contribution of NP for $\ell = e, \mu$ or τ since their SM values are $g_i^{\text{SM}} = 0$, for all $i = (V_L, V_R, S_L, S_R, T)$, by construction. Assuming that the NP is present only in the decay to τ , the one dimensional fits [51, 52, 53, 54, 31, 55, 56, 57, 58], allow for a $V - A$ scenario beyond the SM with the presence of a single coupling g_{V_L} . This feature is similar to the one in $b \rightarrow s$ anomalies where a left-handed scenario is actually also preferred. Nonetheless there is also the possibility to obtain a good one dimensional fit by imposing the combination $g_{S_L} = \pm 4g_T$ to the NP at the TeV scale, allowing for real or imaginary couplings, which can be achieved via right-handed couplings, although this option is slightly disfavoured in the light of the new Belle result.

2.2.5 Simple Models for the Anomalies

With all the experimental information given in the previous sections one may not claim a discovery of NP since none of the mentioned observables deviates more than 5σ from the SM, however the B -physics anomalies are probably the largest coherent set of deviations with respect to the SM we have ever seen. For that reason, simplified models attempting to explain all or some of those flavor anomalies soon appeared on the market.

Those simplified models can address other problems in physics such as the flavor structure of the Yukawa couplings including the origin of massive neutrinos, try to explain dark matter abundance, relate the QCD strong CP problem, or solve other tensions of current data with respect to the SM predictions. This fact makes the work of the community worth the effort to think of a model that explain the anomalies, even if they end up vanishing. In what follows we list some of these models that arise from different theoretical motivations and some of which try to accommodate all the anomalies and others just a subset of them.

Leptoquarks

LQs are colored objects which can be scalar or vector bosons. They appear naturally in many grand unified theories (GUTs), as well as in composite models. Since the $R_{K^{(*)}}$ and $R_{D^{(*)}}$ anomalies indeed refer to the semi-leptonic decays, some involving quarks and leptons, LQs are good candidates to solve the anomalies, and for that reason they draw the attention of the flavor community from past years to present [59, 60, 61, 7, 62, 63, 64, 65, 66, 67, 68, 69, 70, 71, 72, 73, 74, 75, 76, 77, 78, 79, 80, 81, 56, 82, 83, 84, 85, 86, 87, 88, 89]⁷. Their contribution to $b \rightarrow s\mu^+\mu^-$ is depicted in the left side of Fig. 2.3 where LQs have to couple to the second generation of leptons and the 3rd and 2nd generation of down quarks. As for $b \rightarrow c\tau\bar{\nu}$ the LQ contribution arises from the right diagram in Fig. 2.3, and in this case it has to couple to the third generation of leptons, the third generation of down quarks and the second generation of up quarks.

What concerns the $b \rightarrow s$ anomaly, one needs to generate $C_9^{\mu\text{NP}} = -C_{10}^{\mu\text{NP}}$ which can be achieved by LQ with left-handed couplings to the quarks and similar happens with the $R_{D^{(*)}}$ anomaly. The problem arises when we try to solve both anomalies at the same time. In Ref. [56], it has been shown that in order to address the anomalies, the only candidate considering one single mediator is the U_1 vector leptoquark, that can account for $R_{D^{(*)}} > R_{D^{(*)}}^{\text{SM}}$ and $R_{K^{(*)}} < R_{K^{(*)}}^{\text{SM}}$ at the same time using only left-handed couplings while passing all constraints arising from direct searches. This fact has triggered a lot of activity in designing a possible UV completion, given that U_1 is a vector particle not associated to a gauge symmetry realised at $\mathcal{O}(\text{TeV})$ scales. Such examples are the so called PS^3 model and the 4321 model [76, 84] which besides B -anomalies try to address other problems related to flavor physics.

Scalar LQs are a very good alternative in constructing simple models since their scalar nature makes possible to cancel all the divergences without any explicit UV completion. There are plenty of works on solving one of the anomalies or just solving a part of them, since they are not able to account for all the anomalies at the same time when considering one single mediator. However, the abovementioned cancellation of the divergences has been exploited in order to construct models with two scalar LQs which can account for the two types of flavor anomalies. From that point of view there are two combinations of scalar LQs which can accommodate both types of the B -anomalies:

⁷In general, LQs address the anomalies at loop level although there are some cases where the $b \rightarrow s\mu^+\mu^-$ anomaly is addressed via loop diagrams [90, 91]

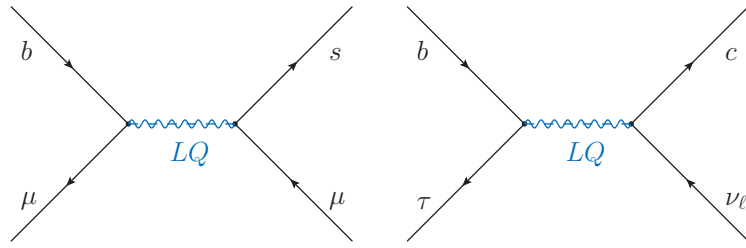


Figure 2.3: Left: Leptoquark contribution to $b \rightarrow s\mu^+\mu^-$ via tree level. Right: Leptoquark contribution to $b \rightarrow c\tau\nu_\tau$ via tree level.

- A model with S_3 and R_2 scalar LQs, with the structure of Yukawa couplings that can be embedded in a $SU(5)$ GUT scenario [56].
- The combination of S_3 and S_1 scalar LQs, which cannot be embedded in a $SU(5)$ GUT scenario but it can accommodate the anomalous magnetic moment of the muon, $(g - 2)_\mu$, depending on the structure of the Yukawa couplings [74, 80, 92].

Apart from explaining the anomalies, one can explore these models further to explain dark matter candidates, neutrino masses and CP problems, specially in the UV complete theories where many new particles need to arise.

Scalar and Fermionic Loop Models

There are many solutions which only focus in one type of anomaly. In this case the so called scalar and fermionic loop models only try to account for $b \rightarrow s\mu^+\mu^-$ anomalies [93, 94, 95]. The proposal of these kind of models is to generate the contribution to $b \rightarrow s\mu^+\mu^-$ at the loop level via box diagrams, as in Fig. 2.4, with at least 3 new particles: two scalars and one fermion or viceversa. This fact resembles the SM behaviour where the FCNC contributions enter at loop level. In general, these models require introducing a number of new particles extending the SM and can account for solutions involving left-handed and right-handed couplings, to verify all the experimental constraints at low and high energies.

As in the LQ case these models are also built to explain other problems such as the muon anomalous magnetic moment, $a_\mu = (g - 2)_\mu/2$ with a possible chirality enhancement due to the inclusion of right-handed couplings and some dark matter investigation has been carried out with neutral scalars or fermions that can accommodate for direct searches limits and dark matter abundances.

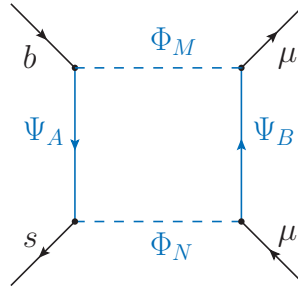


Figure 2.4: Example of box diagram contributing to $b \rightarrow s\mu^+\mu^-$ at loop level within a generic model with new scalars and fermions.

Two Higgs Doublet Models

When the Higgs boson was first detected in the LHC in 2012, the idea to extend the Higgs sector with a 2HDM as embedded in the supersymmetric extensions of the SM, such as Minimal Supersymmetric SM (MSSM) and next-to-MSSM (NMSSM), triggered a considerable activity in the community to look for the particles that arise in the 2HDM models. When the flavor anomalies appeared, this simple extension of the SM was considered by many model builders with intentions to study the anomalies and predict or constrain the possible mass of other Higgs particles mediating the interaction. It turns out, however, that with this model it is not possible to accommodate $R_{K^{(*)}} < R_{K^{(*)}}^{\text{SM}}$ at low q^2 unless one allows for the presence of right-handed neutrinos [96, 97, 98]. However, since there are many types of these models which are famous due to Supersymmetry (SUSY), it is interesting to analyse the $b \rightarrow s\mu^+\mu^-$ anomaly and explore which are the constraints imposed to diverse kinds of 2HDM. Moreover, if the tension of $R_{K^{(*)}}$ with respect to the Standard Model is reduced, there is the possibility that the branching ratio of $B_s \rightarrow \mu^+\mu^-$ can be explained with pseudo-scalar operators, making the 2HDM a viable and attractive scenario of BSM physics. The diagram structure contributing to the $b \rightarrow s\mu^+\mu^-$ process are depicted on the left side of Fig. 2.5.

In these kind of models, the contribution to $b \rightarrow c\tau\nu$ can be achieved via the interaction of a charged Higgs (H^-) as in the right picture of Fig. 2.5 which can accommodate the anomaly with both left and right handed couplings.

Z' and W'

One simple way to extend the SM is to add vector bosons that act as mediators of the interactions that we want to address, in this case a Z' for the $b \rightarrow s\mu^+\mu^-$ anomaly and a W' for the $b \rightarrow c\tau\nu$

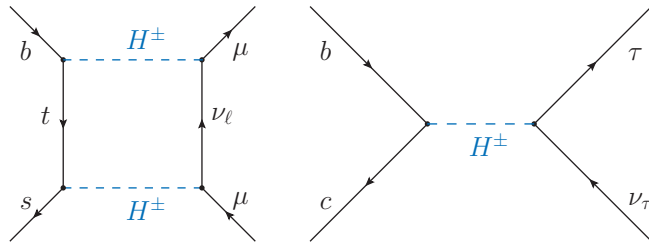


Figure 2.5: Left: Example of box diagram contributing to $b \rightarrow s\mu^+\mu^-$ at loop level in a 2HDM. Right: Example of a tree-level diagram contributing to $b \rightarrow s\tau\nu_\tau$ in a 2HDM. In both cases it is a charged Higgs contribution.

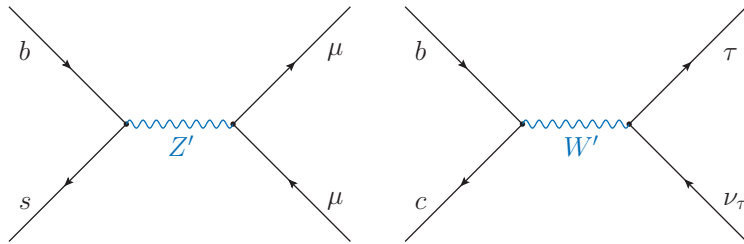


Figure 2.6: Z' contribution to $b \rightarrow s\mu^+\mu^-$ at tree level and W' contribution to $b \rightarrow s\tau\nu_\tau$ also at tree level.

process Fig. 2.6. The presence of the new gauge bosons requires the addition of a new gauge symmetry which has to break into $SU(3)_c \times SU(2)_L \times U(1)_Y$ and hence the addition of new scalars acquiring a vev at the NP scale [99, 100, 101, 102, 103, 104, 105, 106, 107, 108, 109, 110, 111, 112, 113, 114, 115, 116, 117, 118, 119, 120, 121, 122].

There is also the possibility of only explaining the $R_{K^{(*)}}$ anomaly with the Z' which requires only an extra $U(1)$ symmetry, simplifying the scenario but paying the price of not being able to explain $R_{D^{(*)}}$. One remarkable feature of these models is that in principle the gauge coupling to the SM fermions should not be flavor universal, and hence they should have different charge under the new gauge group. This fact however can be avoided by the addition of a 4th family of new heavy vector-like fermions which couple to the Z' boson, and at the same time couple to the SM fermions, generating a $b \rightarrow s\mu^+\mu^-$ contribution with LFU couplings.

These new Z' bosons are very constrained in direct detections due to their tree-level contributions, this fact also makes Z' models very sensitive to many other indirect constraints.

Chapter 3

Left-Handed Scalars and Fermions at One Loop

As stated in the previous Chapter, the FCNCs in the SM arise at loop level. One can use this fact to motivate building a NP model where the contribution to $b \rightarrow s\mu^+\mu^-$ anomalies also appears at loop level. We want to stress that in this chapter we do not aim to explain $b \rightarrow c$ anomaly, i.e CC anomaly, since it is impossible to give a sizable effect at loop level, and therefore if this anomaly is confirmed, one should assume that it comes from another NP source. Explanation of the anomalies via loop effects, on the other hand, typically leads to correlated imprints on other observables like the anomalous magnetic moment of the muon (a_μ). It is thus appealing to investigate the possibility of a simultaneous solution of the $b \rightarrow s$ anomalies and the long-standing tension in $(g-2)_\mu$ at the loop level, for example by light Z' bosons [123, 124, 125, 126, 127, 128, 129, 130, 131, 132], leptoquarks [133, 134, 90] or new fermions and scalars [135, 136, 137, 138, 139, 140, 141, 142, 143, 93, 144].

In this chapter, we examine in detail the possibility proposed in Ref. [93] that the anomalies in the $b \rightarrow s\mu^+\mu^-$ data and $(g-2)_\mu$ are explained by loop effects involving heavy new scalars and fermions that couple to the SM fermions via Yukawa-like interactions. In order to generate the Wilson coefficient C_9 , the new particles must couple to the left-handed SM quark doublets Q . We study the minimal setup in which the new particles do not couple to right-handed SM fields, implying $C_9 = -C_{10}$ which is one of the favored patterns for the solution of the $b \rightarrow s\mu^+\mu^-$ anomalies as pointed out in Sec. 3.2.1. We explore in more detail the phenomenological consequences in a general class of models: We consider those representations which are realized in the SM (singlet, fundamental and adjoint) and study also the case of the fermions (scalars)

being Majorana particles (real scalars).

The chapter is organized as follows: In Sec. 3.1 we define the model and classify the various representations under the SM gauge group for the new particles. In Sec. 3.2 we give the formulae for the Wilson coefficients and the observables relevant for our numerical analysis in Sec. 3.3.

3.1 Setup

In the spirit of Ref. [93], we introduce new heavy scalars and vector-like fermions in such a way that a one-loop box contribution to $b \rightarrow s\mu^+\mu^-$ is generated (see Fig. 3.1) in analogy to FCNC processes in the SM. We will assume that the new particles only couple to left-handed SM fermions. This assumption minimizes the number of free parameters and is phenomenologically well motivated because the resulting pattern $C_9 = -C_{10}$ is one of the scenarios that are suited best for the description of $b \rightarrow s\mu^+\mu^-$ data. To draw the diagram on the left-hand side of Fig. 3.1, we need a new scalar Φ that couples to both quarks and leptons, and two different fermionic particles (with different color quantum numbers), one of them coupling to quarks and one of them to leptons. Alternatively, exchanging the roles played by the scalars and fermions, we get the diagram on the right-hand side of Fig. 3.1. Therefore, we construct the following two distinct models:

1. One additional scalar Φ and two additional fermions Ψ_Q and Ψ_ℓ with interactions described by the Lagrangian

$$\mathcal{L}_{\text{int}}^{(a)} = \Gamma_i^Q \bar{\Psi}_Q P_L Q_i \Phi + \Gamma_i^L \bar{\Psi}_\ell P_L L_i \Phi + \text{h.c.} \quad (3.1)$$

2. Two additional scalars Φ_Q and Φ_ℓ and one additional fermion Ψ with interactions described by the Lagrangian

$$\mathcal{L}_{\text{int}}^{(b)} = \Gamma_i^Q \bar{\Psi} P_L Q_i \Phi_Q + \Gamma_i^L \bar{\Psi} P_L L_i \Phi_\ell + \text{h.c.} \quad (3.2)$$

In Eqs. (3.1) and (3.2), Q_i and L_i denote the left-handed quark and lepton doublets with family index i . The box-diagrams contributing to $b \rightarrow s\ell^+\ell^-$ and $b \rightarrow s\bar{\nu}\nu$ for the model classes a) and b) are shown in Fig. 3.1. Notice that these diagram structure is the one also depicted in Fig. 2.4 in Chapter 2. Analogous box diagrams induce $B_s - \bar{B}_s$ mixing (see upper row in Fig. 3.3).

One-loop contributions to $b \rightarrow s\ell^+\ell^-$ can also be generated by the crossed box diagrams shown in Fig. 3.2. Whereas the standard box contributions in Fig. 3.1 derive from the Lagrangian $\mathcal{L}_{\text{int}}^a$ ($\mathcal{L}_{\text{int}}^b$) with Φ (Ψ) coupling both to quarks and to leptons, crossed boxes are induced by a variant $\mathcal{L}_{\text{int}}^{a'}$ ($\mathcal{L}_{\text{int}}^{b'}$) of the Lagrangian where Φ (Ψ) couples to quarks and the charge-conjugated field Φ^c (Ψ^c) to leptons. Therefore, in the case of a neutral scalar $\Phi = \Phi^c$ (Majorana fermion $\Psi = \Psi^c$) one has $\mathcal{L}_{\text{int}}^a = \mathcal{L}_{\text{int}}^{a'}$ ($\mathcal{L}_{\text{int}}^b = \mathcal{L}_{\text{int}}^{b'}$), and both crossed and uncrossed boxes are present. In the other cases, it turns out that the primed Lagrangians lead to a very similar phenomenology¹ as the unprimed ones, and so we will only consider the two cases $\mathcal{L}_{\text{int}}^a$ and $\mathcal{L}_{\text{int}}^b$ in the following, including the possible situation of neutral scalars (Majorana fermions).

Through EWSB, the SM fermions acquire masses, giving rise to the chirality-flipping process $b \rightarrow s\gamma$ and to non-zero contributions to the anomalous magnetic moment of the muon. The corresponding diagrams are shown in Fig. 3.4. Note that we do not introduce any additional source of chirality violation beyond the SM. In particular, the Higgs mechanism does not contribute to the masses of the new heavy particles which are supposed to be exclusively generated from explicit mass terms in the respective free-particle Lagrangian.

Moving from the weak to the mass eigenbasis of the quarks results in a rotation of the couplings Γ_i^Q in flavor space in Eqs. (3.1) and (3.2). This rotation is unphysical in our setup where we consider the couplings Γ_i^Q as independent free parameters. In the mass eigenbasis, we denote the couplings to muons, bottom- and strange-quarks, as Γ_μ , Γ_b and Γ_s , respectively. We further assume negligible couplings to the first fermion generation. This assumption allows for an explanation of the $R_{K^{(*)}}$ anomaly and moreover weakens the bounds on the masses of the new particles from direct searches.

Let us now discuss the possible representations for the new particles under the SM gauge group. To this end, recall that the SM fermions carry the following gauge quantum numbers:

	$SU(3)$	$SU(2)_L$	$U(1)_Y$
Q	3	2	1/6
u	3	1	2/3
d	3	1	-1/3
L	1	2	-1/2
e	1	1	-1

(3.3)

¹Predictions for observables involving only quarks or only leptons are identical for the primed and unprimed Lagrangians. For $b \rightarrow s\ell^+\ell^-$ the impact on our phenomenological analysis consists in a sign change of the Wilson coefficient $C_9 = -C_{10}$ which can, however, be absorbed by a redefinition of the product of couplings $\Gamma_s^*\Gamma_b$.

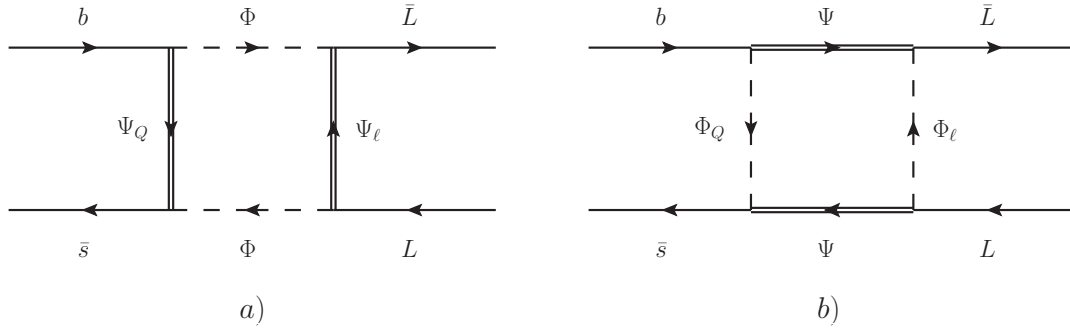


Figure 3.1: Box-diagrams contributing to $b \rightarrow s\ell^+\ell^-$ and $b \rightarrow s\nu\bar{\nu}$ in case a) and b).

In the case of the non-abelian groups we label the respective representations by their dimension. Applying this notation, the fundamental representations of $SU(3)$ and $SU(2)$ are indicated by 3 and 2 in the table above, while the corresponding adjoint representations would be labeled as 8 and 3, and singlets are marked as 1.

In the SM, all particles transform under $SU(2)_L$ and $SU(3)$ either as singlets, in the fundamental, or in the adjoint representation. We thus only consider these three possibilities also for the transformation of the new heavy particles. The requirement of gauge invariance of the Lagrangian in Eq. (3.1) or Eq. (3.2) further acts as a constraint on the allowed combinations of representations for the three new particles. We end up with the following possibilities with respect to $SU(2)$ and $SU(3)$:

$SU(2)$	Ψ_Q, Φ_Q	Ψ_ℓ, Φ_ℓ	Φ, Ψ	$SU(3)$	Ψ_Q, Φ_Q	Ψ_ℓ, Φ_ℓ	Φ, Ψ
<i>I</i>	2	2	1	<i>A</i>	3	1	1
<i>II</i>	1	1	2	<i>B</i>	1	$\bar{3}$	3
<i>III</i>	3	3	2	<i>C</i>	3	8	8
<i>IV</i>	2	2	3	<i>D</i>	8	$\bar{3}$	3
<i>V</i>	3	1	2				
<i>VI</i>	1	3	2				

The hypercharge Y can be freely chosen for one of the new particles. We define $Y_\Phi \equiv X$ for the particle Φ in model class a) and $Y_\Psi = -X$ for the particle Ψ in model class b). The values for the other two particles $\Psi_{Q,\ell}$ respectively $\Phi_{Q,\ell}$ are then fixed from charge conservation in the

Lagrangian (3.1) or (3.2):

$$\begin{array}{c|ccc}
 Y & \Psi_Q, \Phi_Q & \Psi_\ell, \Phi_\ell & \Phi, \Psi \\
 \hline
 & 1/6 + X & -1/2 + X & -X
 \end{array} \tag{3.5}$$

Motivated by the SM charges, we will assume X to be quantized² in units of $1/6$ with $-1 \leq X \leq 1$. After EW symmetry breaking, the electric charge Q_{em} derives from the hypercharge and the third component of $SU(2)$ according to

$$Q_{\text{em}} = T_3 + Y. \tag{3.6}$$

As we have found six possibilities (denoted by I, II, III, IV, V, VI) for the $SU(2)$ representations, and four possibilities (denoted by A, B, C, D) for the $SU(3)$ representations, there are in total 24 scenarios for each model class a) and b). In addition, in each of these scenarios one can freely choose the value of X .

The primed Lagrangian $\mathcal{L}_{\text{int}}^{a')}$ ($\mathcal{L}_{\text{int}}^{b')}$) in principle allows for all $SU(2)$ representations, but only representation I and IV can give non-zero contributions to $b \rightarrow s\mu^+\mu^-$ processes since the corresponding group factors vanish for the other representations. Concerning $SU(3)$ all options A, B, C, D are permitted (with $\bar{3} \rightarrow 3$ for Ψ_ℓ, Φ_ℓ in the cases B and D). The hypercharge of Ψ_ℓ, Φ_ℓ would change to $1/2 - X$. Therefore, the cases with $SU(2) \in \{I, IV\}$, $SU(3) \in \{A, C\}$ and $X = 0$ allow for Φ (Ψ) being a real scalar (a Majorana fermion) contributing to $b \rightarrow s\mu^+\mu^-$ and $B_s - \bar{B}_s$ mixing. We will put a special emphasis on this situation in our numerical analysis in Sec. 3.3 because the presence of additional crossed boxes in $b \rightarrow s\ell\ell$ and $B_s - \bar{B}_s$ (see Fig. 3.2 and second row in Fig. 3.3) can lead to interesting phenomenological consequences.

3.2 Observables and Bounds on Wilson Coefficients

In the previous section we constructed two classes of NP models aiming at an explanation of the $b \rightarrow s\mu^+\mu^-$ anomalies through one-loop box contributions. The relevant free model parameters governing this transition are the couplings Γ_b, Γ_s and Γ_μ together with the masses of the three new particles, $m_\Phi, m_{\Psi_Q}, m_{\Psi_\ell}$ in case a) and $m_\Psi, m_{\Phi_Q}, m_{\Phi_\ell}$ in case b). Unavoidably, the Lagrangian in Eq. (3.1) (in Eq. (3.2)) also generates contributions to $b \rightarrow s\nu\bar{\nu}$, $b \rightarrow s\gamma$ and $B_s - \bar{B}_s$ mixing, and in particular the latter sets an important constraint on the subspace spanned

²The assumption on the quantization of X has no impact on the phenomenological discussion.

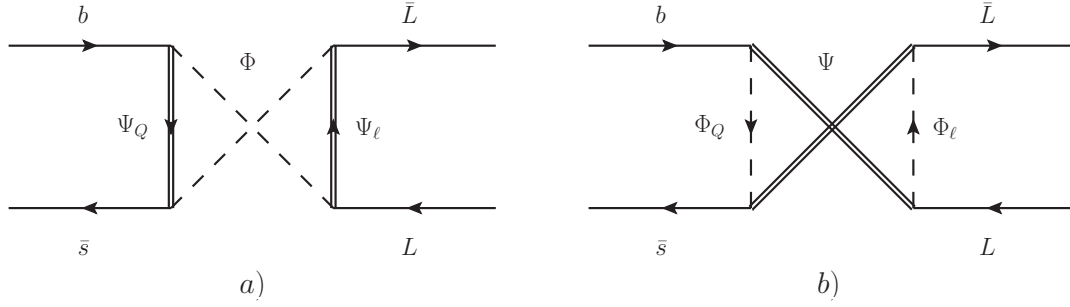


Figure 3.2: Crossed boxes contributing to $b \rightarrow s\ell^+\ell^-$ and $b \rightarrow s\nu\bar{\nu}$ in case a) (b)) if Φ (Ψ) is a real scalar (Majorana fermion).

by the couplings Γ_b , Γ_s and the masses m_Φ , m_{Ψ_Q} (m_Ψ , m_{Φ_Q}). Furthermore, depending on the coupling Γ_μ and the masses m_Φ , m_{Ψ_ℓ} (m_Ψ , m_{Φ_ℓ}), a contribution to the anomalous magnetic moment $(g-2)_\mu$ of the muon emerges that could have the potential to solve the long-standing anomaly in this observable. A complete phenomenological analysis must take into account all these processes. In this section we thus provide the Wilson coefficients needed for their theoretical description in the models under consideration and derive the experimental bounds on them.

3.2.1 $b \rightarrow s\mu^+\mu^-$

In our models, the only relevant NP contributions to $b \rightarrow s\mu^+\mu^-$ transitions reside inside a subset of the effective Hamiltonian in 2.30

$$\mathcal{H}_{\text{eff}}^{\mu^+\mu^-} = -\frac{4G_F}{\sqrt{2}}V_{tb}V_{ts}^*(C_9\mathcal{O}_9 + C_{10}\mathcal{O}_{10}), \quad (3.7)$$

with

$$\mathcal{O}_9 = \frac{\alpha_{\text{EM}}}{4\pi} [\bar{s}\gamma^\nu P_L b] [\bar{\mu}\gamma_\nu\mu], \quad \mathcal{O}_{10} = \frac{\alpha_{\text{EM}}}{4\pi} [\bar{s}\gamma^\nu P_L b] [\bar{\mu}\gamma_\nu\gamma^5\mu], \quad (3.8)$$

as defined in the previous chapter. These operators receive NP contributions from box diagrams, photon- and Z -penguins. Since we do not introduce any additional source of $SU(2)$ breaking compared to the SM, Z -penguin diagrams are necessarily suppressed by m_b^2/M_Z^2 and we will neglect them in the following.

The box contributions are depicted in Fig. 3.1 for both case a) and b). If the new scalar Φ (fermion Ψ) that couples both to quarks and leptons is in a real representation with respect to all gauge transformations, i.e. if it is a singlet or in the adjoint representation with respect to $SU(2)$ and $SU(3)$ and has hypercharge $X = 0$, one can consider the possibility that it is a real scalar (Majorana fermion). In this case, also the crossed diagrams (shown in Fig. 3.2) exist and have to be taken into account. In the models of class a) and b), we have

$$\begin{aligned} C_9^{\text{box}, a) } &= -C_{10}^{\text{box}, a) } = -\mathcal{N} \frac{\Gamma_s^* \Gamma_b |\Gamma_\mu|^2}{32\pi\alpha_{\text{EM}} m_\Phi^2} (\chi\eta - \chi^M \eta^M) F(y_Q, y_\ell) , \\ C_9^{\text{box}, b) } &= -C_{10}^{\text{box}, b) } = \mathcal{N} \frac{\Gamma_s^* \Gamma_b |\Gamma_\mu|^2}{32\pi\alpha_{\text{EM}} m_\Psi^2} (\chi\eta F(x_Q, x_\ell) - \chi^M \eta^M G(x_Q, x_\ell)) , \end{aligned} \quad (3.9)$$

with $y_Q = m_{\Psi_Q}^2/m_\Phi^2$, $y_\ell = m_{\Psi_\ell}^2/m_\Phi^2$ and $x_Q = m_{\Phi_Q}^2/m_\Psi^2$, $x_\ell = m_{\Phi_\ell}^2/m_\Psi^2$, respectively. Moreover, we have introduced the abbreviation

$$\mathcal{N}^{-1} = \frac{4G_F}{\sqrt{2}} V_{tb} V_{ts}^* . \quad (3.10)$$

The dimensionless loop functions are defined in Appendix C.1 in order to ease the notation of this chapter. Here we only write their value in the limit of equal masses

$$F(1, 1) = -G(1, 1) = \frac{1}{3} . \quad (3.11)$$

The $SU(2)$ - and $SU(3)$ -factors η , η^M and χ , χ^M are tabulated³ in Tabs. 3.1, 3.2 and Tab. 3.3, respectively. The term involving the G -function in Eq. (3.9) stems from the crossed box and is only present if Φ (Ψ) is a real scalar (Majorana fermion). If Φ (Ψ) is a complex scalar (Dirac fermion), χ^M and η^M are zero. We have cross-checked our formulae Eq. (3.9) against Ref. [145] where results had been given for the gluino-squark and the chargino-squark box in Supersymmetry, corresponding to our representations C-I and A-IV, respectively.

The photon penguin induces a contribution to C_9 , whereas it does not generate C_{10} because

³Note that for both the $SU(3)$ and the $SU(2)$ generators we use the canonical normalization $[T^a, T^b] = \delta^{ab}/2$, and that we do not absorb a normalization factor into the couplings $\Gamma_b, \Gamma_s, \Gamma_\mu$. This convention has to be kept in mind when comparing for instance with SUSY results in the literature since Supersymmetry dictates the normalization of the gluino-squark-quark coupling to be $\sqrt{2}g_s T_{ij}^a$.

$SU(2)$	η	$\eta^M = \eta_{B\bar{B}}^M$	η_L	η_L^M	$\eta_{B\bar{B}}$
<i>I</i>	1	1	1	1	1
<i>II</i>	1	−	0	−	1
<i>III</i>	5/16	−	1/4	−	5/16
<i>IV</i>	5/16	1/16	1/16	5/16	5/16
<i>V</i>	1/4	−	1/2	−	5/16
<i>VI</i>	1/4	−	1/2	−	1

Table 3.1: Table of the $SU(2)$ -factors entering the Wilson coefficients for the processes involving box diagrams. Results are given for the six representations I-VI defined in Eq. (3.4).

$SU(2)$	η_7	$\tilde{\eta}_7$	η_8	η_{a_μ}	$\tilde{\eta}_{a_\mu}$	η_3	$\tilde{\eta}_3$
<i>I</i>	$-\frac{1}{3} + X$	$-X$	1	$-1 + X$	$-X$	1	0
<i>II</i>	$\frac{1}{6} + X$	$-\frac{1}{2} - X$	1	$-\frac{1}{2} + X$	$-\frac{1}{2} - X$	0	1
<i>III</i>	$-\frac{3}{8} + \frac{3}{4}X$	$\frac{1}{8} - \frac{3}{4}X$	$\frac{3}{4}$	$-\frac{7}{8} + \frac{3}{4}X$	$\frac{1}{8} - \frac{3}{4}X$	1	$-\frac{1}{4}$
<i>IV</i>	$\frac{1}{4} + \frac{3}{4}X$	$-\frac{1}{2} - \frac{3}{4}X$	$\frac{3}{4}$	$-\frac{1}{4} + \frac{3}{4}X$	$-\frac{1}{2} - \frac{3}{4}X$	$-\frac{1}{4}$	1
<i>V</i>	$-\frac{3}{8} + \frac{3}{4}X$	$\frac{1}{8} - \frac{3}{4}X$	$\frac{3}{4}$	$-\frac{1}{2} + X$	$-\frac{1}{2} - X$	0	1
<i>VI</i>	$\frac{1}{6} + X$	$-\frac{1}{2} - X$	1	$-\frac{7}{8} + \frac{3}{4}X$	$\frac{1}{8} - \frac{3}{4}X$	1	$-\frac{1}{4}$

Table 3.2: Table of the $SU(2)$ -factors entering the Wilson coefficients for the penguin diagram processes. Results are given for the six representations I-VI defined in Eq. (3.4).

of the vector coupling of the photon to muons. For the cases a) and b), the C_9 contribution reads

$$C_9^{\gamma, a)} = \mathcal{N} \frac{\Gamma_s \Gamma_b^*}{2m_\Phi^2} \chi_7 \left[\tilde{\eta}_7 \tilde{F}_9(y_Q) - \eta_7 \tilde{G}_9(y_Q) \right], \quad C_9^{\gamma, b)} = \mathcal{N} \frac{\Gamma_s \Gamma_b^*}{2m_\Psi^2} \chi_7 \left[\eta_7 F_9(x_Q) - \tilde{\eta}_7 G_9(x_Q) \right], \quad (3.12)$$

where F_9 , $\tilde{F}_9(x)$, G_9 and \tilde{G}_9 are defined also in Appendix C.1, where in the simplifying limit of equal masses we have

$$F_9(1) = -\frac{1}{24}, \quad G_9(1) = \frac{1}{8}. \quad (3.13)$$

The terms proportional to F_9 and \tilde{F}_9 in Eq. (3.12) stem from the diagram where the photon is emitted by the scalar $\Phi_{(Q)}$, whereas the terms proportional to G_9 and \tilde{G}_9 stem from the diagram where the photon is emitted by the fermion $\Psi_{(Q)}$. The $SU(2)$ - and $SU(3)$ -factors η_7 , $\tilde{\eta}_7$ and χ_7 can again be read off from Tabs. 3.1, 3.2 and 3.3. In the case where the new scalar and the new fermion are singlets under $SU(2)$, η_7 and $\tilde{\eta}_7$ are simply given by the charges of the new particles, $\tilde{\eta}_7 = q_\Phi$ and $\eta_7 = q_{\Psi_Q} = -1/3 + q_\Phi$ for case a), $\tilde{\eta}_7 = q_\Psi$ and $\eta_7 = q_{\Phi_Q} = -1/3 + q_\Psi$

$SU(3)$	$\chi = \chi_7$	χ^M	$\chi_{B\bar{B}}$	$\chi_{B\bar{B}}^M$	χ_8	$\tilde{\chi}_8$	$\chi_{a_\mu} = \chi_Z$
A	1	1	1	1	1	0	1
B	1	–	1	–	0	1	3
C	4/3	4/3	11/18	1/9	–1/6	3/2	8
D	4/3	–	11/18	–	3/2	–1/6	3

Table 3.3: Table of the $SU(3)$ -factors entering the Wilson coefficients for the various processes. Results are given for the four representations A-D defined in Eq. (3.4).

for case b). For higher $SU(2)$ representations, η_7 and $\tilde{\eta}_7$ in addition take care of summing the contributions from each isospin component of the new particles. For the representations C-I and A-IV, the results of Eq. (3.12) have again been checked against Ref. [145].

Unlike the box contribution, the photon penguin does not involve the muon coupling Γ_μ but exclusively depends on the combination $\Gamma_s^* \Gamma_b / m_{\Phi(\Psi)}^2$ constrained from $b \rightarrow s\gamma$ and $B_s - \bar{B}_s$ mixing. We will explicitly demonstrate in Sec. 3.3 that the resulting bounds, together with the requirement of perturbative couplings Γ_s and Γ_b , typically render C_9^γ negligibly small. The same statement applies to the Wilson coefficient C_7 of the magnetic operator operator \mathcal{O}_7 (discussed in Sec. 3.2.4) that contributes to $b \rightarrow s\ell^+\ell^-$ transitions in the effective theory via tree-level photon exchange. Therefore, to a good approximation a solution of the $b \rightarrow s\mu^+\mu^-$ anomalies must proceed in our model via the pattern $C_9 = C_9^{\text{box}} + C_9^\gamma \simeq C_9^{\text{box}} \equiv -C_{10}^{\text{box}} = -C_{10}$ and $C_7 \ll C_9$. The current bounds on the generic scenario $C_9 = -C_{10}$, obtained from the combined fit to $b \rightarrow s\mu^+\mu^-$ data, are taken from [28]

$$\begin{aligned}
 -0.59 &\leq C_9 = -C_{10} \leq -0.41 & (\text{at } 1\sigma), \\
 -0.68 &\leq C_9 = -C_{10} \leq -0.32 & (\text{at } 2\sigma).
 \end{aligned} \tag{3.14}$$

These ranges are consistent with the other ones determined in the literature.

3.2.2 $b \rightarrow s\nu\bar{\nu}$

Following Ref. [146], we write the relevant effective Hamiltonian as

$$\mathcal{H}_{\text{eff}}^{\nu_i\nu_j} = -\frac{4G_F}{\sqrt{2}} V_{tb}V_{ts}^* C_L^{ij} \mathcal{O}_L^{ij}, \quad \text{where} \quad \mathcal{O}_L^{ij} = \frac{\alpha}{4\pi} [\bar{s}\gamma^\mu P_L b][\bar{\nu}_i\gamma_\mu (1 - \gamma^5)\nu_j]. \tag{3.15}$$

Due to $SU(2)$ invariance, $b \rightarrow s\nu\bar{\nu}$ is linked to $b \rightarrow s\ell^+\ell^-$, implying

$$C_L^{22,a} = -\mathcal{N} \frac{\Gamma_s^* \Gamma_b |\Gamma_\mu|^2}{32\pi\alpha_{\text{EM}} m_\Phi^2} (\chi\eta_L - \chi^M \eta_L^M) F(y_Q, y_\ell), \quad (3.16)$$

$$C_L^{22,b} = \mathcal{N} \frac{\Gamma_s^* \Gamma_b |\Gamma_\mu|^2}{32\pi\alpha_{\text{EM}} m_\Psi^2} (\chi\eta_L F(x_Q, x_\ell) + 2\chi^M \eta_L^M G(x_Q, x_\ell)), \quad (3.17)$$

with the functions F and G defined again in Appendix C.1 and η_L, η_L^M and χ, χ^M given in Tabs. 3.1, 3.2 and 3.3.

Since the different neutrino flavors in the related decays $B \rightarrow K^{(*)}\nu\bar{\nu}$ are not distinguished experimentally, the total branching ratio, normalized to its SM prediction, reads

$$R_{K^{(*)}}^{\nu\bar{\nu}} = \frac{\sum_{i,j=1}^3 |C_L^{\text{SM}}\delta^{ij} + C_L^{ij}|^2}{3|C_L^{\text{SM}}|^2}, \quad (3.18)$$

where $C_L^{\text{SM}} \approx -1.47/\sin^2\theta_W = -6.35$ with θ_W being the weak mixing angle. The current experimental limits for $B \rightarrow K^{(*)}\nu\bar{\nu}$ are [147] (at 90% C.L.)

$$R_K^{\nu\bar{\nu}} < 3.9, \quad R_{K^*}^{\nu\bar{\nu}} < 2.7. \quad (3.19)$$

While C_L^{22} , given in Eq. (3.17), involves the muonic coupling Γ_μ , any other coefficient C_L^{ij} with $(i, j) \neq (2, 2)$ would depend on the couplings Γ_e, Γ_τ of the new particles to electrons or tauons. Since we do not want to make any assumptions on the size of these couplings, we will implement the bound from $B \rightarrow K^{(*)}\nu\bar{\nu}$ according to

$$\left| 1 + \frac{C_L^{22}}{C_L^{\text{SM}}} \right|^2 \leq \sum_{i,j=1}^3 \left| \delta^{ij} + \frac{C_L^{ij}}{C_L^{\text{SM}}} \right|^2 \leq 12.9 \quad (\text{at } 90\% \text{ C.L.}), \quad (3.20)$$

leading to the following bound on C_L^{22} :

$$-16.5 \leq C_L^{22} \leq 29.2 \quad (\text{at } 90\% \text{ C.L.}). \quad (3.21)$$

Since this constraint is more than an order of magnitude weaker than the bound in Eq. (3.14) on the $SU(2)$ -related coefficient C_9 of $b \rightarrow s\mu^+\mu^-$, we will not consider it in our numerical analysis.

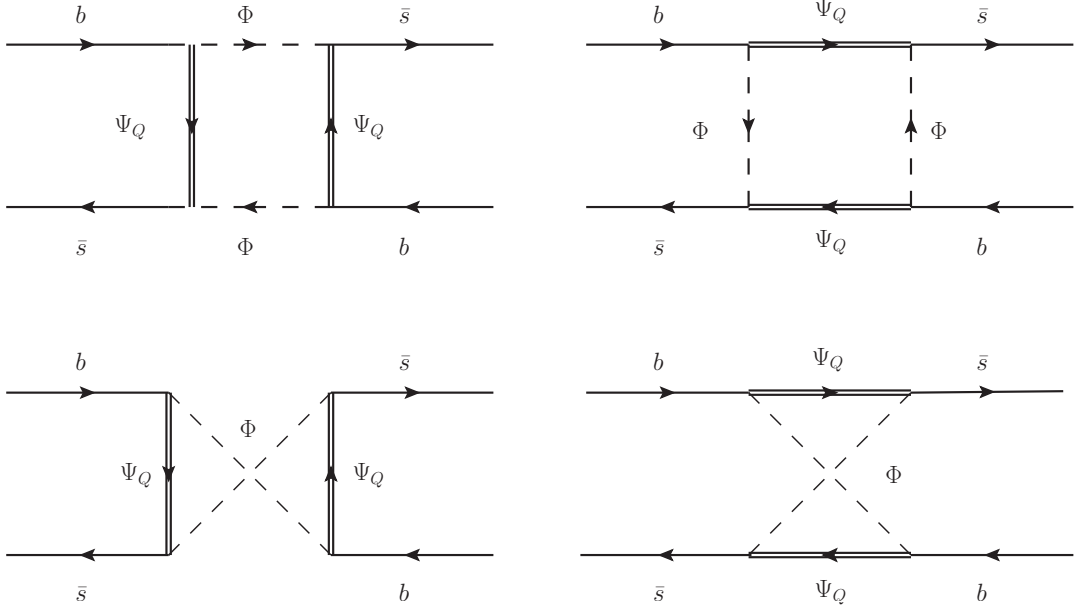


Figure 3.3: Loop contributions to $B_s - \bar{B}_s$ mixing in the case a). The crossed diagrams only exist if Φ is a real scalar. The case b) is obtained by the replacement $\Phi \rightarrow \Psi_Q$ and $\Psi_Q \rightarrow \Phi$.

3.2.3 $B_s - \bar{B}_s$ Mixing

Contributions to $B_s - \bar{B}_s$ mixing arise from box diagrams mediated in models of class a) by the scalar Φ and the fermion Ψ_Q and in models of class b) by the scalar Φ_Q and the fermion Ψ (see Fig. 3.3). If Φ is a real scalar (or Ψ is a Majorana fermion), also the corresponding crossed boxes have to be taken into account. Since the new particles only couple to left-handed SM fermions, the effective Hamiltonian only involves one operator:

$$\mathcal{H}_{\text{eff}}^{B\bar{B}} = C_{B\bar{B}} (\bar{s}_\alpha \gamma^\mu P_L b_\alpha) (\bar{s}_\beta \gamma^\mu P_L b_\beta), \quad (3.22)$$

where α and β are color indices. The NP contribution to the Wilson coefficient reads at the TeV scale

$$\begin{aligned} C_{B\bar{B}}^a &= \frac{(\Gamma_s \Gamma_b^*)^2}{128\pi^2 m_\Phi^2} (\chi_{B\bar{B}} \eta_{B\bar{B}} - \chi_{B\bar{B}}^M \eta_{B\bar{B}}^M) F(y_Q, y_Q), \\ C_{B\bar{B}}^b &= \frac{(\Gamma_s \Gamma_b^*)^2}{128\pi^2 m_\Psi^2} (\chi_{B\bar{B}} \eta_{B\bar{B}} F(x_Q, x_Q) + 2\chi_{B\bar{B}}^M \eta_{B\bar{B}}^M G(x_Q, x_Q)), \end{aligned} \quad (3.23)$$

with the loop functions F and G defined in Appendix C.1 and $\eta_{B\bar{B}}, \eta_{B\bar{B}}^M$ and $\chi_{B\bar{B}}, \chi_{B\bar{B}}^M$ given in Tabs. 3.1, 3.2 and 3.3. For the representations C-I and A-IV, Eq. (3.23) agrees with the results of Ref.[148] for the gluino-squark and the chargino-squark boxes.

To derive bounds on the Wilson coefficient $C_{B\bar{B}}$ at the bottom scale, we define the ratio

$$\frac{\Delta M_s^{\text{exp}}}{\Delta M_s^{\text{SM}}} = \left| 1 + \frac{C_{B\bar{B}}(\mu_b)}{C_{B\bar{B}}^{\text{SM}}(\mu_b)} \right|, \quad (3.24)$$

where in this case we compute the coefficients at the bottom scale μ_b as

$$C_{B\bar{B}}^{\text{SM}}(\mu_b) = \frac{G_F^2 M_W^2}{4\pi^2} \lambda_t^2 \eta(\mu_b, \mu_t) S_0(x_t) \quad \text{and} \quad C_{B\bar{B}}(\mu_b) = \eta(\mu_b, \mu_{\text{TeV}}) C_{B\bar{B}}, \quad (3.25)$$

where $\lambda_t = V_{ts}^* V_{tb}$ is related to the CKM matrix, $S_0(m_t^2/m_W^2) = 2.46$, and the $\eta(\mu_1, \mu_2)$ encode the running of the high scale μ_2 down to the lower one μ_1 . We perform the computation at the μ_b scale since we can write $\eta(\mu_b, \mu_{\text{TeV}}) = \eta(\mu_b, \mu_t) \eta(\mu_t, \mu_{\text{TeV}})$ which allows for a cancellation of the running of the top to the bottom scale, giving

$$\frac{\Delta M_s^{\text{exp}}}{\Delta M_s^{\text{SM}}} = \left| 1 + \frac{\eta(\mu_t, \mu_{\text{TeV}}) C_{B\bar{B}}}{\frac{G_F^2 M_W^2}{4\pi^2} \lambda_t^2 S_0(x_t)} \right|, \quad (3.26)$$

thus we are only left with the running from the TeV to the top scale which can be computed at leading order as

$$\eta(\mu_t, \mu_{\text{TeV}}) = \left(\frac{\alpha_s(1 \text{ TeV})}{\alpha_s(\mu_t)} \right)^{2/7} = 0.95 \quad \text{with 6 flavors.} \quad (3.27)$$

Here for the SM prediction ΔM_s^{SM} , we use the results of Ref. [149], where they take into account the SM average from FLAG 2019 [48] for the hadronic matrix element $f_{B_s}^2 B_{B_s}$ averaged with the HPQCD collaboration computation of ΔM_s^{SM} [150] and with another computation using QCD sum rules [151]. With this value, we find

$$\frac{\Delta M_s^{\text{exp}}}{\Delta M_s^{\text{SM}}} = 0.98 \pm 0.02, \quad (3.28)$$

i.e. the experimental value ΔM_s^{exp} is below the SM prediction ΔM_s^{SM} by a bit less than 1σ . For

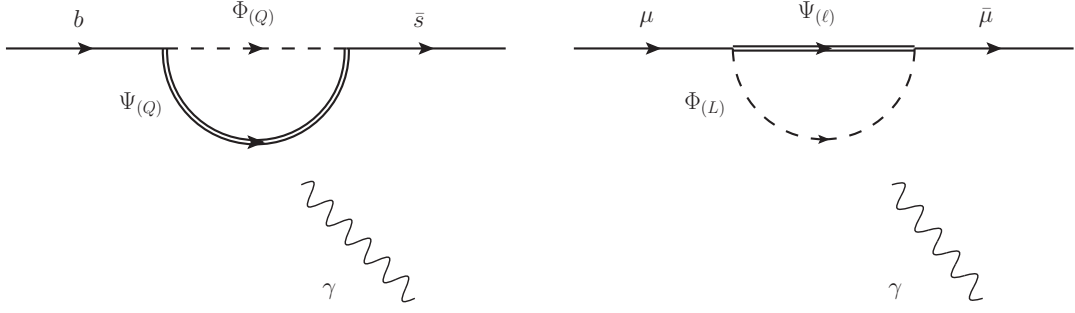


Figure 3.4: Loop contributions to $b \rightarrow s\gamma$ and the anomalous magnetic moment of the muon.

the bound on $C_{B\bar{B}}$ we finally get

$$\begin{aligned} C_{B\bar{B}} &\in [-0.6, 0.2] \times 10^{-5} \text{ TeV}^{-2} \quad (\text{at } 2\sigma), \\ C_{B\bar{B}} &\in [-0.8, 0.4] \times 10^{-5} \text{ TeV}^{-2} \quad (\text{at } 3\sigma). \end{aligned} \quad (3.29)$$

Note that the $SU(2)_L$ symmetry of the SM links the up-type couplings Γ_u to the down-type couplings through a CKM rotation. Therefore, non-vanishing couplings to up-quarks are generated in our model, namely

$$\Gamma_u = V_{us}\Gamma_s + V_{ub}\Gamma_b \quad \text{and} \quad \Gamma_c = V_{cs}\Gamma_s + V_{cb}\Gamma_b. \quad (3.30)$$

These couplings control the size of the contributions to $D_0 - \bar{D}_0$ mixing. The corresponding coefficient $C_{D\bar{D}}$ is obtained from $C_{B\bar{B}}$ by replacing $\Gamma_s \rightarrow \Gamma_u$ and $\Gamma_b \rightarrow \Gamma_c$ in Eq. (3.23).

Since a precise SM prediction for $D_0 - \bar{D}_0$ is lacking, we constrain the NP contribution to $C_{D\bar{D}}$ by the requirement that it does not generate a larger mass difference than the one measured experimentally:

$$\begin{aligned} |C_{D\bar{D}}| &< 2.7 \times 10^{-7} \text{ TeV}^{-2} \quad (\text{at } 2\sigma), \\ |C_{D\bar{D}}| &< 3.4 \times 10^{-7} \text{ TeV}^{-2} \quad (\text{at } 3\sigma). \end{aligned} \quad (3.31)$$

To obtain these bounds, we used the recent results for the $D_0 - \bar{D}_0$ system in Ref. [152] and lattice inputs from Ref. [153].

3.2.4 $b \rightarrow s\gamma$

In our models, $b \rightarrow s\gamma$ is affected by NP contributions to the effective Hamiltonian

$$\mathcal{H}_{\text{eff}}^\gamma = -\frac{4G_F}{\sqrt{2}}V_{tb}V_{ts}^*(C_7\mathcal{O}_7 + C_8\mathcal{O}_8), \quad (3.32)$$

with the operators defined in 2.32 as

$$\mathcal{O}_7 = \frac{e}{16\pi^2}m_b\bar{s}\sigma^{\mu\nu}P_R bF_{\mu\nu}, \quad \mathcal{O}_8 = \frac{g_s}{16\pi^2}m_b\bar{s}_\alpha\sigma^{\mu\nu}P_R T_{\alpha\beta}^a b_\beta G_{\mu\nu}^a. \quad (3.33)$$

While the operator \mathcal{O}_7 generates the process $b \rightarrow s\gamma$ at tree-level, the operator \mathcal{O}_8 contributes via its QCD mixing into \mathcal{O}_7 .

In the cases a) and b) we find the Wilson coefficients

$$C_7^{(a)} = \mathcal{N}\frac{\Gamma_s\Gamma_b^*}{2m_\Phi^2}\chi_7\left[\tilde{\eta}_7\tilde{F}_7(y_Q) - \eta_7F_7(y_Q)\right], \quad C_8^{(a)} = \mathcal{N}\frac{\Gamma_s\Gamma_b^*}{2m_\Phi^2}\eta_8\left[\tilde{\chi}_8\tilde{F}_7(y_Q) - \chi_8F_7(y_Q)\right]. \quad (3.34)$$

and

$$C_7^{(b)} = \mathcal{N}\frac{\Gamma_s\Gamma_b^*}{2m_\Psi^2}\chi_7\left[\eta_7F_7(x_Q) - \tilde{\eta}_7\tilde{F}_7(x_Q)\right], \quad C_8^{(b)} = \mathcal{N}\frac{\Gamma_s\Gamma_b^*}{2m_\Psi^2}\eta_8\left[\chi_8F_7(x_Q) - \tilde{\chi}_8\tilde{F}_7(x_Q)\right], \quad (3.35)$$

where the loop functions are given in Appendix C.1, taking the value $F_7(1) = \tilde{F}_7(1) = 1/24$ in the limit of equal masses. For the $SU(2)$ - and $SU(3)$ -factors $\eta_7, \tilde{\eta}_7, \eta_8$ and $\chi_7, \chi_8, \tilde{\chi}_8$ we refer the reader to Tabs. 3.1, 3.2 and 3.3 as usual. As in the case of C_9^γ , we identify $\tilde{\eta}_7, \eta_7$ with the charges of the new particles if they are $SU(2)$ singlets. Our results of $C_{7,8}$ for the representations C-I and A-IV are in agreement with the ones of Refs.[154, 155] for the gluino-squark and the chargino-squark contributions in Supersymmetry.

The most recent experimental result [45] and SM prediction [156, 157] for the branching ratio of $b \rightarrow s\gamma$ are given by

$$\begin{aligned} \text{Br}(b \rightarrow s\gamma)^{\text{exp}} &= (3.32 \pm 0.15) \times 10^{-4}, \\ \text{Br}(b \rightarrow s\gamma)^{\text{SM}} &= (3.36 \pm 0.23) \times 10^{-4}. \end{aligned}$$

In order to implement the constraint from $b \rightarrow s\gamma$ on the NP coefficients C_7, C_8 (defined at the

high scale $\mu_H = 1 \text{ TeV}$), we introduce the ratio ⁴

$$R_{b \rightarrow s\gamma} = \frac{\text{Br}(b \rightarrow s\gamma)^{\text{exp}}}{\text{Br}(b \rightarrow s\gamma)^{\text{SM}}} - 1 = -2.87 [C_7 + 0.19 C_8] = (-0.7 \pm 8.2) \times 10^{-2}, \quad (3.36)$$

where the combination $C_7 + 0.19 C_8$ takes into account QCD effects [156, 157]. Adding the statistical and the systematic experimental error in quadrature, and combining it linearly with the theory error linearly, we find $-0.17 \leq R_{b \rightarrow s\gamma} \leq 0.16$ at the 2σ level, being equivalent to

$$|C_7 + 0.19 C_8| \leq 0.06 \quad (2\sigma). \quad (3.37)$$

3.2.5 Anomalous Magnetic Moment of the Muon

The anomalous magnetic moment of the muon, $a_\mu \equiv (g-2)_\mu/2$, also receives a NP contribution in our setup. Using the effective Hamiltonian (see for example [158])

$$\mathcal{H}_{\text{eff}}^{a_\mu} = -a_\mu \frac{e}{4m_\mu} (\bar{\mu} \sigma^{\mu\nu} \mu) F_{\mu\nu}, \quad (3.38)$$

we find

$$\begin{aligned} \Delta a_\mu^a &= \frac{m_\mu^2 |\Gamma_\mu|^2}{8\pi^2 m_\Phi^2} \chi_{a_\mu} \left[\tilde{\eta}_{a_\mu} \tilde{F}_7(y_\ell) - \eta_{a_\mu} F_7(y_\ell) \right], \\ \Delta a_\mu^b &= \frac{m_\mu^2 |\Gamma_\mu|^2}{8\pi^2 m_\Psi^2} \chi_{a_\mu} \left[\eta_{a_\mu} F_7(x_\ell) - \tilde{\eta}_{a_\mu} \tilde{F}_7(x_\ell) \right]. \end{aligned} \quad (3.39)$$

The group factors η_{a_μ} , $\tilde{\eta}_{a_\mu}$ and χ_{a_μ} are again given in Tabs. 3.1, 3.2 and 3.3. If the new particles are SU(2) singlets, we have $\tilde{\eta}_{a_\mu} = q_\Phi$ and $\eta_{a_\mu} = q_{\Psi_\ell} = -1 + q_\Phi$ for case a), and $\tilde{\eta}_{a_\mu} = q_\Psi$ and $\eta_{a_\mu} = q_{\Phi_\ell} = -1 + q_\Psi$ for case b). Our result for Δa_μ has been cross-checked for the representation A-IV by comparison with the chargino-squark and the neutralino-squark results in Refs. [159, 160].

The experimental value of $a_\mu^{\text{exp}} = (116\,592\,091 \pm 54 \pm 33) \times 10^{-11}$ (where the first error is statistical and the second systematic) is completely dominated by the Brookhaven experiment E821 [161], but improvements by experiments at Fermilab [162] and J-PARC [163] (see also [164]) are expected in the future. The SM prediction is given by [165, 166, 167, 168, 169, 170, 171, 172, 173, 174, 175, 176, 177, 178, 179, 180, 181, 182, 183, 184, 185, 186, 187,

⁴ $C_{7,8}$ in Eqs. (3.34,3.35) are given in the same sign convention as $C_{7,8}^{\text{SM}}$ in Refs. [156, 157], where $C_7^{\text{SM}}(\mu_H) = -0.197$ and $C_8^{\text{SM}}(\mu_H) = -0.098$ at leading order in QCD.

188]⁵ $a_\mu^{\text{SM}} = (116\,591\,821 \pm 59) \times 10^{-11}$, where almost the entire uncertainty is due to hadronic effects. The difference between the SM prediction and the experimental value,

$$\Delta a_\mu = a_\mu^{\text{exp}} - a_\mu^{\text{SM}} = (270 \pm 85) \times 10^{-11}, \quad (3.40)$$

amounts to a 2.7σ deviation⁶.

The measurement of R_K by LHCb hints towards lepton-flavor universality violation. In global fits to the full set of $b \rightarrow s\ell^+\ell^-$ data this manifests itself as a preference for scenarios with NP contributions $|C_9^e| \ll |C_9^\mu|$ [190, 191]. In our model this pattern transforms into $|\Gamma_e| \ll |\Gamma_\mu|$, and for simplicity we assume $\Gamma_e = 0$ in our phenomenological analysis. In the presence of a non-zero Γ_e , the transition $\mu \rightarrow e\gamma$ is generated in a similar manner as a_μ and the measured branching ratio sets a constraint on the product $\Gamma_\mu\Gamma_e^*$.

The decay $\mu \rightarrow e\gamma$ is described by the effective Hamiltonian

$$\mathcal{H}_{\text{eff}}^{\mu \rightarrow e\gamma} = -C_{\mu \rightarrow e\gamma} m_\mu (\bar{e} \sigma^{\mu\nu} P_R \mu) F_{\mu\nu}, \quad (3.41)$$

from which the branching ratio is obtained according to

$$\text{Br}(\mu \rightarrow e\gamma) = \frac{m_\mu^5}{4\pi} \tau_\mu |C_{\mu \rightarrow e\gamma}|^2, \quad (3.42)$$

where τ_μ denotes the life-time of the muon. In our models, the Wilson coefficient $C_{\mu \rightarrow e\gamma}$ is directly related to the NP contribution to the anomalous magnetic moment of the muon as

$$C_{\mu \rightarrow e\gamma} = \frac{e}{m_\mu^2} \frac{\Gamma_e^*}{\Gamma_\mu^*} \Delta a_\mu. \quad (3.43)$$

The experimental upper limit [192] is currently given by

$$\text{Br}(\mu \rightarrow e\gamma)^{\text{exp}} \leq 4.2 \times 10^{-13}, \quad (3.44)$$

which translates into

$$m_\mu^2 |C_{\mu \rightarrow e\gamma}| < 3.9 \times 10^{-15} \quad (3.45)$$

⁵Here we do not take into account the very recent result of [189] where the value of the SM is compatible with the experiment, since it carries another problems in EW precision observables.

⁶Less conservative estimates lead to discrepancies up to 3.6σ

for the Wilson coefficient. The relation Eq. (3.43) between a_μ and $\mu \rightarrow e\gamma$ then implies that a solution of anomaly in a_μ requires a strong suppression of Γ_e with respect to Γ_μ . Already a minimal shift $\Delta a_\mu = 61 \times 10^{-11}$, as needed to reduce the tension from 2.7σ to 2.0σ , is consistent with the bound from $\mu \rightarrow e\gamma$ only for $|\Gamma_e/\Gamma_\mu| < 2 \times 10^{-5}$.

3.2.6 $Z\mu^+\mu^-$ Coupling

Exchanging the photon in the diagrams of Fig. 3.4 with the Z boson, effective $Zq_i\bar{q}_j$ and $Z\mu^+\mu^-$ vertices are generated. Note that our model does not break the $SU(2)_L$ symmetry of the SM and that the Z boson acts like a $U(1)_Z$ gauge boson in neutral-current processes in the absence of $SU(2)_L$ -breaking sources. For this reason the QED Ward identity holds for the NP corrections to the $Zq_i\bar{q}_j$ and $Z\mu^+\mu^-$ vertices and it follows that the vertex correction and the fermionic field renormalization for on-shell fermions cancel in the limit $q^2 \rightarrow 0$ with q being the momentum carried by the (off-shell) Z boson⁷. This implies that the NP contribution exhibits a $q^2/m_{\Phi(\Psi)}^2$ suppression when the vertex is probed for $q^2 \ll m_{\Phi(\Psi)}^2$, rendering the Z -penguin contribution irrelevant for B decays where $q^2 = \mathcal{O}(m_b^2)$. At LEP, however, the couplings of the Z boson have been measured for $q^2 = M_Z^2$ and the less severe suppression of the NP contribution at this scale together with the high precision of the LEP data could lead to relevant constraints for the model.

The LEP bounds are most important for the $Z\mu^+\mu^-$ coupling because this coupling has been determined most accurately and, moreover, the corrections involve the coupling Γ_μ which is required to be large to solve both the $b \rightarrow s\mu^+\mu^-$ and the a_μ anomalies. As mentioned above, the Z boson behaves like a heavy photon in the Z penguin contribution and the corresponding formula is thus related to the one of the photon penguin in Eq. (3.12). The correction proportional to $|\Gamma_\mu|^2$ to the left-handed $Z\mu^+\mu^-$ coupling is given by

$$\begin{aligned} \frac{\delta g_{L\mu}^a}{g_{L\mu}^{\text{SM}}}(q^2) &= \frac{1}{32\pi^2} \left(\frac{1}{1-2s_W^2} \right) \frac{q^2}{m_\Psi^2} |\Gamma_\mu|^2 \chi_Z \left[\tilde{\eta}_Z \tilde{F}_9(y_\ell) - \eta_Z \tilde{G}_9(y_\ell) \right], \\ \frac{\delta g_{L\mu}^b}{g_{L\mu}^{\text{SM}}}(q^2) &= \frac{1}{32\pi^2} \left(\frac{1}{1-2s_W^2} \right) \frac{q^2}{m_\Psi^2} |\Gamma_\mu|^2 \chi_Z \left[\eta_Z F_9(x_\ell) - \tilde{\eta}_Z G_9(x_\ell) \right], \end{aligned} \quad (3.46)$$

where $\eta_Z = \eta_3 + 2s_W^2\eta_{a_\mu}$ and $\tilde{\eta}_Z = \tilde{\eta}_3 + 2s_W^2\tilde{\eta}_{a_\mu}$. The group factors $\chi_Z, \eta_3, \tilde{\eta}_3$ are again given in

⁷The correction to the self-energy of the Z boson does not cancel but involves the weak gauge coupling and not the potentially large new couplings $\Gamma_{b,s,\mu}$.

Tabs. 3.1, 3.2 and 3.3, and we have introduced the abbreviation $s_W = \sin \theta_W$ with θ_W being the weak mixing angle. For the representation A.I in case a) (A.II in case b)), our model generates the same NP contribution to the $Z\mu^+\mu^-$ coupling as the model considered in Ref. [63], and we explicitly cross-checked our formulae Eq. (3.46) for this special case against the corresponding formula in [63].

From the LEP measurement [193] $g_{L\mu}^{\text{exp}}(m_Z^2) = -0.2689 \pm 0.0011$ we infer the following bound at the 2σ level:

$$\left| \frac{\delta g_{L\mu}}{g_{L\mu}^{\text{SM}}}(m_Z^2) \right| \leq 0.8\% \quad (2\sigma). \quad (3.47)$$

3.3 Phenomenological Analysis

The processes described in the previous section depend in our models on five independent free parameters: the product of couplings $\Gamma_s^*\Gamma_b$ and the absolute value of the coupling $|\Gamma_\mu|$, as well as the three masses $m_{\Psi(\Phi)}$, $m_{\Phi_Q(\Psi_Q)}$, $m_{\Phi_\ell(\Psi_\ell)}$. The decay $b \rightarrow s\gamma$ and $B_s - \bar{B}_s$ mixing, both exclusively related to the quark sector, are experimentally and theoretically very precise observables and thus set stringent constraints on the subspace spanned by $\Gamma_s^*\Gamma_b$ and $m_{\Psi(\Phi)}$, $m_{\Phi_Q(\Psi_Q)}$. In this section we will address the question whether these constraints still allow to choose $|\Gamma_\mu|$ and $m_{\Phi_\ell(\Psi_\ell)}$ in such way that a solution of the anomalies in $b \rightarrow s\mu^+\mu^-$ and a_μ is provided.

Since the loop functions that appear in the Wilson coefficients are smooth functions of the squared mass ratios, the general phenomenological features can in a first approximation be studied in the limit of equal masses $m_{\Psi(\Phi)} = m_{\Phi_Q(\Psi_Q)} = m_{\Phi_\ell(\Psi_\ell)}$, reducing the number of free parameters from five to three. The corresponding analysis will be presented in Sec. 3.3.1. An exception occurs if Ψ is a Majorana fermion: In this case we encounter negative interference between the loop functions F and G in the coefficient $C_{B\bar{B}}$ which can be used to avoid or to weaken the stringent bound from $B_s - \bar{B}_s$ mixing in a setup with unequal masses of the new particles. This possibility will be discussed in Sec. 3.3.2.

3.3.1 Degenerate Masses: $m_{\Psi(\Phi)} = m_{\Phi_Q(\Psi_Q)} = m_{\Phi_\ell(\Psi_\ell)}$

Under the assumption of equal masses $m_{\Psi(\Phi)} = m_{\Phi_Q(\Psi_Q)} = m_{\Phi_\ell(\Psi_\ell)}$, both setups a) and b) give identical results for all Wilson coefficients and we can discuss them together. We will denote the common mass as m_Ψ in the following. As a benchmark point we will assume a mass of 1 TeV which is save with respect to direct LHC searches from Run I and current Run II data. The

$\xi_{B\bar{B}}$	I	II	III	IV	V	VI	ξ_9^{box}		I	II	III	IV	V	VI
A	1 (0)	1	$\frac{5}{16}$	$\frac{5}{16} \left(\frac{1}{4}\right)$	$\frac{5}{16}$	1	A		1 (0)	1	$\frac{5}{16}$	$\frac{5}{16} \left(\frac{1}{4}\right)$	$\frac{1}{4}$	$\frac{1}{4}$
B	1	1	$\frac{5}{16}$	$\frac{5}{16}$	$\frac{5}{16}$	1	B		1	1	$\frac{5}{16}$	$\frac{5}{16}$	$\frac{1}{4}$	$\frac{1}{4}$
C	$\frac{11}{18} \left(\frac{1}{2}\right)$	$\frac{11}{18}$	$\frac{55}{288}$	$\frac{55}{288} \left(\frac{53}{288}\right)$	$\frac{55}{288}$	$\frac{11}{18}$	C		$\frac{4}{3} (0)$	$\frac{4}{3}$	$\frac{5}{12}$	$\frac{5}{12} \left(\frac{1}{3}\right)$	$\frac{1}{3}$	$\frac{1}{3}$
D	$\frac{11}{18}$	$\frac{11}{18}$	$\frac{55}{288}$	$\frac{55}{288}$	$\frac{55}{288}$	$\frac{11}{18}$	D		$\frac{4}{3}$	$\frac{4}{3}$	$\frac{5}{12}$	$\frac{5}{12}$	$\frac{1}{3}$	$\frac{1}{3}$

Table 3.4: Group factor for $B_s - \bar{B}_s$ mixing and C_9^{box} for the case equal masses. The number in brackets are for the case of Majorana fermions or real scalars.

collider signature of our model is similar to the one of sbottom searches in the MSSM if the fermion is not charged under QCD and electrically neutral. The corresponding mass limits at the LHC with 13 TeV can reach up to 800 GeV from Atlas and CMS [194, 195]. Note further that the limits strongly depend on the embedding of the set-up in a more complete theory and that the bounds can be expected to be significantly weaker in our case since we assume approximately degenerate $m_{\Psi(\Phi)} \approx m_{\Phi_Q(\Psi_Q)} \approx m_{\Phi_\ell(\Psi_\ell)}$

It turns out that $B_s - \bar{B}_s$ mixing imposes very stringent constraints in the $(\Gamma_s^* \Gamma_b, m_\Psi)$ -plane. This is caused by the fact that $C_{B\bar{B}}$ is positive and thus increases ΔM_s , pushing it even further away from the experimental central value. At 2σ , we find

$$|\Gamma_s^* \Gamma_b| \leq 0.15 \frac{1}{\sqrt{\xi_{B\bar{B}}}} \frac{m_\Psi}{1 \text{ TeV}}, \quad (3.48)$$

where the combinatorial factor $\xi_{B\bar{B}} = \chi_{B\bar{B}} \eta_{B\bar{B}} - \chi_{B\bar{B}}^M \eta_{B\bar{B}}^M$, tabulated in Tab. 3.4, can weaken the bound at most by a factor $1/\sqrt{(\xi_{B\bar{B}})_{\min}} \approx 2.3$. The constraint heavily affects the photon penguin contributions to C_7 and C_9^γ which depend on the same free parameters $\Gamma_s^* \Gamma_b$ and m_Ψ . In the most favorable representation, and allowing for hypercharges $X \in [-1, +1]$, we find these contributions to be completely negligible:

$$|C_7 + 0.19C_8| \leq 0.018 \frac{1 \text{ TeV}}{m_\Psi}, \quad |C_9^\gamma| \leq 0.02 \frac{1 \text{ TeV}}{m_\Psi}. \quad (3.49)$$

As discussed in Sec. 3.2.3, the CKM-induced couplings $\Gamma_{u,c}$ (see Eq. (3.30)) lead to additional constraints from $D_0 - \bar{D}_0$ mixing. Since the impact of Γ_b entering through Γ_u and Γ_c from Eq. (3.30) is suppressed by small CKM factors ($\mathcal{O}(\lambda^3)$ and $\mathcal{O}(\lambda^2)$, respectively), the constraint from $D_0 - \bar{D}_0$ mixing can be reduced in a scenario with $|\Gamma_b| > |\Gamma_s|$. The choice $|\Gamma_b| \sim 1$ and $|\Gamma_s| \sim 0.35$ saturates the bound from $B_s - \bar{B}_s$ mixing on the product $\Gamma_s^* \Gamma_b$, while it leads to

a suppression by a factor $|V_{us}|^2 |\Gamma_s|^2 \sim 5 \times 10^{-3}$ of $C_{D\bar{D}}$ with respect to $C_{B\bar{B}}$. The constraint on $C_{D\bar{D}}$ given in Eq. (3.31) is then automatically fulfilled once the constraint on $C_{B\bar{B}}$ from Eq. (3.31) is imposed.

In the case of the box contribution to $b \rightarrow s\mu^+\mu^-$, the coupling Γ_μ enters as an additional free parameter, limited to values $\Gamma_\mu \lesssim \mathcal{O}(1)$ in order to ensure perturbativity. The 2σ -bound from $B_s - \bar{B}_s$ mixing constrains $C_9^{\text{box}} = -C_{10}^{\text{box}}$ to

$$|C_9^{\text{box}}| \leq 0.05 \frac{\xi_9^{\text{box}}}{\sqrt{\xi_{B\bar{B}}}} |\Gamma_\mu|^2 \frac{1 \text{ TeV}}{m_\Psi}, \quad (3.50)$$

with the group factors $\xi_9^{\text{box}} = \chi\eta - \chi^M\eta^M$ given in Tab. 3.4. Considering the maximum value of the ratio $\xi_9^{\text{box}}/\sqrt{\xi_{B\bar{B}}}$, namely $4\sqrt{2/11} \simeq 1.7$ for the representations C-I, C-II and D-I, D-II, we find from Eq. (3.50) that a solution of the $b \rightarrow s\mu^+\mu^-$ anomalies at the 2σ -level requires a rather large coupling

$$|\Gamma_\mu| \geq 2.1 \sqrt{\frac{m_\Psi}{1 \text{ TeV}}}. \quad (3.51)$$

Let us now turn to the anomalous magnetic moment of the muon. In the limit of equal masses, the NP contribution is given by

$$\Delta a_\mu = \mp(5.8 \times 10^{-12}) \xi_{a_\mu} |\Gamma_\mu|^2 \left(\frac{1 \text{ TeV}}{m_\Psi} \right)^2, \quad (3.52)$$

with $\xi_{a_\mu} = \chi_{a_\mu}(\eta_{a_\mu} - \tilde{\eta}_{a_\mu})$ in Tab. 3.5. The minus applies to case a) while the plus applies to case b). In order to end up with a value for a_μ that falls within the experimental 2σ range, a positive NP contribution $\Delta a_\mu = 6.2 \times 10^{-10}$ is needed to have constructive interference with the SM. This in turn implies the need for a negative (positive) group factor ξ_{a_μ} for case a) (b)), which can be accomplished for all representations by choosing an appropriate hypercharge $X \in [-1, +1]$. Selecting the representation C-II or C-V (C-I) and maximizing the effect in the anomalous magnetic moment by setting $X = 1$ ($X = -1$), we find $\xi_{a_\mu} = 16$ ($\xi_{a_\mu} = -24$) and that a_μ can be brought into agreement with the experimental measurement at the 2σ -level for

$$|\Gamma_\mu| \geq 2.6(2.1) \frac{m_\Psi}{\text{TeV}}. \quad (3.53)$$

We see that both the tensions in $b \rightarrow s\mu^+\mu^-$ data and in the anomalous magnetic moment of the muon, a_μ , can be reduced below the 2σ level for NP masses at the TeV scale and a coupling

ξ_{a_μ}	<i>I</i>	<i>II</i>	<i>III</i>	<i>IV</i>	<i>V</i>	<i>VI</i>
<i>A</i>	$2X - 1$	$2X$	$\frac{3}{2}X - 1$	$\frac{1}{4}(6X + 1)$	$2X$	$\frac{3}{2}X - 1$
<i>B</i>	$6X - 3$	$6X$	$\frac{9}{2}X - 3$	$\frac{3}{4}(6X + 1)$	$6X$	$\frac{9}{2}X - 3$
<i>C</i>	$16X - 8$	$16X$	$12X - 8$	$12X + 2$	$16X$	$12X - 8$
<i>D</i>	$6X - 3$	$6X$	$\frac{9}{2}X - 3$	$\frac{3}{4}(6X + 1)$	$6X$	$\frac{9}{2}X - 3$

Table 3.5: Group factors for the various representations entering the anomalous magnetic moment of the muon.

$|\Gamma_\mu| \geq 2.1$. In light of this large value one might wonder, whether the LEP bounds on the $Z\mu^+\mu^-$ coupling discussed in Sec. 3.2.6 could become relevant. Evaluation of Eq. (3.46) gives

$$\frac{\delta g_{L\mu}^{\text{SM}}(m_Z^2)}{g_{L\mu}^{\text{SM}}} = -0.0006\% \xi_Z |\Gamma_\mu|^2 \left(\frac{1 \text{ TeV}}{m_\Psi} \right)^2, \quad (3.54)$$

with $\xi_Z = \chi_Z(\tilde{\eta}_Z/3 + \eta_Z)$ in case a) and $\xi_Z = \chi_Z(\eta_Z/3 + \tilde{\eta}_Z)$ in case b). For $|X| \leq 1$, the group factor maximally reaches $\xi_Z \sim 10$ and the correction to the $Z\mu^+\mu^-$ vertex thus stays two orders of magnitude below the experimental sensitivity at LEP (see Eq. (3.47)) for masses of the new particle at the TeV scale.

In order to decide, whether a coupling Γ_μ of size $|\Gamma_\mu| \geq 2.1$ is still viable, it is further instructive to study the scale of the Landau pole of this coupling at the one-loop level. This scale signals the break-down of the perturbative regime. Therefore, it provides an upper limit on the UV cut-off beyond which the theory needs to be complemented with new degrees of freedom if perturbativity shall be conserved. The Landau pole is obtained by evaluation of the renormalization-group equations (RGEs), which were determined at two loop for Yukawa couplings in a general quantum field theory e.g. in Refs. [196, 197, 144]. For Yukawa-like couplings beyond the SM, the RGEs depend on the representations of the new particles under the SM gauge group. We studied the issue of the Landau pole for our models by implementing some of the possible scenarios in the public code SARAH [198] and found that the running is dominated by $\mathcal{O}(\Gamma_\mu^2)$ corrections. For $|\Gamma_\mu| \leq 2.4$, the respective terms in the RGE lead to a Landau pole at $\gtrsim 10^3$ TeV.

In the case of $b \rightarrow s\mu^+\mu^-$, the requirement of a large coupling $|\Gamma_\mu| \geq 2.1$ is a consequence of the tight constraint from $B_s - \bar{B}_s$ mixing, and we will discuss in the following the possibility to relax this constraint by considering non-degenerate masses for the new particles.

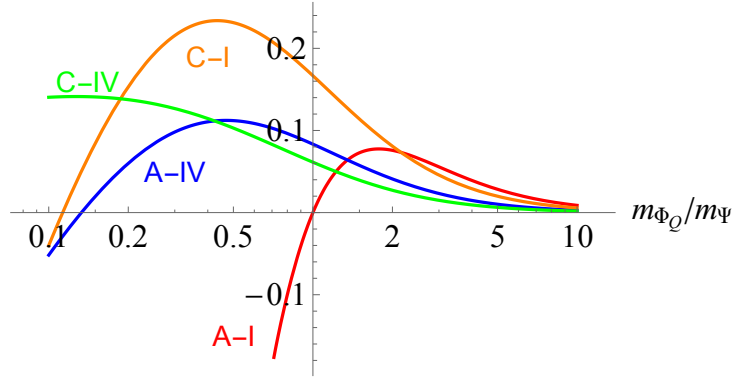


Figure 3.5: The function $H^b(m_{\Phi_Q}/m_\Psi)$ entering $C_{B\bar{B}}$ for the four Majorana representations A-I, A-IV, C-I and C-IV. Note that representation C-IV only has a zero crossing for very small values of m_{Φ_Q}/m_Ψ outside the plot range.

3.3.2 Majorana Case with Non-degenerate Masses

In this section, we address the question whether the impact of the constraint from $B_s - \bar{B}_s$ mixing can be reduced by considering a non-degenerate spectrum for the masses of the new particles. In the model classes a) and b), the Wilson coefficient $C_{B\bar{B}}$ for $B_s - \bar{B}_s$ mixing is proportional to the function

$$\begin{aligned} H^a(m_{\Psi_Q}/m_\Phi) &= (\chi_{B\bar{B}}\eta_{B\bar{B}} - \chi_{B\bar{B}}^M\eta_{B\bar{B}}^M)F(y_Q, y_Q), \\ H^b(m_{\Phi_Q}/m_\Psi) &= \chi_{B\bar{B}}\eta_{B\bar{B}}F(x_Q, x_Q) + 2\chi_{B\bar{B}}^M\eta_{B\bar{B}}^MG(x_Q, x_Q), \end{aligned} \quad (3.55)$$

with $y_Q = m_{\Psi_Q}^2/m_\Phi^2$ and $x_Q = m_{\Phi_Q}^2/m_\Psi^2$. Note that both loop functions F and G have a smooth behavior with respect to their arguments and never switch sign. Therefore, a reduction of the effect in $B_s - \bar{B}_s$ mixing by varying the mass ratio m_{Ψ_Q}/m_Φ or m_{Φ_Q}/m_Ψ is only possible through a (partial) cancellation between the F - and G -term in the function H . Such a cancellation can only occur in the model class b) with the additional condition of Ψ being a Majorana fermion because in all other cases only one loop-function F is present. Among the various representations, only four permit the Majorana option: A-I, A-IV, C-I and C-IV. In Fig. 3.5 we show the function $H^b(m_{\Phi_Q}/m_\Psi)$ for these four representations in the Majorana case. Each of the curves has a zero-crossing, given by $m_{\Phi_Q}/m_\Psi = 1, 0.11, 0.13$ for A-I, A-IV and C-I, respectively, while it lies outside the plotted range for C-IV.

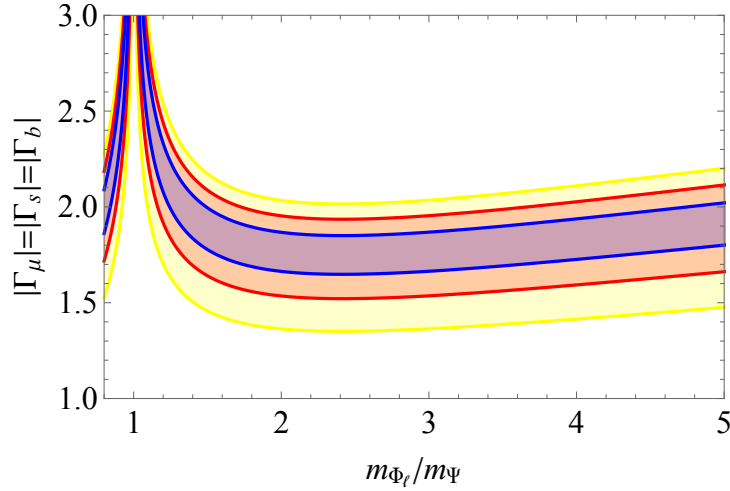


Figure 3.6: Allowed regions for the coupling strength to muon, bottom and strange quarks from $b \rightarrow s\mu^+\mu^-$ data as a function of m_{Φ_ℓ}/m_Ψ for case A-I in scenario b) with $m_{\Phi_Q} = m_\Psi = 1$ TeV. Blue, red and yellow correspond to 1σ , 2σ and 3σ , respectively.

Obviously, choosing a mass configuration that corresponds to the zero of the function H completely avoids any constraint from $\Delta F = 2$ processes. Let us study the consequences for the representation A-I where this situation occurs for $m_\Psi = m_{\Phi_Q}$. Note that the mass m_{Φ_ℓ} of the scalar Φ_ℓ has to be split from the one of the other two particles in order to get a non-vanishing contribution to C_9^{box} . Under the simplifying assumption $|\Gamma_b| = |\Gamma_s| = |\Gamma_\mu|$, we show in Fig. 3.6 as a function of m_{Φ_ℓ}/m_Ψ the generic coupling size needed to explain the $b \rightarrow s\mu^+\mu^-$ data. We see that the larger space available in $\Gamma_s^*\Gamma_b$ in the absence of the bound from $B_s - \bar{B}_s$ mixing, allows to obtain a solution at the 2σ level for a generic coupling size of $|\Gamma_b| = |\Gamma_s| = |\Gamma_\mu| \gtrsim 1.6$ for a mass splitting $m_{\Phi_\ell}/m_\Psi \gtrsim 2$ and $m_\Psi \sim 1$ TeV. The Majorana property of Ψ constrains the photon penguin contribution because it fixes $q_\Psi = 0$ and $q_{\Phi_Q} = -1/3$, leading to

$$C_7 = -C_9^\gamma = -0.005 V_{ts}^* V_{tb} \left(\frac{1 \text{ TeV}}{m_\Psi} \right)^2. \quad (3.56)$$

For $|\Gamma_b|, |\Gamma_s| < 3$ and $m_\Psi = 1$ TeV, we encounter values $|C_7| = |C_9^\gamma| < 0.044$, which are too small to have a relevant impact.

In the case $m_{\Phi_Q}/m_\Psi < 1$, a negative NP contribution to ΔM_s is generated, as preferred by current lattice data. An improvement in $B_s - \bar{B}_s$ mixing can be achieved simultaneously with

a solution of the $b \rightarrow s\mu^+\mu^-$ anomalies if a small mass splitting $0.98 \lesssim m_{\Phi_Q}/m_{\Psi} \lesssim 1.0$ is introduced.

Chapter 4

General Scenario with New Scalars and Fermions at One Loop

In the previous chapter we focused on solving the $b \rightarrow s\mu^+\mu^-$ anomalies with a simple extension of the SM containing three fields and left-handed couplings only. However, while $R_{K^{(*)}}$ is perfectly accommodated, the anomalous magnetic moment of the muon anomaly required very large muon couplings since there are no chirality-changing sources which could enhance the contribution to this observable.

Therefore, we extend in this chapter the analysis of Chapter 3 to include the possibility of new sources of EW symmetry breaking within the NP sector. In doing so, we are giving the possibility to have new fields coupling to the right-handed sector of the SM apart from left-handed one. This new feature allows for an enhancement of the anomalous magnetic moment of the muon and it can also fit at the same time $b \rightarrow s\mu^+\mu^-$ data. In fact, while before Moriond 2019 scenarios with left-handed current were in general preferred, now including right-handed contributions (both in quark and leptonic sectors) can even give a good fit to data [28, 29, 30, 31, 32].

At the same time we generalise the model by considering an arbitrary number of BSM fields from which we compute the contribution to some of the observables mentioned in 3. We use these general formulae to test a UV complete example of such a setup with new scalars and fermions couplings to left- and right-handed SM fermions is a model with a vector-like 4th generation. With respect to Ref. [199, 200], also aiming at an explanation of the $b \rightarrow s\ell^+\ell^-$ anomalies, we add not only a 4th generation of leptons but also of quarks [201, 202, 203, 204] to the SM.

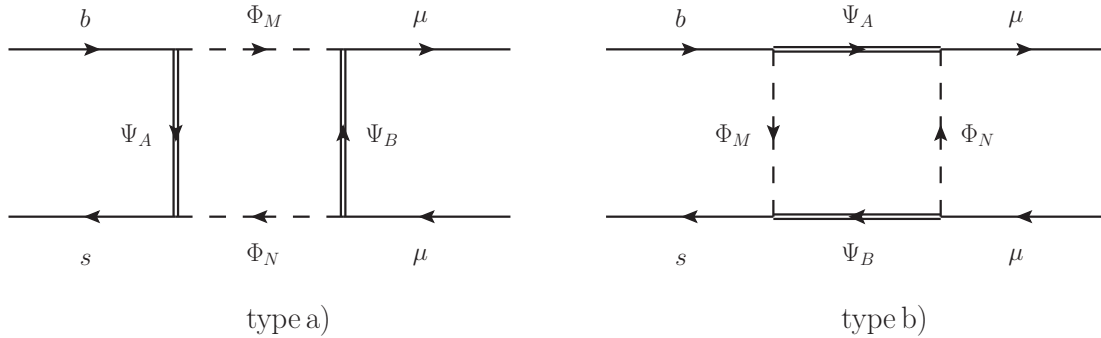


Figure 4.1: Box diagrams contributing to $b \rightarrow s \mu^+ \mu^-$ transitions. The diagram on the left is generated in models in which the fermions couples only to SM quarks or only to SM leptons, which corresponds to type a). The diagram on the right refers to models with scalars connecting b to s and μ to μ , i.e. type b).

This chapter is organised as follows: In Sec. 4.1 we define our generic setup, in which new scalars and fermions couple to SM quarks and leptons via Yukawa-like interactions. There, we also provide completely general expressions for the formulae of the relevant Wilson coefficients. We review the corresponding observables together with the current experimental situation in Sec. 4.2. Our generic approach of Sec. 4.1 is then applied to a specific UV complete model in Sec. 4.3, which contains a vector-like fourth generation of fermions and a neutral scalar.

4.1 Generic Setup and Wilson Coefficients

In this section we define our generic setup and calculate completely general one-loop expressions for contributions to $b \rightarrow s$ processes and the anomalous magnetic moment of the muon.

As outlined in the introduction, in the spirit of the previous chapter, we add to the SM particle content a NP sector with vector-like fermions Ψ_A and new scalars Φ_M such that $b \rightarrow s \mu^+ \mu^-$ transitions can be generated via box diagrams, as depicted in Fig. 4.1. In this respect, we generalize the previous analysis by including in addition couplings of new particles to $SU(2)$ singlet SM fermions. Moreover, we do not impose limitations on the number of fields added to the SM and allow for couplings of the new sector to the SM Higgs.

In order to generate box diagrams as the ones shown in Fig. 4.1 it is necessary that either the scalars $\Phi_{M,N}$ or the fermions $\Psi_{A,B}$ couple both to quarks and leptons, corresponding to case a) and b), respectively. This means that in diagrams of type a) the amplitudes (before using any Fierz identities) have the structure $(\bar{s}\Gamma b)(\bar{\mu}\Gamma\mu)$, while in type b) amplitudes of the form

$(\bar{\mu}\Gamma b)(\bar{s}\Gamma\mu)$ are generated. Here, Γ denotes an arbitrary Dirac structure. Since semi-leptonic operators are commonly given in the form $(\bar{s}\Gamma b)(\bar{\mu}\Gamma\mu)$, Fierz identities must be used in case b) in order to transform the expressions to this standard basis. We give the relevant Fierz identities in Appendix B.

The Yukawa-like couplings of new scalars Φ_M and fermions Ψ_A to bottom/strange quarks and muons can be parameterized completely generically (below the EW symmetry breaking scale) by the Lagrangian

$$\mathcal{L}_{\text{int}} = \left[\bar{\Psi}_A (L_{AM}^b P_L b + L_{AM}^s P_L s + L_{AM}^\mu P_L \mu) \Phi_M + \bar{\Psi}_A (R_{AM}^b P_R b + R_{AM}^s P_R s + R_{AM}^\mu P_R \mu) \Phi_M \right] + \text{h.c.} . \quad (4.1)$$

Here Ψ_A and Φ_M have to be understood as generic lists containing in principle an arbitrary number of fields, meaning that A and M also include implicitly $SU(2)$ and color indices. Therefore, the couplings $L_{AM}^{s,b}$ and $R_{AM}^{s,b}$ are generic matrices in $(A-M)$ space with the restriction that $U(1)_{\text{EM}}$ and $SU(3)$ are respected¹.

In the same spirit as in Chap 3, this Lagrangian will not only affect $b \rightarrow s\mu^+\mu^-$ transitions but also unavoidably generate effects in $B_s - \bar{B}_s$ mixing, $b \rightarrow s\gamma$ decays, the anomalous magnetic moment of the muon a_μ as well as Z couplings and decays to SM fermions. Furthermore, $b \rightarrow s\nu\bar{\nu}$ processes and $D_0 - \bar{D}_0$ mixing can give relevant constraints once $SU(2)$ invariance at the NP scale is imposed. Therefore, all these processes have to be taken into account in a complete phenomenological analysis. In order to perform such an analysis, the Wilson coefficients of the relevant effective Hamiltonian must be known. We will calculate them in the following subsections. Contrary to the previous Chapter, we compute the experimental bounds in another section since formulae are now more involved.

¹Here we only consider coupling to muons in order to explain the anomalies in $b \rightarrow s\ell^+\ell^-$. The reason for this is that in our setup sizable couplings to electrons would in general generate effects in $\mu \rightarrow e\gamma$, which would contradict experimental bounds [192] by orders of magnitude.

$SU(3)$	$b \rightarrow s\ell\bar{\ell}$ type a)				$b \rightarrow s\ell\bar{\ell}$ type b)				χ
	Ψ_A	Ψ_B	Φ_M	Φ_N	Ψ_A	Ψ_B	Φ_M	Φ_N	
I	3	1	1	1	1	1	$\bar{3}$	1	1
II	1	$\bar{3}$	$\bar{3}$	$\bar{3}$	3	3	1	3	1
III	3	8	8	8	8	8	$\bar{3}$	8	4/3
IV	8	$\bar{3}$	$\bar{3}$	$\bar{3}$	3	3	8	3	4/3
V	$\bar{3}$	3	3	3	$\bar{3}$	$\bar{3}$	3	$\bar{3}$	2

Table 4.1: Table of the possible $SU(3)$ representations that can give an effect in $b \rightarrow s\ell^+\ell^-$ or $b \rightarrow s\nu\nu$ transitions via box diagrams. χ denotes the resulting group factor appearing in Eqs. (4.4)-(4.8) which also enters in $b \rightarrow s\nu\nu$ transitions.

4.1.1 $b \rightarrow s\mu^+\mu^-$ and $b \rightarrow s\gamma$ Transitions

The dimension-6 operators governing $b \rightarrow s\mu^+\mu^-$ and $b \rightarrow s\gamma$ transitions are contained in the effective Hamiltonian:

$$\mathcal{H}_{\text{eff}}^{\mu\mu} = -\frac{4G_F}{\sqrt{2}}V_{tb}V_{ts}^* \sum_i \left(C_i \mathcal{O}_i + C'_i \mathcal{O}'_i \right) + \text{h.c.}, \quad (4.2)$$

where we focus only in the muon sector

$$\begin{aligned} \mathcal{O}_7 &= \frac{e}{16\pi^2} m_b \bar{s} \sigma^{\mu\nu} P_R b F_{\mu\nu}, & \mathcal{O}_8 &= \frac{g_s}{16\pi^2} m_b \bar{s} \sigma^{\mu\nu} P_R T_{\alpha\beta}^a b_\beta G_{\mu\nu}^a, \\ \mathcal{O}_9 &= \frac{\alpha_{\text{EM}}}{4\pi} (\bar{s} \gamma_\mu P_L b) (\bar{\mu} \gamma^\mu \mu), & \mathcal{O}_{10} &= \frac{\alpha_{\text{EM}}}{4\pi} (\bar{s} \gamma_\mu P_L b) (\bar{\mu} \gamma^\mu \gamma_5 \mu), \\ \mathcal{O}_S &= \frac{\alpha_{\text{EM}}}{4\pi} (\bar{s} P_R b) (\bar{\mu} \mu), & \mathcal{O}_P &= \frac{\alpha_{\text{EM}}}{4\pi} (\bar{s} P_R b) (\bar{\mu} \gamma_5 \mu), \\ \mathcal{O}_T &= \frac{\alpha_{\text{EM}}}{4\pi} (\bar{s} \sigma_{\mu\nu} b) (\bar{\mu} \sigma^{\mu\nu} P_R \mu), \end{aligned} \quad (4.3)$$

with e being the electron charge, α_{EM} the fine structure constant and g_s the $SU(3)$ gauge coupling. The primed operators are obtained by interchanging L and R . NP contributions from box diagrams will generate effects in $C_{9,10}^{(\prime)}$, $C_{S,P}^{(\prime)}$ and $O_T^{(\prime)}$, while on-shell photon (gluon) penguins generate $C_{7(8)}^{(\prime)}$ and $C_9^{(\prime)}$, and Z -penguins $C_{9,10}^{(\prime)}$.

The box diagrams in Fig. 4.1, result in the following Wilson coefficients (here and in the remainder of the section, an implicit sum over all NP particles, i.e. A, B, M, N , is understood):

$$C_9^{\text{box}, a)} = -\mathcal{N} \frac{\chi L_{AN}^{s*} L_{AM}^b}{32\pi \alpha_{\text{EM}} m_{\Phi_M}^2} [L_{BM}^{\mu*} L_{BN}^\mu + R_{BM}^{\mu*} R_{BN}^\mu] F(x_{AM}, x_{BM}, x_{NM}),$$

$$C_9^{\text{box},b) = \mathcal{N} \frac{\chi L_{BM}^{s*} L_{AM}^b}{32\pi\alpha_{\text{EM}} m_{\Phi_M}^2} \left[L_{AN}^{\mu*} L_{BN}^\mu F(x_{AM}, x_{BM}, x_{NM}) - R_{AN}^{\mu*} R_{BN}^\mu \frac{m_{\Psi_A} m_{\Psi_B}}{m_{\Phi_M}^2} G(x_{AM}, x_{BM}, x_{NM}) \right], \quad (4.4)$$

$$C_{10}^{\text{box},a) = \mathcal{N} \frac{\chi L_{AN}^{s*} L_{AM}^b}{32\pi\alpha_{\text{EM}} m_{\Phi_M}^2} [L_{BM}^{\mu*} L_{BN}^\mu - R_{BM}^{\mu*} R_{BN}^\mu] F(x_{AM}, x_{BM}, x_{NM}),$$

$$C_{10}^{\text{box},b) = -\mathcal{N} \frac{\chi L_{BM}^{s*} L_{AM}^b}{32\pi\alpha_{\text{EM}} m_{\Phi_M}^2} \left[L_{AN}^{\mu*} L_{BN}^\mu F(x_{AM}, x_{BM}, x_{NM}) + R_{AN}^{\mu*} R_{BN}^\mu \frac{m_{\Psi_A} m_{\Psi_B}}{m_{\Phi_M}^2} G(x_{AM}, x_{BM}, x_{NM}) \right], \quad (4.5)$$

$$C_S^{\text{box},a) = -\mathcal{N} \frac{\chi L_{AN}^{s*} R_{AM}^b}{16\pi\alpha_{\text{EM}} m_{\Phi_M}^2} [R_{BM}^{\mu*} L_{BN}^\mu + L_{BM}^{\mu*} R_{BN}^\mu] \frac{m_{\Psi_A} m_{\Psi_B}}{m_{\Phi_M}^2} G(x_{AM}, x_{BM}, x_{NM}),$$

$$C_S^{\text{box},b) = \mathcal{N} \frac{\chi L_{BM}^{s*} R_{AM}^b}{16\pi\alpha_{\text{EM}} m_{\Phi_M}^2} \left[R_{AN}^{\mu*} L_{BN}^\mu F(x_{AM}, x_{BM}, x_{NM}) + L_{AN}^{\mu*} R_{BN}^\mu \frac{m_{\Psi_A} m_{\Psi_B}}{2m_{\Phi_M}^2} G(x_{AM}, x_{BM}, x_{NM}) \right], \quad (4.6)$$

$$C_P^{\text{box},a) = \mathcal{N} \frac{\chi L_{AN}^{s*} R_{AM}^b}{16\pi\alpha_{\text{EM}} m_{\Phi_M}^2} [R_{BM}^{\mu*} L_{BN}^\mu - L_{BM}^{\mu*} R_{BN}^\mu] \frac{m_{\Psi_A} m_{\Psi_B}}{m_{\Phi_M}^2} G(x_{AM}, x_{BM}, x_{NM}),$$

$$C_P^{\text{box},b) = \mathcal{N} \frac{\chi L_{BM}^{s*} R_{AM}^b}{16\pi\alpha_{\text{EM}} m_{\Phi_M}^2} \left[R_{AN}^{\mu*} L_{BN}^\mu F(x_{AM}, x_{BM}, x_{NM}) - L_{AN}^{\mu*} R_{BN}^\mu \frac{m_{\Psi_A} m_{\Psi_B}}{2m_{\Phi_M}^2} G(x_{AM}, x_{BM}, x_{NM}) \right], \quad (4.7)$$

$$C_T^{\text{box},b) = \mathcal{N} \frac{\chi L_{BM}^{s*} R_{AM}^b L_{AN}^{\mu*} R_{BN}^\mu}{16\pi\alpha_{\text{EM}} m_{\Phi_M}^2} \frac{m_{\Psi_A} m_{\Psi_B}}{m_{\Phi_M}^2} G(x_{AM}, x_{BM}, x_{NM}), \quad (4.8)$$

$$C_{9,S,T}^{\text{box}} = C_{9,S,T}^{\text{box}} (L \leftrightarrow R), \quad C_{10,P}^{\text{box}} = -C_{10,P}^{\text{box}} (L \leftrightarrow R), \quad (4.9)$$

$SU(3)$	Ψ_A	Φ_M	χ_γ	χ_g	$\tilde{\chi}_g$
I	3	1	1	1	0
II	1	$\bar{3}$	1	0	1
III	3	8	4/3	-1/6	3/2
IV	8	$\bar{3}$	4/3	3/2	-1/6
V	$\bar{3}$	3	2	-1	1

Table 4.2: Table of the different $SU(3)$ representations that can give non-zero effects via photon- and gluon-penguin diagrams to $b \rightarrow s\mu^+\mu^-$ transitions. χ_γ denotes the resulting group factor for the former contribution, while χ_g and $\tilde{\chi}_g$ represent the resulting group factors for the latter.

where we have defined

$$x_{AM} \equiv (m_{\Psi_A}/m_{\Phi_M})^2, \quad x_{BM} \equiv (m_{\Psi_B}/m_{\Phi_M})^2, \quad x_{NM} \equiv (m_{\Phi_N}/m_{\Phi_M})^2, \quad (4.10)$$

and

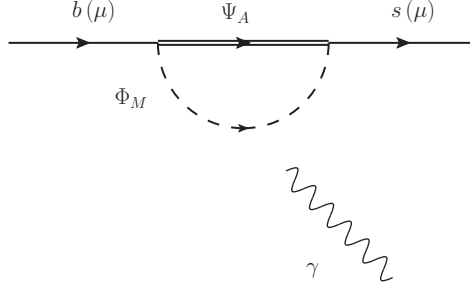
$$\mathcal{N}^{-1} = \frac{4G_F}{\sqrt{2}} V_{tb} V_{ts}^*. \quad (4.11)$$

In the equations above, the labels A , B , M and N denote the particle (in case of several representations) and also include $SU(2)$ components, while the sum over $SU(3)$ indices is encoded in the group factors χ . The dimensionless loop functions F and G are defined in Appendix C.1.

Such box contributions are only possible if both color and electric charge are conserved. While the Wilson coefficients of $b \rightarrow s\ell\ell$ operators are insensitive to the electric charge of the particle in the box, concerning $SU(3)$, the different possible representations of the new particles lead to distinct group factors χ in Eqs. (4.4)-(4.8). These group factors are different for type a) and b) and are given for all the possible representations in Tab. 4.1. Furthermore, crossed box diagrams can be constructed in some particular cases. We give the corresponding expressions for such in Appendix C.2.1 for the real scalar (or Majorana fermion) case and in Appendix C.3 for the crossed diagrams arising with complex scalars.

On-shell photon penguins diagrams in Fig. 4.2 affect $C_7^{(l)}$ while off-shell ones enter $C_9^{(l)}$:

$$C_7 = \mathcal{N} \frac{\chi_\gamma L_{AM}^b}{2m_{\Phi_M}^2} \left[L_{AM}^{s*} \left(Q_{\Phi_M} \tilde{F}_7(x_{AM}) - Q_{\Psi_A} F_7(x_{AM}) \right) + R_{AM}^{s*} \frac{4m_{\Psi_A}}{m_b} \left(Q_{\Phi_M} \tilde{G}_7(x_{AM}) - Q_{\Psi_A} G_7(x_{AM}) \right) \right], \quad (4.12)$$


 Figure 4.2: Photon-penguin diagrams contributing to $b \rightarrow s\gamma$ transitions and a_μ .

$$C_9^\gamma = \mathcal{N} \frac{\chi_\gamma L_{AM}^{s*} L_{AM}^b}{2m_{\Phi_M}^2} \left[Q_{\Phi_M} \tilde{F}_9(x_{AM}) - Q_{\Psi_A} \tilde{G}_9(x_{AM}) \right], \quad (4.13)$$

$$C_7' = C_7(L \leftrightarrow R), \quad C_9^{\gamma'} = C_9^\gamma(L \leftrightarrow R), \quad (4.14)$$

where m_b is the b quark mass. Q_{Φ_M} and Q_{Ψ_A} are the electric charges of the NP fields Φ_M and Ψ_A , respectively. The conservation of electric charge imposes that $Q_{\Phi_M} + Q_{\Psi_A} = Q_d \equiv -1/3$. The color factors χ_γ , which depend on the $SU(3)$ representations of the new particles in the loop, are given in Tab. 4.2. The loop functions are defined in Appendix C.1. Note that the terms proportional to \tilde{F}_7 , \tilde{G}_7 and \tilde{F}_9 in Eqs. (4.12)-(4.14) stem from the diagram where the photon couples to the scalar Φ_M , while the terms proportional to F_7 , G_7 and \tilde{G}_9 stem from the diagram where the photon couples to the fermion Ψ_A .

Similarly, the gluon-penguin generates

$$C_8 = \mathcal{N} \frac{L_{AM}^b}{2m_{\Phi_M}^2} \left[L_{AM}^{s*} \left(\chi_g \tilde{F}_7(x_{AM}) - \tilde{\chi}_g F_7(x_{AM}) \right) + R_{AM}^{s*} \frac{4m_{\Psi_A}}{m_b} \left(\chi_g \tilde{G}_7(x_{AM}) - \tilde{\chi}_g G_7(x_{AM}) \right) \right], \quad (4.15)$$

$$C_8' = C_8(L \leftrightarrow R), \quad (4.16)$$

where the color factors χ_g and $\tilde{\chi}_g$ for the different possible $SU(3)$ representations are given in Tab. 4.2.

The contribution of Z -penguins to $C_{9,10}^{(\prime)}$ is given in Sec. 4.1.6 together with a discussion of Z decays.

4.1.2 $b \rightarrow s\nu\bar{\nu}$

As stated at the beginning of this section, $b \rightarrow s\nu_\mu\bar{\nu}_\mu$ processes have to be taken into account once $SU(2)$ invariance at the NP scale is imposed. This implies that, in the generic description in Eq. (4.1), one has to replace the left-handed muon fields with neutrinos. The box diagrams generating $b \rightarrow s\nu_\mu\bar{\nu}_\mu$ are therefore obtained from Fig. 4.1 by replacing muons with neutrinos.

The effective Hamiltonian describing this process reads (following the conventions of Ref. [146] as in the previous chapter)

$$\mathcal{H}_{\text{eff}}^{\nu_\mu} = -\frac{4G_F}{\sqrt{2}} V_{tb} V_{ts}^* (C_L \mathcal{O}_L + C_R \mathcal{O}_R) + \text{h.c.}, \quad (4.17)$$

where

$$\mathcal{O}_{L(R)} = \frac{\alpha_{\text{EM}}}{4\pi} [\bar{s}\gamma^\mu P_{L(R)} b] [\bar{\nu}_\mu \gamma_\mu (1 - \gamma^5) \nu_\mu]. \quad (4.18)$$

The resulting Wilson coefficients are:

$$\begin{aligned} C_L^a &= -\mathcal{N} \frac{\chi L_{AN}^{s*} L_{AM}^b L_{BM}^{\mu*} L_{BN}^\mu}{32\pi\alpha_{\text{EM}} m_{\Phi_M}^2} F(x_{AM}, x_{BM}, x_{NM}), \\ C_L^b &= \mathcal{N} \frac{\chi L_{BN}^{s*} L_{AM}^b L_{AN}^{\mu*} L_{BN}^\mu}{32\pi\alpha_{\text{EM}} m_{\Phi_M}^2} F(x_{AM}, x_{BM}, x_{NM}), \end{aligned} \quad (4.19)$$

$$\begin{aligned} C_R^a &= -\mathcal{N} \frac{\chi R_{AN}^{s*} R_{AM}^b L_{BM}^{\mu*} L_{BN}^\mu}{32\pi\alpha_{\text{EM}} m_{\Phi_M}^2} F(x_{AM}, x_{BM}, x_{NM}), \\ C_R^b &= \mathcal{N} \frac{\chi R_{BN}^{s*} R_{AM}^b L_{AN}^{\mu*} L_{BN}^\mu}{32\pi\alpha_{\text{EM}} m_{\Phi_M}^2} \frac{m_{\Psi_A} m_{\Psi_B}}{m_{\Phi_M}^2} G(x_{AM}, x_{BM}, x_{NM}), \end{aligned} \quad (4.20)$$

where the normalization factor \mathcal{N} has been introduced in Eq. (4.11), and the loop functions $F(x, y, z)$ and $G(x, y, z)$ are defined in Appendix C.1. The colour factor χ is the same as for $b \rightarrow s\mu^+\mu^-$ transitions and is given in Tab. 4.1 for the different representations.

4.1.3 $\Delta B = \Delta S = 2$ Processes

The presence of $L_{AM}^{b,s}$ and $R_{AM}^{b,s}$ implies NP contributions to the $B_s - \bar{B}_s$ mixing which, using the conventions of Refs. [205, 206], is governed by

$$\mathcal{H}_{\text{eff}}^{B_s \bar{B}_s} = C_i \sum_{i=1}^5 \mathcal{O}_i + \tilde{C}_i \sum_{i=1}^3 \tilde{\mathcal{O}}_i + \text{h.c.}, \quad (4.21)$$

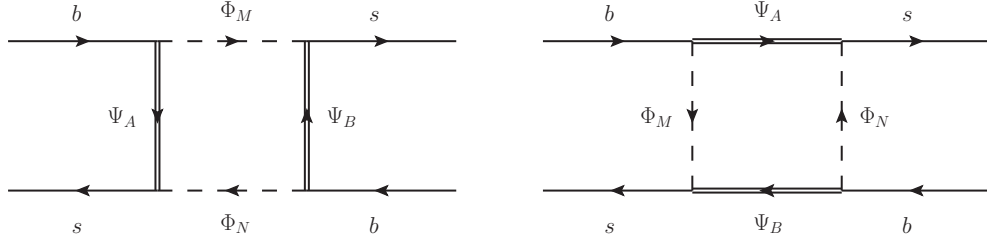


Figure 4.3: Box diagrams contributing to $B_s - \bar{B}_s$ mixing. Both diagrams arise independently of the nature of the mediator involved in $b \rightarrow s\mu^+\mu^-$ transitions.

$SU(3)$	Ψ_A	Ψ_B	Φ_M	Φ_N	χ_{BB}	$\tilde{\chi}_{BB}$
I	3	3	1	1	1	0
II	1	1	$\bar{3}$	$\bar{3}$	0	1
III	3	3	8	8	1/36	7/12
IV	8	8	$\bar{3}$	$\bar{3}$	7/12	1/36
V	3	3	(1,8)	(8,1)	-1/6	1/2
VI	(1,8)	(8,1)	$\bar{3}$	$\bar{3}$	1/2	-1/6
VII	$\bar{3}$	$\bar{3}$	3	3	1	1

Table 4.3: Table of the different $SU(3)$ representations that can give a non-zero effect via box diagrams to $B_s - \bar{B}_s$ mixing. χ_{BB} and $\tilde{\chi}_{BB}$ denote the resulting group factors.

with

$$\begin{aligned}
 \mathcal{O}_1 &= (\bar{s}_\alpha \gamma^\mu P_L b_\alpha) (\bar{s}_\beta \gamma^\mu P_L b_\beta), & \tilde{\mathcal{O}}_1 &= (\bar{s}_\alpha \gamma^\mu P_R b_\alpha) (\bar{s}_\beta \gamma^\mu P_R b_\beta), \\
 \mathcal{O}_2 &= (\bar{s}_\alpha P_L b_\alpha) (\bar{s}_\beta P_L b_\beta), & \tilde{\mathcal{O}}_2 &= (\bar{s}_\alpha P_R b_\alpha) (\bar{s}_\beta P_R b_\beta), \\
 \mathcal{O}_3 &= (\bar{s}_\alpha P_L b_\beta) (\bar{s}_\beta P_L b_\alpha), & \tilde{\mathcal{O}}_3 &= (\bar{s}_\alpha P_R b_\beta) (\bar{s}_\beta P_R b_\alpha), \\
 \mathcal{O}_4 &= (\bar{s}_\alpha P_L b_\alpha) (\bar{s}_\beta P_R b_\beta), \\
 \mathcal{O}_5 &= (\bar{s}_\alpha P_L b_\beta) (\bar{s}_\beta P_R b_\alpha).
 \end{aligned} \tag{4.22}$$

The box diagrams contributing to these above operators are shown in Fig. 4.3. Using the Lagrangian from Eq. (4.1), one obtains the following results for the coefficients:

$$C_1 = (\chi_{BB} + \tilde{\chi}_{BB}) \frac{L_{AN}^{s*} L_{AM}^b L_{BM}^{s*} L_{BN}^b}{128\pi^2 m_{\Phi_M}^2} F(x_{AM}, x_{BM}, x_{NM}), \tag{4.23}$$

$$C_2 = \chi_{BB} \frac{R_{AN}^{s*} L_{AM}^b R_{BM}^{s*} L_{BN}^b}{64\pi^2 m_{\Phi_M}^2} \frac{m_{\Psi_A} m_{\Psi_B}}{m_{\Phi_M}^2} G(x_{AM}, x_{BM}, x_{NM}), \tag{4.24}$$

$$C_3 = \tilde{\chi}_{BB} \frac{R_{AN}^{s*} L_{AM}^b R_{BM}^{s*} L_{BN}^b}{64\pi^2 m_{\Phi_M}^2} \frac{m_{\Psi_A} m_{\Psi_B}}{m_{\Phi_M}^2} G(x_{AM}, x_{BM}, x_{NM}) , \quad (4.25)$$

$$C_4 = \chi_{BB} \frac{R_{AN}^{s*} L_{AM}^b L_{BM}^{s*} R_{BN}^b}{32\pi^2 m_{\Phi_M}^2} \frac{m_{\Psi_A} m_{\Psi_B}}{m_{\Phi_M}^2} G(x_{AM}, x_{BM}, x_{NM}) \\ - \tilde{\chi}_{BB} \frac{R_{AN}^{s*} R_{AM}^b L_{BM}^{s*} L_{BN}^b}{32\pi^2 m_{\Phi_M}^2} F(x_{AM}, x_{BM}, x_{NM}) , \quad (4.26)$$

$$C_5 = \tilde{\chi}_{BB} \frac{R_{AN}^{s*} L_{AM}^b L_{BM}^{s*} R_{BN}^b}{32\pi^2 m_{\Phi_M}^2} \frac{m_{\Psi_A} m_{\Psi_B}}{m_{\Phi_M}^2} G(x_{AM}, x_{BM}, x_{NM}) \\ - \chi_{BB} \frac{R_{AN}^{s*} R_{AM}^b L_{BM}^{s*} L_{BN}^b}{32\pi^2 m_{\Phi_M}^2} F(x_{AM}, x_{BM}, x_{NM}) , \quad (4.27)$$

$$\tilde{C}_{1,2,3} = C_{1,2,3} (L \leftrightarrow R) . \quad (4.28)$$

The loop functions $F(x, y, z)$ and $G(x, y, z)$ are defined in Appendix C.1 and the colour factors χ_{BB} and $\tilde{\chi}_{BB}$ are given in Tab. 4.3 for the different allowed representations. Again, in the presence of Majorana fermions or real scalars crossed diagrams can be constructed and the resulting expressions are given in Appendix C.2.2.

4.1.4 $D_0 - \bar{D}_0$ Mixing

NP contributions to the $D_0 - \bar{D}_0$ mixing can be obtained in complete generality (at the low scale) from Eqs. (4.23)-(4.28) by making the substitutions $s \rightarrow u$, $b \rightarrow c$, introducing couplings $L_{AM}^{u,c}$ and $R_{AM}^{u,c}$ of new scalars and fermions to up-quarks in straightforward extension of Eq. (4.1).

In the context a UV complete model, $SU(2)$ invariance imposes at the high scale that couplings to left-handed up-type quarks are related to the couplings to left-handed down-type quarks via CKM rotations. Therefore, working in the down-basis, the “minimal” effect generated in $D_0 - \bar{D}_0$ is induced by the couplings

$$L_{AM}^u = V_{us}^* L_{AM}^s + V_{ub}^* L_{AM}^b , \quad L_{AM}^c = V_{cs}^* L_{AM}^s + V_{cb}^* L_{AM}^b . \quad (4.29)$$

$SU(3)$	Ψ_A	Φ_M	χ_{a_μ}
I	1	1	1
II	$(3, \bar{3})$	$(3, \bar{3})$	3
III	8	8	8

Table 4.4: Table of the different $SU(3)$ representations that can give a non-zero effect to a_μ . χ_{a_μ} denotes the resulting group factor.

4.1.5 Anomalous Magnetic Moment of the Muon

The anomalous magnetic moment of the muon ($a_\mu \equiv (g-2)_\mu/2$) and its electric dipole moments (d_μ) we find from the diagrams in Fig. 4.2

$$\Delta a_\mu = \frac{\chi_{a_\mu} m_\mu^2}{8\pi^2 m_{\Phi_M}^2} \left[(L_{AM}^{\mu*} L_{AM}^\mu + R_{AM}^{\mu*} R_{AM}^\mu) \left(Q_{\Phi_M} \tilde{F}_7(x_{AM}) - Q_{\Psi_A} F_7(x_{AM}) \right) \right. \\ \left. + (L_{AM}^{\mu*} R_{AM}^\mu + R_{AM}^{\mu*} L_{AM}^\mu) \frac{2m_{\Psi_A}}{m_\mu} \left(Q_{\Phi_M} \tilde{G}_7(x_{AM}) - Q_{\Psi_A} G_7(x_{AM}) \right) \right], \quad (4.30)$$

$$d_\mu = \frac{\chi_{a_\mu} m_{\Psi_A}}{8\pi^2 m_{\Phi_M}^2} e (L_{AM}^{\mu*} R_{AM}^\mu - R_{AM}^{\mu*} L_{AM}^\mu) \left(Q_{\Phi_M} \tilde{G}_7(x_{AM}) - Q_{\Psi_A} G_7(x_{AM}) \right), \quad (4.31)$$

where m_μ is the muon mass, χ_{a_μ} is the colour factor given in Table 4.4, and Q_{Φ_M} and Q_{Ψ_A} are the electric charges of the NP fields Φ_M and Ψ_A , respectively. Analogously to photon-penguin contributions to $b \rightarrow s$ transitions, the conservation of electric charge imposes that $Q_{\Phi_M} + Q_{\Psi_A} = Q_\mu \equiv -1$. Finally, the loop functions $F_7(x)$, $\tilde{F}_7(x)$, $G_7(x)$ and $\tilde{G}_7(x)$ are defined in Appendix C.1.

4.1.6 Modified Z Couplings

Here, we study the effects of our new particles on modified Z couplings, i.e. on $Z\bar{\mu}\mu$, $Z\bar{b}b$, $Z\bar{s}s$ and $Z\bar{f}f$ couplings, both for off- and on-shell Z bosons². We define the form-factors governing $Z\bar{f}f$ interactions as [208]

$$-\frac{g_2}{c_W} \bar{f}' \gamma^\mu \left[g_L^{f'f}(q^2) P_L + g_R^{f'f}(q^2) P_R \right] f Z_\mu + \text{h.c.}, \quad (4.32)$$

²Expressions for Z couplings in generic gauge theories can be found in Ref. [207].

where $f = \{b, s, \mu\}$, g_2 is the $SU(2)$ gauge coupling, θ_W the Weinberg angle and q is the Z momentum. Moreover,

$$g_{L(R)}^{f'f}(q^2) = g_{f_L}^{\text{SM}} \delta_{f'f} + \Delta g_{L(R)}^{f'f}(q^2) \quad (4.33)$$

with $g_{f_L}^{\text{SM}} = (T_3^f - Q_f s_W^2)$ and $g_{f_R}^{\text{SM}} = -Q_f s_W^2$ being the Z couplings to SM fermions at tree-level. The relevant Feynman diagrams are shown in Fig. 4.4. We write the coupling of the Z boson to the new scalars and fermions as

$$\mathcal{L}^Z = -\frac{g_2}{c_W} Z_\mu \left(\bar{\Psi}_A \gamma^\mu \left[g_{AB}^{\Psi,L} P_L + g_{AB}^{\Psi,R} P_R \right] \Psi_B + g_{MN}^\Phi \Phi_M^\dagger i \overleftrightarrow{\partial}^\mu \Phi_N \right) + \text{h.c.}, \quad (4.34)$$

where we have introduced the notation $a \overleftrightarrow{\partial}^\mu b = a(\partial^\mu b) - (\partial^\mu a)b$, and with generic couplings $g_{AB}^{\Psi,L,R}$ and g_{MN}^Φ which can only be determined in a UV complete model in which also the couplings of the new particles to the SM Higgs are known. Using the generic Lagrangian from Eq. (4.1), one obtains the following results for the coefficients

$$\begin{aligned} \Delta g_L^{f'f}(q^2) = & \frac{\chi_Z L_{BN}^{f'} L_{AM}^{f*}}{32\pi^2} \\ & \left[2 g_{AB}^{\Psi,L} \delta_{MN} \frac{m_{\Psi_A} m_{\Psi_B}}{m_{\Phi_M}^2} G_Z(x_{AM}, x_{BM}) - g_{AB}^{\Psi,R} \delta_{MN} F_Z(x_{AM}, x_{BM}, m_{\Phi_M}) \right. \\ & + g_{MN}^\Phi \delta_{AB} H_Z(x_{AM}, x_{AN}, m_{\Psi_A}) - \frac{1}{2} (g_{f_L}^{\text{SM}} + g_{f_L}^{\text{SM}}) \delta_{AB} \delta_{MN} I_Z(x_{AM}, m_{\Phi_M}) \\ & + q^2 \left(g_{AB}^{\Psi,L} \delta_{MN} \frac{m_{\Psi_A} m_{\Psi_B}}{m_{\Phi_M}^4} \tilde{G}_Z(x_{AM}, x_{BM}) - \frac{2}{3} \frac{g_{AB}^{\Psi,R} \delta_{MN}}{m_{\Phi_M}^2} \tilde{F}_Z(x_{AM}, x_{BM}) \right. \\ & \left. \left. - \frac{1}{3} \frac{g_{MN}^\Phi \delta_{AB}}{m_{\Psi_A}^2} \tilde{H}_Z(x_{AM}, x_{AN}) \right) \right], \quad (4.35) \end{aligned}$$

$$\Delta g_R^{f'f}(q^2) = \Delta g_L^{f'f}(q^2) (L \leftrightarrow R), \quad (4.36)$$

where the loop functions are defined in Appendix C.1, and the colour factor $\chi_Z = \chi_\gamma$ for $f, f' = b, s$ (see Table 4.2) and $\chi_Z = \chi_{a_\mu}$ (see Table 4.4) for $f = \mu$. Here we have set the masses and momenta of the external fermions to 0 and expanded up to first order in q^2 over the NP scale. If one is considering data from Z decays, Eq. (4.35) has to be evaluated to $q^2 = m_Z^2$ while for processes with an off-shell Z (like $b \rightarrow s \ell^+ \ell^-$) one has to set $q^2 = 0$.

Note that in the absence of EW symmetry breaking in the NP sector, the contribution of the self-energies cancel the one of the genuine vertex correction and Eq. (4.35) vanishes for

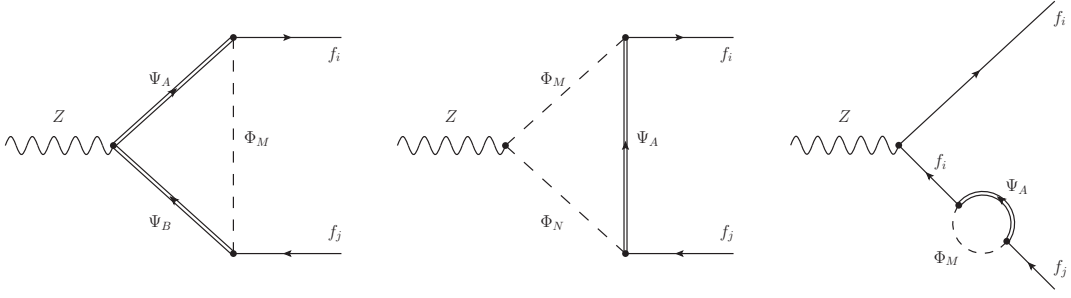


Figure 4.4: Feynman diagrams modifying the $Z \bar{f}_i f_j$ vertex with $f_i = s, b, \mu$.

$q^2 = 0$. Therefore, as noted above, $g_{AB}^{\Psi,L}$, $g_{AB}^{\Psi,R}$ and g_{MN}^{Φ} are only meaningful after EW symmetry breaking and it is not possible to relate them purely to $SU(2) \times U(1)$ quantum numbers. In a specific UV model with a known pattern of EW symmetry breaking, rotation matrices can be used to relate the couplings before and after the breaking. Consequently, the cancellation of UV divergences (present in some of the loop functions in Eq. (4.35)) is only manifest after summation over $SU(2)$ indices, due to a GIM-like cancellation originating from the unitarity of the rotation matrices. We will give a concrete example of this in Sec. 4.3.

The form-factors in Eq. (4.32) includes $Z \bar{s} b$ couplings generating contributions to $C_{9,10}^{(\prime)}$

$$C_9^{(\prime)Z} = \mathcal{N} \frac{\pi g^2}{\alpha_{\text{EM}} c_W^2 m_Z^2} g_{L(R)}^{sb}(q^2 = 0) (1 - 4s_W^2), \quad (4.37)$$

$$C_{10}^{(\prime)Z} = -\mathcal{N} \frac{\pi g^2}{\alpha_{\text{EM}} c_W^2 m_Z^2} g_{L(R)}^{sb}(q^2 = 0). \quad (4.38)$$

Note that these contributions are lepton flavor universal and therefore cannot account for R_K and R_{K^*} . However, a mixture of lepton flavor universal and violating contributions is phenomenologically interesting [27], especially in the light of the recent Belle and LHCb measurements [28]. In a similar fashion, $Z \bar{s} b$ couplings will also generate the following contributions to $b \rightarrow s \nu \bar{\nu}$ contained in $C_{L(R)}$

$$C_{L(R)}^Z = -\mathcal{N} \frac{\pi g^2}{\alpha_{\text{EM}} c_W^2 m_Z^2} g_{L(R)}^{sb}(q^2 = 0). \quad (4.39)$$

Finally, if $SU(2)$ invariance at the NP scale is imposed, the new scalars and fermions couple also the neutrinos. Hence, contributions to $Z \rightarrow \nu \bar{\nu}$ and $W \rightarrow \mu \bar{\nu}$ will arise as well. Concerning $Z \rightarrow \nu \bar{\nu}$, $g_{\nu_L}(q^2 = m_Z^2)$ can be straightforwardly extracted from Eq. (4.35) by appropriate

replacements and the same is true concerning $W\mu\bar{\nu}$ couplings.

4.2 Experimental Constraints on Wilson Coefficients

In this section we review the experimental situation and the resulting constraints on the Wilson coefficients calculated in the previous section.

4.2.1 $b \rightarrow s$ Transitions

The semileptonic operators $\mathcal{O}_{9,10}^{(\prime)}$, $\mathcal{O}_{S,P}^{(\prime)}$ and $\mathcal{O}_T^{(\prime)}$, together with magnetic operators $\mathcal{O}_7^{(\prime)}$, contribute to a plethora of $b \rightarrow s\ell^+\ell^-$ observables. The corresponding measurements include total branching ratios of $B_s \rightarrow \ell^+\ell^-$ [45], of the exclusive decays $B \rightarrow K^*\gamma$ [45], $B \rightarrow \phi\gamma$ [209], the inclusive decay $B \rightarrow X_s\gamma$ [45], the angular analyses of $B \rightarrow K^{(*)}\ell^+\ell^-$ [9, 210, 16, 41, 211, 212, 213] (proposed in Refs. [214, 43, 42]) and $B_s \rightarrow \phi\ell^+\ell^-$ [17], and also the ratios R_K [11] and R_{K^*} [10, 18] measuring LFUV.

First of all, the contributions of scalar operators are helicity-enhanced in the $B_s \rightarrow \mu^+\mu^-$ branching ratio with respect to the \mathcal{O}_{10} contribution of the SM. This results in the bound [46]

$$\begin{aligned} \frac{\text{Br}(B_s \rightarrow \mu^+\mu^-)^{\text{exp}}}{\text{Br}(B_s \rightarrow \mu^+\mu^-)^{\text{SM}}} - 1 &= \left| 1 + \frac{C_{10} - C'_{10}}{C_{10}^{\text{SM}}} + \frac{m_{B_s}^2}{2m_\mu(m_b + m_s)} \frac{C_P - C'_P}{C_{10}^{\text{SM}}} \right|^2 \\ &+ \frac{m_{B_s}^2(m_{B_s}^2 - 4m_\mu^2)}{4m_\mu^2(m_b + m_s)^2} \left| \frac{C_S - C'_S}{C_{10}^{\text{SM}}} \right|^2 - 1 = -0.13 \pm 0.20 \quad (4.40) \end{aligned}$$

which excludes sizable contributions to scalar operators (unless there is a purely scalar quark current) and leads to

$$|C_{S,P}^{(\prime)}| \lesssim 0.03 \quad (2\sigma), \quad (4.41)$$

from the updated one-parameter fit of Ref. [215]. Therefore, we neglect the effects of scalar operators in semi-leptonic B since they anyway cannot explain the corresponding anomalies.

Moreover, the inclusive $b \rightarrow s\gamma$ decay strongly constrains the magnetic operators. From [156,

157], in the limit of vanishing $C'_{7,8}$ ³, we have

$$\frac{\text{Br}(b \rightarrow s\gamma)^{\text{exp}}}{\text{Br}(b \rightarrow s\gamma)^{\text{SM}}} - 1 = -2.87 [C_7 + 0.19 C_8] = (-0.7 \pm 8.2) \times 10^{-2}, \quad (4.42)$$

leading to, as in Chap. 3,

$$|C_7 + 0.19 C_8| \lesssim 0.06 \quad (2\sigma). \quad (4.43)$$

Here, we used $C_{7,8}$ at a matching scale of 1 TeV as input. Again, these constraints are so stringent that the effect of $C_{7,8}$ on the flavor anomalies can be mostly neglected.

On the other hand, vector operators can explain the $b \rightarrow s\ell^+\ell^-$ anomalies. We therefore refer to global fits to constrain $C_{9,10}^{(\prime)}$, where all the relevant observables have been taken into account [19, 20, 21, 22, 23, 24, 25, 26]. The results of the most recent fits find at the 2σ level

$$\begin{aligned} -1.46 \leq C_9^{\text{NP}} \leq -0.78, & \quad -0.09 \leq C_{10}^{\text{NP}} \leq 0.57, \\ -0.39 \leq C'_9 \leq 1.45, & \quad -0.55 \leq C'_{10} \leq 0.41, \end{aligned}$$

according to Ref. [28] (which is compatible with Refs. [29, 30, 31, 32]).

As explained in Sec. 4.1.2, $SU(2)$ invariance implies the presence of contributions to $B \rightarrow K^{(*)}\nu\bar{\nu}$ decays as well. Since there is no experimental way to distinguish different neutrino flavors in these decays, one measures the total branching ratio which we normalize to its SM prediction [146]:

$$R_{K^{(*)}}^{\nu\bar{\nu}} = \frac{\text{Br}^{\text{exp}}(B \rightarrow K^{(*)}\nu\bar{\nu})}{\text{Br}^{\text{SM}}(B \rightarrow K^{(*)}\nu\bar{\nu})} = \frac{2(C_L^{\text{SM}})^2 + (C_L^{\text{SM}} + C_L)^2 - \kappa (C_L^{\text{SM}} + C_L)C_R + C_R^2}{3(C_L^{\text{SM}})^2}. \quad (4.44)$$

In the case of a K in the final state one has $\kappa \equiv -2$, while for the K^* one gets $\kappa = 1.34(4)$ [146]. The current experimental limits at 90% C.L. are [147]

$$R_K^{\nu\bar{\nu}} < 3.9, \quad R_{K^*}^{\nu\bar{\nu}} < 2.7. \quad (4.45)$$

³Note that $C'_{7,8}$ are less constrained since they do not interfere with the SM. For a more detailed analysis including primed operators see e.g. Ref. [216].

4.2.2 Neutral Meson Mixing

The experimental constraint on the Wilson coefficients in Eqs. (4.23)-(4.28) comes from the mass difference ΔM_s of neutral B_s mesons, see e.g. Ref. [205] (in the case of real Wilson coefficients). To compare our results with experiments we make a slight different approach compared to the previous chapter provided that now we are using not just the $V - A$ left-handed operator but the whole basis including right-handed couplings. The comparison with the experimental value is very similar but now one has to take into account the new Wilson coefficient such as

$$\begin{aligned} \frac{\Delta M_s^{\text{exp}}}{\Delta M_s^{\text{SM}}} &= \left| 1 + \sum_{i,j=1}^3 R_i(\mu_b) \frac{\eta_{ij}(\mu_b, \mu_H)}{C_1^{\text{SM}}(\mu_b)} (C_j + \tilde{C}_j) + \sum_{i,j=4}^5 R_i(\mu_b) \frac{\eta_{ij}(\mu_b, \mu_H)}{C_1^{\text{SM}}(\mu_b)} C_j \right| \\ &= \left| 1 + \frac{0.8 (C_1 + \tilde{C}_1) - 1.9 (C_2 + \tilde{C}_2) + 0.5 (C_3 + \tilde{C}_3) + 5.2 C_4 + 1.9 C_5}{C_1^{\text{SM}}(\mu_b)} \right| \end{aligned} \quad (4.46)$$

where $R_i(\mu_b)$ is related to the matrix element of the operators Q_i in Eq. (4.22) at the scale μ_b by the relation

$$R_i(\mu_b) = \frac{\langle \bar{B}_s | Q_i(\mu_b) | B_s \rangle}{\langle \bar{B}_s | Q_1(\mu_b) | B_s \rangle}. \quad (4.47)$$

The coefficients C_i and \tilde{C}_i are the ones in Eqs. (4.23)-(4.28), computed at the NP scale μ_H . The matrix in operator space $\eta_{ij}(\mu_b, \mu_H)$ encodes the QCD evolution from the high scale μ_H to μ_b , which we calculated numerically for a reference scale $\mu_H = 1$ TeV [217]. The matrix elements in Eqs. (4.46)-(4.47) have been computed by a $N_f = 2 + 1$ lattice simulation [218], which found values consistent with the $N_f = 2$ calculation [153], the recent HPQCD computation [150] and the recent sum rules results [151]. It is worth mentioning that FLAG 2019 [48] only provides a lattice average for $\langle \bar{B}_s | Q_1(\mu_b) | B_s \rangle$, which is however dominated by the $N_f = 2 + 1$ results from Ref. [218]. Therefore, we decided to employ the results from Ref. [218] in Eqs. (4.46)-(4.47). The SM value for the Wilson coefficient is $C_1^{\text{SM}}(\mu_b) = \frac{G_F^2 M_W^2}{4\pi^2} \lambda_t^2 \eta_{11}(\mu_b, m_t) S_0(x_t) \simeq 7.2 \times 10^{-11} \text{ GeV}^{-2}$.

The experimental constraint therefore reads

$$\frac{\Delta M_s^{\text{exp}}}{\Delta M_s^{\text{SM}}} = 0.91 \pm 0.08, \quad (4.48)$$

computed with the values from Ref. [218] for $\langle \bar{B}_s | Q_1(\mu_b) | B_s \rangle$. This value shows a slight tension

with the SM as first outlined in Refs. [219, 220]. The tension would be reduced if one considered the results for the matrix element from Ref. [151]: however, in this case one should rely on a separate computation for the decay constant, while in Ref. [218] both quantities are computed together.

Analogously to the B_s system, $D_0 - \bar{D}_0$ mixing is constrained by the mass difference of neutral D_0 mesons [152]:

$$\Delta M_{D_0}^{\text{exp}} = (0.63_{-0.29}^{+0.27}) \times 10^{-11} \text{MeV} . \quad (4.49)$$

Unfortunately, a precise SM prediction is still lacking in this sector but one can constrain the NP contribution by assuming that not more than the total mass difference is generated by it.

4.2.3 Anomalous Magnetic Moment of the Muon

From the experimental side, this quantity has been already measured quite precisely [221], but as stated in the previous chapter further improvements by experiments at Fermilab [162] and J-PARC [163] (see also [164]) are expected in the future. On the theory side, the SM prediction has been improved continuously. The current tension between the two determinations accounts to

$$\Delta a_\mu = a_\mu^{\text{exp}} - a_\mu^{\text{SM}} \sim 270(85) \times 10^{-11} . \quad (4.50)$$

4.2.4 Z Decays

The main experimental measurements of Z couplings have been performed at LEP [193] (at the Z pole).

$$\begin{aligned} g_V^{e, \text{exp}} &= -0.03817(47) , & g_A^{e, \text{exp}} &= -0.50111(35) , \\ g_V^{\mu, \text{exp}} &= -0.0367(23) , & g_A^{\mu, \text{exp}} &= -0.50120(54) , \\ g_V^{\tau, \text{exp}} &= -0.0366(10) , & g_A^{\tau, \text{exp}} &= -0.50204(64) , \end{aligned} \quad (4.51)$$

where $g_{V(A)} = g_L \pm g_R$.

4.3 4th Generation Model

In this section we propose a model with a vector-like 4th generation of fermions and a new complex scalar. This will also allow us to apply and illustrate the generic findings of the previous section to a UV complete model and study the effects in $b \rightarrow s\ell^+\ell^-$ data and a_μ .

4.3.1 Lagrangian

The Lagrangian for our 4th generation model is obtained from the SM one by adding a 4th vector-like generation [199, 200] and a neutral scalar

$$\begin{aligned}
 L^{4\text{th}} &= \sum_i \left(\Gamma_{q_i}^L \bar{\Psi}_q P_L q_i + \Gamma_{\ell_i}^L \bar{\Psi}_\ell P_L \ell_i + \Gamma_{u_i}^R \bar{\Psi}_u P_R u_i + \Gamma_{d_i}^R \bar{\Psi}_d P_R d_i + \Gamma_{e_i}^R \bar{\Psi}_e P_R e_i \right) \Phi + \text{h.c.} \\
 &+ \sum_{C=L,R} \left(\lambda_C^U \bar{\Psi}_q P_C \tilde{h} \Psi_u + \lambda_C^D \bar{\Psi}_q P_C h \Psi_d + \lambda_C^E \bar{\Psi}_\ell P_C h \Psi_e \right) + \text{h.c.} \\
 &+ \sum_{F=q,\ell,u,d,e} M_F \bar{\Psi}_F \Psi_F + \kappa h^\dagger h \Phi^\dagger \Phi + m_\Phi^2 \Phi^\dagger \Phi, \tag{4.52}
 \end{aligned}$$

where i is a family index and h the SM Higgs doublet. The charge assignments for the new vector-like fermions $\Psi = \Psi_L + \Psi_R$ with $P_{L,R}\Psi = \Psi_{L,R}$ and the new scalar Φ are

	$SU(3)$	$SU(2)$	$U(1)$	$U'(1)$
Ψ_q	3	2	1/6	Z
Ψ_u	3	1	2/3	Z
Ψ_d	3	1	-1/3	Z
Ψ_ℓ	1	2	-1/2	Z
Ψ_e	1	1	-1	Z
Φ	1	1	0	- Z

(4.53)

The SM fermions have the same $SU(3) \times SU(2) \times U(1)$ charge assignments of the relative NP fermion partner, and the higgs transforms as a $(1, 2, 1/2)$. Here we assigned to the new particles also charges under a new $U(1)$ group in order to forbid mixing with the SM particles, giving a similar effect as R-parity in the MSSM⁴. From Table 4.53 we see that concerning $SU(3)$ we

⁴We did not assume a Z_2 symmetry because this would allow the scalar Φ to be real and lead to crossed boxes in $b \rightarrow s\ell^+\ell^-$, canceling the desired effect there.

are dealing with cases I of our generic analysis in Tables 4.1-4.4. In particular, concerning $b \rightarrow s\mu^+\mu^-$, this model would generate diagrams of type a) in Fig. 4.1.

After EW symmetry breaking, mass matrices for the new fermions are generated

$$L_{\text{mass}}^{4\text{th}} = \begin{pmatrix} \bar{\Psi}_{q,1} \\ \bar{\Psi}_u \end{pmatrix}^T \mathbf{M}_U P_L \begin{pmatrix} \Psi_{q,1} \\ \Psi_u \end{pmatrix} + \begin{pmatrix} \bar{\Psi}_{q,2} \\ \bar{\Psi}_d \end{pmatrix}^T \mathbf{M}_D P_L \begin{pmatrix} \Psi_{q,2} \\ \Psi_d \end{pmatrix} \\ + \begin{pmatrix} \bar{\Psi}_{\ell,2} \\ \bar{\Psi}_e \end{pmatrix}^T \mathbf{M}_E P_L \begin{pmatrix} \Psi_{\ell,2} \\ \Psi_e \end{pmatrix} + \text{h.c.}, \quad (4.54)$$

where $\mathbf{M}_{U,D,E}$ are non-diagonal mass matrices

$$\mathbf{M}_{D(U)} = \begin{pmatrix} M_q & \sqrt{2}v\lambda_R^{D(U)} \\ \sqrt{2}v\lambda_L^{D(U)*} & M_{d(u)} \end{pmatrix}, \quad \mathbf{M}_E = \begin{pmatrix} M_\ell & \sqrt{2}v\lambda_R^E \\ \sqrt{2}v\lambda_L^{E*} & M_e \end{pmatrix}. \quad (4.55)$$

Here the subscripts 1 and 2 denote the $SU(2)$ component of the doublet. We diagonalize these mass matrices by performing the field redefinitions

$$P_L \begin{pmatrix} \Psi_{q,1} \\ \Psi_u \end{pmatrix}_I \rightarrow W_{IJ}^{UL} \Psi_J^{UL}, \quad P_L \begin{pmatrix} \Psi_{q,2} \\ \Psi_d \end{pmatrix}_I \rightarrow W_{IJ}^{DL} \Psi_J^{DL}, \quad + \quad L \rightarrow R \\ P_L \Psi_{L,1} \rightarrow \Psi^{NL}, \quad P_L \begin{pmatrix} \Psi_{\ell,2} \\ \Psi_e \end{pmatrix}_I \rightarrow W_{IJ}^{EL} \Psi_J^{EL}, \quad + \quad L \rightarrow R \quad (4.56)$$

leading to

$$(W^{FL\dagger} \mathbf{M}_F W^{FR})_{IJ} = m_{F_I} \delta_{IJ}, \quad \text{with } F = U, D, E. \quad (4.57)$$

Therefore, after EW symmetry breaking we have the mass eigenstates $\Psi_I^{UL,R}$, $\Psi_I^{DL,R}$, $\Psi_I^{EL,R}$ and $\Psi^{NL,R}$, with $I = \{1, 2\}$. In particular, $\Psi_I^{UL,R}$ and $\Psi_I^{DL,R}$ ($\Psi_I^{EL,R}$ and $\Psi^{NL,R}$) are $SU(3)$ triplets (singlets) with the same electric charges as up-type and down-type quarks (charged-leptons and neutrinos), respectively.

The rotations introduced at Eq. (4.56) lead to the following Lagrangian for the interactions in the broken phase

$$L_{\text{int}}^{4\text{th}} = (L_I^{d_i} \bar{\Psi}_I^D P_L d_i + L_I^{e_i} \bar{\Psi}_I^E P_L e_i + R_I^{d_i} \bar{\Psi}_I^D P_R d_i + R_I^{e_i} \bar{\Psi}_I^E P_R e_i) \Phi \\ + (L_I^{u_i} \bar{\Psi}_I^U P_L u_i + L_I^{\nu_i} \bar{\Psi}_I^N P_L \nu_i + R_I^{u_i} \bar{\Psi}_I^U P_R u_i) \Phi + \text{h.c.} \quad (4.58)$$

which resembles Eq. (4.1) for the special case of our 4th generation model. Thus identify

$$\begin{aligned}
 L_I^{d_i} &= \Gamma_{q_i}^L W_{1I}^{DR*}, & L_I^{e_i} &= \Gamma_{\ell_i}^L W_{1I}^{ER*}, & L_I^{u_i} &= \Gamma_{q_j}^L V_{ij}^* W_{1I}^{UR*}, & L^{\nu_i} &= \Gamma_{\ell_i}^L, \\
 R_I^{d_i} &= \Gamma_{d_i}^R W_{2I}^{DL*}, & R_I^{e_i} &= \Gamma_{e_i}^R W_{2I}^{EL*}, & R_I^{u_i} &= \Gamma_{u_i}^R W_{2I}^{UL*}.
 \end{aligned} \tag{4.59}$$

Here we worked in the down-basis for the SM quarks which means that CKM matrices V_{ij} appear in vertices involving up-type quarks. The first two columns of the above Lagrangian involves couplings with down-type quarks and charged leptons and can be directly matched on the Lagrangian in Eq. (4.1) for the case of only one scalar, i.e. $\Phi_M \equiv \Phi$ and $\Psi_A \equiv \{\Psi_I^D, \Psi_I^E\}$. The presence of $L_I^{u_i}$ (L^{ν_i}) resembles the fact, mentioned in Sec. 4.1, that left-handed couplings to down-quarks (leptons) lead via $SU(2)$ to couplings to left-handed up-quarks (neutrinos). In addition couplings to right-handed up-quarks $R_I^{u_i}$ appear in our model which are however not relevant for our phenomenology.

4.3.2 Wilson Coefficients

With these conventions we can now easily derive the Wilson coefficients within our model which can be directly obtained from the results of Sec. 4.1. In order to simplify the expressions, we will assume $M_Q = M_d \equiv m_D$ and $M_L = M_e \equiv m_E$ and only take into account couplings to b , s and μ in Eq. (4.52):

$$\{\Gamma_s^L, \Gamma_b^L, \Gamma_\mu^L, \Gamma_s^R, \Gamma_b^R, \Gamma_\mu^R\}, \tag{4.60}$$

Concerning $SU(2)$ breaking effects the couplings $\lambda_{L,R}^D$ and $\lambda_{L,R}^E$ related to the down and charged leptons sector, respectively, can be relevant. However, concerning $\lambda_{L,R}^D$ recall that from Section 4.2.1 that experimental data suggests very small values for $C_{S,P}$ and $C_{7,8}$. In our model this can be achieved by assuming $\lambda_{L,R}^D = 0^5$. In this limit the mass matrix \mathbf{M}^D in Eq. (4.55) is diagonal and the corresponding rotation matrices $W^{DR(L)}$ in Eq. (4.57) are equal to the identity, which implies

$$C_{S,P} \propto L_A^{s*} R_A^b \propto W_{1A}^{DR} W_{2A}^{DL*} = \delta_{1A} \delta_{2A} = 0. \tag{4.61}$$

With this setup, we obtain the following non-vanishing couplings in the quark sector of the

⁵Note that the effect in scalar and magnetic operators can also be suppressed if $\Gamma_{b,s}^R = 0$ or very small. However, we decided to focus on option with $\lambda_{L,R}^D$ being very small.

Lagrangian in Eq. (4.58):

$$\begin{aligned} L_1^s &= \Gamma_s^L, & L_1^b &= \Gamma_b^L, & R_2^s &= \Gamma_s^R, & R_2^b &= \Gamma_b^R, \\ L_1^u &= V_{us}^* \Gamma_s^L + V_{ub}^* \Gamma_b^L, & L_1^c &= V_{cs}^* \Gamma_s^L + V_{cb}^* \Gamma_b^L. \end{aligned} \quad (4.62)$$

with

$$\Gamma^L \equiv L_1^b L_1^{s*}, \quad \Gamma^R \equiv R_2^b R_2^{s*}, \quad x_{D(E)} \equiv \frac{m_{D(E)}^2}{m_\Phi^2}. \quad (4.63)$$

The expressions of Wilson coefficients for $b \rightarrow s$ processes simplify to:

- $b \rightarrow s\mu^+\mu^-$ and $b \rightarrow s\gamma$ (see Eqs. (4.4)-(4.16))

$$C_9^{\text{box}} = -\mathcal{N} \frac{\Gamma^L}{32\pi\alpha_{\text{EM}}m_\Phi^2} (|\Gamma_\mu^L|^2 + |\Gamma_\mu^R|^2) F(x_D, x_E), \quad (4.64)$$

$$C_{10}^{\text{box}} = \mathcal{N} \frac{\Gamma^L}{32\pi\alpha_{\text{EM}}m_\Phi^2} (|\Gamma_\mu^L|^2 - |\Gamma_\mu^R|^2) F(x_D, x_E), \quad (4.65)$$

$$C_9^\gamma = \mathcal{N} \frac{\Gamma^L}{6m_\Phi^2} \tilde{G}_9(x_D), \quad C_7 = \mathcal{N} \frac{\Gamma^L}{6m_\Phi^2} F_7(x_D), \quad C_8 = -\mathcal{N} \frac{\Gamma^L}{2m_\Phi^2} F_7(x_D), \quad (4.66)$$

$$C_9^{\prime\text{box}} = C_9^{\text{box}} (L \leftrightarrow R), \quad C_{10}^{\prime\text{box}} = -C_{10}^{\text{box}} (L \leftrightarrow R), \quad (4.67)$$

$$C_9^{\prime\gamma} = C_9^\gamma (L \leftrightarrow R), \quad C_{7,8}' = C_{7,8} (L \leftrightarrow R). \quad (4.68)$$

- $b \rightarrow s\nu\bar{\nu}$ (see Eqs. (4.19)-(4.20))

$$C_L = -\mathcal{N} \frac{\Gamma^L |\Gamma_\mu^L|^2}{32\pi\alpha_{\text{EM}}m_\Phi^2} F(x_D, x_E), \quad C_R = -\mathcal{N} \frac{\Gamma^R |\Gamma_\mu^L|^2}{32\pi\alpha_{\text{EM}}m_\Phi^2} F(x_D, x_E). \quad (4.69)$$

- $B_s - \bar{B}_s$ (see Eqs. (4.23)-(4.28))

$$C_1 = \frac{|\Gamma^L|^2}{128\pi^2 m_\Phi^2} F(x_D), \quad C_5 = -\frac{\Gamma^L \Gamma^R}{32\pi^2 m_\Phi^2} F(x_D), \quad \tilde{C}_1 = \frac{|\Gamma^R|^2}{128\pi^2 m_\Phi^2} F(x_D), \quad (4.70)$$

where the (simplified) loop function are defined in Appendix C.1. In addition there are contributions to the C_1 analogue in $D^0 - \bar{D}^0$ mixing obtained by substituting $L_1^b \rightarrow L_1^c$ and $L_1^s \rightarrow L_1^u$ within Γ^L .

In the charged-lepton sector $SU(2)$ breaking effects (encoded in $\lambda_{L,R}^E$) can give a sizable

chiral enhancement of the NP effect in a_μ (see Eq. (4.30)) such that the long-standing anomaly in this channel can be addressed. In general one can parametrize the rotation matrices as

$$W^{E_{L,R}} = \begin{pmatrix} \cos(\theta_{L,R}) & -\sin(\theta_{L,R}) \\ \sin(\theta_{L,R}) & \cos(\theta_{L,R}) \end{pmatrix}, \quad (4.71)$$

leading to

$$\begin{aligned} L_1^\mu &= \Gamma_\mu^L \cos \theta_L, & L_2^\mu &= -\Gamma_\mu^L \sin \theta_L, & L^\nu &= \Gamma_\mu^L, \\ R_1^\mu &= \Gamma_\mu^R \sin \theta_R, & R_2^\mu &= \Gamma_\mu^R \cos \theta_R. \end{aligned} \quad (4.72)$$

In our analysis we will consider a simplified setup with $\lambda_R^E = -\lambda_L^E \equiv \lambda^E$ that maximizes the effect in a_μ (which at leading order in v is proportional to $\lambda_R^E - \lambda_L^E$). In this approximation we have for

- a_μ (see Eq. (4.30))

$$\Delta a_\mu = \frac{m_\mu^2}{8\pi^2 m_\Phi^2} \left[(|\Gamma_\mu^L|^2 + |\Gamma_\mu^R|^2) F_7(x_E) + \frac{8}{\sqrt{2}} \frac{v \lambda^E}{m_\mu} \Gamma_\mu^L \Gamma_\mu^R G_7(x_E) \right], \quad (4.73)$$

where we have assumed real values for the couplings, implying a vanishing d_μ . Let us stress that the contributions proportional to $v\lambda^E$, coming from $SU(2)$ breaking terms, is chirally enhanced can give a sizable effect that can explain the a_μ anomaly.

- $Z \rightarrow \mu^+ \mu^-$ (see Eqs. (4.35)-(4.36))

$$\Delta g_{\mu_L}(m_Z^2) = -\frac{|\Gamma_\mu^L|^2}{32\pi^2} \left[\frac{m_Z^2}{m_\Phi^2} \left((1 - 2s_W^2) \tilde{G}_9(x_E) + \frac{2}{3} \left(\frac{v\lambda^E}{m_E} \right)^2 F_9(x_E) \right) + \left(\frac{v\lambda^E}{m_E} \right)^2 F_Z(x_E) \right], \quad (4.74)$$

$$\Delta g_{\mu_R}(m_Z^2) = \frac{|\Gamma_\mu^R|^2}{32\pi^2} \left[\frac{m_Z^2}{m_\Phi^2} \left(2s_W^2 \tilde{G}_9(x_E) + \frac{2}{3} \left(\frac{v\lambda^E}{m_E} \right)^2 F_9(x_E) \right) + \left(\frac{v\lambda^E}{m_E} \right)^2 F_Z(x_E) \right], \quad (4.75)$$

where the simplified loop function $F_Z(x_E)$ has been defined in Appendix C.1. The results for $Z \rightarrow b\bar{b}$ couplings can be easily obtained by suitable substitutions. Note that in our approximation of $\lambda_{L,R}^D = 0$ the correction to the $Z\bar{b}b$ vertex vanishes at $q^2 = 0$. Note that the UV

divergences cancel as required, once for the couplings in Eq. (4.34) the relations

$$g^{\Psi,L(R)} = W^{E_{L(R)}} \dagger \begin{pmatrix} g^{\Psi_{L,2}} & 0 \\ 0 & g^{\Psi_e} \end{pmatrix} W^{E_{L(R)}} = W^{E_{L(R)}} \dagger \begin{pmatrix} g_{\mu L}^{\text{SM}} & 0 \\ 0 & g_{\mu R}^{\text{SM}} \end{pmatrix} W^{E_{L(R)}}, \quad (4.76)$$

and $g_\Phi = 0$ are used. Thus the finiteness of the result can be traced by to the unitarity of the matrices W .

4.3.3 Phenomenology

We are now ready to consider the phenomenology of our 4th generation model. For this purpose we will perform a combined fit to all the relevant and available experimental data, as briefly reviewed in Sec. 4.2. We perform this fit using the publicly available `HEPfit` package [222], performing a Markov Chain Monte Carlo (MCMC) analysis employing the Bayesian Analysis Toolkit (BAT) [223].

Let us first choose specific values for the masses of the scalar Φ and the fermions Ψ . As observed in Ref. [95] a large splitting between the scalar mass and the vector-like lepton mass with respect to the vector-like quark masses is welcome to suppress the relative effect in ΔM_s . Since the vector-like quarks should not be too light anyway because of direct LHC searches [224, 225] we choose $m_\Phi \simeq m_E \simeq 450 \text{ GeV}$ ⁶ and $m_D = 3.15 \text{ TeV}$, corresponding to $x_{E,L} \simeq 1$ and $x_D \simeq 50$. These values are well beyond the reach of direct searches at LHC: Concerning $m_{E,L}$ the bounds come from Drell-Yan production of the new fermions which are subsequently decaying in the neutral scalar and SM leptons. Therefore, the collider signature is similar to the one of MSSM slepton [226, 227]⁷.

Turning to the coupling of the new scalars and fermions to quarks and muons, we assume a flatly distributed priors within the range $|\Gamma| \leq 1.5$ such that perturbativity is respected. In the rest of this section we will focus on one particular benchmark point, that we selected because it lies within all the 1σ regions of the combined fit distributions for the NP couplings. The benchmark values are

$$|\Gamma_\mu^L| = 1.5, \quad |\Gamma_\mu^R| = 1.4, \quad \lambda^E = 0.0015, \quad \Gamma^L = -1.0, \quad \Gamma^R = -0.12 \quad (4.77)$$

⁶Nearly degenerate masses $m_\Phi \simeq m_E$ are also welcome in the light of the dark matter relic density since the stable Φ is a suitable DM candidate. In fact, for $m_\Phi = 450 \text{ GeV}$, $450 \leq m_E \leq 520 \text{ GeV}$ the model allows for an efficient annihilation such that one does not over-shoot the matter density of the universe for order one Γ couplings.

⁷A detailed study recasting these MSSM analysis for our model has been performed in Refs. [228, 229], finding $m_E \gtrsim m_\Phi = 450 \text{ GeV}$ as an allowed solution.

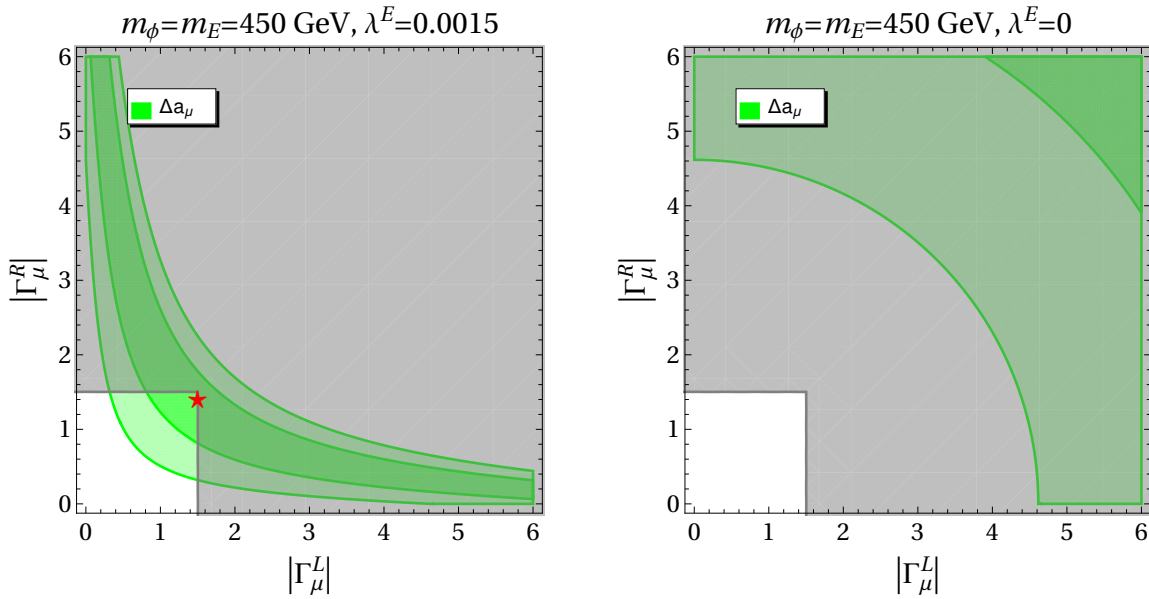


Figure 4.5: Left panel: allowed region for the coupling strength $|\Gamma_\mu^L|$ from the muon anomalous magnetic moment as a function of $|\Gamma_\mu^R|$, assuming $m_\phi = 450 \text{ GeV}$, $x^E=1$ and $\lambda^E = 0.0015$. The excluded region due to the requirement of perturbativity for $|\Gamma_\mu^{L,R}|$ is given in gray. Dark (light) green corresponds to 1σ (2σ) region. The red star marks the benchmark point (1.5, 1.4). Right panel: same as the left panel, but assuming $\lambda^E = 0$.

assuming real values for all couplings. Note that the small value for λ^E is obtained from the fit due to its correlation with $|\Gamma_\mu^R|$. Higher values of λ^E would require lower values of $|\Gamma_\mu^R|$, which is disfavored by the current fit to $b \rightarrow s\ell^+\ell^-$ data.

We observe that it is extremely important to allow for a right-handed coupling Γ_μ^R together a mixing coupling λ^E in the muon sector such that a_μ can be explained. This can be seen from the fit in the $(|\Gamma_\mu^L|, |\Gamma_\mu^R|)$ -plane from the left panel of Fig. 4.5. In the case with $\lambda^E = 0.0015$, corresponding to the benchmark point reported in Eq. (4.77), one can see that it is possible to explain the deviation in a_μ by means of couplings of order unity. However, the situation changes significantly if one did not allow the presence of a coupling of the vector-like leptons to the SM Higgs. As shown in the right panel of Fig. 4.5, with $\lambda^E = 0$, it is not possible to obtain couplings that are perturbative and capable to give a satisfactory explanation of the anomalous magnetic moment of the muon at the same time. The presence of Γ_μ^R ameliorates the tension, but it is still not sufficient by itself to address the anomaly.

Also in the quark sector right-handed couplings are needed to address the B anomalies

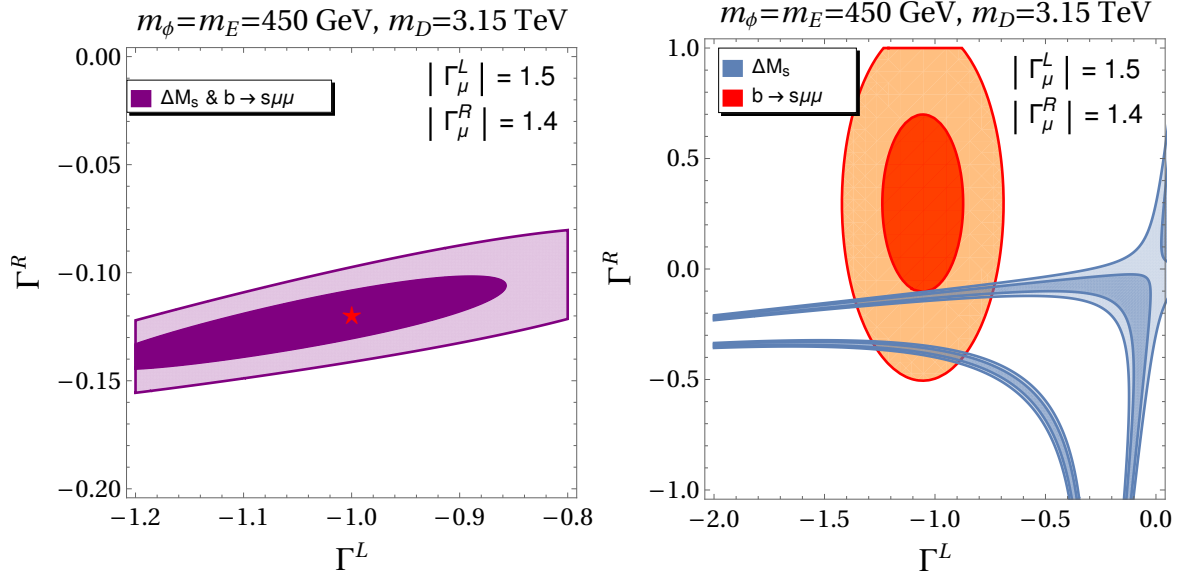


Figure 4.6: Left panel: Allowed region for the coupling $\Gamma^L \equiv \Gamma_b^L \Gamma_s^{L*}$ and $\Gamma^R \equiv \Gamma_b^R \Gamma_s^{R*}$ from $B_s - \bar{B}_s$ mixing and $b \rightarrow s\mu^+\mu^-$ data for $m_\phi = m_E = 450 \text{ GeV}$, $m_D = 3.15 \text{ TeV}$, $|\Gamma_\mu^L| = 1.5$ and $|\Gamma_\mu^R| = 1.4$. The red star marks the values at our benchmark point $(-1, -0.12)$. The dark (light) purple regions is preferred at the 1σ (2σ) level. Right panel: same as the left panel, but showing separately the allowed regions coming from $B_s - \bar{B}_s$ mixing (in blue) and $b \rightarrow s\mu^+\mu^-$ data (in red). The upper branch allowed by $B_s - \bar{B}_s$ mixing corresponds to the one shown on the left.

without spoiling at the same time the measurement for ΔM_s . This is particularly evident by looking at the left panel of Fig. 4.6, where the region allowed by both $b \rightarrow s\mu^+\mu^-$ transitions and $B_s - \bar{B}_s$ is shown. Indeed, if one performs a separate fit to $b \rightarrow s\mu^+\mu^-$ transitions and ΔM_s as shown in the right panel of Fig. 4.6, it is evident that the two channels are incompatible as long as one assumes a vanishing coupling to right-handed bottom and strange quarks, i.e. $\Gamma^R = 0$.

The preference for non-zero couplings (i.e. BSM effects) is in general driven by Δa_μ , the angular analyses of $B \rightarrow K^*\mu^+\mu^-$ and $B_s \rightarrow \phi\mu^+\mu^-$, the branching fraction of $B_s \rightarrow \mu^+\mu^-$ and the ratios R_K and R_{K^*} . On the other hand, the experimental constraints coming from $b \rightarrow s\gamma$ and $B \rightarrow K^{(*)}\nu\bar{\nu}$ and ΔM_s set bounds on $\Gamma^{L,R}$ and $|\Gamma_\mu^L|$ that are less stringent than the ones obtained by the inclusion of the aforementioned channels involving $b \rightarrow s$ transitions in our setup with $\lambda_{L,R}^D = 0$. Analogously, the constraints from $Z \rightarrow \mu^+\mu^-$ are found to give negligible constraints on $|\Gamma_\mu^{L,R}|$. Concerning $D_0 - \bar{D}_0$ mixing, we recall that Eq. (4.62) implies

a relation between $\Gamma^L \equiv L_1^b L_1^{s*}$ and $L_1^{u,c}$. Exploiting the fact that only the product of $L_1^b L_1^{s*}$ enters $b \rightarrow s \ell^+ \ell^-$, together with the suppression of the L_1^b in $L_1^{u,c}$ by small CKM factors ($\mathcal{O}(\lambda^3)$ and $\mathcal{O}(\lambda^2)$, respectively), it is possible arrange the contributions to Γ^L in such a way that the constraint imposed by $D_0 - \bar{D}_0$ mixing is automatically satisfied.

Chapter 5

Two Scalar Leptoquark Model

In this chapter we assess the flavor anomalies via scalar LQ. As we already mentioned in Chapter 2, LQs are good candidates to solve the tension of flavor data with respect to the SM as they can modify the SM prediction through a tree-level or one-loop diagrams, depending on the structure of Yukawa couplings chosen to make the model consistent with the low- and high-energy observables. In [87] the authors stress that using a single scalar LQ it is not sufficient to solve both tensions in charged and neutral currents. Instead, considering a single mediator solution the vector LQ U_1 arises as a good candidate. However to render the loop corrections finite in such a scenario one would need to specify the ultra-violet completion of the theory, which in turn involves a number of new parameters (cf. Refs. [76, 82, 79, 84, 78, 81]). For that reason and to keep the minimality of simple models, we focus on the extension of the SM via two scalar LQs already proposed in Refs. [74, 80, 71, 56]. In these kind of models one has to take into account many observables that act as constraints of the NP model. In the scalar LQ extensions, there are many kinds of observables computed in [230], although a computation of the leptonic decays of Z and W bosons is not available. In Ref [231], they stress the importance of these observables and compute their contribution to the leading logarithm order, whereas in this chapter we make the computation in the next-to-leading logarithm approximation, that is to include the finite terms for each scalar LQ, and demonstrate its phenomenological relevance in a particular model with S_1 and S_3 LQs, already in the literature [74].

Another observable that rules out many models is $B_s - \bar{B}_s$ mixing as we already saw in Chaps. 3& 4. For illustration purposes, we evaluate the same $S_1 + S_3$ model of [74], and check its viability once the $B_s - \bar{B}_s$ constraint is well implemented together with the EW observables.

Implementing the abovementioned constraints we evaluate three different scenarios after

Moriond conference 2019, where a new value of R_D and R_K were presented.

5.1 Scalar Leptoquarks

In this Section we introduce the scalar LQ Lagrangians. We follow the notation of Ref. [230] and specify LQs by their SM quantum numbers, $(SU(3)_c, SU(2)_L)_Y$. In this way the electric charge, $Q = Y + I_3$, is the sum of the hypercharge (Y) and the third component of the weak isospin (I_3). In the left-handed doublets, $Q_i = [(V^\dagger u_L)_i \ d_{Li}]^T$ and $L_i = [(U \nu_L)_i \ \ell_{Li}]^T$, the matrices V and U are respectively the CKM and the PMNS matrices. As the neutrino masses are insignificant for phenomenology of this chapter we can set $U = \mathbb{1}$.

$$R_2 = (\mathbf{3}, \mathbf{2})_{7/6} : \quad \mathcal{L}_{R_2} = - (y_{R_2}^L)_{ij} \bar{u}_{R_i} R_2 i \tau_2 L_j + (y_{R_2}^R)_{ij} \bar{Q}_i R_2 \ell_{R_j} + \text{h.c.}, \quad (5.1)$$

$$\tilde{R}_2 = (\mathbf{3}, \mathbf{2})_{1/6} : \quad \mathcal{L}_{\tilde{R}_2} = - (y_{\tilde{R}_2}^L)_{ij} \bar{d}_{R_i} \tilde{R}_2 i \tau_2 L_j + (y_{\tilde{R}_2}^R)_{ij} \bar{Q}_i \tilde{R}_2 \nu_{R_j} + \text{h.c.}, \quad (5.2)$$

$$S_1 = (\bar{\mathbf{3}}, \mathbf{1})_{1/3} : \quad \mathcal{L}_{S_1} = (y_{S_1}^L)_{ij} \bar{Q}_i^C i \tau_2 S_1 L_j + (y_{S_1}^R)_{ij} \bar{u}_{R_i}^C S_1 \ell_{R_j} \\ + (y_{S_1}^{\prime R})_{ij} \bar{d}_{R_i}^C S_1 \nu_{R_j} + \text{h.c.}, \quad (5.3)$$

$$S_3 = (\bar{\mathbf{3}}, \mathbf{3})_{1/3} : \quad \mathcal{L}_{S_3} = (y_{S_3}^L)_{ij} \bar{Q}_i^C i \tau_2 (\vec{\tau} \cdot \vec{S}_3) L_j + \text{h.c.}, \quad (5.4)$$

$$\tilde{S}_1 = (\bar{\mathbf{3}}, \mathbf{1})_{4/3} : \quad \mathcal{L}_{\tilde{S}_1} = (y_{\tilde{S}_1}^R)_{ij} \bar{d}_{R_i}^C \tilde{S}_1 \ell_{R_j} + \text{h.c.}, \quad (5.5)$$

$$\bar{S}_1 = (\bar{\mathbf{3}}, \mathbf{1})_{-2/3} : \quad \mathcal{L}_{\bar{S}_1} = (y_{\bar{S}_1}^R)_{ij} \bar{u}_{R_i}^C \bar{S}_1 \nu_{R_j} + \text{h.c.}, \quad (5.6)$$

where, as usual, the fermion fields $\psi_{L,R} = P_{L,R} \psi$ with $P_{L,R} = (1 \mp \gamma^5)/2$, and ψ^C stands for a charge conjugated fermion, while τ_k denote the Pauli matrices. Note that we neglected the LQ couplings to diquarks in Eqs. (5.3-5.6) which is necessary for stability of the proton [230]. $y_{LQ}^{L,R}$ are the matrices of Yukawa couplings the components of which correspond to the quark and lepton indices in the weak interaction eigenbasis. It is often useful to label the scalar leptoquarks through its flavor number $F = 3B + L$, where B and L stand for the baryon and the lepton number respectively. In that way R_2 and \tilde{R}_2 are $F = 0$ leptoquarks while S_1, S_3, \tilde{S}_1 and \bar{S}_1 are $|F| = 2$ leptoquarks. For phenomenological considerations it is more convenient to work in the mass eigenbasis. After absorbing the matrices of rotation to the mass eigenstate

basis into the redefinition of Yukawa matrices ($y_{LQ}^{L,R}$), and by accounting for the usual CKM mixing matrix V , we can write

$$\begin{aligned} \mathcal{L}_{R_2} = & - (y_{R_2}^L)_{ij} \bar{u}_i P_L \ell_j R_2^{(5/3)} + (y_{R_2}^L)_{ij} \bar{u}_i P_L \nu_j R_2^{(2/3)} \\ & + (V y_{R_2}^R)_{ij} \bar{u}_i P_R \ell_j R_2^{(5/3)} + (y_{R_2}^R)_{ij} \bar{d}_i P_R \ell_j R_2^{(2/3)} + \text{h.c.} , \end{aligned} \quad (5.7)$$

$$\begin{aligned} \mathcal{L}_{\tilde{R}_2} = & - (y_{\tilde{R}_2}^L)_{ij} \bar{d}_i P_L \ell_j \tilde{R}_2^{(2/3)} + (y_{\tilde{R}_2}^L)_{ij} \bar{d}_i P_L \nu_j \tilde{R}_2^{(-1/3)} \\ & + (V y_{\tilde{R}_2}^R)_{ij} \bar{u}_i P_R \nu_j \tilde{R}_2^{(2/3)} + (y_{\tilde{R}_2}^R)_{ij} \bar{d}_i P_R \nu_j \tilde{R}_2^{(-1/3)} + \text{h.c.} , \end{aligned} \quad (5.8)$$

$$\begin{aligned} \mathcal{L}_{S_1} = & - (y_{S_1}^L)_{ij} \bar{d}_i^C P_L \nu S_1 + (V^* y_{S_1}^L)_{ij} \bar{u}_i^C P_L \ell_j S_1 \\ & + (y_{S_1}^R)_{ij} \bar{u}_i^C P_R \ell_j S_1 + (y_{S_1}^R)_{ij} \bar{d}_i^C P_R \nu_j S_1 + \text{h.c.} , \end{aligned} \quad (5.9)$$

$$\begin{aligned} \mathcal{L}_{S_3} = & - (y_{S_3}^L)_{ij} \bar{d}_i^C P_L \nu_j S_3^{(1/3)} - \sqrt{2} (y_{S_3}^L)_{ij} \bar{d}_i^C P_L \ell_j S_3^{(4/3)} \\ & + \sqrt{2} (V^* y_{S_3}^L)_{ij} \bar{u}_i^C P_L \nu_j S_3^{(-2/3)} - (V^* y_{S_3}^L)_{ij} \bar{u}_i^C P_L \ell_j S_3^{(1/3)} + \text{h.c.} . \end{aligned} \quad (5.10)$$

$$\mathcal{L}_{\tilde{S}_1} = (y_{\tilde{S}_1}^R)_{ij} \bar{d}_i^C P_R \ell_j \tilde{S}_1 + \text{h.c.} , \quad (5.11)$$

$$\mathcal{L}_{\bar{S}_1} = (y_{\bar{S}_1}^R)_{ij} \bar{u}_i^C P_R \nu_j \bar{S}_1 + \text{h.c.} , \quad (5.12)$$

where in the superscript of the non-singlet LQ field we note the component corresponding to the specific electric charge eigenstate which we assume to be mass degenerate. We stress once again that we set the PMNS matrix to $U = \mathbb{1}$.

5.2 Addressing Anomalies with a Single Scalar Leptoquark

The first and more logical approach in order to solve the flavor anomalies is to consider the possibility that the NP contribution comes from a single LQ. In this section we show that it is impossible to solve both $R_{K^{(*)}}$ and $R_{D^{(*)}}$ anomalies using only one scalar LQ. To do that, we list again all the scalar LQs and justify their unavailability to fulfill the deviations respect to the SM.

- R_2

Due the second and fourth Yukawa terms of the R_2 Lagrangian in (5.7), this LQ can

generate a satisfactory contribution to $R_{D^{(*)}}$ with the $g_S = 4g_T$ pattern of the effective couplings, since both left and right-handed couplings are involved. However the tree-level contribution to $b \rightarrow s\mu^+\mu^-$ process generates $C_9 = C_{10}$ pattern, which is disfavoured by data. This issue can be solved by suppressing the tree-level contribution with appropriate choice of the Yukawas as in [91], but since this combination would require to suppress right-handed couplings, it is in conflict with the possible $R_{D^{(*)}}$ solution.

- \tilde{R}_2

In this scalar LQ scenario we generate $C'_9 = -C'_{10}$ contribution to $b \rightarrow s\mu^+\mu^-$ at tree-level. While this combination is good to fulfill $R_K < R_K^{\text{SM}}$, as predicted by the SM, it also predicts $R_{K^*} > R_{K^*}^{\text{SM}}$, which is contrary to the experiment. Concerning charged currents, in Ref. [70] it is shown that it is possible to generate an contribution to $R_{D^{(*)}}$ by using right-handed neutrinos. However, this contribution turns out to be too small since there is no interference with the SM.

- S_1

This LQ was the first proposed to accommodate both of the anomalies [90] since for $m_{S_1} \sim 1$ TeV it can generate the desired combination of WC $C'_9 = -C'_{10}$ at loop-level in $b \rightarrow s\mu^+\mu^-$. It also generates contribution to $R_{D^{(*)}}$ at tree-level at the same mass scale, reproducing its experimental value with left-handed couplings (g_{V_L} coefficient) or even with right-handed couplings (g_{S_L} and g_T coefficients). In Ref. [65] they show that these scenario would lead to huge contributions to observables such as

$$R_D^{\mu/e} = \frac{\text{Br}(B \rightarrow D\mu\bar{\nu})}{\text{Br}(B \rightarrow De\bar{\nu})} \quad (5.13)$$

which is disfavoured by present data. Additionally, one could work with a heavier LQ, although this requires to enlarge the couplings making them disfavoured by direct searches as computed in Ref. [87]

- S_3

This LQ couples to left-handed SM fermions. It can generate at tree-level $C_9 = -C_{10}$, which allows to explain $R_{K^{(*)}}$ anomaly, and its contribution to $R_{D^{(*)}}$ is generated with the effective coefficient g_{V_L} but with an opposite sign as expected by data. Notice that the first and the last terms of (5.10) are the ones giving contribution to $b \rightarrow c\tau\nu$. In S_1 Lagrangian 5.9, where we have the correct sign, the analogous terms generating left-

handed $R_{D^{(*)}}$ contribution are the first with a minus sign, and the second with a plus sign, while in S_3 Lagrangian these terms appear both with a negative sign, generating the opposite sign to g_{VL}

- \tilde{S}_1 & \bar{S}_1

These two last scalar LQs are not suitable candidates since they only relate one type of quarks with one type of leptons. Plus they only couple to right-handed fermions.

The fact that any single scalar LQ explanation is possible, has focused the single LQ activity in exploring vector LQ, and in particular the U_1 LQ, mentioned in Chap. 2. What we do is to explore the possibility of considering an extension of the SM with two scalar LQs. In the following sections, we list and study the two main constraints that our models will face.

5.3 Leptoquark Contributions to $Z \rightarrow \ell\ell$

5.3.1 Effective Field Theory Description

Leptoquarks contribute to the Z couplings to leptons via the loop diagrams illustrated in Fig. 5.1. The effective Lagrangian describing the Z -boson interaction to generic fermions $f_{i,j}$ can be written as

$$\delta\mathcal{L}_{\text{eff}}^Z = \frac{g}{\cos\theta_W} \sum_{f,i,j} \bar{f}_i \gamma^\mu \left[g_{f_L}^{ij} P_L + g_{f_R}^{ij} P_R \right] f_j Z_\mu \quad (5.14)$$

where g is the $SU(2)_L$ gauge coupling, θ_W is the Weinberg angle, and

$$g_{f_{L(R)}}^{ij} = \delta_{ij} g_{f_{L(R)}}^{\text{SM}} + \delta g_{f_{L(R)}}^{ij}, \quad (5.15)$$

with $g_{f_L}^{\text{SM}} = I_3^f - Q^f \sin^2\theta_W$ and $g_{f_R}^{\text{SM}} = -Q^f \sin^2\theta_W$. LQ loop contributions are described by the effective coefficients $\delta g_{f_{L(R)}}^{ij}$. The corresponding Z -boson branching fractions are then

given by ¹

$$\begin{aligned} \text{Br}(Z \rightarrow f_i \bar{f}_j) = \frac{m_Z \lambda_Z^{1/2}}{6\pi v^2 \Gamma_Z} & \left[(|g_{f_L}^{ij}|^2 + |g_{f_R}^{ij}|^2) \left(1 - \frac{m_i^2 + m_j^2}{2m_Z^2} - \frac{(m_i^2 - m_j^2)^2}{2m_Z^4} \right) \right. \\ & \left. + 6 \frac{m_i m_j}{m_Z^2} \text{Re} \left[g_{f_L}^{ij} (g_{f_R}^{ij})^* \right] \right], \end{aligned} \quad (5.16)$$

where $m_{i,j}$ are the fermion masses and $\lambda_Z \equiv [m_Z^2 - (m_i - m_j)^2][m_Z^2 - (m_i + m_j)^2]$.² Contributions to these rates are constrained by the measurement of both flavor conserving and flavor violating Z decays at LEP [152]. In particular, LEP measured the effective couplings [193]

$$\begin{aligned} g_V^{e,\text{exp}} &= -0.03817(47), & g_A^{e,\text{exp}} &= -0.50111(35), \\ g_V^{\mu,\text{exp}} &= -0.0367(23), & g_A^{\mu,\text{exp}} &= -0.50120(54), \\ g_V^{\tau,\text{exp}} &= -0.0366(10), & g_A^{\tau,\text{exp}} &= -0.50204(64), \end{aligned} \quad (5.17)$$

which as in the previous Chapter are related to the couplings in Eq. (5.14) via the relations $g_{V(A)}^{ij} = g_{\ell_L}^{ij} \pm g_{\ell_R}^{ij}$. Note that for $i = j$ we simplify the notation by dropping one superindex. Another important observable is the effective number of neutrinos [193]

$$N_\nu^{\text{exp}} = 2.9840(82), \quad (5.18)$$

which will constraint the LQ couplings to neutrinos via [193]

$$N_\nu = \sum_{i,j} \left[\left| \delta_{ij} + \frac{\delta g_{\nu_L}^{ij}}{g_{\nu_L}^{\text{SM}}} \right|^2 + \left| \frac{\delta g_{\nu_R}^{ij}}{g_{\nu_L}^{\text{SM}}} \right|^2 \right], \quad (5.19)$$

where $i, j \in \{e, \mu, \tau\}$ and neutrino masses have been neglected.

5.3.2 One-loop Matching

We shall now provide an expressions for the couplings $\delta g_{L(R)}^{ij}$ for each of the leptoquark models listed in Sec. 5.1. We focus our discussion onto the leptonic Z couplings since these are the

¹For $i \neq j$ the computation of the branching ratio has to be interpreted as the average $\frac{1}{2} [\text{Br}(Z \rightarrow f_i \bar{f}_j) + \text{Br}(Z \rightarrow f_j \bar{f}_i)]$

²This expression also applies to the decays $Z \rightarrow \nu\nu$ if neutrinos are assumed to be Dirac particles. If lepton number is violated, this expression should be modified. Both formulas, however, agree in the limit $m_{i,j} \rightarrow 0$. See Ref. [232] for a similar discussion in the case of $K \rightarrow \pi\nu\bar{\nu}$ decays.

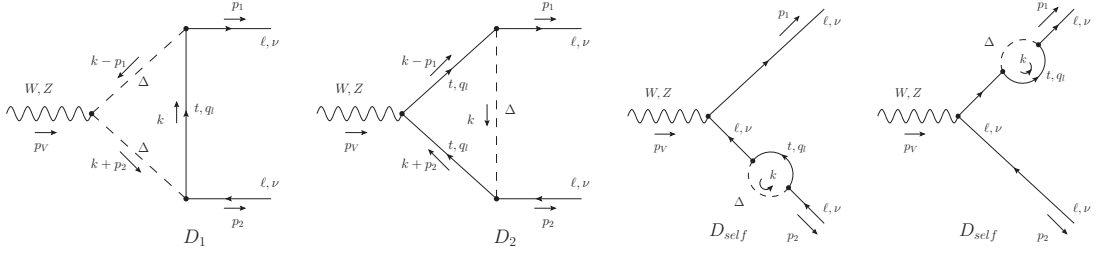


Figure 5.1: Scalar LQ (Δ) contributions at one-loop to $Z \rightarrow \ell_i \ell_j$, $Z \rightarrow \nu_i \nu_j$ and $W \rightarrow \ell_j \nu_i$.

most precisely determined by experiment. Our discussion can be adapted to the Z couplings to quarks. Before presenting our results, we define our convention for the covariant derivative in an analogous way as the one in Chap. 2

$$D_\mu = \partial_\mu + ig' Y B_\mu + ig I^k W_\mu^k + ig_s T^a G_\mu^a, \quad (5.20)$$

where Y is the hypercharge, and T^a and I^k are the relevant $SU(3)_c$ and $SU(2)_L$ generators, respectively. After the EW symmetry breaking, this expression can be rewritten as

$$D_\mu = \partial_\mu + i \frac{g}{\sqrt{2}} (I^+ W_\mu^+ + I^- W_\mu^-) + i \frac{g}{\cos \theta_W} (I_3 - Q \sin^2 \theta_W) Z_\mu + ie Q A^\mu + ig_s T^a G_\mu^a, \quad (5.21)$$

where $e = g \sin \theta_W = g' \cos \theta_W$, $Q = Y + I_3$ and $I^\pm = (I_1 \pm i I_2)$, as usual. To present our results in a compact form, we consider a general Yukawa Lagrangian defined by

$$\mathcal{L}_{\text{yuk.}}^{F=0} = \bar{q}_i [l_{ij} P_R + r_{ij} P_L] \ell_j \Delta + \text{h.c.} \quad (5.22)$$

$$\mathcal{L}_{\text{yuk.}}^{F=2} = \bar{q}_i^C [l_{ij} P_R + r_{ij} P_L] \ell_j \Delta + \text{h.c.} \quad (5.23)$$

where q and ℓ are generic quark and lepton flavors, l_{ij} and r_{ij} denote the generic Yukawa couplings, and Δ is a leptoquark mass eigenstate, which belongs to one of the $SU(2)_L$ multiplets listed in Eq. (5.1)–(5.6). Our results will be presented in such a way that the expression for a specific model can be obtained by simply comparing Eqs. (5.22, 5.23), to the Yukawa Lagrangians listed in Sec. 5.1. In this way, one can determine l_{ij} and r_{ij} for each leptoquark charge eigenstate contributing to $Z \rightarrow \ell\ell$ or $Z \rightarrow \nu\bar{\nu}$, which should then be summed up to give the final expression.

Our computation is performed in two independent ways. We first neglect the light quark

masses (i.e., for $q_u = u, c$ and $q_d = s, d, b$) and expand in the external momenta before integration [233]

$$\frac{1}{(k+p)^2 - M^2} = \frac{1}{k^2 - M^2} \left[1 - \frac{p^2 + 2(k \cdot p)}{k^2 - M^2} + \frac{4(k \cdot p)^2}{(k^2 - M^2)^2} \right] + \mathcal{O}\left(\frac{p}{M}\right)^4, \quad (5.24)$$

where k is the loop momentum, p is a generic external momentum and M stands for the mass of the particle running in the loop. With this method we obtain analytic expressions for the loop functions, systematically accounting for the corrections of order $\mathcal{O}(m_Z/m_\Delta)^n$ (with $n > 0$), but avoiding the difficult computation of Passarino-Veltman functions with nonzero external momenta. We then compare these expressions with the ones computed numerically by using the Mathematica packages LoopTools [234] and Package-X [235]. We find an agreement better than per-mil level between the results obtained numerically and analytically, for leptoquark masses heavier than ≈ 900 GeV, as currently allowed by LHC searches [87].

We present now our analytic results in terms of the Yukawas l_{ij} and r_{ij} , and the quantum numbers of SM fermions. As explained above, we separate the top quark contribution from the light quarks ($q_u = u, c$ and $q_d = s, d, b$), since the relevant scales are different in each case. The final result for $F = 0$ leptoquarks to $\mathcal{O}(m_Z^2/m_\Delta^2)$ reads

$$\left[\delta g_{\ell_{L(R)}}^{ij} \right]_{F=0} = N_C \frac{w_{tj} w_{ti}^*}{16\pi^2} \left[\left(g_{u_{L(R)}} - g_{u_{R(L)}} \right) \frac{x_t(x_t - 1 - \log x_t)}{(x_t - 1)^2} + \frac{x_Z}{12} F_{F=0}^{L(R)}(x_t) \right] \quad (5.25)$$

$$+ x_Z N_C \sum_{k=u,c} \frac{w_{kj} w_{ki}^*}{48\pi^2} \left[-g_{u_{R(L)}} \left(\log x_Z - i\pi - \frac{1}{6} \right) + \frac{g_{\ell_{L(R)}}}{6} \right] \quad (5.26)$$

$$+ x_Z N_C \sum_{k=d,s,b} \frac{w_{kj} w_{ki}^*}{48\pi^2} \left[-g_{d_{R(L)}} \left(\log x_Z - i\pi - \frac{1}{6} \right) + \frac{g_{\ell_{L(R)}}}{6} \right], \quad (5.27)$$

while for $|F| = 2$ leptoquarks we obtain,

$$\left[\delta g_{\ell_{L(R)}}^{ij} \right]_{F=2} = N_C \frac{w_{tj} w_{ti}^*}{16\pi^2} \left[\left(g_{u_{L(R)}} - g_{u_{R(L)}} \right) \frac{x_t(x_t - 1 - \log x_t)}{(x_t - 1)^2} + \frac{x_Z}{12} F_{F=2}^{L(R)}(x_t) \right] \quad (5.28)$$

$$+ x_Z N_C \sum_{k=u,c} \frac{w_{kj} w_{ki}^*}{48\pi^2} \left[g_{u_{L(R)}} \left(\log x_Z - i\pi - \frac{1}{6} \right) + \frac{g_{\ell_{L(R)}}}{6} \right] \quad (5.29)$$

$$+ x_Z N_C \sum_{k=d,s,b} \frac{w_{kj} w_{ki}^*}{48\pi^2} \left[g_{d_{L(R)}} \left(\log x_Z - i\pi - \frac{1}{6} \right) + \frac{g_{\ell_{L(R)}}}{6} \right], \quad (5.30)$$

where $x_t = m_t^2/m_\Delta^2$, $x_Z = m_Z^2/m_\Delta^2$, $N_C = 3$, with $g_L^f = I_3^f - Q_f \sin^2 \theta_W$ and $g_R^f = -Q_f \sin^2 \theta_W$ ($f = u, d, \ell$), as before. In the above expressions, w_{ki} should be replaced by r_{ki} or l_{ki} for δg_L^{ij} or δg_R^{ij} , respectively. These couplings are collected in Table 5.1 for each leptoquark representation listed in Sec. 5.1. One of the novelties of our study is the inclusion of the terms $\mathcal{O}(x_Z \log x_t)$, which have never been considered before and which can induce non-negligible corrections for LQ masses $m_\Delta \lesssim 1.5$ TeV.³ These corrections are collected in the functions $F_0^{L(R)}$ and $F_2^{L(R)}$, which are given by

$$F_{F=0}^{L(R)}(x_t) = g_{u_{R(L)}} \frac{(x_t - 1)(5x_t^2 - 7x_t + 8) - 2(x_t^3 + 2) \log x_t}{(x_t - 1)^4} \quad (5.31)$$

$$+ g_{u_{L(R)}} \frac{(x_t - 1)(x_t^2 - 5x_t - 2) + 6x_t \log x_t}{(x_t - 1)^4} \quad (5.32)$$

$$+ g_{\ell_{L(R)}} \frac{(x_t - 1)(-11x_t^2 + 7x_t - 2) + 6x_t^3 \log x_t}{3(x_t - 1)^4}, \quad (5.33)$$

and

$$F_{F=2}^{L(R)}(x_t) = - g_{u_{L(R)}} \frac{(x_t - 1)(5x_t^2 - 7x_t + 8) - 2(x_t^3 + 2) \log x_t}{(x_t - 1)^4} \quad (5.34)$$

$$- g_{u_{R(L)}} \frac{(x_t - 1)(x_t^2 - 5x_t - 2) + 6x_t \log x_t}{(x_t - 1)^4} \quad (5.35)$$

$$+ g_{\ell_{L(R)}} \frac{(x_t - 1)(-11x_t^2 + 7x_t - 2) + 6x_t^3 \log x_t}{3(x_t - 1)^4}. \quad (5.36)$$

The phenomenological relevance of these terms and the other finite contributions we computed for the first time will be illustrated in the following.

5.3.3 Relevance of the Finite Terms in $Z \rightarrow \ell\ell$

We now discuss the relevance of the new contributions we computed, namely the $\mathcal{O}(x_Z \log x_t)$ terms and the finite terms in the matching. To this end, we compare our results to the formulas given in Ref. [231], obtained in an effective field theory context by employing a renormalization-

³Note, in particular, that much lower masses are allowed by current LHC searches for leptoquarks, which exclude masses of order ≈ 900 GeV for LQs with mostly couplings to the third generation, see e.g. Ref. [87].

Decay	w_{ij}	q	R_2	\tilde{R}_2	S_1	S_3	\tilde{S}_1	\bar{S}_1
$Z \rightarrow \ell\ell$	r_{ij}	q_u	$-\left(y_{R_2}^L\right)_{ij}$	0	$\left(V^* y_{S_1}^L\right)_{ij}$	$-\left(V^* y_{S_3}^L\right)_{ij}$	0	0
		q_d	0	$-\left(y_{\tilde{R}_2}^L\right)_{ij}$	0	$-\sqrt{2}\left(y_{S_3}^L\right)_{ij}$	0	0
	l_{ij}	q_u	$\left(V y_{R_2}^R\right)_{ij}$	0	$\left(y_{S_1}^R\right)_{ij}$	0	0	0
		q_d	$\left(y_{R_2}^R\right)_{ij}$	0	0	0	$\left(y_{\tilde{S}_1}^R\right)_{ij}$	0
$Z \rightarrow \nu\nu$	r_{ij}	q_u	$\left(y_{R_2}^L\right)_{ij}$	0	0	$\sqrt{2}\left(V^* y_{S_3}^L\right)_{ij}$	0	0
		q_d	0	$\left(y_{\tilde{R}_2}^L\right)_{ij}$	$-\left(y_{S_1}^L\right)_{ij}$	$-\left(y_{S_3}^L\right)_{ij}$	0	0
	l_{ij}	q_u	0	$\left(V y_{R_2}^R\right)_{ij}$	0	0	0	$\left(y_{\tilde{S}_1}^R\right)_{ij}$
		q_d	0	$\left(y_{\tilde{R}_2}^R\right)_{ij}$	$\left(y_{S_1}^R\right)_{ij}$	0	0	0

Table 5.1: Expressions for the coefficients w_{ij} in Eq. (5.25) and (5.28) obtained by the matching of Eq. (5.22) and (5.23) onto the Yukawa Lagrangians listed in Sec. 5.1 for LQs with fermion number $F = 0$ and $|F| = 2$, respectively.

group-equations approach to a leading-logarithmic approximation (LLA). The latter approach only accounts for the terms $x_t \log x_t$ and $x_Z \log x_Z$ from the general expressions, where one assumes that $v_{EW} \approx m_Z \approx m_t$ in the logarithms.

In Fig. 5.2, we show the ratio between the full and simplified formulas for $Z \rightarrow \ell^- \ell^+$ and for $Z \rightarrow \nu \bar{\nu}$ as a function of the LQ mass, for the different $SU(2)_L \times U(1)_Y$ representations. For illustration, we have only considered Yukawa couplings to third generation fermions in Eq. (5.1)–(5.6). We find that the new corrections we have computed can be as large as $\mathcal{O}(20\%)$ for values of LQ mass below 1.5 TeV, as allowed by the present limits from the direct searches at the LHC [87]. Furthermore, we see that these relative corrections decrease with the LQ mass, becoming less relevant for larger masses, in which case the LLA is satisfied to a good extent. The conclusion of this exercise is that, given the present limits from LHC, one should consider the full formulas to reliably assess the viability of any scenario with low-energy scalar LQ. We will illustrate this feature in Sec. 5.4 with a concrete model for the B -anomalies, which presents a tension with current data if the formulas from Ref. [231] are used, but which turns out to be perfectly consistent when the full formulas are considered.

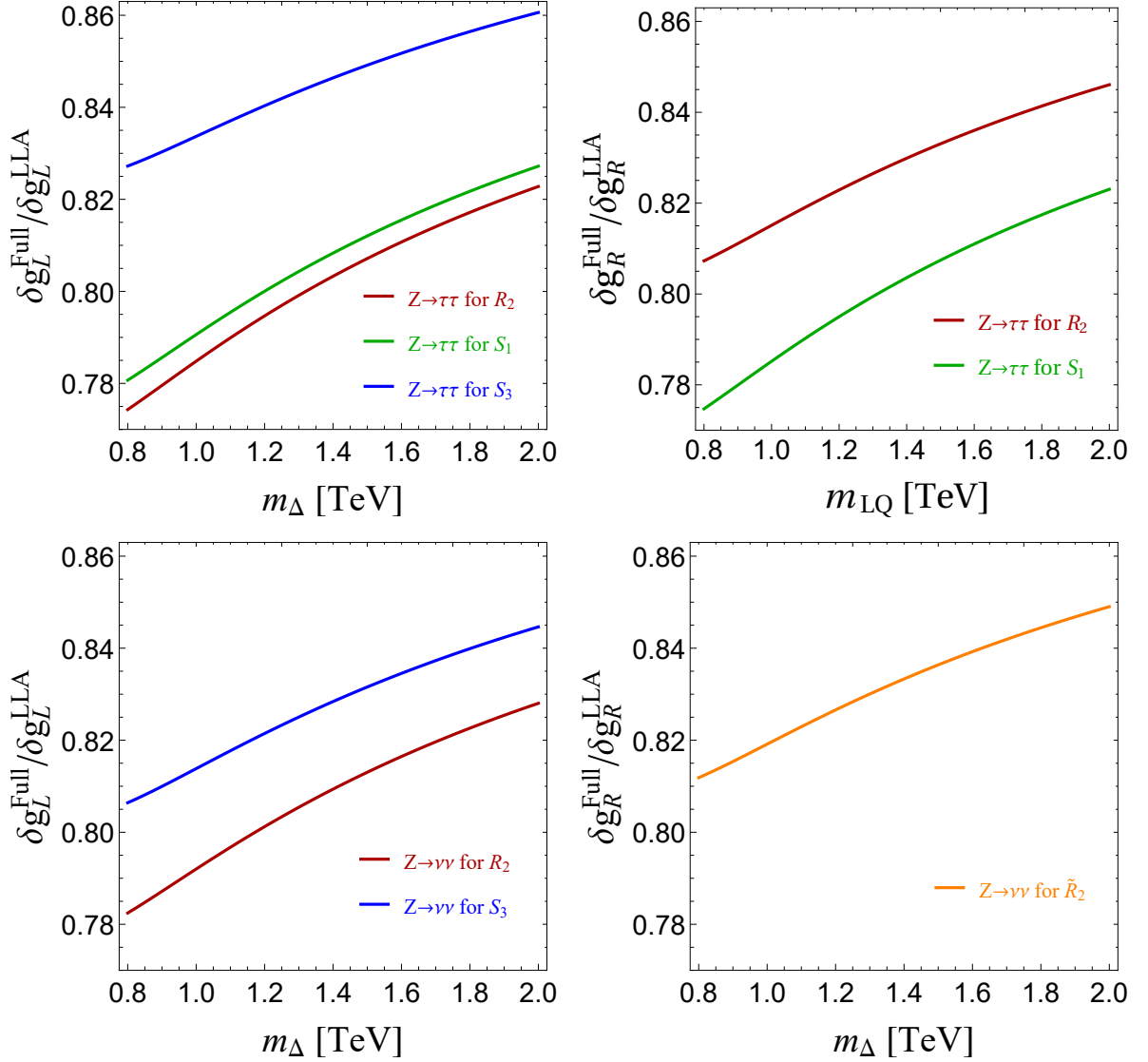


Figure 5.2: Comparison of the full expressions given in Eq. (5.25) and (5.28) for $Z \rightarrow \ell^+\ell^-$ and $Z \rightarrow \nu\bar{\nu}$ with the ones obtained by employing a RGE approach with a leading logarithmic approximation (LLA) [231]. We consider all LQ representations listed in Sec. 5.1 and we assume, for illustration, that the LQs only have couplings to third generation fermions in Eq. (5.1)–(5.6). The contributions from the new terms we have computed can be as large as $\mathcal{O}(20\%)$, for masses allowed by the direct searches at the LHC, being therefore non-negligible in phenomenological analyses.

Before closing this Section we need to compare our results with previous computations in the literature. We agree with the results from Ref. [90], where the light fermion and top-

quark contributions have been computed for the S_1 model. To that result we included terms of $\mathcal{O}(x_Z \log x_t)$, which amount to a $\mathcal{O}(10\%)$ relative effect. We also agree with the results presented in Ref. [91], where the R_2 contribution was computed for both light and heavy fermions. Again, our result goes a step beyond in that we include also the $\mathcal{O}(x_Z \log x_t)$ terms. Similarly, if we neglect the $\mathcal{O}(x_Z \log x_t)$ terms, we agree with the results of Ref. [69] where the top-quark contribution was computed for S_1 and R_2 LQs. Note, however, that we disagree with their sign of $\delta g_{L(R)}$ for the R_2 LQ. Before moving on, we stress that the expressions given above can be easily adapted to other scenarios of new physics containing scalar particles coupled to fermions, such as the two-Higgs doublet models [236].

5.4 Leptoquark Contributions to $W \rightarrow \ell \bar{\nu}$

5.4.1 Effective Field Theory Description

We now turn to the W couplings to leptons. Similar to the above discussion, the W interactions can be generically written as

$$\delta \mathcal{L}_{\text{eff}}^W = \frac{g}{\sqrt{2}} \sum_{i,j} \bar{\ell}_i \gamma^\mu \left[(\delta^{ij} + h_{\ell_L}^{ij}) P_L + \delta h_{\ell_R}^{ij} P_R \right] \nu_j W_\mu^- + \text{h.c.}, \quad (5.37)$$

where $h_{\ell_{L,R}}^{ij}$ describes the loop-level contributions illustrated in Fig. 5.1. In this expression, we also consider the possibility of light right-handed neutrinos, which we assume to be Dirac particles for simplicity.⁴ The corresponding branching ratio can then be written as

$$\text{Br}(W \rightarrow \ell_i \nu_j) = \frac{m_W^3}{12\pi v^2 \Gamma_W} \left(|\delta_{ij} + \delta h_{\ell_L}^{ij}|^2 + |\delta h_{\ell_R}^{ij}|^2 \right) \left(1 - \frac{m_i^2}{2m_W^2} - \frac{m_i^4}{2m_W^4} \right), \quad (5.38)$$

where $m_i \equiv m_{\ell_i}$ and neutrinos masses have been neglected. This expression should be compared to the LEP measurements [152]

$$\text{Br}(W \rightarrow \tau \bar{\nu})^{\text{exp}} = 11.38(21) \times 10^{-2}, \quad (5.39)$$

$$\text{Br}(W \rightarrow \mu \bar{\nu})^{\text{exp}} = 10.63(15) \times 10^{-2}, \quad (5.40)$$

$$\text{Br}(W \rightarrow e \bar{\nu})^{\text{exp}} = 10.71(16) \times 10^{-2}. \quad (5.41)$$

⁴For W decays, the expression for Majorana neutrinos is a trivial extension of the results presented above (cf. e.g. Ref. [232] for further discussion).

In particular, the ratio $R_W^{\tau/\mu} = \text{Br}(W \rightarrow \tau\nu)^{\text{exp}}/\text{Br}(W \rightarrow \mu\nu)^{\text{exp}} = 1.07(3)$ is about 2.4σ above the SM prediction, $R_W^{\tau/\mu, \text{SM}} \approx 0.999$. It is very challenging to explain such a large deviation in a new physics model, since these contributions would be correlated, via $SU(2)_L \times U(1)_Y$ gauge invariance, with the tightly measured Z couplings to τ -leptons [237]. Alternatively, the $W_{\tau\nu}$ coupling can also be inferred from the τ -lepton decays. Current PDG average [152]

$$\text{Br}(\tau \rightarrow \mu\nu\bar{\nu})^{\text{exp}} = 17.33(5) \times 10^{-2}, \quad (5.42)$$

in a good agreement with the SM prediction, $\text{Br}(\tau \rightarrow \mu\nu\bar{\nu}) = 17.29(3) \times 10^{-2}$ [110]. Leptoquarks would also contribute to τ -decays via box-type diagrams. Since these contributions are proportional to $y_{\text{LQ}}^4/m_\Delta^2 = m_\Delta^2 \times (y_{\text{LQ}}/m_\Delta)^4$, where y_{LQ} denotes a generic LQ coupling, we know these are subdominant contributions for low values of m_Δ and fixed values of y_{LQ}/m_Δ , as in the case of the B -anomalies. For completeness we provide the expression for $\text{Br}(\tau \rightarrow \mu\nu\bar{\nu})$ in Appendix D.

5.4.2 One-loop Matching

We now give the expressions for $h_{\ell_L}^{ij}$ and $h_{\ell_R}^{ij}$ for each LQ model listed in Sec. 5.1. From Eq. (5.5) and (5.6), we see that the models $\tilde{S}_1 = (\bar{\mathbf{3}}, \mathbf{1})_{4/3}$ and $\bar{S}_1 = (\bar{\mathbf{3}}, \mathbf{1})_{-2/3}$ do not contribute to $W \rightarrow \ell\bar{\nu}$, since these are singlets of $SU(2)_L$ which do not have couplings to both up- and down-type quarks, neither to the W . For the scenarios with weak doublet leptoquarks, we obtain

$$\left[\delta h_{\ell_L}^{ij} \right]_{R_2} = N_c \frac{x_W}{288\pi^2} \left[\left(y_{R_2}^{L\dagger} \right)_{it} \left(y_{R_2}^L \right)_{tj} G_{R_2}(x_t) + \sum_{k=u,c} \left(y_{R_2}^{L\dagger} \right)_{ik} \left(y_{R_2}^L \right)_{kj} \right], \quad (5.43)$$

$$\left[\delta h_{\ell_L}^{ij} \right]_{\tilde{R}_2} = N_c \frac{x_W}{288\pi^2} \left(y_{\tilde{R}_2}^{L\dagger} y_{\tilde{R}_2}^L \right)_{ij}, \quad (5.44)$$

where $x_W = m_W^2/m_\Delta^2$ and $x_t = m_t^2/m_\Delta^2$, as before, and the function G_{R_2} is defined by

$$G_{R_2}(x_t) = \frac{-11x_t^3 + 6x_t^3 \log x_t + 18x_t^2 - 9x_t + 2}{2(x_t - 1)^4}, \quad (5.45)$$

Note, in particular, that these contributions cannot be accounted for by the effective field theory computation with leading-logarithmic approximation [231]. For the two remaining scenarios, we find

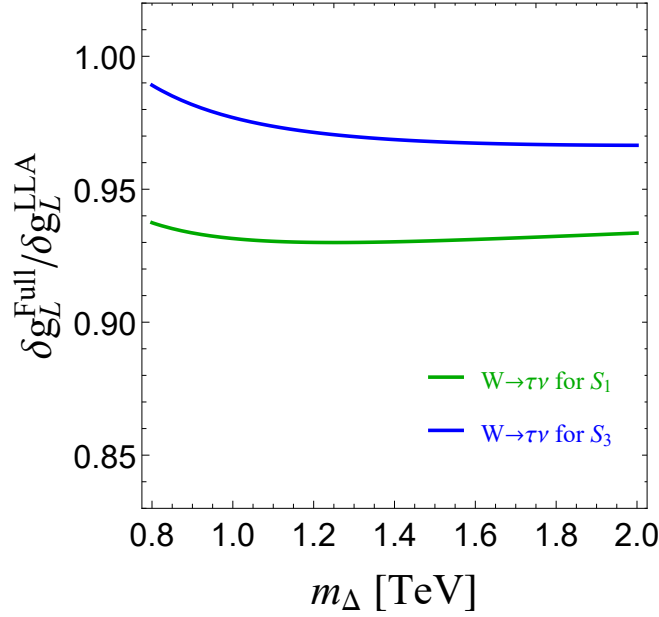


Figure 5.3: Comparison of the full expressions given in Eq. (5.47) and (5.49) for $W \rightarrow \ell \bar{\nu}$ with the ones obtained by employing a RGE approach with a leading logarithmic approximation (LLA) [231]. For illustration, we assume once again that the LQs only have couplings to the third generation fermions in Eq. (5.1)–(5.6). We do not display the results for the R_2 and \tilde{R}_2 LQs, since the RGE approach cannot encapsulate the contributions from these states, which have no logarithmic dependence. Furthermore, note that the LQs \tilde{S}_1 and \tilde{S}_1 do not contribute to these decays to one-loop order.

$$\left[\delta h_{\ell L}^{ij} \right]_{S_1} = N_C \left(V^* y_{S_1}^L \right)_{ti}^* \left(V^* y_{S_1}^L \right)_{tj} \left[- \frac{x_t (x_t - 1 + (x_t - 2) \log x_t)}{64\pi^2 (x_t - 1)^2} + \frac{x_W}{288\pi^2} G_{S_1}(x_t) \right] \quad (5.46)$$

$$+ N_C \frac{x_W}{144\pi^2} \sum_{k=u,c} \left(V^* y_{S_1}^L \right)_{ki}^* \left(V^* y_{S_1}^L \right)_{kj} (-1 - 3 \log x_W + 3\pi i), \quad (5.47)$$

and

$$\left[\delta h_{\ell L}^{ij} \right]_{S_3} = N_C \left(V^* y_{S_3}^L \right)_{ti}^* \left(V^* y_{S_3}^L \right)_{tj} \left[\frac{x_t (x_t - 1 + (x_t - 2) \log x_t)}{64\pi^2 (x_t - 1)^2} + \frac{x_W}{288\pi^2} G_{S_3}(x_t) \right] \quad (5.48)$$

$$+ N_C \frac{x_W}{144\pi^2} \sum_{k=u,c} \left(V^* y_{S_3}^L \right)_{ki}^* \left(V^* y_{S_3}^L \right)_{kj} (1 - 3 \log x_W + 3\pi i), \quad (5.49)$$

where we separate the top-quark contributions from the other light quarks. The functions G_{S_1} and G_{S_3} are given by

$$G_{S_1}(x_t) = \frac{6(x_t - 1 - \log x_t)}{(x_t - 1)^2}, \quad (5.50)$$

$$G_{S_3}(x_t) = \frac{6 [x_t (x_t^2 + x_t - 2) + 1] \log x_t + x_t - 1 [x_t (x_t (2x_t - 23) + 25) - 10]}{(x_t - 1)^4}. \quad (5.51)$$

Finally, note that none of the scalar LQ particles contribute at one-loop order to $h_{\ell_R}^{ij}$.

5.4.3 Relevance of the Finite Terms in $W \rightarrow \ell\nu$

We should now comment on the phenomenological implications of the results presented above. Similarly to the discussion of leptonic Z couplings in Sec. 5.3, we compared our full formulas to the ones obtained within a leading logarithmic approximation [231]. These results are illustrated in Fig. 5.3 for the models S_1 and S_3 , where we considered couplings only to the third generation fermions. For both scenarios, we find a negative correction coming from finite terms of order $\mathcal{O}(5\%)$, with a very mild dependence on the LQ mass m_Δ . For the other scenarios, namely R_2 and \tilde{R}_2 , we cannot perform such a comparison since the leading logarithmic approximation of Eq. (5.43) and (5.44) would give a vanishing contribution. In this case, the finite terms are essential to consider.

5.5 Illustration: S_1 & S_3 Explanation of $R_{K^{(*)}}$ and $R_{D^{(*)}}$

In this Section we illustrate our results in a specific scalar LQ model proposed to simultaneously explain the $b \rightarrow s$ and $b \rightarrow c$ anomalies [71, 74, 80]. This model contains the LQs $S_1 = (\bar{\mathbf{3}}, \mathbf{1})_{1/3}$ and $S_3 = (\bar{\mathbf{3}}, \mathbf{3})_{1/3}$, with couplings only to left-handed fermions, namely

$$\mathcal{L}_{\text{Yuk}} = (y_{S_1}^L)_{ij} \bar{Q}_i^C i\tau_2 S_1 L_j + (y_{S_3}^L)_{ij} \bar{Q}_i^C i\tau_2 (\vec{\tau} \cdot \vec{S}_3) L_j + \text{h.c.} \quad (5.52)$$

We adopt the same Yukawa pattern of Ref. [74, 80], namely

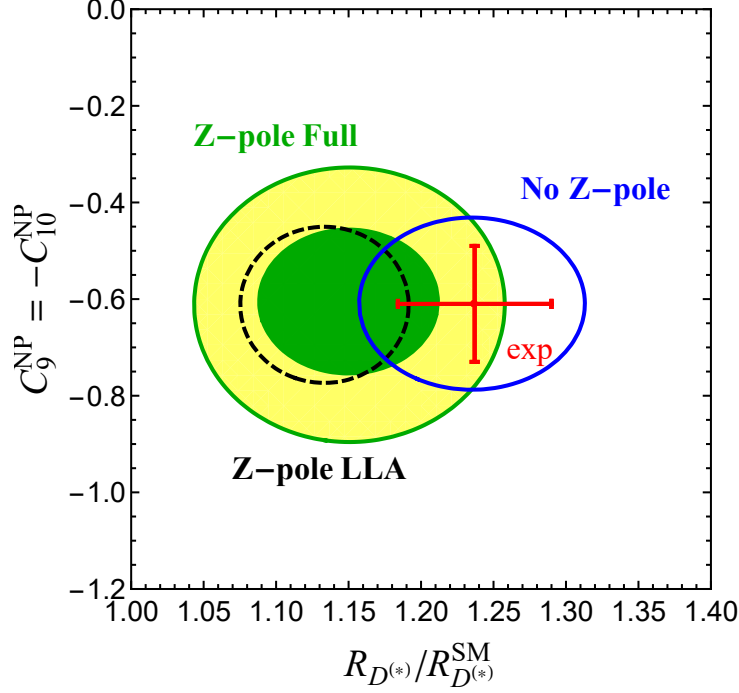


Figure 5.4: Results of the low-energy fit considering the full expressions computed in this section are depicted in the plane $R_{D^{(*)}}/R_{D^{(*)}}^{\text{SM}}$ vs. $C_9^{\text{NP}} = -C_{10}^{\text{NP}}$ by the green (yellow) regions to 1σ (2σ) accuracy. Leptoquark masses are fixed to $m_{S_1} = m_{S_3} = 2$ TeV and Yukawa couplings are scanned over the ranges described in the text. In the same plot we show the 1σ results of the fit by neglecting Z -pole constraints (blue line) and by including Z -poles observables with a leading-log approximation (black dashed line) [231]. As discussed in the text, the inclusion of finite terms reduces the tension between $R_{D^{(*)}}^{\text{exp}}$ and Z -pole data.

$$y_{S_1}^L = g_{S_1} \times \begin{pmatrix} 0 & 0 & 0 \\ 0 & \beta_{s\mu}^{S_1} & \beta_{s\tau}^{S_1} \\ 0 & \beta_{b\mu}^{S_1} & \beta_{b\tau}^{S_1} \end{pmatrix}, \quad y_{S_3}^L = g_{S_3} \times \begin{pmatrix} 0 & 0 & 0 \\ 0 & \beta_{s\mu}^{S_3} & \beta_{s\tau}^{S_3} \\ 0 & \beta_{b\mu}^{S_3} & \beta_{b\tau}^{S_3} \end{pmatrix}, \quad (5.53)$$

where $g_{S_{1(3)}}$ describe the overall strength of LQ Yukawa interactions, while $\beta_{ij}^{S_{1(3)}}$ contain the flavor structure. Couplings to the first generation are set to zero to avoid stringent bounds from kaon physics observables and atomic parity violation. Following Ref. [74, 80], we further assume that $\beta_{b\tau}^{S_1} = \beta_{b\tau}^{S_3} = 1$, and that $\beta_{q\mu} \equiv \beta_{q\mu}^{S_1} = \beta_{q\mu}^{S_3}$, with $q = s, b$. The $s\tau$ couplings are considered to be in general different, as needed to explain current deviations. We are then left with six couplings to be fixed by the data, namely g_{S_1} , g_{S_3} , $\beta_{s\mu}$, $\beta_{b\mu}$ and $\beta_{s\tau}^{S_{1(3)}}$, as well as two

masses m_{S_1} and m_{S_3} .

Several low-energy observables are sensitive to the couplings defined above. To illustrate the impact of the expressions we computed, we consider the same experimental constraints of Ref. [74]: (i) the LFU ratios $R_{D^{(*)}}$ and $R_{K^{(*)}}$ (via $C_9 = -C_{10}$ data fit), (ii) LFU tests in $R_D^{\mu/e}$, (iii) limits on the branching fractions $\text{Br}(B \rightarrow K^{(*)}\nu\bar{\nu})$, and (iv) the decays $Z \rightarrow \tau^+\tau^-$ and $Z \rightarrow \nu\bar{\nu}$ ⁵. Concerning the latter observables, we perform a fit by using the leading-log approximation (LLA) of Ref. [231], which is also considered in Ref. [74, 80], and by considering our complete formulas, cf. Sec. 5.3. We consider the same range of parameters as in Ref. [74], namely $\beta_{s\mu}, \beta_{s\tau}^{S_{1(3)}} \in (-5V_{cb}, 5V_{cb})$ and $\beta_{b\mu} \in (-1, 1)$.

Our results are depicted in Fig. 5.4 in the plane $R_{D^{(*)}}/R_{D^{(*)}}^{\text{SM}}$ vs. $C_9^{\text{NP}} = -C_{10}^{\text{NP}}$ for LQ masses $m_{S_1} = m_{S_3} = 2$ TeV. In the analysis considering the leading-log approximation, we obtain a value $\chi_{\text{min}}^2 \approx 8.0$, which shows a mild tension between the observed deviations $R_{D^{(*)}}$ and Z -pole data, as depicted by the 2σ contour (black dashed line). If, instead, one considers the formulas computed in the previous section, the tension is milder as shown by the green/yellow contours in Fig. 5.4, for which we obtain $\chi_{\text{min}}^2 \approx 6.5$. This example illustrates the importance of the finite one-loop terms in the computation of $Z \rightarrow \ell\ell$ and $Z \rightarrow \nu\nu$, which have a non-negligible effect for the models aiming at explaining the B -physics anomalies. Finally, it should be noted that similar conclusions have been reached in Refs. [78, 81] in which the authors considered an ultraviolet complete scenario which includes vector LQ states.

5.6 On the Importance of $B_s - \bar{B}_s$ Mixing in S_1 & S_3

The oscillations or mixing of neutral mesons have played a crucial role in particle physics history. Since these processes convert a particle to its anti-particle or viceversa they are suitable to study matter anti-matter interaction, and thus explore CP violation effects that could explain the amount of matter nowadays. They are labeled as $\Delta F = 2$ processes, where $F = S$ for the strange quark in kaons and $F = B$ for the bottom quark in B -meson oscillation. They are loop-suppressed in the SM, and thus they are good observables for testing the presence of NP. Indeed, oscillations such as $K^0 - \bar{K}^0$ became also good test for the SM, allowing to predict the existence of the charm quark as well as the GIM mechanism. The oscillations with $\Delta B = 2$ $B - \bar{B}$ mixing and later on the $B_s - \bar{B}_s$ mixing were produced in the so called B factories, which in the same spirit as the kaon mixing, were measured experimentally having a little excess in

⁵Analytic expressions for the observables that do not appear in this Chapter are displayed in the Appendix E

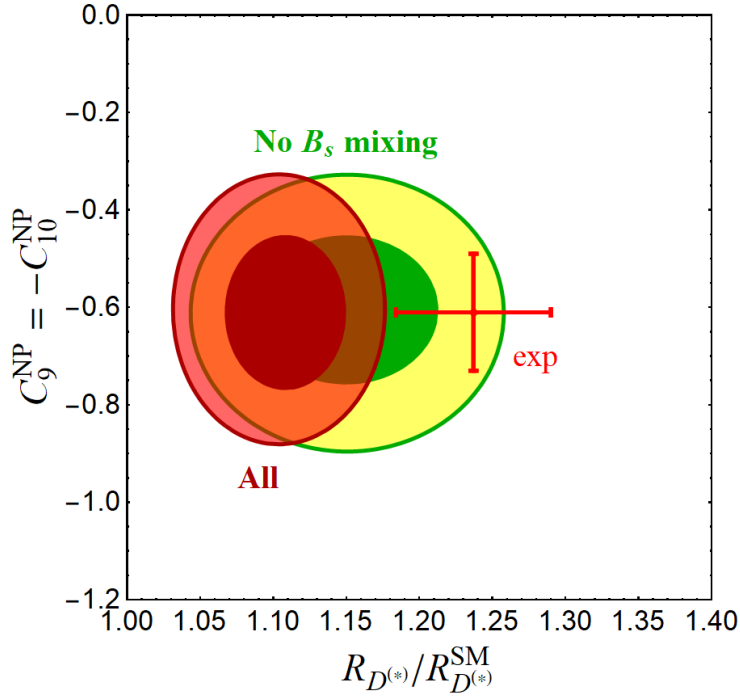


Figure 5.5: In (Dark)Red, results of the (1)2 σ low-energy fit considering the full Z -pole expressions and including $B_s - \bar{B}_s$ mixing, which are depicted in the plane $R_{D^{(*)}}/R_{D^{(*)}}^{\text{SM}}$ vs. $C_9^{\text{NP}} = -C_{10}^{\text{NP}}$. Leptoquark masses are fixed to $m_{S_1} = m_{S_3} = 2$ TeV and Yukawa couplings are scanned over the ranges described in the text. In the same plot we show the 1 and 2 σ results of the fit with the same colors described in Fig. 5.4.

ΔM_s respect to the SM. This fact allowed to predict for the first time the mass of the top quark. In models tested nowadays these observables impose huge constraints which have to be taken into account.

In the previous section we showed that including Z -pole observables in the fit computed at NLLA is quite relevant in order to improve the fit with respect to experimental data. However, the purpose of this section is to show that including the $B - \bar{B}$ mixing constraint in the fit it becomes impossible to explain the $b \rightarrow c\tau\nu$ anomalies with 2018 data. Indeed, in the previous chapters we saw that this observable is quite constraining and reduces a lot the available parameter space for NP. For this reason, we first write down the most general Yukawa setup in a S_1 & S_3 LQ scenario without couplings to the first generation.

$$y_{S_1}^L = \begin{pmatrix} 0 & 0 & 0 \\ 0 & y_{s\mu}^{S_1} & y_{s\tau}^{S_1} \\ 0 & y_{b\mu}^{S_1} & y_{b\tau}^{S_1} \end{pmatrix}, \quad y_{S_3}^L = \begin{pmatrix} 0 & 0 & 0 \\ 0 & y_{s\mu}^{S_3} & y_{s\tau}^{S_3} \\ 0 & y_{b\mu}^{S_3} & y_{b\tau}^{S_3} \end{pmatrix}, \quad (5.54)$$

On the other hand, the effective Hamiltonian for $B - \bar{B}$ mixing reads as in Sec. 3.2.3

$$\mathcal{H}_{B\bar{B}}^{\text{NP}} = C_{B\bar{B}}(\bar{s}_\alpha \gamma^\mu P_L b_\alpha) (\bar{s}_\beta \gamma^\mu P_L b_\beta), \quad (5.55)$$

where the WC is computed at the matching scale $\mu_{\text{LQ}} \sim \text{TeV}$. For this process in this model, there are two box diagrams with the single presence of S_1 , 4 diagrams with the single presence of S_3 , and 4 diagrams combining both S_1 and S_3 . Once performed the matching one obtains

$$C_{B\bar{B}}^{\text{NP}} = \frac{1}{128\pi^2 m_{S_1}^2} (y_{s\mu}^{S_1*} y_{b\mu}^{S_1} + y_{s\tau}^{S_1*} y_{b\tau}^{S_1})^2 + \frac{5}{128\pi^2 m_{S_3}^2} (y_{s\mu}^{S_3*} y_{b\mu}^{S_3} + y_{s\tau}^{S_3*} y_{b\tau}^{S_3})^2 \quad (5.56)$$

$$+ \frac{1}{32\pi^2 (m_{S_1}^2 - m_{S_3}^2)} (y_{s\mu}^{S_1*} y_{b\mu}^{S_3} + y_{s\tau}^{S_1*} y_{b\tau}^{S_3}) (y_{s\mu}^{S_3*} y_{b\mu}^{S_1} + y_{s\tau}^{S_3*} y_{b\tau}^{S_1}) \log\left(\frac{m_{S_1}}{m_{S_3}}\right),$$

which has to be compared with the experiment via

$$\frac{\Delta M_s^{\text{exp}}}{\Delta M_s^{\text{SM}}} = \left| 1 + \frac{C_{B\bar{B}}^{\text{NP}}(\mu_b)}{C_{B\bar{B}}^{\text{SM}}(\mu_b)} \right|, \quad (5.57)$$

that was already discussed in Chap. 3 in Sec. 3.2.3. Obtaining the following bound:

$$\frac{\Delta M_s^{\text{exp}}}{\Delta M_s^{\text{SM}}} = 0.98 \pm 0.02. \quad (5.58)$$

Returning to the illustration of the previous section, if we adopt the Yukawa pattern of (5.54), we can perform the same fit but now considering the $B_s - \bar{B}_s$ mixing. Interestingly, the minimum obtained now with the χ^2 minimization is $\chi_{\text{min}}^2 \simeq 13$ which is higher than the value obtained using Z -poles using the NLLA. In Fig. 5.5 we show in red the 1 and 2 σ regions of the fit superposed to the fit obtained in the previous section. Indeed this new fit is not able to explain $R_{D^{(*)}}$ anomaly (with 2018 data) even at 2 σ level with a purely left-handed scenario. This feature is also observed in other works of the literature such as in [71].

Therefore, one could introduce a right-handed coupling to c -quark τ -lepton in order to en-

hance the contribution to $R_{D^{(*)}}$ with scalar operators without spoiling any other observables considering in the fit. Nonetheless there are many other observables such as $\tau \rightarrow \mu\gamma$ which would become a relevant constraint to take into account

5.7 S_1 & S_3 Status After Moriond 2019

After the Moriond conference in 2019, a new measurement of R_K lowered the value of the best fit $C_9^{\text{NP}} = -C_{10}^{\text{NP}}$ but the discrepancy with respect to the SM remained the same because the error bars shrank. On the other hand, the world average of $R_{D^{(*)}}$ was updated due to a new measurement of BELLE experiment. As stated in Chapter 2, the tension with respect to the SM was reduced, and therefore it gave the possibility to reassess the viability of the S_1 & S_3 left-handed scenario. Here we present three models with different Yukawa patterns which became viable after Moriond 2019 reports. In this case we set the mass of both LQs to 1.5 TeV to ensure that we compare properly the 3 models. Moreover, for completion we use more observables in the fits, apart from the ones mentioned above, which are listed in Appendix E. The first scenario that we test is the one with the Yukawas in (5.54) which we used in 5.5 and 5.6 to illustrate the importance of the Z -pole and the $B_s - \bar{B}_s$ observables. We can see in Scenario 1 of Fig. 5.6 that the experimental value for $R_{D^{(*)}}$ is now lower than in the previous plot, and this allows the same model in the previous section to be 1σ compatible with data, even when $B_s - \bar{B}_s$ and more observables are considered in the fit (see Appendix E for details on all the observables).

The second scenario is inspired in [71], where its structure allows for an exact cancellation of the $B \rightarrow K\nu\bar{\nu}$ observable, namely

$$y_{S_1}^L = \begin{pmatrix} 0 & 0 & 0 \\ 0 & \lambda_{s\mu} & \lambda_{s\tau} \\ 0 & \lambda_{b\mu} & \lambda_{b\tau} \end{pmatrix}, \quad y_{S_3}^L = \begin{pmatrix} 0 & 0 & 0 \\ 0 & \lambda_{s\mu} & \lambda_{s\tau} \\ 0 & -\lambda_{b\mu} & -\lambda_{b\tau} \end{pmatrix}. \quad (5.59)$$

Looking at Scenario 2 of Fig. 5.6 we see that this model can also accommodate new data, while before the new results appeared it was not even compatible at 2σ level.

Finally, since muon couplings are basically included in order to generate contribution to $R_{K^{(*)}}$ which is only affected by S_3 at tree-level, in the third scenario we work with vanishing muon couplings for the S_1 leptoquark and without setting any particular correlation between

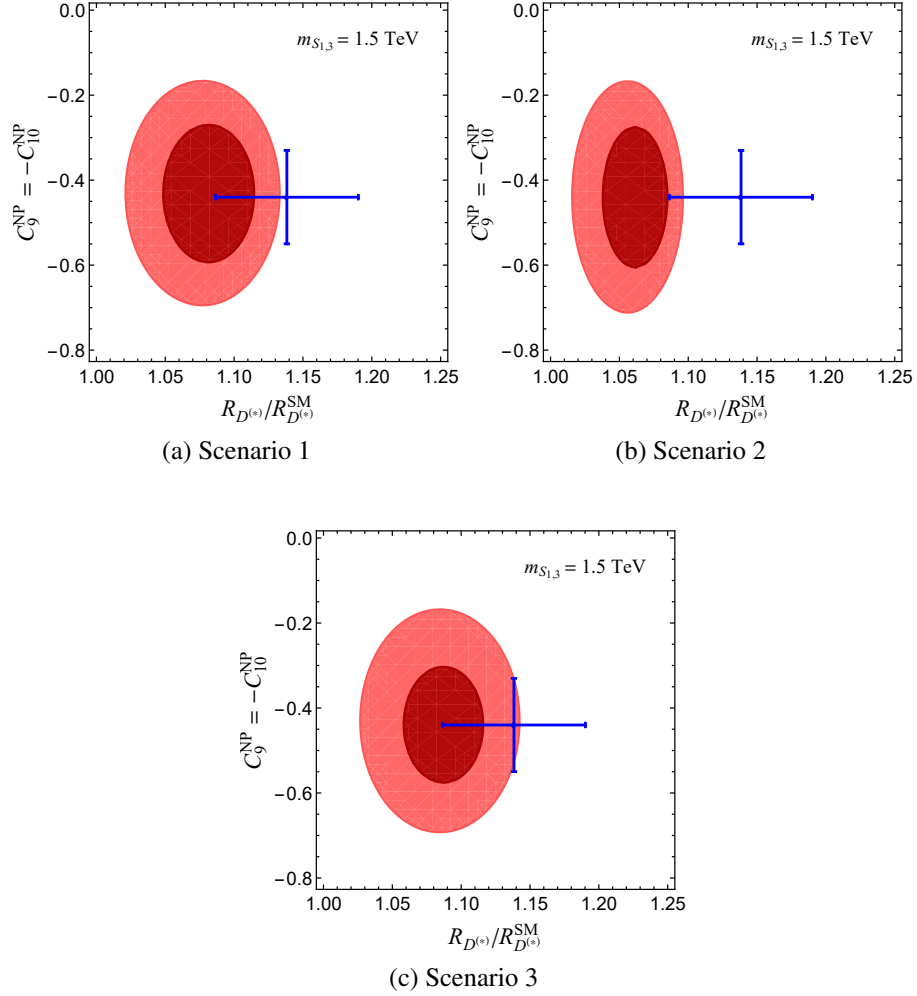


Figure 5.6: In (Dark)Red, results of the (1)2 σ low-energy fit considering the full Z -pole expressions and including $B_s - \bar{B}_s$ mixing, which are depicted in the plane $R_{D^{(*)}}/R_{D^{(*)}}^{SM}$ vs. $C_9^{NP} = -C_{10}^{NP}$. Leptoquark masses are fixed to $m_{S_1} = m_{S_3} = 1.5$ TeV and each best fit point is depicted in yellow. The three plots are obtained by fitting each model to all the observables of the tables in Appendix E

different couplings. The Yukawas in this case read

$$y_{S_1}^L = \begin{pmatrix} 0 & 0 & 0 \\ 0 & 0 & y_{s\tau}^{S_1} \\ 0 & 0 & y_{b\tau}^{S_1} \end{pmatrix}, \quad y_{S_3}^L = \begin{pmatrix} 0 & 0 & 0 \\ 0 & y_{s\mu}^{S_3} & y_{s\tau}^{S_3} \\ 0 & y_{b\mu}^{S_3} & y_{b\tau}^{S_3} \end{pmatrix}, \quad (5.60)$$

where in Scenario 3 of Fig. 5.6 we see that data is also well accommodated at 1σ and we do not need a new right-handed coupling to explain the anomalies.

In Appendix E we show the considered observables in every fit with their analytical expression, and write down the χ^2 value for each observable. This allows us to disentangle which observable can be important in the fit as well as which fit can handle more observables. In this case, since the last scenario does not impose any particular hierarchy between the Yukawas, we are able to explain the experimental values of 16 observables up to one sigma. Including the flavor anomalies.

Chapter 6

Two Higgs Doublet Model

Despite of the great success of the SM with the Higgs boson discovery at the LHC, the pending question of hierarchy of scales remains open and a quest for physics BSM continues. One of the minimalistic approaches to build a model of physics BSM is to extend the Higgs sector by introducing an extra Higgs doublet. This extension of the SM is called 2HDM.

The new particles arising in the 2HDM are additional Higgs bosons which are being searched in the LHC, specially the charged one. Including fermions in a 2HDM, results in a plethora of new parameters whose number is typically reduced by certain assumptions such as forbidding FCNCs at tree level as in the SM and imposing a softly broken \mathbb{Z}_2 symmetry on the Higgs doublets.

In this chapter, we do not aim to explain the anomalies, but rather to see the phenomenological implications of a 2HDM in $b \rightarrow s\mu^+\mu^-$ processes. Concretely we explore two observables such as $\text{Br}(B_s \rightarrow \mu^+\mu^-)^{2\text{HDM}}$ and $\text{Br}(B \rightarrow K\mu^+\mu^-)_{\text{high-}q^2}^{2\text{HDM}}$ which are very well measured experimentally and for which the theoretical control of the corresponding hadronic uncertainties is established by the lattice QCD computations [48]. For other observables the theoretical uncertainties are not as well assessed and one might run a risk of interpreting the unknown hadronic uncertainties as signals of physics BSM. We should also emphasize that in our scenarios we ignore the channels with electrons in the final state.

First we present the 2HDM and apply the general constraints, we then compute the effective coefficients of the $b \rightarrow s\mu^+\mu^-$ processes arising from the 2HDM. In Sec 6.5 we explore in detail the matching of the effective theory with the full theory and then we compare our Wilson coefficient results with Ref [238]. Then we proceed to evaluate phenomenologically different types of 2HDM with the abovementioned observables, and also including the possibility for

τ -lepton decays.

6.1 General Constraints on 2HDM

In this Section we remind the reader of the basic ingredients of 2HDM, enumerate the parameters of the model and list the main general constraints on the spectrum of scalars which are then used to perform a scan of allowed parameters to obtain the allowed ranges of the Higgs masses and couplings.

6.1.1 2HDM

We consider a general CP-conserving 2HDM with a softly broken \mathbb{Z}_2 symmetry. The most general potential can then be written as

$$V(\Phi_1, \Phi_2) = m_{11}^2 \Phi_1^\dagger \Phi_1 + m_{22}^2 \Phi_2^\dagger \Phi_2 + m_{12}^2 (\Phi_1^\dagger \Phi_2 + \Phi_2^\dagger \Phi_1) + \frac{\lambda_1}{2} (\Phi_1^\dagger \Phi_1)^2 + \frac{\lambda_2}{2} (\Phi_2^\dagger \Phi_2)^2 + \lambda_3 \Phi_1^\dagger \Phi_1 \Phi_2^\dagger \Phi_2 + \lambda_4 \Phi_1^\dagger \Phi_2 \Phi_2^\dagger \Phi_1 + \frac{\lambda_5}{2} \left[(\Phi_1^\dagger \Phi_2)^2 + (\Phi_2^\dagger \Phi_1)^2 \right], \quad (6.1)$$

where the term proportional to m_{12}^2 accounts for the soft breaking of \mathbb{Z}_2 .¹ The scalar doublets Φ_a ($a = 1, 2$) can be parameterized as

$$\Phi_a(x) = \begin{pmatrix} \phi_a^+(x) \\ \frac{1}{\sqrt{2}} [v_a + \rho_a(x) + i\eta_a(x)] \end{pmatrix}, \quad (6.2)$$

with $v_{1,2} \geq 0$ being the vacuum expectation values satisfying $v^{\text{SM}} = \sqrt{v_1^2 + v_2^2}$, already known from experiments, $v^{\text{SM}} = 246$ GeV. In the following, for notational simplicity, we will drop the argument of the Higgs fields. Two of the six fields are Goldstone bosons, while the remaining ones are four massive scalars: two CP-even states (h, H), one CP-odd state (A), and one charged

¹We remind the reader that the \mathbb{Z}_2 symmetry ($\Phi_1 \rightarrow \pm\Phi_1, \Phi_2 \rightarrow \mp\Phi_2$) of the Lagrangian forbids transitions $\Phi_1 \leftrightarrow \Phi_2$. Soft breaking of \mathbb{Z}_2 means that such transitions may occur only due to dimension-2 operators (terms proportional to m_{12}^2 in Eq. (6.1)) so that \mathbb{Z}_2 remains preserved at very short distances.

Higgs (H^\pm). These fields are defined as

$$\begin{pmatrix} \phi_1^+ \\ \phi_2^+ \end{pmatrix} = \begin{pmatrix} \cos \beta & -\sin \beta \\ \sin \beta & \cos \beta \end{pmatrix} \begin{pmatrix} G^+ \\ H^+ \end{pmatrix}, \quad \begin{pmatrix} \eta_1 \\ \eta_2 \end{pmatrix} = \begin{pmatrix} \cos \beta & -\sin \beta \\ \sin \beta & \cos \beta \end{pmatrix} \begin{pmatrix} G^0 \\ A \end{pmatrix}, \quad (6.3)$$

and

$$\begin{pmatrix} \rho_1 \\ \rho_2 \end{pmatrix} = \begin{pmatrix} \cos \alpha & -\sin \alpha \\ \sin \alpha & \cos \alpha \end{pmatrix} \begin{pmatrix} H \\ h \end{pmatrix}, \quad (6.4)$$

The mixing angles α and β satisfy

$$\tan \beta = \frac{v_2}{v_1}, \quad \tan 2\alpha = \frac{2(-m_{12}^2 + \lambda_{345}v_1v_2)}{m_{12}^2(v_2/v_1 - v_1/v_2) + \lambda_1v_1^2 - \lambda_2v_2^2}, \quad (6.5)$$

with $\lambda_{345} \equiv \lambda_3 + \lambda_4 + \lambda_5$. The masses of the physical scalars can be written in terms of parameters which appear in the potential as

$$m_H^2 = M^2 \sin^2(\alpha - \beta) + \left(\lambda_1 \cos^2 \alpha \cos^2 \beta + \lambda_2 \sin^2 \alpha \sin^2 \beta + \frac{\lambda_{345}}{2} \sin 2\alpha \sin 2\beta \right) v^2, \quad (6.6)$$

$$m_h^2 = M^2 \cos^2(\alpha - \beta) + \left(\lambda_1 \sin^2 \alpha \cos^2 \beta + \lambda_2 \cos^2 \alpha \sin^2 \beta - \frac{\lambda_{345}}{2} \sin 2\alpha \sin 2\beta \right) v^2, \quad (6.7)$$

$$m_A^2 = M^2 - \lambda_5 v^2, \quad (6.8)$$

$$m_{H^\pm}^2 = M^2 - \frac{\lambda_4 + \lambda_5}{2} v^2, \quad (6.9)$$

where the \mathbb{Z}_2 breaking term is now parameterized via $M^2 \equiv \frac{m_{12}^2}{\sin \beta \cos \beta}$. In the Yukawa sector, the \mathbb{Z}_2 symmetry becomes particularly important as it prevents the flavor changing processes to appear at tree level. Furthermore it enforces that each type of the right-handed fermion couples to a single Higgs doublet. Four choices are then possible and they are called Type I, II, X (Lepton Specific) and Z (Flipped) 2HDM [236].² To be more specific, we first write the

²The model that we call Type Z or Flipped 2HDM is sometimes referred to as Type Y.

Model	ζ_d	ζ_u	ζ_ℓ
Type I	$\cot \beta$	$\cot \beta$	$\cot \beta$
Type II	$-\tan \beta$	$\cot \beta$	$-\tan \beta$
Type X (lepton specific)	$\cot \beta$	$\cot \beta$	$-\tan \beta$
Type Z (flipped)	$-\tan \beta$	$\cot \beta$	$\cot \beta$

 Table 6.1: Couplings ζ_f in various types of 2HDM.

Yukawa Lagrangian as

$$\begin{aligned}
 \mathcal{L}_Y = & -\frac{\sqrt{2}}{v} H^+ \left\{ \bar{u} [\zeta_d V m_d P_R - \zeta_u m_u V P_L] d + \zeta_\ell \bar{\nu} m_\ell P_R \ell \right\} \\
 & -\frac{1}{v} \sum_{f, \varphi_i^0 \in \{h, H, A\}} \xi_f^{\varphi_i^0} \varphi_i^0 \left[\bar{f} m_f P_R f \right] + \text{h.c.}, \tag{6.10}
 \end{aligned}$$

where u and d stand for the up- and down-type quark, ℓ is a lepton flavor, f stands for a generic fermion, V for the CKM matrix, and $P_{L,R} = (1 \mp \gamma_5)/2$. A specific choice of parameters ζ_f corresponds to the above mentioned types of 2HDM, which we also summarize in Table 6.1. Notice that the couplings $\xi_f^{\varphi_i^0}$ appearing in the neutral Lagrangian part can be mapped onto the charged ones via

$$\begin{aligned}
 \xi_f^h &= \sin(\beta - \alpha) + \cos(\beta - \alpha) \zeta_f, \\
 \xi_f^H &= \cos(\beta - \alpha) - \sin(\beta - \alpha) \zeta_f, \\
 \xi_u^A &= -i \zeta_u, \quad \xi_{d,\ell}^A = i \zeta_{d,\ell}. \tag{6.11}
 \end{aligned}$$

6.1.2 General Constraints and Scan of Parameters

To perform a thorough scan of scalars in a general 2HDM we use the general constraints summarized below.

- **Stability:**

To ensure that the scalar potential is bounded from below, the quartic couplings should satisfy the relations [239]

$$\lambda_{1,2} > 0, \quad \lambda_3 > -(\lambda_1\lambda_2)^{1/2}, \quad \text{and} \quad \lambda_3 + \lambda_4 - |\lambda_5| > -(\lambda_1\lambda_2)^{1/2}. \quad (6.12)$$

Furthermore, the stability of the EW vacuum implies that

$$m_{11}^2 + \frac{\lambda_1 v_1^2}{2} + \frac{\lambda_3 v_2^2}{2} = \frac{v_2}{v_1} \left[m_{12}^2 - (\lambda_4 + \lambda_5) \frac{v_1 v_2}{2} \right], \quad (6.13)$$

$$m_{22}^2 + \frac{\lambda_2 v_2^2}{2} + \frac{\lambda_3 v_1^2}{2} = \frac{v_1}{v_2} \left[m_{12}^2 - (\lambda_4 + \lambda_5) \frac{v_1 v_2}{2} \right], \quad (6.14)$$

which then allows us to express m_{11}^2 and m_{22}^2 in terms of the soft \mathbb{Z}_2 breaking term m_{12}^2 and the quartic couplings λ_{1-5} . These constraints should be combined with the necessary and sufficient condition that the minimum developed at (v_1, v_2) is global [240]:

$$m_{12}^2 \left(m_{11}^2 - m_{22}^2 \sqrt{\lambda_1/\lambda_2} \right) \left(\tan \beta - \sqrt[4]{\lambda_1/\lambda_2} \right) > 0. \quad (6.15)$$

- **Perturbative Unitarity:**

An important constraint on the spectrum of scalars within 2HDM stems from the unitarity requirement of the S -wave component of the scalar scattering amplitudes. That condition implies the following inequalities [241, 242]

$$|a_{\pm}|, |b_{\pm}|, |c_{\pm}|, |f_{\pm}|, |e_{1,2}|, |f_1|, |p_1| < 8\pi, \quad (6.16)$$

where

$$\begin{aligned} a_{\pm} &= \frac{3}{2}(\lambda_1 + \lambda_2) \pm \sqrt{\frac{9}{4}(\lambda_1 - \lambda_2)^2 + (2\lambda_3 + \lambda_4)^2}, \\ b_{\pm} &= \frac{1}{2}(\lambda_1 + \lambda_2) \pm \frac{1}{2}\sqrt{(\lambda_1 - \lambda_2)^2 + 4\lambda_4^2}, \\ c_{\pm} &= \frac{1}{2}(\lambda_1 + \lambda_2) \pm \frac{1}{2}\sqrt{(\lambda_1 - \lambda_2)^2 + 4\lambda_5^2}, \\ e_1 &= \lambda_3 + 2\lambda_4 - 3\lambda_5, & e_2 &= \lambda_3 - \lambda_5, \\ f_+ &= \lambda_3 + 2\lambda_4 + 3\lambda_5, & f_- &= \lambda_3 + \lambda_5, \\ f_1 &= \lambda_3 + \lambda_4, & p_1 &= \lambda_3 - \lambda_4. \end{aligned} \quad (6.17)$$

• **EW Precision Tests:**

Finally, the additional scalars contribute to the gauge boson vacuum polarization. As a result, the EW precision data provide important constraint. In particular the T parameter bounds the mass splitting between m_H and m_{H^\pm} in the scenario in which h is identified with the SM-like Higgs, cf. Ref. [243] for example. The general expressions for the parameters S , T and U in 2HDM can be found in Ref. [244]. To derive the bounds on the scalar spectrum we consider the following values and the corresponding correlation matrix [245],

$$\begin{aligned} \Delta S^{\text{SM}} &= 0.05 \pm 0.11, \\ \Delta T^{\text{SM}} &= 0.09 \pm 0.13, \\ \Delta U^{\text{SM}} &= 0.01 \pm 0.11, \end{aligned} \quad \text{corr} = \begin{pmatrix} 1 & 0.90 & -0.59 \\ 0.90 & 1 & -0.83 \\ -0.59 & -0.83 & 1 \end{pmatrix}. \quad (6.18)$$

The χ^2 function is then expressed as

$$\chi^2 = \sum_{i,j} (X_i - X_i^{\text{SM}})(\sigma^2)_{ij}^{-1}(X_j - X_j^{\text{SM}}), \quad (6.19)$$

where the vector of central values and uncertainties are denoted as $X = (\Delta S, \Delta T, \Delta U)$ and $\sigma = (0.11, 0.13, 0.11)$, while the elements of the covariance matrix are obtained via $\sigma_{ij}^2 \equiv \sigma_i \text{corr}_{ij} \sigma_j$.

As mentioned above, we identify the lightest CP-even state h with the SM-like scalar observed at the LHC with mass $m_h = 125.10(14)$ GeV [152]. To forbid the dangerous decays $h \rightarrow AA$ which could over-saturate the total width of h ($\simeq \Gamma_h^{\text{SM}}$), we assume that $m_A > m_h/2$. Moreover, we impose the alignment condition $|\cos(\beta - \alpha)| \leq 0.3$, in order to ensure that the couplings of h to $V = W, Z$ remain consistent with the values measured so far, which appear to be in good agreement with the SM predictions [246, 247]. The constraints are then imposed onto a set of randomly generated points in the intervals:

$$\begin{aligned} \tan \beta &\in (0.2, 50), & \alpha &\in \left(-\frac{\pi}{2}, \frac{\pi}{2}\right), & |M^2| &\leq (1.2 \text{ TeV})^2, \\ m_{H^\pm} &\in (m_W, 1.2 \text{ TeV}), & m_H &\in (m_h, 1.2 \text{ TeV}), & m_A &\in (m_h/2, 1.2 \text{ TeV}). \end{aligned} \quad (6.20)$$

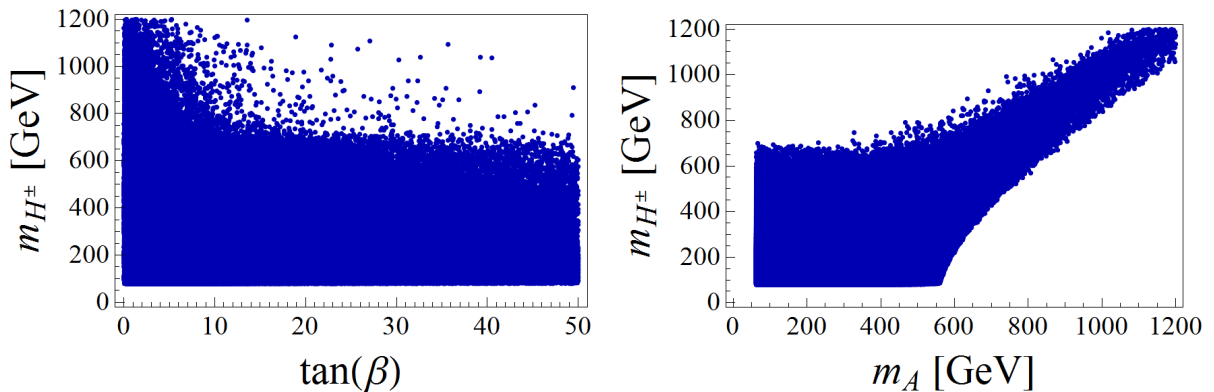


Figure 6.1: Results of the scan described in the text.

A scan of parameters consistent with the constraints listed above favors the moderate and small values of $\tan \beta \in (0.2, 15]$. In order to access large $\tan \beta$ values, and in addition to the free scan, we perform a second scan with $m_H \approx |M|$, which helps us probing higher values of $\tan \beta$, and we then combine results of both scans. The combined results are shown in Fig. 6.1 in two planes, $(\tan \beta, m_{H^\pm})$ and (m_A, m_{H^\pm}) . From the right panel of Fig. 6.1 we observe that the additional scalars become mass degenerate in the decoupling region ($M^2 \gg v^2$), as it can be easily deduced from Eqs. (6.6)–(6.9). We should also emphasize that the results of our scans agree with what has been previously reported in the literature, cf. [248, 249, 250, 251].

In Sec. 6.7 we will confront the points allowed by our scan with the experimental measurements of exclusive $b \rightarrow s$ decays.

6.2 Effective Hamiltonian

The most general effective Hamiltonian describing the $b \rightarrow s\ell\ell$ transitions, made of dimension six operators, is given by Eq. 4.2

$$\mathcal{H}_{\text{eff}} = -\frac{4G_F}{\sqrt{2}} V_{tb} V_{ts}^* \sum_i \left(C_i \mathcal{O}_i + C'_i \mathcal{O}'_i \right) + \text{h.c.} \quad (6.21)$$

The dimension six operators appearing in this Hamiltonian are sufficient to match the one-loop amplitude when the external fermion momenta are neglected. This, however, is not true if the computation is made with external momenta different from zero which is, in general, necessary when dealing with (pseudo-)scalar operators. For example, in order to get a correct expression

for the Wilson coefficient C_P one needs to consider the external momenta, which then leads to $C_P \propto m_\ell m_b / m_W^2$, c.f. [238]. We therefore need to select all situations in which one can obtain the terms of the form $(m_\ell m_b / m_W^2) \mathcal{O}_P$, such as

$$\frac{e^2}{(4\pi)^2} \frac{m_\ell}{m_W^2} (\bar{s} \not{q} P_i b) (\bar{\ell} P_j \ell), \quad \text{or} \quad \frac{e^2}{(4\pi)^2} \frac{m_b}{m_W^2} (\bar{s} P_i b) (\bar{\ell} \not{q} P_j \ell), \quad (6.22)$$

which can obviously be reduced to $(m_\ell m_b / m_W^2) \mathcal{O}_P$. As an example,

$$\begin{aligned} \frac{\alpha}{4\pi} \frac{m_\ell}{m_W^2} (\bar{s} \not{q} P_L b) (\bar{\ell} \gamma_5 \ell) &= \frac{\alpha}{4\pi} \frac{m_\ell m_b}{m_W^2} (\bar{s} P_R b) (\bar{\ell} \gamma_5 \ell) - \frac{\alpha}{4\pi} \frac{m_\ell m_s}{m_W^2} (\bar{s} P_L b) (\bar{\ell} \gamma_5 \ell) \\ &= \frac{m_\ell m_b}{m_W^2} \mathcal{O}_P - \frac{m_\ell m_s}{m_W^2} \mathcal{O}'_P \simeq \frac{m_\ell m_b}{m_W^2} \mathcal{O}_P. \end{aligned} \quad (6.23)$$

A complication arises when encountering the operators with insertion of $\not{p}_b + \not{p}_s$ in the leptonic current, with the convention $b(p_b) \rightarrow s(p_s) \ell^-(p_-) \ell^+(p_+)$, where we also use $q = p_b - p_s = p_+ + p_-$. A way to deal with that, adopted in Ref. [238], consists in setting $p_s = 0$, so that $\not{p}_b + \not{p}_s = \not{q} + 2\not{p}_s = \not{q} = \not{p}_+ + \not{p}_-$, and in this way one can again, like in the previous example, use the equations of motion. That way to deal with the problem in hands, however, leads to an incomplete expression for C_P , for example. If, instead, one keeps all the momenta non-zero, we get a complete result. At this point we just emphasize that the matching should be performed by keeping all the external momenta different from zero and the contributions stemming from dimension-seven operators can be neglected at the very end of computation. We further elucidate this problem in Sec. 6.5 where we also propose a general framework for the appropriate matching between the full and effective theories in a case in which the (pseudo-)scalar bosons are explicitly taken into account. Before closing this section we could also argue that a term $(m_\ell m_b / m_W^2) \mathcal{O}_P$ could be obtained from the dimension-eight operators such as,

$$\frac{\alpha}{4\pi} \frac{1}{m_W^2} \left(\bar{s} (\not{p}_+ - \not{p}_-) P_i b \right) \left(\bar{\ell} (\not{p}_b + \not{p}_s) P_j \ell \right). \quad (6.24)$$

Such terms, however, never appear in our calculations and we will limit our discussion to the dimension-seven operators only.

6.3 Wilson coefficients

After unambiguously matching the full with the effective theories we obtain the one-loop expressions for the Wilson coefficients generated by the additional scalar particles. We summarize our results in this Section. For clarity we will write them as,

$$C_7 = C_7^{\text{NP},\gamma}, \quad (6.25)$$

$$C_9 = C_9^{\text{NP},\gamma} + C_9^{\text{NP},Z}, \quad (6.26)$$

$$C_{10} = C_{10}^{\text{NP},Z}, \quad (6.27)$$

$$C_P = C_P^{\text{NP},\text{box}} + C_P^{\text{NP},Z} + C_P^{\text{NP},A} \quad (6.28)$$

$$C_S = C_S^{\text{NP},\text{box}} + C_S^{\text{NP},h} + C_S^{\text{NP},H} \quad (6.29)$$

where the superscripts denote the types of diagrams that contributes to a given Wilson coefficient, namely, the box diagrams, the γ , Z -penguins and the (pseudo-)scalar penguins. These coefficients should be added to the (effective) ones obtained in the SM: $C_7 = -0.304$, $C_9 = 4.211$, $C_{10} = -4.103$, and $C_{S,P} \simeq 0$ [252].³

Henceforth, we neglect the s -quark mass and give all our results in the unitary gauge. To check the consistency of our formulas, we also performed the computation in the Feynman gauge. In the remainder of this Section we present our resulting expressions for each of the coefficients appearing in Eqs. (6.27)–(6.29). We use the standard notation,

$$x_q = \frac{m_q^2}{m_W^2}, \quad x_{H^\pm} = \frac{m_{H^\pm}^2}{m_W^2}, \quad x_{\varphi_i^0} = \frac{m_{\varphi_i^0}^2}{m_W^2}, \quad (6.30)$$

where $q \in \{b, t\}$, and $\varphi_i^0 \in \{h, H, A\}$.

6.3.1 γ -penguins in 2HDM

The γ -penguin diagrams induced by the charged Higgs are shown in Fig. 6.2. The off-shell and on-shell contributions can be matched onto the Wilson coefficients C_7 and C_9 , respectively, we obtain,

³Special attention should be paid to the scalar penguin with the SM-like Higgs to avoid the double counting since it also appears with modifications in aligned-2HDM.

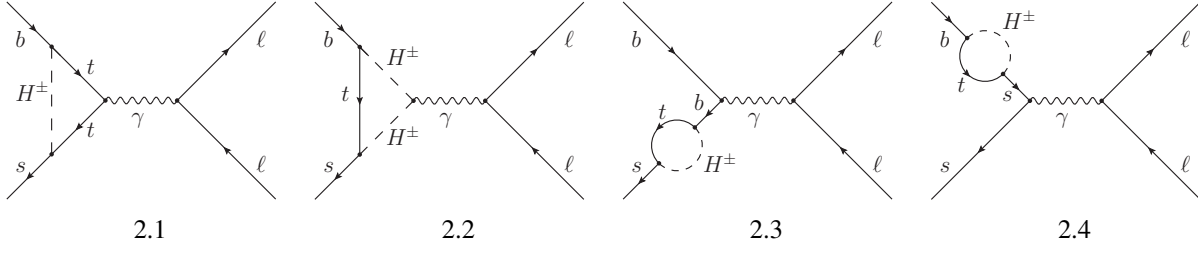
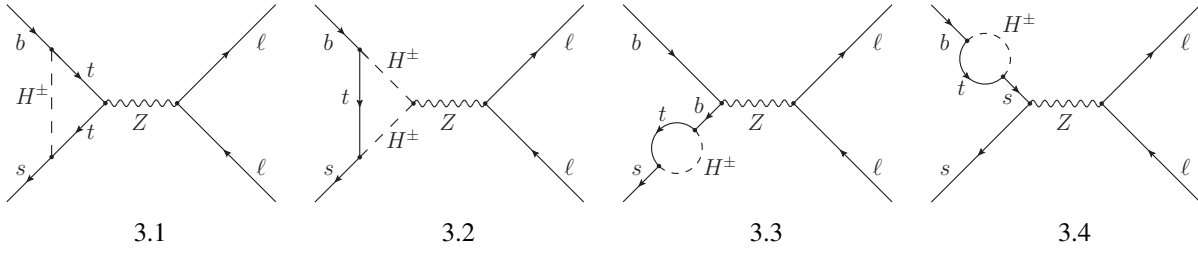


Figure 6.2: Photon penguin diagrams generated by the charged Higgs bosons.


 Figure 6.3: Z penguin diagrams generated by the additional scalars.

$$\begin{aligned}
 C_7^{\text{NP},\gamma} = & -|\zeta_u|^2 \frac{x_t}{72} \left[\frac{7x_{H^\pm}^2 - 5x_{H^\pm}x_t - 8x_t^2}{(x_{H^\pm} - x_t)^3} + \frac{6x_{H^\pm}x_t(3x_t - 2x_{H^\pm})}{(x_{H^\pm} - x_t)^4} \log\left(\frac{x_{H^\pm}}{x_t}\right) \right] \\
 & - \zeta_u^* \zeta_d \frac{x_t}{12} \left[\frac{3x_{H^\pm} - 5x_t}{(x_t - x_{H^\pm})^2} + \frac{2x_{H^\pm}(3x_t - 2x_{H^\pm})}{(x_t - x_{H^\pm})^3} \log\left(\frac{x_t}{x_{H^\pm}}\right) \right], \quad (6.31)
 \end{aligned}$$

and

$$\begin{aligned}
 C_9^{\text{NP},\gamma} = & |\zeta_u|^2 \frac{x_t}{108} \left[\frac{38x_{H^\pm}^2 - 79x_{H^\pm}x_t + 47x_t^2}{(x_{H^\pm} - x_t)^3} - \frac{6(4x_{H^\pm}^3 - 6x_{H^\pm}^2x_t + 3x_t^3)}{(x_{H^\pm} - x_t)^4} \log\left(\frac{x_{H^\pm}}{x_t}\right) \right] \\
 & + \zeta_u^* \zeta_d \frac{x_t x_b}{108} \left[\frac{-37x_{H^\pm}^2 + 8x_{H^\pm}x_t + 53x_t^2}{(x_{H^\pm} - x_t)^4} + \frac{6(2x_{H^\pm}^3 + 6x_{H^\pm}^2x_t - 9x_{H^\pm}x_t^2 - 3x_t^3)}{(x_{H^\pm} - x_t)^5} \log\left(\frac{x_{H^\pm}}{x_t}\right) \right]. \quad (6.32)
 \end{aligned}$$

The dominant terms in both $C_7^{\text{NP},\gamma}$ and $C_9^{\text{NP},\gamma}$ come from the top quark contribution and are proportional to $|\zeta_u|^2$. The terms proportional to $\zeta_u^* \zeta_d$ are suppressed by m_b^2 , thus indeed subdominant.

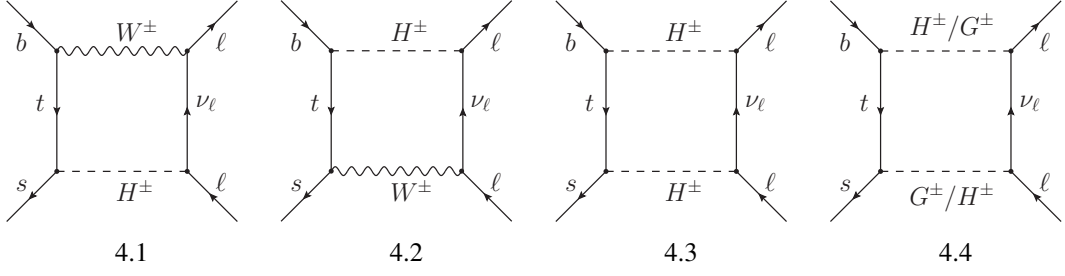


Figure 6.4: Box diagrams generated by the additional scalars.

6.3.2 Z -penguins in 2HDM

The Z -penguin diagrams contribute significantly to the Wilson coefficients C_P , C_9 and C_{10} through the diagrams shown in Fig. 6.3. The leading order expressions for C_9 and C_{10} read

$$C_9^{\text{NP},Z} = C_{10}^{\text{NP},Z}(-1 + 4 \sin^2 \theta_W), \quad (6.33)$$

$$C_{10}^{\text{NP},Z} = |\zeta_u|^2 \frac{x_t^2}{8 \sin^2 \theta_W} \left[\frac{1}{x_{H^\pm} - x_t} - \frac{x_{H^\pm}}{(x_{H^\pm} - x_t)^2} \log \left(\frac{x_{H^\pm}}{x_t} \right) \right] + \zeta_u^* \zeta_d \frac{x_t x_b}{16 \sin^2 \theta_W} \left[\frac{x_{H^\pm} + x_t}{(x_{H^\pm} - x_t)^2} - \frac{2x_t x_{H^\pm}}{(x_{H^\pm} - x_t)^3} \log \left(\frac{x_{H^\pm}}{x_t} \right) \right]. \quad (6.34)$$

Similarly, for C_P we obtain,

$$C_P^{\text{NP},Z} = \zeta_u^* \zeta_d \frac{\sqrt{x_b x_\ell} x_t}{16 \sin^2 \theta_W} \left[\frac{x_t - 3x_{H^\pm}}{(x_{H^\pm} - x_t)^2} + \frac{2x_{H^\pm}^2}{(x_{H^\pm} - x_t)^3} \log \left(\frac{x_{H^\pm}}{x_t} \right) \right] \quad (6.35)$$

$$+ |\zeta_u|^2 \frac{\sqrt{x_b x_\ell} x_t}{216} \left\{ \frac{38x_{H^\pm}^2 + 54x_{H^\pm}^2 x_t - 79x_{H^\pm} x_t - 108x_{H^\pm} x_t^2 + 47x_t^2 + 54x_t^3}{(x_{H^\pm} - x_t)^3} \right. \quad (6.36)$$

$$\left. - \frac{6(4x_{H^\pm}^3 + 9x_{H^\pm}^3 x_t - 6x_{H^\pm}^2 x_t - 18x_{H^\pm}^2 x_t^2 + 9x_{H^\pm} x_t^3 + 3x_t^3)}{(x_{H^\pm} - x_t)^4} \log \left(\frac{x_{H^\pm}}{x_t} \right) \right. \quad (6.37)$$

$$\left. - \frac{3}{2 \sin^2 \theta_W} \left[\frac{2x_{H^\pm}^2 + 36x_{H^\pm}^2 x_t - 7x_{H^\pm} x_t - 72x_{H^\pm} x_t^2 + 11x_t^2 + 36x_t^3}{(x_{H^\pm} - x_t)^3} \right. \right. \quad (6.38)$$

$$\left. \left. - \frac{6x_t(6x_{H^\pm}^3 - 12x_{H^\pm}^2 x_t + 6x_{H^\pm} x_t^2 + x_t^2)}{(x_{H^\pm} - x_t)^4} \log \left(\frac{x_{H^\pm}}{x_t} \right) \right] \right\}. \quad (6.39)$$

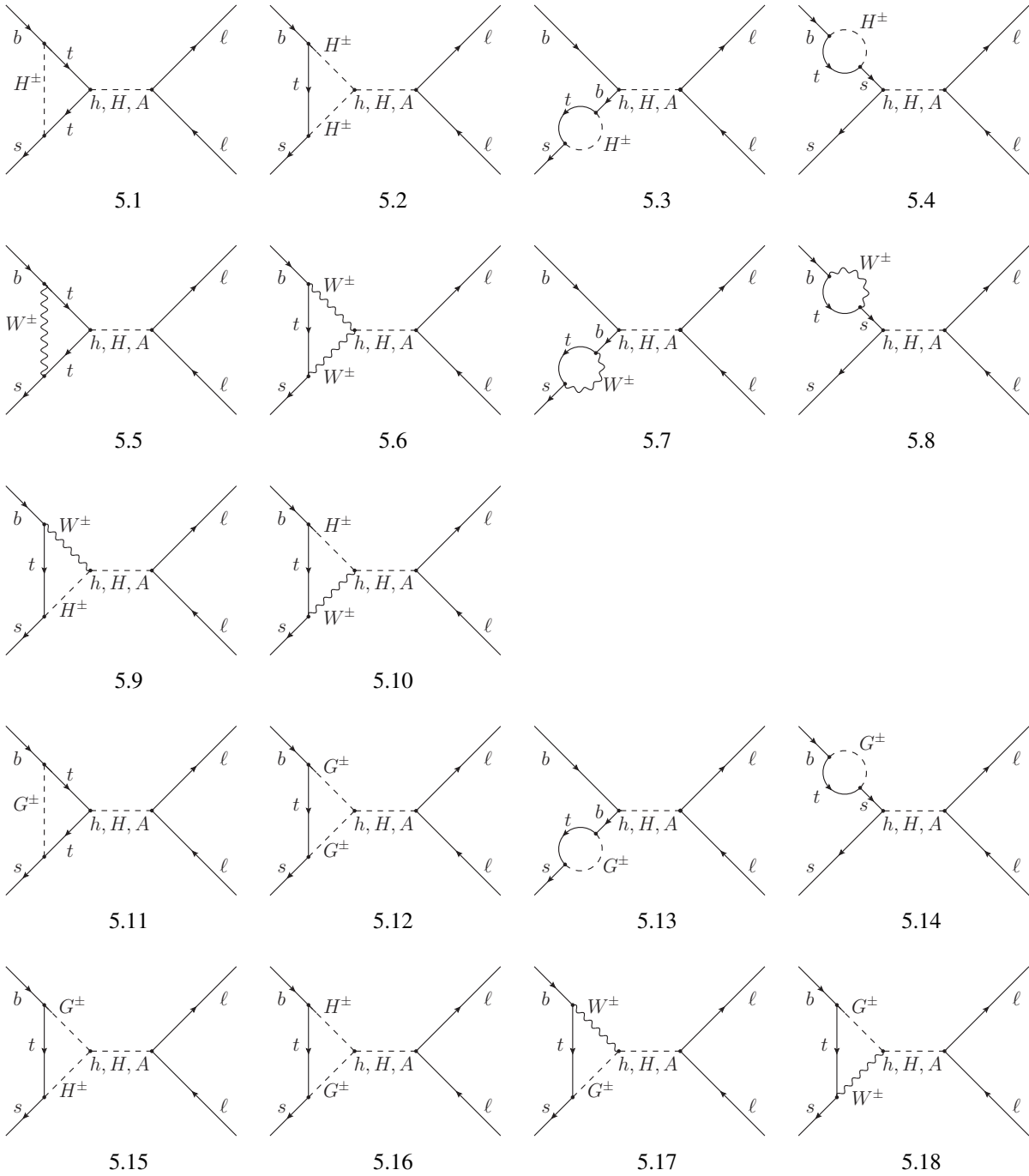


Figure 6.5: Higgs penguin diagrams generated by the additional scalars.

6.3.3 Charged Higgs Boxes in 2HDM

The box diagrams, peculiar for 2HDM, are drawn in Fig. 6.4. At low-energy they contribute to the Wilson coefficients C_S and C_P as,

$$\begin{aligned}
C_S^{\text{NP, box}} = & \frac{\sqrt{x_\ell x_b} x_t}{8(x_{H^\pm} - x_t) \sin^2 \theta_W} \left\{ \zeta_\ell \zeta_u^* \left(\frac{x_t}{x_t - 1} \log x_t - \frac{x_{H^\pm}}{x_{H^\pm} - 1} \log x_{H^\pm} \right) \right. \\
& + \zeta_u \zeta_\ell^* \left[1 - \frac{x_{H^\pm} - x_t^2}{(x_{H^\pm} - x_t)(x_t - 1)} \log x_t - \frac{x_{H^\pm}(x_t - 1)}{(x_{H^\pm} - x_t)(x_{H^\pm} - 1)} \log x_{H^\pm} \right] \\
& \left. + 2\zeta_d \zeta_\ell^* \log \left(\frac{x_t}{x_{H^\pm}} \right) \right\}, \quad (6.40)
\end{aligned}$$

and

$$\begin{aligned}
C_P^{\text{NP, box}} = & \frac{\sqrt{x_\ell x_b} x_t}{8(x_{H^\pm} - x_t) \sin^2 \theta_W} \left\{ \zeta_\ell \zeta_u^* \left(\frac{x_t}{x_t - 1} \log x_t - \frac{x_{H^\pm}}{x_{H^\pm} - 1} \log x_{H^\pm} \right) \right. \\
& - \zeta_u \zeta_\ell^* \left[1 - \frac{x_{H^\pm} - x_t^2}{(x_{H^\pm} - x_t)(x_t - 1)} \log x_t - \frac{x_{H^\pm}(x_t - 1)}{(x_{H^\pm} - x_t)(x_{H^\pm} - 1)} \log x_{H^\pm} \right] \\
& \left. - 2\zeta_d \zeta_\ell^* \log \left(\frac{x_t}{x_{H^\pm}} \right) \right\}. \quad (6.41)
\end{aligned}$$

In addition to $C_{S,P}^{\text{NP, box}}$, the tensor and (axial-)vector operators receive contributions but suppressed by the lepton mass, i.e. by $x_\ell = m_\ell^2/m_W^2$. These coefficients are negligible even for decays with τ 's in the final state as it can be verified by using the expressions we provide in Appendix F.2.

6.3.4 Scalar penguins in 2HDM

We now turn to the effective coefficients $C_P^{\text{NP, A}}$, $C_S^{\text{NP, h}}$ and $C_S^{\text{NP, H}}$, generated by the scalar penguin diagrams shown in Fig. 6.5. We recall that the total ultraviolet divergence coming from these diagrams is proportional to the factor $(1 + \zeta_u \zeta_d)(\zeta_u - \zeta_d)$, which vanishes due to the \mathbb{Z}_2 symmetry (cf. Table 6.1).⁴

The penguins with the CP-odd Higgs give rise to,

⁴Notice that this is not true in general. For instance, in the aligned-2HDM the divergences are canceled by contributions coming from the radiatively induced misalignment of the Yukawa matrices. The alignment is only preserved at all scales in the context of \mathbb{Z}_2 -symmetric models [238].

$$\begin{aligned}
 C_P^{\text{NP}, A} = & -\frac{\sqrt{x_\ell x_b} \zeta_\ell x_t}{\sin^2 \theta_W 2x_A} \left\{ \frac{\zeta_u^3 x_t}{2} \left[\frac{1}{x_{H^\pm} - x_t} - \frac{x_{H^\pm}}{(x_{H^\pm} - x_t)^2} \log \left(\frac{x_{H^\pm}}{x_t} \right) \right] \right. \\
 & + \frac{\zeta_u}{4} \left[-\frac{3x_{H^\pm} x_t - 6x_{H^\pm} - 2x_t^2 + 5x_t}{(x_t - 1)(x_{H^\pm} - x_t)} + \frac{x_{H^\pm}(x_{H^\pm}^2 - 7x_{H^\pm} + 6x_t)}{(x_{H^\pm} - x_t)^2(x_{H^\pm} - 1)} \log x_{H^\pm} \right. \\
 & \left. \left. - \frac{x_{H^\pm}^2(x_t^2 - 2x_t + 4) + 3x_t^2(2x_t - 2x_{H^\pm} - 1)}{(x_{H^\pm} - x_t)^2(x_t - 1)^2} \log x_t \right] \right\}, \quad (6.42)
 \end{aligned}$$

where we used that $\zeta_f \in \mathbb{R}$, and $(1 + \zeta_u \zeta_d)(\zeta_u - \zeta_d) = 0$. Similarly, the penguins with the CP-even Higgs lead to:

$$\begin{aligned}
 C_S^{\text{NP}, h} = & \frac{\sqrt{x_\ell x_b} x_t}{\sin^2 \theta_W 2x_h} [\sin(\beta - \alpha) + \cos(\beta - \alpha)\zeta_\ell] \\
 & \times \left[g_1 \sin(\beta - \alpha) + g_2 \cos(\beta - \alpha) - g_0 \frac{2v^2}{m_W^2} \lambda_{H^+H^-}^h \right], \\
 C_S^{\text{NP}, H} = & \frac{\sqrt{x_\ell x_b} x_t}{\sin^2 \theta_W 2x_H} [\cos(\beta - \alpha) - \sin(\beta - \alpha)\zeta_\ell] \\
 & \times \left[g_1 \cos(\beta - \alpha) - g_2 \sin(\beta - \alpha) - g_0 \frac{2v^2}{m_W^2} \lambda_{H^+H^-}^H \right], \quad (6.43)
 \end{aligned}$$

where $\lambda_{H^+H^-}^i$ are the trilinear couplings defined in Appendix F.3. The functions $g_{0,1,2}$ are given in Appendix F.2 along with the amplitudes generated by each of the diagrams shown in Fig. 6.5.

6.4 Comparison with Other Computations

In this Section we compare our Wilson coefficients with the results obtained in previous studies. Before doing so we should emphasize the novelties of this work:

- (i) The result for C_9 in a general 2HDM with a \mathbb{Z}_2 symmetry is new;
- (ii) The subleading terms $\mathcal{O}(m_b)$ to $C_{9,10}$ have been neglected in the previous computations, and they are included here;

- (iii) We provided an independent computation of the coefficients C_S and C_P , and elucidate inconsistencies present in Ref. [238], cf. Sec. 6.5 where we propose a general prescription for matching procedure when the external momenta are not neglected.

The effective coefficients C_S and C_P , in the context of Type II 2HDM, were first computed in Refs. [253, 254, 255, 256, 257, 258]. In these papers $\tan\beta$ was assumed to be very large, which considerably simplifies the computation because in that case only the box diagrams give significant contributions. We agree with these results if we keep only the leading terms in $\tan\beta$ in our expressions. Along the same lines, the leading order QCD corrections to the same coefficients were included in Ref. [259].

Recently, the computation of C_S and C_P was extended to the context of a general aligned-2HDM, which comprises all four types of 2HDM with \mathbb{Z}_2 symmetry discussed here but without the usual assumption of large $\tan\beta$ [238]. We agree with their general results, except for the expression for $C_P^{\text{NP},Z}$ which differs from the one reported in the present paper. The disagreement comes from the fact that the authors of Ref. [238] worked with the assumption $p_s = 0$, which appears not to be fully appropriate.⁵ By keeping $p_s \neq 0$ one realizes that the computation of Z -penguin leads to two independent terms, one proportional to $p_H = p_b + p_s$ and the other to $q = p_b - p_s$. By using equations of motion, $C_{P,S}$ correctly receive contributions from the terms proportional to q , but not from those proportional to p_H . With $p_s = 0$ only one invariant appears, because $p_H \equiv q$, and thus the resulting $C_{P,S}$ also receive spurious contributions from p_H .

Regarding the other Wilson coefficients, the first computations of C_7 for a general 2HDM have been performed in Ref. [145], then in Refs. [260, 261] and [262] where the leading and subleading QCD corrections were included too. Our results are consistent with those, as well as with the expression for C_{10} presented in Ref. [257] and more recently in Ref. [238]. The only difference with respect to those results is that we include the subleading terms in m_b .

6.5 Matching Procedure

In this section we discuss in more detail the matching of the one-loop amplitudes when the nonzero external momenta are considered. We stress once again that keeping external momenta

⁵We should emphasize that we were able to reproduce the expression for $C_P^{\text{NP},Z}$ reported in Ref. [238] by taking $p_s = 0$.

non-zero is necessary to obtain the correct values for the Wilson coefficients $C_{S,P}$. As we mentioned in Sec. 6.2 the insertion of external momenta result in dimension-seven operators which can be simplified by using equations of motion, except in the cases when the lepton momenta are to be contracted with the quark current and/or the quark momenta to be contracted with the lepton current. The amplitudes which need a special treatment, which give rise to the terms $\propto m_\ell m_b/m_W^2$, are:

$$\begin{aligned}\mathcal{A}_{ij}^\ell &= \frac{\alpha}{4\pi} \frac{1}{m_W} (\bar{s}(\not{p}_- - \not{p}_+)P_i b)(\bar{\ell}P_j \ell), & \mathcal{A}_{ij}^q &= \frac{\alpha}{4\pi} \frac{1}{m_W} (\bar{s}P_i b)(\bar{\ell}(\not{p}_b + \not{p}_s)P_j \ell), \\ \mathcal{A}_{ij}^{V\ell} &= \frac{\alpha}{4\pi} \frac{1}{m_W} (\bar{s}(\not{p}_- - \not{p}_+)\gamma_\mu P_i b)(\bar{\ell}\gamma^\mu P_j \ell), & \mathcal{A}_{ij}^{Vq} &= \frac{\alpha}{4\pi} \frac{1}{m_W} (\bar{s}\gamma_\mu P_i b)(\bar{\ell}(\not{p}_b + \not{p}_s)\gamma^\mu P_j \ell),\end{aligned}\tag{6.44}$$

where $i, j = L, R$ and s, b, ℓ are the fermion spinors. Note again that our convention is $b(p_b) \rightarrow s(p_s)\ell^-(p_-)\ell^+(p_+)$, and $q = p_b - p_s = p_+ + p_-$. In our calculation, specifically, the amplitude \mathcal{A}_{ij}^q appears in the computation of the Z -penguin diagrams, while we find \mathcal{A}_{ij}^ℓ and \mathcal{A}_{ij}^{Vq} when computing the box diagrams.

In order to keep our discussion general, we first extend the Hamiltonian (6.21) and include the following operators

$$\mathcal{H}'_{\text{eff}} = -\frac{4G_F}{\sqrt{2}} V_{tb} V_{ts}^* \sum_{i,j=L,R} \left(C_{ij}^{\mathcal{T}\ell} \mathcal{O}_{ij}^{\mathcal{T}\ell} + C_{ij}^{\mathcal{T}q} \mathcal{O}_{ij}^{\mathcal{T}q} \right) + \text{h.c.},\tag{6.45}$$

where

$$\begin{aligned}\mathcal{O}_{ij}^{\mathcal{T}\ell} &= \frac{e^2}{(4\pi)^2} \frac{1}{m_W} (\bar{s}\gamma^\mu P_i b) \partial^\nu (\bar{\ell}\sigma_{\mu\nu} P_j \ell), \\ \mathcal{O}_{ij}^{\mathcal{T}q} &= -\frac{e^2}{(4\pi)^2} \frac{1}{m_W} \partial^\nu (\bar{s}\sigma_{\mu\nu} P_i b) (\bar{\ell}\gamma^\mu P_j \ell),\end{aligned}\tag{6.46}$$

with $i, j = L, R$.⁶ We reiterate that even though these operators are suppressed by $1/m_W$, they are necessary to unambiguously match the loop induced amplitudes with the effective field theory. The above choice of the basis of dimension-seven operators is convenient since they do not contribute to $\text{Br}(B_s \rightarrow \mu^+ \mu^-)$, while for the other decays their hadronic matrix elements

⁶Notice that we are not computing the QCD corrections to the Wilson coefficients and therefore, at this order, we do not make distinction between the ordinary and the covariant $SU(3)_c$ derivative.

are easy to calculate.

By using the Fierz rearrangement and by applying the field equations, the amplitudes (6.44) are reduced to

$$\mathcal{A}_{LL}^\ell \leftrightarrow -\mathcal{O}_{LL}^{\mathcal{T}\ell} + \mathcal{O}_9 \frac{m_\ell}{m_W}, \quad (6.47)$$

$$\mathcal{A}_{LR}^\ell \leftrightarrow -\mathcal{O}_{LR}^{\mathcal{T}\ell} + \mathcal{O}_9 \frac{m_\ell}{m_W}, \quad (6.48)$$

$$\mathcal{A}_{LL}^{V\ell} \leftrightarrow -\mathcal{O}_{LL}^{\mathcal{T}q} + \left(\mathcal{O}'_S - \frac{\mathcal{O}_T - \mathcal{O}_{T5}}{4} \right) \frac{m_\ell}{m_W}, \quad (6.49)$$

$$\mathcal{A}_{LR}^{V\ell} \leftrightarrow \mathcal{O}_{LR}^{\mathcal{T}q} + \left(\mathcal{O}'_S + \frac{\mathcal{O}_T - \mathcal{O}_{T5}}{4} \right) \frac{m_\ell}{m_W}, \quad (6.50)$$

$$\mathcal{A}_{LL}^q \leftrightarrow \mathcal{O}_{LL}^{\mathcal{T}q} + \frac{\mathcal{O}'_9 - \mathcal{O}'_{10}}{2} \frac{m_b}{m_W} + \frac{\mathcal{O}_9 - \mathcal{O}_{10}}{2} \frac{m_s}{m_W}, \quad (6.51)$$

$$\mathcal{A}_{LR}^q \leftrightarrow \mathcal{O}_{LR}^{\mathcal{T}q} + \frac{\mathcal{O}'_9 + \mathcal{O}'_{10}}{2} \frac{m_b}{m_W} + \frac{\mathcal{O}_9 + \mathcal{O}_{10}}{2} \frac{m_s}{m_W}, \quad (6.52)$$

$$\mathcal{A}_{LL}^{Vq} \leftrightarrow \mathcal{O}_{LL}^{\mathcal{T}\ell} + \frac{\mathcal{O}_S - \mathcal{O}_P}{2} \frac{m_b}{m_W} + \left(\mathcal{O}'_S - \mathcal{O}'_P - \frac{\mathcal{O}_T - \mathcal{O}_{T5}}{2} \right) \frac{m_s}{2m_W}, \quad (6.53)$$

$$\mathcal{A}_{LR}^{Vq} \leftrightarrow -\mathcal{O}_{LR}^{\mathcal{T}\ell} + \frac{\mathcal{O}'_S + \mathcal{O}'_P}{2} \frac{m_s}{m_W} + \left(\mathcal{O}_S + \mathcal{O}_P + \frac{\mathcal{O}_T + \mathcal{O}_{T5}}{2} \right) \frac{m_b}{2m_W}. \quad (6.54)$$

To remain completely general, in the above equations we also kept the lepton mass and the mass of s -quark different from zero. Clearly, for the appropriate matching of these amplitudes to the effective theory, the operators appearing in Eq. (6.21) are not enough and the extended basis given in Eq. (6.45) is necessary. Once the matching is performed, the operators from Eq. (6.21) could be neglected since they are $1/m_W$ suppressed with respect to the dominant (dimension six) ones.

This delicate point can then be verified explicitly by computing the Wilson coefficients $C_{RL}^{\mathcal{T}q}$ and $C_{RR}^{\mathcal{T}q}$ which come from the Z -penguin diagrams and the coefficients $C_{LL}^{\mathcal{T}\ell} = (C_{LR}^{\mathcal{T}\ell})^*$ generated by the box diagrams. Their explicit expression is given in Appendix F.2.

Now, if one sets $p_s = 0$ in \mathcal{A}_{RR}^q of Eq. (6.44), then just like in Ref. [238] one could write $\not{p}_b + \not{p}_s = \not{p}_b = \not{q}$ which, by means of equations of motion, yields

$$\mathcal{A}_{RR}^q = \frac{m_\ell}{m_W} \frac{\alpha}{4\pi} (\bar{s} P_R b) (\bar{\ell} (P_R - P_L) \ell) = \sqrt{x_\ell} \mathcal{O}_P, \quad (6.55)$$

which then in the actual computation gives a contribution to C_P . With our procedure, we understand that this contribution does not come from C_P but actually from $\sqrt{x_\ell} C_{RL}^{\mathcal{T}q}$. In other words, and by using our definition of operators and of the effective Hamiltonian, we find

$$\mathcal{A}_{RR}^q = \sqrt{x_\ell} \mathcal{O}_P + 2 \frac{\alpha}{4\pi} (\bar{s} P_R b) \left(\bar{\ell} \not{\phi}_s P_R \ell \right). \quad (6.56)$$

Had we set $p_s = 0$ we would have missed the contribution of the dimension-seven operator. We emphasize it, once again, that \mathcal{A}_{RR}^q is a non-trivial operator with derivative which cannot be straightforwardly simplified by means of equations of motion.

Finally, after a comparison between ours and the result for C_P presented in Ref. [238] we find ⁷

$$C_P^{\text{Ref.}[238]} = \left[C_P + \frac{\sqrt{x_\ell}}{2 \sin^2 \theta_W} C_{RR}^{\mathcal{T}q} \right]^{(\text{this work})}. \quad (6.57)$$

In other words, the Wilson coefficient C_P of Ref. [238] contains the Wilson coefficient of the operator $\mathcal{O}_{RR}^{\mathcal{T}q}$, the matrix element of which is not equal to the matrix element of the operator \mathcal{O}_P but is, instead, suppressed by m_W as we explicitly check in the next section. For that reason the Wilson coefficient of Ref. [238] is not well defined unless the basis of dimension-seven operators is explicitly specified.

6.6 $B_s \rightarrow \mu^+ \mu^-$ and $B \rightarrow K \mu^+ \mu^-$ in 2HDM

In this Section we give the expressions for $\text{Br}(B_s \rightarrow \mu^+ \mu^-)$ and $\text{Br}(B \rightarrow K \mu^+ \mu^-)$ to which we also include the contributions of the operators given in Eq. (6.46). Those additional operators were necessary for the appropriate matching procedure between the full and the effective theories. However, since they are suppressed by $1/m_W$ they are expected to be negligible with respect to the dominant operators entering the effective Hamiltonian (6.21). The purpose of this exercise is to check whether or not the size of the matrix elements of the operators (6.46) is indeed numerically insignificant for phenomenology.

⁷Notice also that the notation of Ref. [238] is such that their Wilson coefficient C_P , which we can call \tilde{C}_P , is related to our's via $C_P = \sqrt{x_\ell x_b} \tilde{C}_P / \sin^2 \theta_W$.

6.6.1 $B_s \rightarrow \mu^+ \mu^-$

On the basis of Lorentz invariance and invariance of the strong interaction with respect to parity, one can easily verify that $B_s \rightarrow \mu^+ \mu^-$ is not affected by the operators $\mathcal{O}_{i,j}^{\mathcal{T}q}$ and $\mathcal{O}_{i,j}^{\mathcal{T}\ell}$, with $i, j = L, R$. The expression for the decay rate of this process remains the standard one

$$\begin{aligned} \text{Br}(B_s \rightarrow \ell^+ \ell^-)^{\text{th}} = \tau_{B_s} \frac{\alpha^2 G_F^2 m_{B_s} \beta_\ell}{16\pi^3} |V_{tb} V_{ts}^*|^2 f_{B_s}^2 m_\ell^2 & \left[\left| C_{10} - C'_{10} + \frac{m_{B_s}^2 (C_P - C'_P)}{2m_\ell (m_b + m_s)} \right|^2 \right. \\ & \left. + |C_S - C'_S|^2 \frac{m_{B_s}^2 (m_{B_s}^2 - 4m_\ell^2)}{4m_\ell^2 (m_b + m_s)^2} \right], \end{aligned} \quad (6.58)$$

where $\beta_\ell = \sqrt{1 - 4m_\ell^2/m_{B_s}^2}$. To compare Eq. (6.58) with the available experimental value, we proceed analogously as in (4.40) of Chap. 4, using the averaged branching ratios from the fit in Ref. [46].

As we mentioned before, the dimension-seven operators (6.46) were chosen in such a way that they do not contribute the $B_s \rightarrow \ell^+ \ell^-$ decay amplitude.

6.6.2 $B \rightarrow K \mu^+ \mu^-$

In contrast to $B_s \rightarrow \ell^+ \ell^-$, the decay $B \rightarrow K \ell^+ \ell^-$ receives contributions from the operators of the extended basis (6.46). To write the decay amplitude in a compact form, it is convenient to use the formalism of helicity amplitudes (HA's) Ref. [110]. Using this process described in Ref. [110] but adding the dimension 7 operators, we obtain

$$\begin{aligned} \frac{d}{dq^2} \text{Br}(B \rightarrow K \ell^+ \ell^-)^{\text{th}} = \frac{2(q^2 - m_\ell^2)}{3} & [|A_0^L|^2 + |A_0^R|^2] + 2m_\ell^2 |A_t|^2 + \frac{q^2 - 4m_\ell^2}{2} |A_S|^2 \\ & + \frac{q^2 + 2m_\ell^2}{3} [|A_{t0}^L - A_{0t}^L|^2 + |A_{t0}^R - A_{0t}^R|^2] + 4m_\ell^2 \text{Re} [A_0^{L*} A_0^R] \\ & + \frac{8(q^2 - 4m_\ell^2)}{3} |A_{T5}|^2 + \frac{4(q^2 - 4m_\ell^2)}{3} \text{Re} [A_{T5}^* (A_{t0}^L - A_{0t}^L) - (L \leftrightarrow R)] \\ & + 4m_\ell^2 \text{Re} [A_{0t}^{L*} (A_{0t}^R - A_{t0}^R) - A_{t0}^{L*} (A_{0t}^R - A_{t0}^R)] \\ & - 2m_\ell \sqrt{q^2} \text{Im} [(A_0^L + A_0^R)^* (A_{t0}^L - A_{0t}^L + (L \leftrightarrow R))], \end{aligned} \quad (6.59)$$

and the explicit expressions for the helicity amplitudes are the q^2 -dependent functions which read:

$$A_0^{L(R)}(q^2) = \mathcal{N}_K \frac{\lambda_B^{1/2}}{2\sqrt{q^2}} \left[f_+(q^2) [(C_9 + C'_9) \mp (C_{10} + C'_{10})] + f_T(q^2) \frac{2m_b}{m_B + m_K} (C_7 + C'_7) - f_T(q^2) \frac{q^2}{m_W(m_B + m_K)} [C_{L,L(R)}^{\mathcal{T}q} + C_{R,L(R)}^{\mathcal{T}q}] \right], \quad (6.60)$$

$$A_t(q^2) = -\mathcal{N}_K f_0(q^2) \frac{m_B^2 - m_K^2}{\sqrt{q^2}} \left[C_{10} + C'_{10} + \frac{q^2 (C_P + C'_P)}{2m_\ell(m_b - m_s)} \right], \quad (6.61)$$

$$A_S(q^2) = \mathcal{N}_K f_0(q^2) \frac{m_B^2 - m_K^2}{m_b - m_s} (C_S + C'_S), \quad (6.62)$$

$$A_{0t}^{L(R)}(q^2) = i\mathcal{N}_K \lambda_B^{1/2} \left[f_T(q^2) \frac{C_T}{m_B + m_K} + f_+(q^2) \frac{C_{L,L(R)}^{\mathcal{T}\ell} + C_{R,L(R)}^{\mathcal{T}\ell}}{2m_W} \right], \quad (6.63)$$

$$A_{t0}^{L(R)}(q^2) = -i\mathcal{N}_K f_T(q^2) \frac{C_T \lambda_B^{1/2}}{m_B + m_K}, \quad (6.64)$$

$$A_{T5}(q^2) \equiv A_{+-}^{L(R)} = i\mathcal{N}_K f_T(q^2) \frac{C_{T5} \lambda_B^{1/2}}{m_B + m_K}, \quad (6.65)$$

where the normalization factor also accounts for the remaining phase space, namely,

$$|\mathcal{N}_K(q^2)|^2 = \tau_{Ba} \frac{\alpha_{\text{em}}^2 G_F^2 |V_{tb} V_{ts}^*|^2 \lambda_q^{1/2}}{512\pi^5 m_B^3} \lambda_B^{1/2}. \quad (6.66)$$

For shortness, in the above formulas, we used $\lambda_q = \lambda(\sqrt{q^2}, m_\ell, m_\ell)$ and $\lambda_B = \lambda(m_B, m_K, \sqrt{q^2})$, where $\lambda(a, b, c) \equiv [a^2 - (b - c)^2][a^2 - (b + c)^2]$. The kinematic conventions and the form factor definitions are collected in Appendix F. In the limit in which the derivative operators vanish we retrieve the usual expression for differential branching fraction [110]. The choice of dimension-seven operators (6.46) is convenient also because their matrix elements are proportional to the original hadronic matrix elements multiplied by iq^μ . As it can be seen from the above expressions the coefficients $C_{i,j}^{\mathcal{T}\ell}$ and $C_{i,j}^{\mathcal{T}q}$ enters the above formulas with the explicit $1/m_W$ -suppression factor. In other words, with the above formulas and by using the Wilson coefficients presented in the previous Sections, we see that the derivative operators (6.46) are

indeed irrelevant for phenomenology. Their presence is therefore essential for the unambiguous matching procedure in the computation of Wilson coefficients but they do not alter the phenomenological analysis even at the sub-percent level.

6.7 Phenomenology and Discussion

In this Section we use our results for Wilson coefficients and compare the experimental data for the exclusive $b \rightarrow s\ell^+\ell^-$ modes with various types of 2HDM. We decided to focus on $\text{Br}(B_s \rightarrow \mu^+\mu^-)^{\text{exp}} = (3.1 \pm 0.6) \times 10^{-9}$ [45], and $\text{Br}(B \rightarrow K\mu^+\mu^-)_{\text{high } q^2}^{\text{exp}} = (8.5 \pm 0.3 \pm 0.4) \times 10^{-8}$ [263], where “high q^2 ” means that the decay rate has been integrated over the interval $q^2 \in [15, 22]$ GeV^2 . The reason for opting for these decay modes is that the relevant hadronic uncertainties are under good theoretical control. The hadronic quantity entering the $B_s \rightarrow \mu^+\mu^-$ decay amplitude is the decay constant, f_{B_s} . It has been abundantly computed by means of numerical simulations of QCD on the lattice and its value is nowadays one of the most accurately computed hadronic quantities as far as $B_{(s)}$ -mesons are concerned [48]. The hadronic form factors entering the $B \rightarrow K\mu^+\mu^-$ decay amplitude have been directly computed in lattice QCD only in the region of large q^2 's [264, 265], which explains why we use $\text{Br}(B \rightarrow K\mu^+\mu^-)_{\text{high } q^2}^{\text{exp}}$ to do phenomenology. Furthermore, since the bin corresponding to $q^2 \in [15, 22]$ GeV^2 is rather wide and away from the very narrow charmonium resonances, the assumption of quark-hadron duality is likely to be valid [266]. By using the recent lattice QCD results for the form factors provided by HPQCD [264] and MILC Collaborations [265], the SM results are

$$\text{Br}(B \rightarrow K\mu^+\mu^-)_{\text{high } q^2} = \left\{ (10.0 \pm 0.5) \times 10^{-8} \Big|_{\text{HPQCD}}, (10.7 \pm 0.5) \times 10^{-8} \Big|_{\text{MILC}} \right\}, \quad (6.67)$$

both being about 2σ larger than the experimental value measured at LHCb.⁸ Since the current disagreement between theory and experiment needs to be corroborated by more data, we decided to impose all the constraints to 3σ accuracy. We will then discuss the impact of $\text{Br}(B \rightarrow K\mu^+\mu^-)_{\text{high } q^2}^{\text{exp}}$ on 2HDM if the current discrepancy remains, i.e. by requiring the 2HDM to compensate the disagreement between theory (SM) and experiment at the level of 2σ

⁸In the following we will average the results obtained by using the two sets of form factors obtained in lattice QCD.

Model	Type I	Type II	Type X	Type Z
$\tan \beta$	> 1.0	> 0.9	> 1.0	> 0.9

Table 6.2: Allowed values of low $\tan \beta$ (at 99% CL) for the different 2HDMs. See text for details.

and more. Notice also that the measured $\text{Br}(B_s \rightarrow \mu^+ \mu^-)^{\text{exp}}$ is slightly smaller than predicted, $\text{Br}(B_s \rightarrow \mu^+ \mu^-)^{\text{SM}} = (3.57 \pm 0.17) \times 10^{-9}$ [46].

We now use the results of our scan from Sec. 6.1.2, require the 3σ agreement between experiment and theory, which means that we add the generic 2HDM Wilson coefficients derived in the previous Section to the SM values. The result, in the plane $(\tan \beta, m_{H^\pm})$, is shown in Fig. 6.6 for each type of 2HDM discussed in Sec. 6.1. We learn that both $\text{Br}(B_s \rightarrow \mu^+ \mu^-)$ and $\text{Br}(B \rightarrow K \mu^+ \mu^-)_{\text{high } q^2}$ exclude the low $\tan \beta \lesssim 1$ region regardless of the type of 2HDM considered. The limit of exclusion of low $\tan \beta$ coming from $\text{Br}(B \rightarrow K \mu^+ \mu^-)_{\text{high } q^2}$ is slightly larger than the one arising from $\text{Br}(B_s \rightarrow \mu^+ \mu^-)$. The limit on low $\tan \beta$ obtained in this way for each of our four models is given in Tab. 6.2.

Besides excluding $\tan \beta \lesssim 1$, it may appear as a surprise that the large $\tan \beta$ are not excluded by these data. The reason for that is the fact that the (pseudo-)scalar Wilson coefficient, with respect to the dominant (axial-)vector one, comes with a term proportional to $(m_{B_s}/m_W)^2$ which suppresses the large $\tan \beta$ values. This feature can be easily verified in the Type II model for which the coefficients $C_{S,P}$, in the large $\tan \beta$ limit. This is why only a small number of points have been eliminated from our scan of Type II model at large $\tan \beta$ but relatively light m_{H^\pm} .

Since the SM value is in slight tension with $\text{Br}(B \rightarrow K \mu^+ \mu^-)_{\text{high } q^2}^{\text{exp}}$ at the 2.1σ level, we can now check which of the models discussed in this paper can be made consistent with the experimental data if any disagreement beyond 2σ between theory (SM) and experiment is to be attributed to 2HDM. It turns out that two such models are Type II and Type Z 2HDM, which we illustrate in Fig. 6.7. For the other two scenarios (Type I and Type X) the NP contributions are either too small or already in conflict with $\text{Br}(B_s \rightarrow \mu^+ \mu^-)^{\text{exp}}$. From Figs. 6.7 and 6.8 we see that in order to explain the discrepancy one needs a relatively light charged scalar: (i) $m_{H^\pm} \lesssim 735$ GeV and $\tan \beta > 2.3$ in the Type II scenario, and (ii) $m_{H^\pm} \lesssim 380$ GeV and $\tan \beta > 3.5$ for the Type Z scenario. Since the masses of the additional scalars are correlated, we see that m_H and m_A become bounded as well, cf. Fig. 6.8. In the case of Type II and

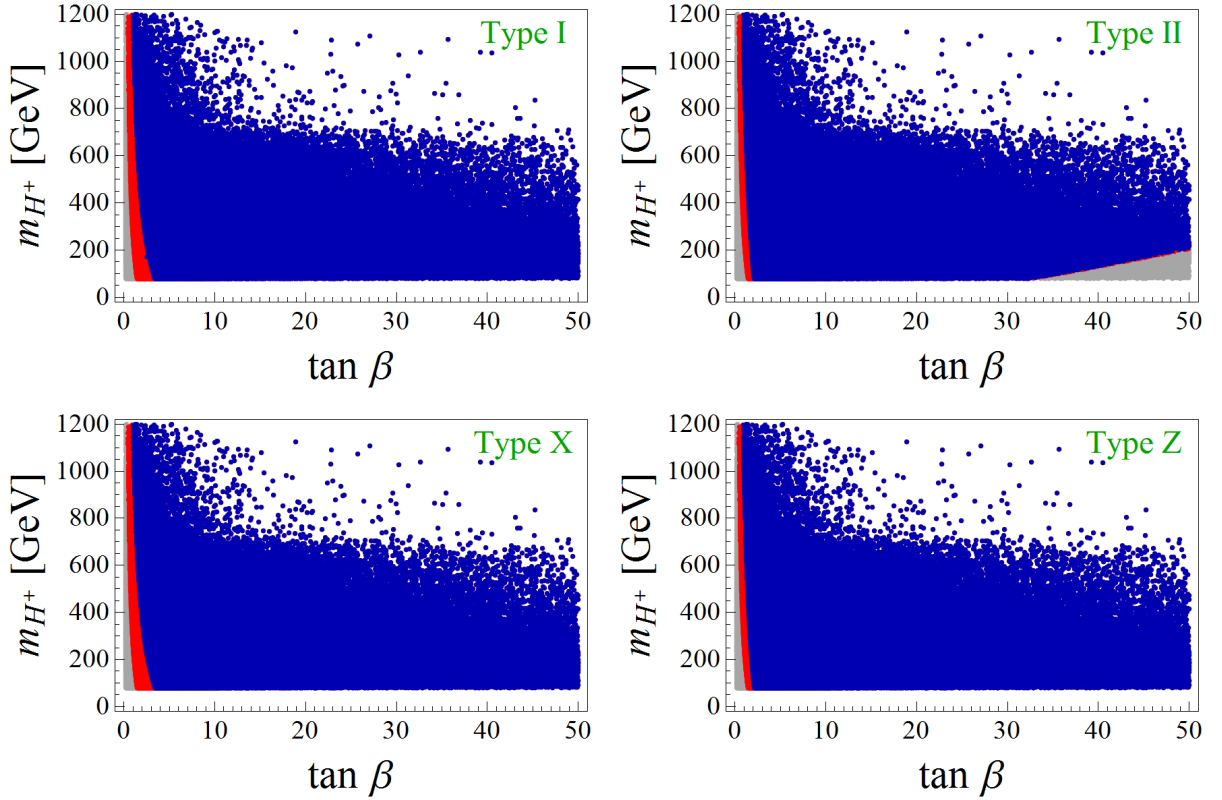


Figure 6.6: Results of the scan given in Fig. 6.1 after imposing the constraints coming from $\text{Br}(B_s \rightarrow \mu^+ \mu^-)^{\text{exp}}$ and $\text{Br}(B \rightarrow K \mu^+ \mu^-)_{\text{high } q^2}^{\text{exp}}$ to 3σ accuracy. Blue points are allowed by all observables, while gray points are excluded by $\text{Br}(B_s \rightarrow \mu^+ \mu^-)^{\text{exp}}$, and the red ones are excluded by $\text{Br}(B \rightarrow K \mu^+ \mu^-)_{\text{high } q^2}$.

Type Z 2HDM an additional bound on the charged Higgs has been recently derived from the inclusive mode $\text{Br}(B \rightarrow X_s \gamma)$. After comparing the experimental spectra with theoretical expressions in which the higher order QCD corrections have been included, the lower bound $m_{H^\pm} > 570$ GeV (95% CL) was obtained in Ref. [267] (c.f. also Ref.[157]). This bound is superposed on our results in Figs. 6.7 and 6.8, which then also eliminates Type Z 2HDM. Furthermore, we can say that the requirement of agreement between theory and experiment to 2σ , for the quantities discussed in this Section, reduces the available space of parameters for Type II 2HDM to $m_{H^\pm} \in (570, 735)$ GeV, and $\tan \beta \in (16, 35)$, while the available range of values for the mass of the CP-odd Higgs becomes $m_A \in (145, 865)$ GeV.

In what follows we will assume that the 2σ disagreement of the measure $\text{Br}(B \rightarrow K \mu^+ \mu^-)_{\text{high } q^2}^{\text{exp}}$ with respect to the SM prediction indeed remains as such in the future and discuss the conse-

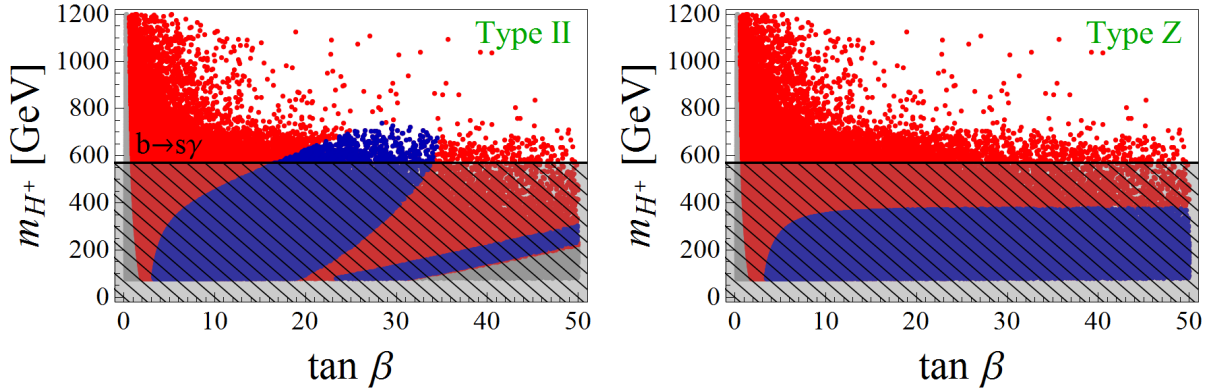


Figure 6.7: Results of the scan in Fig. 6.1 after imposing the $b \rightarrow s$ constraints to 2σ accuracy. The hatched area is excluded by $\text{Br}(B \rightarrow X_s \gamma)$ at 95% [267]. See Fig. 6.6 for the color code.

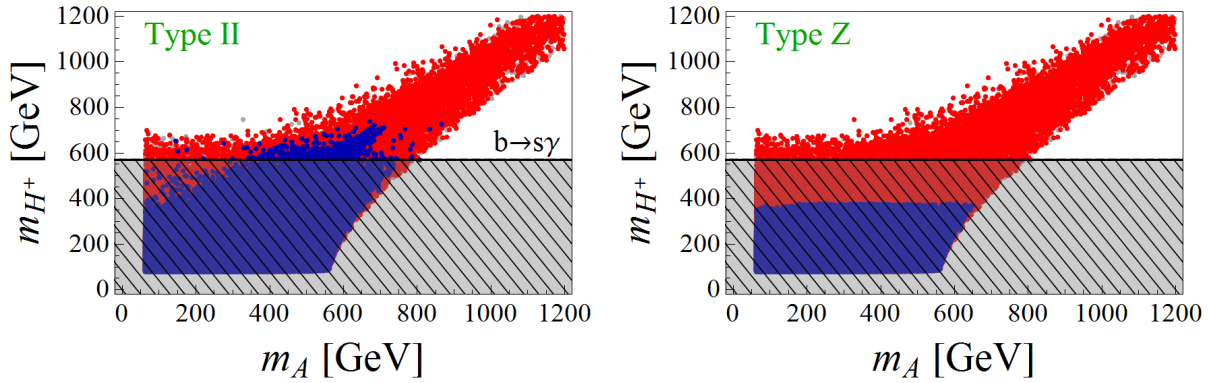


Figure 6.8: Same as in Fig. 6.7 but in the (m_A, m_{H^\pm}) plane.

quences on the decays $\text{Br}(B_s \rightarrow \tau^+ \tau^-)$ and $\text{Br}(B \rightarrow K \tau^+ \tau^-)_{\text{high } q^2}$ if the Type II 2HDM is used to explain the disagreement. From Eq. (6.58) we can see that

$$\frac{\text{Br}(B_s \rightarrow \tau^+ \tau^-)}{\text{Br}(B_s \rightarrow \tau^+ \tau^-)^{\text{SM}}} = \frac{\text{Br}(B_s \rightarrow \mu^+ \mu^-)}{\text{Br}(B_s \rightarrow \mu^+ \mu^-)^{\text{SM}}} - \frac{|C_S^{\tau\tau}|^2}{|C_{10}^{\text{SM}}|^2} \frac{m_{B_s}^2}{(m_b + m_s)^2}, \quad (6.68)$$

where the only remaining m_ℓ dependence comes from the last numerator in the factor multiplying $|C_S - C'_S|^2$ in Eq. (6.58). In Fig. 6.9 we illustrate the validity of the above equality. Notice that a tiny departure from equality comes from the large $\tan \beta$ values which enhance the C_S contribution. In other words, the current experimental result $\text{Br}(B_s \rightarrow \mu^+ \mu^-)^{\text{exp}}$, which is slightly lower than the one predicted in the SM, is expected to lead to $\text{Br}(B_s \rightarrow \tau^+ \tau^-)^{\text{exp}}$ compatible or slightly lower than predicted in the SM. The cancellation of the lepton mass in

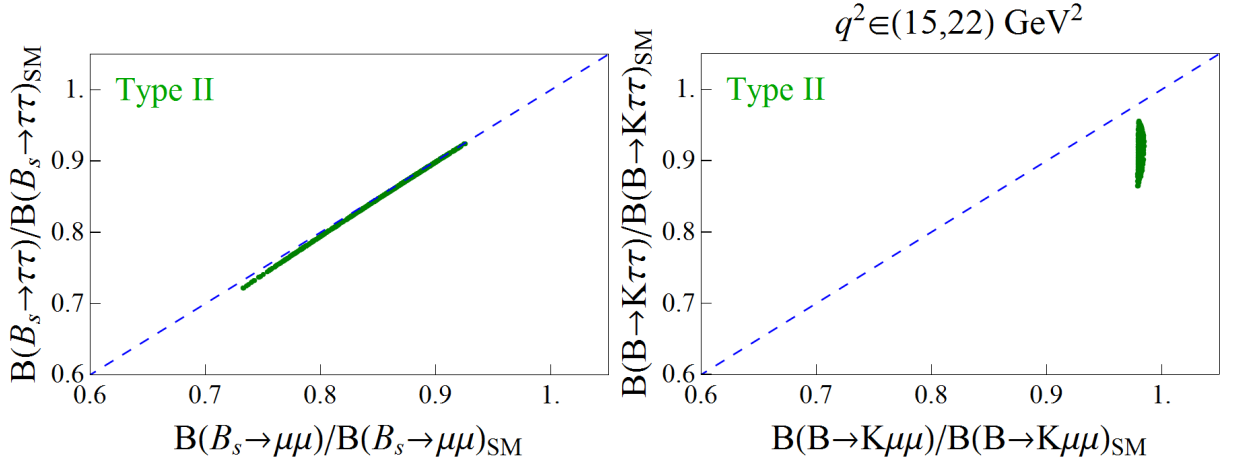


Figure 6.9: We show the branching fractions of the decay to τ -leptons with respect to their SM predictions, as obtained in the Type II 2HDM, consistent with experimental results for the decays to muons in the final state.

$\text{Br}(B_s \rightarrow \ell^+ \ell^-)^{2\text{HDM}}$, discussed above, does not occur in $\text{Br}(B \rightarrow K \ell^+ \ell^-)_{\text{high-}q^2}^{2\text{HDM}}$. As a result we obtain,

$$\frac{\text{Br}(B \rightarrow K \tau^+ \tau^-)^{\text{Type II}}}{\text{Br}(B \rightarrow K \tau^+ \tau^-)^{\text{SM}}} \lesssim \frac{\text{Br}(B \rightarrow K \mu^+ \mu^-)^{\text{Type II}}}{\text{Br}(B \rightarrow K \mu^+ \mu^-)^{\text{SM}}}, \quad (6.69)$$

where we omitted the subscript “high- q^2 ” to avoid a too heavy notation. Illustration is provided in Fig. 6.9. We can rephrase this observation with an equivalent statement:

$$\frac{\text{Br}(B \rightarrow K \tau^+ \tau^-)^{\text{Type II}}}{\text{Br}(B \rightarrow K \mu^+ \mu^-)^{\text{Type II}}} < \frac{\text{Br}(B \rightarrow K \tau^+ \tau^-)^{\text{SM}}}{\text{Br}(B \rightarrow K \mu^+ \mu^-)^{\text{SM}}}. \quad (6.70)$$

To be fully explicit, we obtain

$$\left. \frac{\text{Br}(B \rightarrow K \tau^+ \tau^-)}{\text{Br}(B \rightarrow K \mu^+ \mu^-)} \right|_{\text{high-}q^2} \in (1.12, 1.14)_{\text{SM}}, (1.0, 1.1)_{\text{Type II}}. \quad (6.71)$$

Chapter 7

Summary and Conclusions

Nowadays, in order to look for the effects of new physics, i.e. physics beyond the Standard Model, one searches for disagreements between the results predicted by the accurate theoretical expressions derived in the Standard Model and those precisely measured in the experiments. Thanks to the LHC and various flavor physics experiments this can be done in two ways: (a) through direct searches of new particles at the high energy and high luminosity experiments at LHC, and (b) through indirect searches in the low energy flavor physics experiments. Obviously both ways are complementary to each other. Recent LHC results concerning the exclusive $b \rightarrow s\ell\ell$ modes exhibited several interesting discrepancies which spurred a great deal of theoretical activity in looking for the effects of new physics in various observables, of which the most intriguing one is the ratio of the mode with $\mu^+\mu^-$ in the final state with respect to the one in which, instead of muons, one has e^+e^- in the final state. More specifically, it has been observed that $R_K^{\text{exp}} < R_K^{\text{SM}}$, $R_{K^*}^{\text{exp}} < R_{K^*}^{\text{SM}}$ and $R_{pK}^{\text{exp}} < R_{pK}^{\text{SM}}$ (see text for definitions). Although none of these measurements exhibits a deviation larger than 5σ , all of them point towards the violation of the lepton flavor universality, which came as a big surprise.

In this thesis we explored the (b) option and examined various new physics scenarios that could accommodate the above-mentioned B -physics anomalies and which are consistent with the whole plethora of experimental flavor physics data. We first described both the $b \rightarrow s\ell\ell$ and the $b \rightarrow c\ell\bar{\nu}$ processes by means of an effective field theory in which the most general new physics couplings are considered. The constraints on those couplings (Wilson coefficients) are deduced from fit to a large number of observables. With these constraints in hands we then proceeded to build a specific model/theory of physics beyond the Standard Model. In that respect, one sees that our model building is fully data driven.

In Chapter 3 we have studied the impact of extending the Standard Model by introducing new heavy scalars and fermions on $b \rightarrow s\mu^+\mu^-$ processes. In particular, we considered (i) a model with two extra fermions (Ψ_Q and Ψ_ℓ) and one extra scalar (scalar Φ), and (ii) a model with two additional scalars (Φ_Q and Φ_ℓ) and one additional fermion Ψ . Both models are consistent with $C_9^\mu = -C_{10}^\mu$, relation between the Wilson coefficients which seems to be preferred by the data.

Considering representations up to the adjoint one under the SM gauge group, we classified all possible combinations of representations for the new particles that are allowed by charge conservation in the new Yukawa-type vertices. In this setup we calculated the new physics contributions to $b \rightarrow s\mu^+\mu^-$ processes, $B_s - \bar{B}_s$ mixing, $b \rightarrow s\gamma$, $b \rightarrow s\nu\bar{\nu}$, in addition to the anomalous magnetic moment of the muon a_μ . We found that the constraint from $B_s - \bar{B}_s$ mixing is very stringent due to the new lattice data favoring destructive interference with the SM, which in our case translates to a requirement for a large value of the Yukawa-like coupling of the new physics particles to muon, $|\Gamma_\mu| \gtrsim 2.1$, for the masses of new particles $\mathcal{O}(1 \text{ TeV})$. The $B_s - \bar{B}_s$ constraint can be avoided in a model with two scalars if Ψ is a Majorana fermion. In such a case we show that, for $m_{\Phi_q} \leq m_\Psi$, the contribution to the $B_s - \bar{B}_s$ mixing amplitude can be zero. Notice that a_μ , the anomalous magnetic moment of the muon, depends only on Γ_μ and the 2σ agreement between theory and experiment can be achieved for $|\Gamma_\mu| \gtrsim 2$, with the new heavy particles being $\mathcal{O}(1 \text{ TeV})$.

In Chapter 4 we generalized the analysis of Chapter 3 by allowing the non-zero couplings of the new particles to right-handed SM fermion as and calculated the general expressions for the Wilson coefficients governing $b \rightarrow s$ processes ($b \rightarrow sl^+\ell^-$, $b \rightarrow s\nu\bar{\nu}$, $b \rightarrow s\gamma$ and $B_s - \bar{B}_s$ mixing). Moreover, we computed the contributions to a_μ as well as to the accurately measured $\text{Br}(Z \rightarrow \mu^+\mu^-)$, which is also included in our analysis.

Furthermore, we proposed a viable UV complete model which, besides a scalar (Φ) contains two vector-like fermions of 4th generation, namely Ψ^E and Ψ^D . From the phenomenological analysis we show that a good description of the experimental flavor physics $b \rightarrow s$ data, consistent with results of the direct searches at the LHC, can be made for e.g. $m_E \approx m_\Phi \simeq 0.5 \text{ TeV}$, and $m_D \simeq 3 \text{ TeV}$. Interestingly, Φ can also be viewed as a viable candidate for the Dark Matter particle. Indeed, we showed that if $m_{\Psi^E} \sim m_\Phi$ one gets the amount of relic density consistent with the limits of the direct Dark Matter searches.

In Chapter 5 we discussed another family of new physics scenarios in which the Standard Model is extended by including one or two light [$\mathcal{O}(1 \text{ TeV})$] leptoquark states. In these scenar-

ios one can explain both types of B -anomalies, $b \rightarrow s\ell\ell$ and $b \rightarrow c\ell\bar{\nu}$. One of the main requirements in specifying such a model is to provide consistency with the measured $\text{Br}(Z \rightarrow \ell\ell)$ and $\text{Br}(Z \rightarrow \nu\bar{\nu})$. Such processes are loop induced and have not been fully included in the previous analyses. We computed the contribution of all of the possible scalar leptoquarks propagating in the loops, by admitting the most generic structure of the Yukawa couplings. In doing so we did not limit ourselves to the computation of the leading logarithms ($\mathcal{O}(x_t \log x_t)$). Instead, we also computed the finite terms in addition to the terms $\mathcal{O}(x_{Z(W)} \log x_t)$. We find that these new contributions are sizeable and their inclusion in the phenomenological analyses is mandatory. Instead, the contributions to $W \rightarrow \ell\nu$ arising from the loops involving scalar leptoquarks are tiny.

We illustrate the importance of including the Z -pole observables on a specific model in which the new physics comes from two light scalar leptoquarks, S_1 and S_3 , and how using the NNLA can lead to a compatible explanation of data. We also showed that one of the most important constraints in such models comes from the observed frequency of oscillations in the $B_s - \bar{B}_s$ system. We provide the expression coming from the loop diagrams and derive the Wilson coefficient to the $B_s - \bar{B}_s$ mixing in this scenario. Including this constrain, that S_1+S_3 model was unable to explain $R_{D^{(*)}}$ experimental value before a new measurement of Belle lowered its value in Moriond Conference 2019. The same occurred with the other two S_1+S_3 models with different Yukawa structure proposed in Chapter 5

In Chapter 6 we computed the leading order Wilson coefficients relevant to the exclusive $b \rightarrow s\ell^+\ell^-$ decays in the framework of 2HDM with a softly broken \mathbb{Z}_2 symmetry. Most of these Wilson coefficients have been computed previously but in the limit of large $\tan\beta$, which we have extended to a generic setup. We also included $\mathcal{O}(m_b)$ corrections, which were neglected in the previous computations. Regarding the (pseudo-)scalar Wilson coefficients, we elucidated the issue of unambiguous matching of the one-loop amplitudes between the full and effective theories which requires extending the basis of operators in the effective theory by including two types of operators suppressed by $1/m_W$ (altogether, eight new operators). We pointed out that for the appropriate identification of the Z -penguin contribution to the Wilson coefficient C_P it is necessary to keep all external momenta different from zero.

After having computed the full set of Wilson coefficients we were able to make a phenomenological analysis by focusing on $\text{Br}(B_s \rightarrow \mu^+\mu^-)$ and $\text{Br}(B \rightarrow K\mu^+\mu^-)_{\text{high-}q^2}$, the quantities which are measured at LHC and for which the hadronic uncertainties are under good theoretical control (computed in LQCD). After carefully scanning the parameter space

of 2HDM with a softly broken \mathbb{Z}_2 symmetry, we tested various types of 2HDM against the experimental data and found that to 3σ the values of low $\tan\beta \lesssim 1$ are excluded for all types of 2HDM's. We also discussed the repercussions of the current results on the decays $\text{Br}(B_s \rightarrow \tau^+\tau^-)$ and $\text{Br}(B \rightarrow K\tau^+\tau^-)_{\text{high-}q^2}$. Notice that 2HDM models can be used to describe $R_{D^{(*)}}^{\text{exp}} > R_{D^{(*)}}^{\text{SM}}$, but not to describe $R_{K^{(*)}}^{\text{exp}} < R_{K^{(*)}}^{\text{SM}}$. Therefore, even if the B -anomalies do not resist the test of time and appear to be merely statistical fluctuations, the current measurements will be a very important in relaxing the \mathbb{Z}_2 symmetry requirement on the Yukawa couplings and to constrain the Yukawa couplings in a more model-independent way. The mechanism to generate such Yukawa couplings is beyond the scope of this thesis and is one of the directions that can be pursued in the future.

The research and results presented in this thesis demonstrate that we entered the era in which the high precision experimental data are giving main directions to our model building efforts. With the new results, in the years to come, from many ongoing experiments will make the model building efforts more and more restrictive, which will further help us solving the most fundamental question of the origin of flavor.

Appendix A

Matching of a $b \rightarrow s\mu^+\mu^-$ Transition

In this Appendix, we show an example of the matching procedure for a $b \rightarrow s\mu^+\mu^-$ process between a full theory and an effective theory. In this case, we propose a full theory with new heavy scalars and fermions (Φ_Q, Φ_ℓ, Ψ) coupling to the SM b, s quarks and muons, similar to the model b) in Chap. 3. With that in mind, we write the full theory Lagrangian as

$$\mathcal{L}^{\text{full}} = \Gamma_s \bar{\Psi} P_L s \Phi_Q + \Gamma_b \bar{\Psi} P_L b \Phi_Q + \Gamma_\mu \bar{\Psi} P_L \mu \Phi_\ell + \text{h.c.}, \quad (\text{A.1})$$

where we choose the same representation A-I of Chap 3 with $Q_\Psi \neq 0$ in order to avoid crossed diagrams. Then, the only Feynman diagram that contributes to $b \rightarrow s\mu^+\mu^-$ in this model is depicted in Fig. A.1.

In a similar way, the Hamiltonian¹ governing the $b \rightarrow s\mu^+\mu^-$ left-handed interactions in the effective theory is

$$\mathcal{H}^{\text{eff}} = C_9 \mathcal{O}_9 + C_{10} \mathcal{O}_{10} + \text{h.c.}, \quad (\text{A.2})$$

with C_9 and C_{10} being the Wilson coefficients and here we define the operators without normalization factors for simplicity as

$$\mathcal{O}_9 = (\bar{s}\gamma_\mu P_L b)(\bar{\mu}\gamma_\mu \mu) \quad \text{and} \quad \mathcal{O}_{10} = (\bar{s}\gamma_\mu P_L b)(\bar{\mu}\gamma_\mu \gamma_5 \mu), \quad (\text{A.3})$$

which establish the operator basis needed for this process.

Once specified the full and the effective theory, we have to define the external momentum

¹Usually in effective theories, especially in the flavor sector, one uses Hamiltonian instead of Lagrangian for historical reasons. However the relation between them in this case is just $\mathcal{H} = -\mathcal{L}$

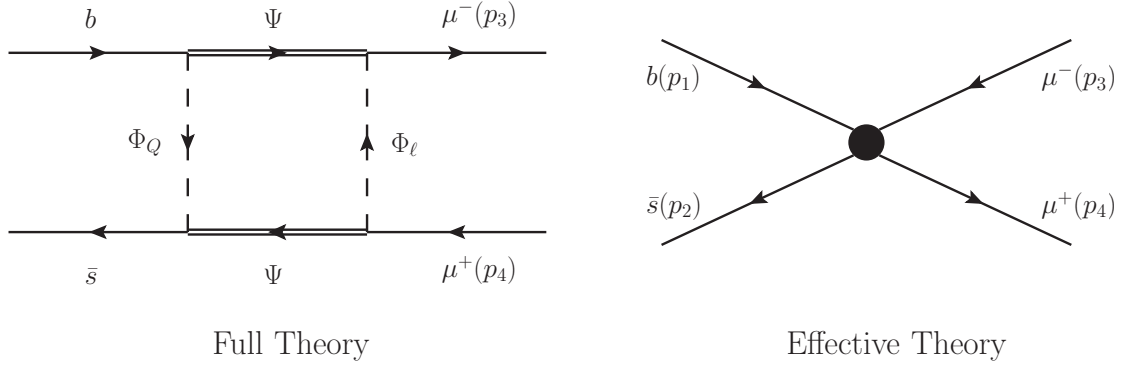


Figure A.1: Feynman diagrams contributing to $b \rightarrow s\mu^+\mu^-$ in the full theory (left) and in the effective theory (right).

for each particle in the process, namely $b(p_1) \rightarrow s(p_2)\mu^+(p_4)\mu^-(p_3)$, and we are ready to match the two amplitudes describing the same process that arise from two different theories.

We first compute the amplitude for the effective theory. Notice that since there is only one vertex in the right picture of Fig. A.1, it is straightforward to write down the amplitude from the Lagrangian (A.2) as

$$\mathcal{A}^{\text{eff}} = -i\langle\mu^-(p_3)\mu^+(p_4)|\mathcal{H}^{\text{eff}}|b(p_1)s(p_2)\rangle = -i(C_9\langle\mathcal{O}_9\rangle + C_{10}\langle\mathcal{O}_{10}\rangle), \quad (\text{A.4})$$

where

$$\langle\mathcal{O}_9\rangle = \langle\mu^-(p_3)\mu^+(p_4)|\mathcal{O}_9|b(p_1)s(p_2)\rangle = [\bar{s}(p_2)\gamma_\mu P_L b(p_1)][\bar{\mu}(p_3)\gamma_\mu\mu(p_4)], \quad (\text{A.5})$$

$$\langle\mathcal{O}_{10}\rangle = \langle\mu^-(p_3)\mu^+(p_4)|\mathcal{O}_{10}|b(p_1)s(p_2)\rangle = [\bar{s}(p_2)\gamma_\mu P_L b(p_1)][\bar{\mu}(p_3)\gamma_\mu\gamma_5\mu(p_4)]. \quad (\text{A.6})$$

Notice that the expected value or matrix element of the operators results in spinors which we distinguish from the operators by labeling the momenta and using brackets instead of parentheses. What follows now is to compare this effective amplitude with the one obtained with the full theory.

In order to compute the amplitude for the $b(p_1) \rightarrow s(p_2)\mu^+(p_4)\mu^-(p_3)$ process in the full theory we use the Lagrangian in (A.1), yielding the diagram in Fig. A.1. As we said, we assume that the particles in the loop are much heavier compared to the ones in the external legs, hence we neglect the external momenta. Applying the full Lagrangian in the four vertices $(x_1, x_2, x_3$

and x_4) of the loop, the amplitude $\mathcal{A}^{\text{full}}$ reads

$$\begin{aligned}\mathcal{A}^{\text{full}} &= \frac{i^4}{4!} \langle \mu^-(p_3) \mu^+(p_4) | \mathcal{T} \{ \mathcal{L}^{\text{full}}(x_1) \mathcal{L}^{\text{full}}(x_2) \mathcal{L}^{\text{full}}(x_3) \mathcal{L}^{\text{full}}(x_4) \} | b(p_1) s(p_2) \rangle \\ &= -i \frac{\Gamma_s^* \Gamma_b |\Gamma_\mu|^2}{64\pi^2 m_\Psi^2} F(x_Q, x_\ell) [\bar{\mu}(p_3) \gamma_\mu P_L b(p_1)] [\bar{s}(p_2) \gamma_\mu P_L \mu(p_4)],\end{aligned}\quad (\text{A.7})$$

where $F(x_Q, x_\ell)$ is defined in the Appendix C.1, and $x_Q = m_{\Phi_Q}^2/m_\Psi^2$, $x_\ell = m_{\Phi_\ell}^2/m_\Psi^2$. Notice again that we end up with spinors. In order to get the spinor in the correct order so we can compare it with the effective theory, we apply the Fierz transformation for spinors, which are the same as for the operators but with an overall minus sign. We have

$$\begin{aligned}\mathcal{A}^{\text{full}} &= i \frac{\Gamma_s^* \Gamma_b |\Gamma_\mu|^2}{64\pi^2 m_\Psi^2} F(x_Q, x_\ell) [\bar{s}(p_2) \gamma_\mu P_L b(p_1)] [\bar{\mu}(p_3) \gamma_\mu P_L \mu(p_4)] \\ &= i \frac{\Gamma_s^* \Gamma_b |\Gamma_\mu|^2}{128\pi^2 m_\Psi^2} F(x_Q, x_\ell) (\langle \mathcal{O}_9 \rangle - \langle \mathcal{O}_{10} \rangle),\end{aligned}\quad (\text{A.8})$$

where in the last line we used that $P_L = (1 - \gamma_5)/2$ and identified the $\langle \mathcal{O}_9 \rangle$ and $\langle \mathcal{O}_{10} \rangle$ matrix elements.

Finally, equating the two amplitudes $\mathcal{A}^{\text{eff}} = \mathcal{A}^{\text{full}}$ we obtain

$$-i(C_9 \langle \mathcal{O}_9 \rangle + C_{10} \langle \mathcal{O}_{10} \rangle) = i \frac{\Gamma_s^* \Gamma_b |\Gamma_\mu|^2}{128\pi^2 m_\Psi^2} F(x_Q, x_\ell) (\langle \mathcal{O}_9 \rangle - \langle \mathcal{O}_{10} \rangle) \quad (\text{A.9})$$

where \mathcal{O}_9 and \mathcal{O}_{10} are independent operators, thus we can obtain C_9 and C_{10} by equating the $\langle \mathcal{O}_{10} \rangle$ and $\langle \mathcal{O}_9 \rangle$ coefficients in the right-hand side and the left-hand side of (A.9). Obtaining

$$C_9 = -\frac{\Gamma_s^* \Gamma_b |\Gamma_\mu|^2}{128\pi^2 m_\Psi^2} F(x_Q, x_\ell) \quad \text{and} \quad C_{10} = \frac{\Gamma_s^* \Gamma_b |\Gamma_\mu|^2}{128\pi^2 m_\Psi^2} F(x_Q, x_\ell) \quad (\text{A.10})$$

with $C_9 = -C_{10}$, as expected because we were only dealing with left-handed couplings to the SM fermions. In this matching we integrated out the heavy degrees of freedom Φ_Q , Φ_ℓ and Ψ . In other words, we have encoded the physics of the full theory in the Wilson coefficients of the effective theory at a certain energy scale. Now we could use renormalization-group equations in order to run the Wilson coefficients to another scale, although in this particular case they would remain the same since we only have left-handed vector operators.

Appendix B

Fierz Identities

Here we list the Fierz identities for spinors used in the computations. With i, j, k and l representing Dirac indices here we find

$$(\gamma_\mu P_{L,R})_{ij} (\gamma_\mu P_{L,R})_{kl} = -(\gamma_\mu P_{L,R})_{il} (\gamma_\mu P_{L,R})_{kj} \quad (\text{B.1})$$

$$(\gamma_\mu P_{L,R})_{ij} (\gamma_\mu P_{R,L})_{kl} = 2(P_{R,L})_{il} (P_{L,R})_{kj} \quad (\text{B.2})$$

$$(P_{L,R})_{ij} (P_{L,R})_{kl} = \frac{1}{2} (P_{L,R})_{il} (P_{L,R})_{kj} + \frac{1}{8} (\sigma_{\mu\nu})_{il} (\sigma_{\mu\nu} P_{L,R})_{kj} \quad (\text{B.3})$$

$$(P_{L,R})_{ij} (P_{R,L})_{kl} = \frac{1}{2} (\gamma_\mu P_{R,L})_{il} (\gamma_\mu P_{L,R})_{kj} \quad (\text{B.4})$$

$$(\sigma_{\mu\nu})_{ij} (\sigma_{\mu\nu} P_{L,R})_{kl} = 6(\gamma_\mu P_{L,R})_{il} (\gamma_\mu P_{L,R})_{kj} - \frac{1}{2} (\sigma_{\mu\nu})_{il} (\sigma_{\mu\nu} P_{L,R})_{kj} , \quad (\text{B.5})$$

where $P_{L,R} = (1 \mp \gamma_5)/2$ and $\sigma_{\mu\nu} = \frac{i}{2} [\gamma_\mu, \gamma_\nu]$. When dealing with diagrams with crossed fermion lines, one needs Fierz identities involving charge conjugation matrices. Here, exchanging the second and the third Dirac index we find

$$(\gamma_\mu P_{L,R} C)_{ij} (C \gamma_\mu P_{L,R})_{kl} = -2(P_{R,L})_{ik} (P_{L,R})_{jl} \quad (\text{B.6})$$

$$(\gamma_\mu P_{L,R} C)_{ij} (C \gamma_\mu P_{R,L})_{kl} = -(\gamma_\mu P_{L,R})_{ik} (\gamma_\mu P_{R,L})_{jl} \quad (\text{B.7})$$

$$(P_{L,R} C)_{ij} (C P_{L,R})_{kl} = \frac{1}{2} (P_{L,R})_{ik} (P_{L,R})_{jl} - \frac{1}{8} (\sigma_{\mu\nu})_{ik} (\sigma_{\mu\nu} P_{L,R})_{jl} \quad (\text{B.8})$$

$$(P_{L,R} C)_{ij} (C P_{R,L})_{kl} = -\frac{1}{2} (\gamma_\mu P_{R,L})_{ik} (\gamma_\mu P_{R,L})_{jl} , \quad (\text{B.9})$$

with the charge conjugation matrix defined as $C = i\gamma_0\gamma_2$. If we were dealing with fields, every identity would get a minus sign due to the Dirac algebra.

Appendix C

New Scalars and Fermions

In this appendix we list the complementary information that has been used or mentioned in Chapters 3&4

C.1 Loop Functions

Here we list the dimensionless loop functions introduced in Sections 4.1 and 4.3. The loop functions appearing in box diagrams that involve four different masses are defined as

$$F(x, y, z) = \frac{x^2 \log(x)}{(x-1)(x-y)(x-z)} + \frac{y^2 \log(y)}{(y-1)(y-x)(y-z)} + \frac{z^2 \log(z)}{(z-1)(z-x)(z-y)}, \quad (\text{C.1})$$

$$G(x, y, z) = 2 \left(\frac{x \log(x)}{(x-1)(x-y)(x-z)} + \frac{y \log(y)}{(y-1)(y-x)(y-z)} + \frac{z \log(z)}{(z-1)(z-x)(z-y)} \right), \quad (\text{C.2})$$

which in the equal mass limit read

$$F(1, 1, 1) = -G(1, 1, 1) = \frac{1}{3}. \quad (\text{C.3})$$

In the presence of only three different masses in the loop, one gets the functions

$$F(x, y) \equiv F(x, y, 1) = \frac{1}{(1-x)(1-y)} + \frac{x^2 \log(x)}{(1-x)^2(x-y)} + \frac{y^2 \log(y)}{(1-y)^2(y-x)}, \quad (\text{C.4})$$

$$G(x, y) \equiv G(x, y, 1) = 2 \left(\frac{1}{(1-x)(1-y)} + \frac{x \log(x)}{(1-x)^2(x-y)} + \frac{y \log(y)}{(1-y)^2(y-x)} \right), \quad (\text{C.5})$$

while, in the presence of only two different masses in the loop, one gets

$$\begin{aligned} F(x) \equiv F(x, x) &= \frac{x+1}{(x-1)^2} - \frac{2x \log(x)}{(x-1)^3}, \\ G(x) \equiv G(x, x) &= \frac{2}{(x-1)^2} - \frac{(x+1) \log(x)}{(x-1)^3}. \end{aligned} \quad (\text{C.6})$$

The loop functions appearing in photon- and gluon-penguin diagrams and the Z -penguin diagrams of Chap. 3 are defined as

$$F_7(x) = \frac{x^3 - 6x^2 + 3x + 2 + 6x \log x}{12(x-1)^4}, \quad \tilde{F}_7(x) = x^{-1} F_7(x^{-1}), \quad (\text{C.7})$$

$$G_7(x) = \frac{x^2 - 4x + 3 + 2 \log x}{8(x-1)^3}, \quad \tilde{G}_7(x) = \frac{x^2 - 2x \log x - 1}{8(x-1)^3}, \quad (\text{C.8})$$

$$F_9(x) = \frac{-2x^3 + 9x^2 - 18x + 11 + 6 \log x}{36(x-1)^4}, \quad \tilde{F}_9(x) = x^{-1} F_9(x^{-1}), \quad (\text{C.9})$$

$$G_9(x) = \frac{-16x^3 + 45x^2 - 36x + 7 + 6(2x-3)x^2 \log x}{36(x-1)^4}, \quad \tilde{G}_9(x) = x^{-1} G_9(x^{-1}), \quad (\text{C.10})$$

which in the equal mass limit read

$$F_7(1) = \tilde{F}_7(1) = \frac{G_7(1)}{2} = \tilde{G}_7(1) = -F_9(1) = -\tilde{F}_9(1) = \frac{G_9(1)}{3} = \frac{\tilde{G}_9(1)}{3} = \frac{1}{24}. \quad (\text{C.11})$$

Finally, the loop functions for the calculation of Z -penguins of Chap. 4 are defined as

$$\begin{aligned} G_Z(x, y) &= x F_V(x, y) + x \leftrightarrow y, \\ F_Z(x, y, m) &\equiv \bar{F}_Z(x, y) - \overline{div}_\varepsilon = (x^2 F_V(x, y) + x \leftrightarrow y) - \overline{div}_\varepsilon, \\ H_Z(x, y, m) &\equiv \bar{H}_Z(x, y) + \overline{div}_\varepsilon = (y F_V(x, y) + x \leftrightarrow y) + 1 + \overline{div}_\varepsilon, \\ I_Z(x, m) &\equiv \bar{I}_Z(x) + \overline{div}_\varepsilon = \frac{x}{x-1} - x^2 F_V(x, 1) + \overline{div}_\varepsilon, \\ \tilde{G}_Z(x, y) &= x K_V(x, y) + x \leftrightarrow y, \\ \tilde{F}_Z(x, y) &= \left(x^2 K_V(x, y) - \frac{x^2}{x-y} F_V(x, y) \right) + x \leftrightarrow y, \end{aligned}$$

$$\tilde{H}_Z(x, y) = \left(\frac{x^2 y}{(y-1)(x-y)^2} - \frac{x^2 y^2 (3x-y-2) \log(x)}{(x-1)^2 (x-y)^3} \right) + x \leftrightarrow y, \quad (\text{C.12})$$

where we have defined $\overline{\text{div}}_\varepsilon = \Delta_\varepsilon - \log\left(\frac{m^2}{\mu^2}\right)$ and

$$F_V(x, y) = \frac{\log(x)}{(x-1)(x-y)}, \quad K_V(x, y) = \frac{(x^2 + xy - 2y) \log(x)}{(x-1)^2 (x-y)^3} - \frac{1}{(x-1)(x-y)^2}. \quad (\text{C.13})$$

It is interesting to notice that the following relations hold between particular limits of the penguin induced functions:

$$\begin{aligned} H_Z\left(\frac{m^2}{n^2}, \frac{m^2}{n^2}, m\right) &= I_Z\left(\frac{m^2}{n^2}, n\right), \\ -\frac{m^2}{n^2} G_Z\left(\frac{m^2}{n^2}, \frac{m^2}{n^2}\right) &+ \frac{1}{2} F_Z\left(\frac{m^2}{n^2}, \frac{m^2}{n^2}, n\right) + \frac{1}{4} H_Z\left(\frac{m^2}{n^2}, \frac{m^2}{n^2}, m\right) + \frac{1}{4} I_Z\left(\frac{m^2}{n^2}, n\right) = 0, \\ \frac{1}{2} x \tilde{G}_Z(x, x) - \frac{1}{3} \tilde{F}_Z(x, x) &= \tilde{G}_9(x), \\ \frac{1}{6} \tilde{F}_Z(x, x) &= F_9(x). \end{aligned} \quad (\text{C.14})$$

$$\frac{1}{6x} \tilde{H}_Z(x, x) = \tilde{F}_9(x). \quad (\text{C.15})$$

Moreover, it is useful to define the limit

$$F_Z(x) \equiv \overline{F}_Z(x, x) = \frac{x}{x-1} + \frac{(x-2)x \log x}{(x-1)^2}. \quad (\text{C.16})$$

Finally, the equal mass limits read

$$G_Z(1, 1) = \frac{\overline{F}_Z(1, 1)}{3} = -\overline{H}_Z(1, 1) = -\overline{I}_Z(1) = 6\tilde{G}_Z(1, 1) = -2\tilde{F}_Z(1, 1) = -2\tilde{H}_Z(1, 1) = \frac{1}{2}. \quad (\text{C.17})$$

C.2 Crossed Diagrams

If the NP fields have the appropriate quantum numbers they can be either real scalars or Majorana fermions. If this is the case, crossed diagrams as shown in Fig. C.1 can be constructed and

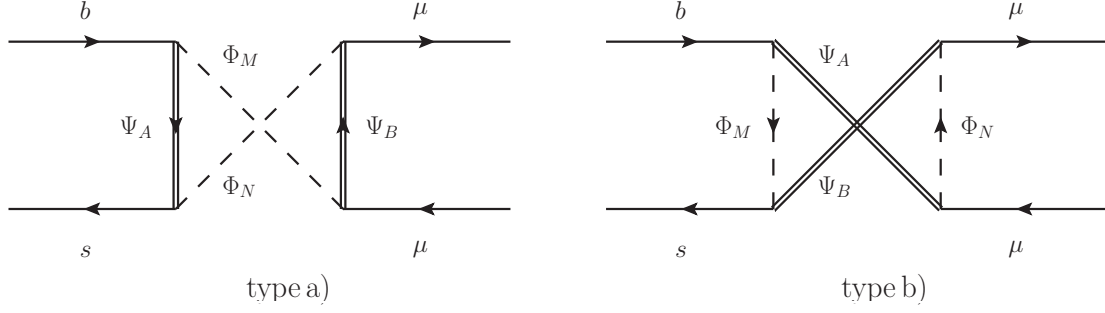


Figure C.1: Crossed box diagrams contributing to $b \rightarrow s\mu^+\mu^-$ transitions. The diagram on the left appears in models with real scalars, while the one on the right can be constructed in models with Majorana fermions.

$SU(3)$, type a)	Ψ_A	Ψ_B	Φ_M	Φ_N	$SU(3)$, type b)	Ψ_A	Ψ_B	Φ_M	Φ_N	χ
I	3	1	1	1	I	1	1	3	1	1
III	3	8	8	8	III	8	8	3	8	4/3

Table C.1: Table of $SU(3)$ -factors entering the box induced Wilson coefficients involved in $b \rightarrow s$ transitions for real scalars, type a), and Majorana fermions, type b). The numbers of each representation refer to the ones in Table 4.1.

contribute to $b \rightarrow s\mu^+\mu^-$ transitions in addition to the ones shown in Fig. 4.1. Similarly, there are contributions from crossed boxes to $B_s - \bar{B}_s$ mixing (in addition to the ones in Fig. 4.3) arising due to the diagrams in Fig. C.2.

C.2.1 $b \rightarrow s\mu^+\mu^-$

In $b \rightarrow s\mu^+\mu^-$ the possible representations that give rise to additional crossed diagrams with real scalars or Majorana fermions are listed in Tab. C.1. For type a) the only possibility is to have real scalars, while for type b) one can only have crossed diagrams in the presence of Majorana fermions.

The contribution to the Wilson coefficients stemming from the diagrams in Fig. C.1a) corresponds to the ones listed for a)-type in Eqs. (4.4)-(4.7), after inverting $M \leftrightarrow N$ in the muon couplings and changing $F(x_{AM}, x_{BM}, x_{NM}) \rightarrow -F(x_{AM}, x_{BM}, x_{NM})$. For case b) (see right diagram in Fig. C.1) the Wilson coefficients are given by

$$C_9^{\text{box } b)} = -\mathcal{N} \frac{\chi L_{BM}^{s*} L_{AM}^b}{32\pi\alpha_{\text{EM}} m_{\Phi_M}^2} \left[L_{BN}^{\mu*} L_{AN}^\mu \frac{m_{\Psi_A} m_{\Psi_B}}{m_{\Phi_M}^2} G(x_{AM}, x_{BM}, x_{NM}) \right]$$

$SU(3)$	Ψ_A	Ψ_B	Φ_M	Φ_N	χ_{BB}^M	$\tilde{\chi}_{BB}^M$	
I	3	3	1	1	1	0	Real Φ
II	1	1	3	3	0	1	Majorana Ψ
III	3	3	8	8	5/18	-1/6	Real Φ
IV	8	8	3	3	-1/6	5/18	Majorana Ψ
V	3	3	(1,8)	(8,1)	1/6	-1/2	Real Φ
VI	(1,8)	(8,1)	3	3	-1/2	1/6	Majorana Ψ

Table C.2: Table of $SU(3)$ -factors entering the box induced Wilson coefficients involved in $B_s - \bar{B}_s$ mixing for real scalars and Majorana fermions.

$$\left. -R_{BN}^{\mu*} R_{AN}^\mu F(x_{AM}, x_{BM}, x_{NM}) \right], \quad (\text{C.18})$$

$$C_{10}^{\text{box } b} = \mathcal{N} \frac{\chi L_{BM}^{s*} L_{AM}^b}{32\pi\alpha_{\text{EM}} m_{\Phi_M}^2} \left[L_{BN}^{\mu*} L_{AN}^\mu \frac{m_{\Psi_A} m_{\Psi_B}}{m_{\Phi_M}^2} G(x_{AM}, x_{BM}, x_{NM}) \right. \\ \left. + R_{BN}^{\mu*} R_{AN}^\mu F(x_{AM}, x_{BM}, x_{NM}) \right], \quad (\text{C.19})$$

$$C_S^{\text{box } b} = \mathcal{N} \frac{\chi L_{BM}^{s*} L_{AM}^b}{16\pi\alpha_{\text{EM}} m_{\Phi_M}^2} \left[R_{BN}^{\mu*} L_{AN}^\mu F(x_{AM}, x_{BM}, x_{NM}) \right. \\ \left. + L_{BN}^{\mu*} R_{AN}^\mu \frac{m_{\Psi_A} m_{\Psi_B}}{2m_{\Phi_M}^2} G(x_{AM}, x_{BM}, x_{NM}) \right], \quad (\text{C.20})$$

$$C_P^{\text{box } b} = \mathcal{N} \frac{\chi L_{BM}^{s*} L_{AM}^b}{16\pi\alpha_{\text{EM}} m_{\Phi_M}^2} \left[R_{BN}^{\mu*} L_{AN}^\mu F(x_{AM}, x_{BM}, x_{NM}) \right. \\ \left. - L_{BN}^{\mu*} R_{AN}^\mu \frac{m_{\Psi_A} m_{\Psi_B}}{2m_{\Phi_M}^2} G(x_{AM}, x_{BM}, x_{NM}) \right], \quad (\text{C.21})$$

$$C_T^{\text{box } b} = -\mathcal{N} \frac{\chi L_{BM}^{s*} R_{AM}^b L_{BN}^{\mu*} R_{AN}^\mu}{16\pi\alpha_{\text{EM}} m_{\Phi_M}^2} \frac{m_{\Psi_A} m_{\Psi_B}}{m_{\Phi_M}^2} G(x_{AM}, x_{BM}, x_{NM}), \quad (\text{C.22})$$

$$C_{9,S}^{\text{box}} = C_{9,S}^{\text{box}} (L \leftrightarrow R), \quad C_{P,10}^{\text{box}} = -C_{P,10}^{\text{box}} (L \leftrightarrow R), \quad (\text{C.23})$$

C.2.2 Meson Mixing

For B_s mixing we can either have real scalars or Majorana fermions. In Tab. C.2 we list the possible representations of the diagrams in Fig. C.2 writing explicitly if we have a real scalar contribution (diagrams on the left side of the figure) or a Majorana fermion (diagrams

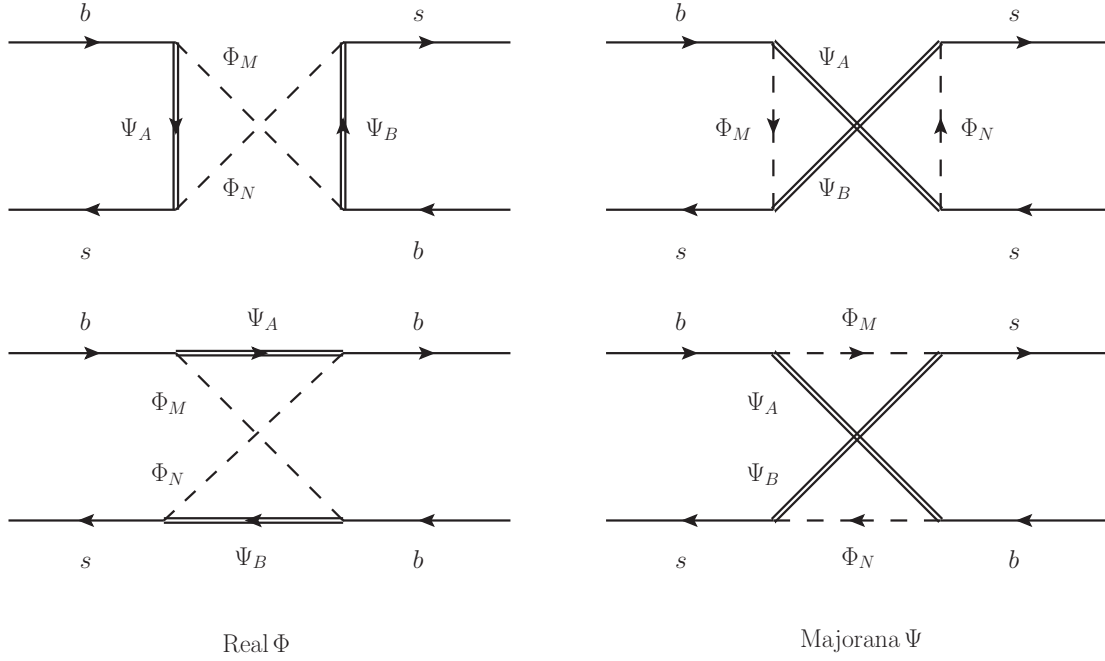


Figure C.2: Box diagrams contributing to $B_s - \bar{B}_s$ mixing. The diagram on the left is relative to models with real scalars, while the one on the right refers to models with Majorana fermions.

on the right). The Wilson coefficients for real scalar crossed diagrams correspond to the ones listed in Eqs. (4.4)-(4.7), after inverting $M \leftrightarrow N$ in two of the four couplings and changing $F(x_{AM}, x_{BM}, x_{NM}) \rightarrow -F(x_{AM}, x_{BM}, x_{NM})$, whereas matching to the generic Lagrangian from Eq. (4.1) with the crossed fermion contributions, one obtains the following results for the coefficients:

$$C_1 = (\chi_{BB}^M + \tilde{\chi}_{BB}^M) \frac{L_{AN}^{s*} L_{BM}^b L_{AM}^{s*} L_{BN}^b}{128\pi^2 m_{\Phi_M}^2} \frac{m_{\Psi_A} m_{\Psi_B}}{m_{\Phi_M}^2} G(x_{AM}, x_{BM}, x_{NM}), \quad (\text{C.24})$$

$$C_{2,3} = -(\chi_{BB}^M + \tilde{\chi}_{BB}^M) \frac{R_{AN}^{s*} L_{BM}^b R_{AM}^{s*} L_{BN}^b}{64\pi^2 m_{\Phi_M}^2} \frac{m_{\Psi_A} m_{\Psi_B}}{m_{\Phi_M}^2} G(x_{AM}, x_{BM}, x_{NM}), \quad (\text{C.25})$$

$$C_4 = \frac{L_{AM}^b R_{AN}^b}{32\pi^2 m_{\Phi_M}^2} [\chi_{BB}^M L_{BM}^{s*} R_{BN}^{s*} - \tilde{\chi}_{BB}^M R_{BM}^{s*} L_{BN}^{s*}] F(x_{AM}, x_{BM}, x_{NM}), \quad (\text{C.26})$$

$$C_5 = \frac{L_{AM}^b R_{AN}^b}{32\pi^2 m_{\Phi_M}^2} [\tilde{\chi}_{BB}^M L_{BM}^{s*} R_{BN}^{s*} - \chi_{BB}^M R_{BM}^{s*} L_{BN}^{s*}] F(x_{AM}, x_{BM}, x_{NM}), \quad (\text{C.27})$$

$$\tilde{C}_i = C_i (L \rightarrow R), \quad \text{for } i = \{1, 2, 3\}, \quad (\text{C.28})$$

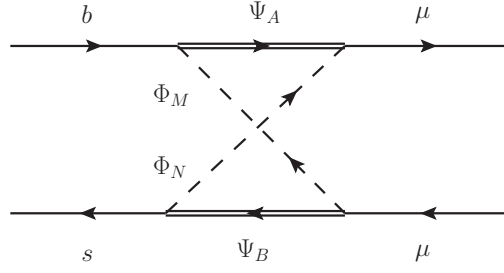


Figure C.3: Crossed box diagrams contributing to $b \rightarrow s\mu^+\mu^-$ transitions. The diagram appears when a complex scalar couples to b, s quarks and its conjugate couples to the muons.

$SU(3)$	Ψ_A	Ψ_B	Φ_M	Φ_N	χ
I	(1,3)	(3,1)	($\bar{3}$,1)	(1, $\bar{3}$)	1
II	(8,3)	(3,8)	($\bar{3}$,8)	(8, $\bar{3}$)	4/3
III	$\bar{3}$	$\bar{3}$	3	3	2

Table C.3: Table of $SU(3)$ -factors entering the box induced Wilson coefficients involved in $b \rightarrow s$ transitions for crossed diagrams with complex scalars.

The corresponding contributions to $D_0 - \bar{D}_0$ mixing are obtained from Eqs. (4.22)-(4.28) via the replacements $s \rightarrow u$ and $b \rightarrow c$.

C.3 Crossed Diagrams with Complex Scalars

There is also the possibility that a complex scalar couples to the down-type quarks whereas its hermitian conjugated version couples to muons. This means that the Lagrangian in Eq. (4.1) takes a slightly different form, namely

$$\mathcal{L}_{\text{int}} = \left[\bar{\Psi}_A (L_{AM}^b P_L b + L_{AM}^s P_L s + R_{AM}^b P_R b + R_{AM}^s P_R s) \Phi_M + \bar{\Psi}_A (L_{AM}^\mu P_L + R_{AM}^\mu P_R \mu) \Phi_M^\dagger \right] + \text{h.c.} \quad (\text{C.29})$$

Also this Lagrangian generates a contribution to $b \rightarrow s\mu^+\mu^-$ via the diagram shown in Fig. C.3. The possible representations under the $SU(3)$ of the new scalars and fermions in the loop are listed in Tab. C.3. The corresponding Wilson Coefficients can be obtained from the ones calculated for the type b diagrams in Eqs. (4.4)-(4.7) by exchanging $M \leftrightarrow N$ in the couplings R, L

and replacing $F(x_{AM}, x_{BM}, x_{NM}) \rightarrow -F(x_{AM}, x_{BM}, x_{NM})$.

Appendix D

$\ell_i \rightarrow \ell_j \nu_i \bar{\nu}_j$ with Scalar Leptoquarks

In this Appendix we collect the complete expression for $\ell_i \rightarrow \ell_j \nu_i \bar{\nu}_j$, with $i, j \in \{e, \mu, \tau\}$, and $m_{\ell_i} > m_{\ell_j}$. The most general dimension six effective Lagrangian describing these decays without taking into account right-handed neutrinos can be written as

$$\delta\mathcal{L}_{\text{eff}}^\tau = -\frac{2}{v^2} \left[(1 + \delta C_{LL}^{ij}) (\bar{\nu}_i \gamma^\mu P_L \ell_i) (\bar{\ell}_j \gamma_\mu P_L \nu_j) + \delta C_{LR}^{ij} (\bar{\nu}_i P_R \ell_i) (\bar{\ell}_j P_L \nu_j) \right] + \text{h.c.}, \quad (\text{D.1})$$

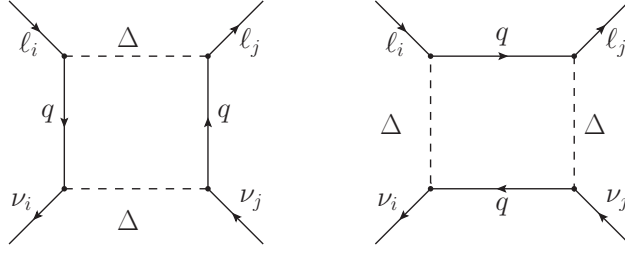
where δC_{LL}^{ij} and δC_{LR}^{ij} are the Wilson coefficients. For simplicity, we have considered only the lepton flavor conserving couplings since the LFV ones would not interfere with the SM. The relevant decay rate then reads,

$$\frac{\Gamma(\ell_i \rightarrow \ell_j \nu_i \bar{\nu}_j)}{\Gamma(\ell_i \rightarrow \ell_j \nu_i \bar{\nu}_j)^{\text{SM}}} = 1 + |1 + \delta C_{LL}^{ij}|^2 + \frac{1}{4} |\delta C_{LR}^{ij}|^2 + \frac{2m_{\ell_i}}{m_{\ell_j}} \text{Re} \left[(1 + \delta C_{LL}^{ij}) \delta C_{LR}^{ij} \right], \quad (\text{D.2})$$

normalized with respect to the SM value, $\Gamma(\ell_i \rightarrow \ell_j \nu_i \bar{\nu}_j)^{\text{SM}} = G_F^2 m_{\ell_i}^5 / (192\pi^3)$, after neglecting the terms $\mathcal{O}(m_{\ell_j}^2/m_{\ell_i}^2)$. LQs contributes to the effective Wilson coefficients in Eq. (D.2) at the one-loop level via two types of diagrams: (i) W -penguins and (ii) box diagrams. The former ones can be expressed in terms of the $W\tau\nu$ effective vertices defined in Eq. (5.37). In the limit of small transferred momenta (i.e. $m_{\ell_i}^2/m_W^2 \ll 1$) we find

$$\left[\delta C_{LL}^{ij} \right]^{\text{W-penguin}} = \delta h_{\ell_L}^{ii}(x_W = 0) + \delta h_{\ell_L}^{jj}(x_W = 0) + \dots, \quad (\text{D.3})$$

where $\delta h_{\ell_L}^{ij}$ are the effective coefficients reported in Sec. 5.4, in which x_W should be set to zero. In practice we truncate the series and neglect all the terms represented by ‘dots’ in Eq. (D.3).


 Figure D.1: Box diagrams contributing to $\ell_i \rightarrow \ell_j \nu_i \bar{\nu}_j$.

The box diagram contributions are schematically illustrated in Fig. D.1. For the LQ doublets, we find

$$\left[\delta C_{LL}^{ij} \right]_{R_2}^{\text{box}} = \frac{N_c v^2}{128 \pi^2 m_{R_2}^2} \left(y_{R_2}^{L\dagger} \cdot y_{R_2}^L \right)_{jj} \left(y_{R_2}^{L\dagger} \cdot y_{R_2}^L \right)_{ii}, \quad (\text{D.4})$$

$$\left[\delta C_{LR}^{ij} \right]_{R_2}^{\text{box}} = -\frac{N_c v^2}{64 \pi^2 m_{R_2}^2} \left(y_{R_2}^{R\dagger} \cdot y_{R_2}^R \right)_{ji} \left(y_{R_2}^{L\dagger} \cdot y_{R_2}^L \right)_{ij}, \quad (\text{D.5})$$

and

$$\left[\delta C_{LL}^{ij} \right]_{\tilde{R}_2}^{\text{box}} = -\frac{N_c v^2}{128 \pi^2 m_{\tilde{R}_2}^2} \left(y_{\tilde{R}_2}^{L\dagger} \cdot y_{\tilde{R}_2}^L \right)_{jj} \cdot \left(y_{\tilde{R}_2}^{L\dagger} \cdot y_{\tilde{R}_2}^L \right)_{ii}, \quad (\text{D.6})$$

where $y_{LQ}^\dagger \cdot y_{LQ}$ denotes a matrix product. The coefficient δC_{LR} is not generated by \tilde{R}_2 because this LQ does not couple to the right-handed leptons in Eq. (5.2). Also note that none of these box contributions can be captured by an EFT computation to leading logarithms. For the remaining LQ models, we find

$$\begin{aligned} \left[\delta C_{LL}^{ij} \right]_{S_1}^{\text{box}} &= +\frac{N_c v^2}{128 m_{S_1}^2} \left(y_{S_1}^{L\dagger} y_{S_1}^L \right)_{ji} \left(y_{S_1}^{L\dagger} y_{S_1}^L \right)_{ij}, \\ \left[\delta C_{LR}^{ij} \right]_{S_1}^{\text{box}} &= -\frac{N_c v^2}{64 \pi^2 m_{S_1}^2} \left(y_{S_1}^{R\dagger} \cdot y_{S_1}^R \right)_{ji} \left(y_{S_1}^{L\dagger} \cdot y_{S_1}^L \right)_{ij}. \end{aligned} \quad (\text{D.7})$$

and

$$\left[\delta C_{LL}^{ij} \right]_{S_3}^{\text{box}} = \frac{N_c v^2}{128 m_{S_3}^2} \left(y_{S_3}^{L\dagger} \cdot y_{S_3}^L \right)_{ji} \left(y_{S_3}^{L\dagger} \cdot y_{S_3}^L \right)_{ij} + \frac{N_c v^2}{32 m_{S_3}^2} \left(y_{S_3}^{L\dagger} \cdot y_{S_3}^L \right)_{jj} \left(y_{S_3}^{L\dagger} \cdot y_{S_3}^L \right)_{ii}. \quad (\text{D.8})$$

These contributions should be added to the ones, presented in Eq. (D.3).

Appendix E

S_1 & S_3 Observables

In this section we list the analytic expression of the observables appearing in the fits that are not shown in Chapter 5. The general Yukawa structure for S_1 and S_3 LQs is the same, without couplings to the first generation of quarks and leptons

$$y_{S_1}^L = \begin{pmatrix} 0 & 0 & 0 \\ 0 & y_{s\mu}^{S_1} & y_{s\tau}^{S_1} \\ 0 & y_{b\mu}^{S_1} & y_{b\tau}^{S_1} \end{pmatrix}, \quad y_{S_3}^L = \begin{pmatrix} 0 & 0 & 0 \\ 0 & y_{s\mu}^{S_3} & y_{s\tau}^{S_3} \\ 0 & y_{b\mu}^{S_3} & y_{b\tau}^{S_3} \end{pmatrix}. \quad (\text{E.1})$$

For each observable, we display the effective Hamiltonian or Lagrangian with effective coefficients, and we write these coefficients as functions of the Yukawas. All the form factors to compute the meson decays with B, B_s, D and D_s have been obtained from Ref. [48]. The form factors of vector mesons are taken from Ref [268], while the experimental values used are specified in each section

E.1 $b \rightarrow c\tau\nu$

These charged current transition is governed by the Hamiltonian in (2.39). Considering only the third generation operators, the only contribution from the LQs is at tree-level to the g_{V_L} coefficient in our setup.

$$g_{V_L} = \frac{1}{4\sqrt{2}G_F V_{cb}} \left[\frac{(V_{cs}y_{s\tau}^{S_1*} + V_{cb}y_{b\tau}^{S_1*})y_{b\tau}^{S_1}}{m_{S_1}^2} - \frac{(V_{cs}y_{s\tau}^{S_3*} + V_{cb}y_{b\tau}^{S_3*})y_{b\tau}^{S_3}}{m_{S_3}^2} \right] \quad (\text{E.2})$$

Assuming that the relevant contribution only comes from the τ leptons we can write [269]

$$\frac{R_{D^{(*)}}}{R_{D^{(*)}}^{\text{SM}}} = |1 + g_{VL}|^2. \quad (\text{E.3})$$

where before Moriond the experimental value was

$$R_D^{\text{exp old}} = 0.407 \pm 0.046 \quad \text{and} \quad R_{D^*}^{\text{exp old}} = 0.306 \pm 0.015, \quad (\text{E.4})$$

while after it became

$$R_D^{\text{exp}} = 0.334 \pm 0.029 \quad \text{and} \quad R_{D^*}^{\text{exp}} = 0.297 \pm 0.014. \quad (\text{E.5})$$

E.2 $b \rightarrow s\mu^+\mu^-$

The effective Hamiltonian governing this transition is the same as in (4.2) with the pattern of $C_9^{\text{NP}} = -C_{10}^{\text{NP}}$ in the muon since we only have left-handed couplings. In this case the leading contribution comes from a S_3 leptoquark exchanged at tree-level in the t -channel. The coefficient is

$$C_9^{\text{NP}} = -C_{10}^{\text{NP}} = \frac{\pi}{\sqrt{2}G_F V_{ts}^* V_{tb} \alpha_{\text{em}}} \frac{y_{s\mu}^{S_3^*} y_{b\mu}^{S_3}}{m_{S_3}^2}, \quad (\text{E.6})$$

and we use the value in [28].

E.3 $b \rightarrow s\nu\nu$

The effective Hamiltonian of this transition was also mentioned in Chapters 3 and 4. The effective coefficients involve the two LQs at tree level

$$C_L^{\mu\mu} = \frac{\pi}{2\sqrt{2}G_F V_{ts}^* V_{tb} \alpha_{\text{em}}} \left(\frac{y_{s\mu}^{S_1^*} y_{b\mu}^{S_1}}{m_{S_1}^2} + \frac{y_{s\mu}^{S_3^*} y_{b\mu}^{S_3}}{m_{S_3}^2} \right), \quad (\text{E.7})$$

$$C_L^{\mu\tau} = \frac{\pi}{2\sqrt{2}G_F V_{ts}^* V_{tb} \alpha_{\text{em}}} \left(\frac{y_{s\tau}^{S_1^*} y_{b\mu}^{S_1}}{m_{S_1}^2} + \frac{y_{s\tau}^{S_3^*} y_{b\mu}^{S_3}}{m_{S_3}^2} \right), \quad (\text{E.8})$$

$$C_L^{\tau\mu} = \frac{\pi}{2\sqrt{2}G_F V_{ts}^* V_{tb} \alpha_{\text{em}}} \left(\frac{y_{s\mu}^{S_1^*} y_{b\tau}^{S_1}}{m_{S_1}^2} + \frac{y_{s\mu}^{S_3^*} y_{b\tau}^{S_3}}{m_{S_3}^2} \right), \quad (\text{E.9})$$

$$C_L^{\tau\tau} = \frac{\pi}{2\sqrt{2}G_F V_{ts}^* V_{tb} \alpha_{\text{em}}} \left(\frac{y_{s\tau}^{S_1^*} y_{b\tau}^{S_1}}{m_{S_1}^2} + \frac{y_{s\tau}^{S_3^*} y_{b\tau}^{S_3}}{m_{S_3}^2} \right), \quad (\text{E.10})$$

The related observable is described in other chapters and we adopt the same experimental value as in Chaps. 3 and 4.

E.4 $b \rightarrow c\ell\nu$ with $\ell = \mu, e$

The observable related to this process is $R_D^{\mu/e}$ and the Hamiltonian related to this process is the same as in the τ sector but with muons. Since we do not have NP related to electrons, we write the effective coefficient contribution of this process as

$$g_{V_L}^\mu = \frac{1}{4\sqrt{2}G_F V_{cb}} \left[\frac{(V_{cs} y_{s\mu}^{S_1^*} + V_{cb} y_{b\mu}^{S_1^*}) y_{b\mu}^{S_1}}{m_{S_1}^2} - \frac{(V_{cs} y_{s\mu}^{S_3^*} + V_{cb} y_{b\mu}^{S_3^*}) y_{b\mu}^{S_3}}{m_{S_3}^2} \right], \quad (\text{E.11})$$

then the observable reads the same as for $R_{D^{(*)}}$.

$$R_D^{\mu/e} = R_D^{\mu/e \text{ SM}} |1 + g_{V_L}^\mu|^2. \quad (\text{E.12})$$

Obtaining $R_D^{\mu/e \text{ exp}} = 0.995 \pm 0.044$ from the branching ratios in [270]. This observable ensures that the couplings of the muons are smaller respect to the tau ones.

E.5 τ decays

Here we list the τ decays that we use as constraints. They are LFV decays therefore they are not predicted by the SM.

$\tau \rightarrow \mu\gamma$

This decay is a good constraint in order to assess LFV in NP models. The Hamiltonian of this decay is very similar to the one of $b \rightarrow s\gamma$ as it occurs also at loop-level, but instead of quarks we have a muon and a tau:

$$\mathcal{H}_{\text{eff}}^{\tau \rightarrow \mu\gamma} = m_\tau \sigma_L (\bar{\mu} \sigma^{\mu\nu} P_L \tau) F_{\mu\nu}. \quad (\text{E.13})$$

Since it is an electromagnetic interaction we split the results by the electric charge eigenstates. At leading order we have

$$\begin{aligned}
 \sigma_L^{\Delta^{1/3}} &= - \sum_{\Delta=S_1, S_3} \frac{N_c}{192\pi^2 m_\Delta^2} \sum_{q=u,c,t} (V_{qb} y_{b\mu}^\Delta + V_{qs} y_{s\mu}^{\Delta*}) (V_{qb}^* y_{b\tau}^\Delta + V_{qs}^* y_{s\tau}^\Delta), \\
 \sigma_L^{\Delta^{4/3}} &= - \frac{N_c}{48\pi^2 m_{S_3}^2} (y_{b\mu}^{S_3*} y_{b\tau}^{S_3} + y_{s\mu}^{S_3*} y_{s\tau}^{S_3}), \\
 \sigma_L &= \sigma_L^{\Delta^{1/3}} + \sigma_L^{\Delta^{4/3}}.
 \end{aligned} \tag{E.14}$$

with the branching ratio

$$\text{Br}(\tau \rightarrow \mu\gamma) = \tau_\tau \frac{(m_\tau^2 - m_\mu^2)^3}{4m_\tau^3} |\sigma_L|^2, \tag{E.15}$$

where τ_τ is the life-time of the τ . The experimental bound on this observable states that $\text{Br}(\tau \rightarrow \mu\gamma) < 4.4 \times 10^{-8}$, taking this data from [152].

$\tau \rightarrow \mu\phi$

This observable is also a LFV test for a NP model. This time, it is a tree-level induced process where ϕ is a vector meson made of a strange and anti-strange quark. In our model the branching ratio is

$$\text{Br}(\tau \rightarrow \mu\phi) = \tau_\tau f_\phi^2 \frac{m_\phi^4 (m_\tau^2 - m_\phi^2)}{4m_\tau^3} \left(\frac{m_\tau^4}{m_\phi^4} + \frac{m_\tau^2}{m_\phi^2} - 1 \right) \left| \frac{y_{s\mu}^{S_3*} y_{s\tau}^{S_3}}{m_{S_3}^2} \right|^2, \tag{E.16}$$

where f_ϕ is the form factor defined in Ref. [268], while the experimental prediction is taken from [152] and it is $\text{Br}(\tau \rightarrow \mu\phi) < 8.4 \times 10^{-8}$ at 90% C.L.

E.6 $K \rightarrow \ell\nu_\ell$ with $\ell = e, \mu$ and $\tau \rightarrow K\nu_\tau$

The effective vertex of this observable in our model concerns only the muon and the tau, since we do not have NP in the electron. The Hamiltonian for the decay involving the muon reads

$$\mathcal{H}_{\text{eff}}^{us\mu\nu\mu} = -2\sqrt{2}G_F V_{us} (1 + g_{V_L}^{us\mu\nu\mu}) (\bar{s}\gamma_\mu P_L u) (\bar{\mu}\gamma^\mu P_L \nu_\mu) + \text{h.c.}, \tag{E.17}$$

where in our $S_1 + S_3$ model we have

$$g_{V_L}^{us\mu\nu_\mu} = \frac{1}{4\sqrt{2}G_F V_{us}} \left[\frac{(V_{us}y_{s\mu}^{S_1*} + V_{ub}y_{b\mu}^{S_1*})y_{s\mu}^{S_1}}{m_{S_1}^2} - \frac{(V_{us}y_{s\mu}^{S_3*} + V_{ub}y_{b\mu}^{S_3*})y_{b\mu}^{S_3}}{m_{S_3}^2} \right]. \quad (\text{E.18})$$

We can construct the ratio of branching fractions defining

$$r_K^{e/\mu} = \frac{\text{Br}(K \rightarrow e\nu_e)}{\text{Br}(K \rightarrow \mu\nu_\mu)} \quad (\text{E.19})$$

with

$$\frac{r_K^{e/\mu}}{(r_K^{e/\mu})_{\text{SM}}} = \frac{1}{|1 + g_{V_L}^{us\mu\nu_\mu}|^2}. \quad (\text{E.20})$$

We can also construct the Hamiltonian for the τ decay in a similar way

$$\mathcal{H}_{\text{eff}}^{us\tau\nu_\tau} = -2\sqrt{2}G_F V_{us}(1 + g_{V_L}^{us\tau\nu_\tau})(\bar{s}\gamma_\mu P_L u)(\bar{\tau}\gamma^\mu P_L \nu_\tau) + \text{h.c.}, \quad (\text{E.21})$$

with

$$g_{V_L}^{us\tau\nu_\tau} = \frac{1}{4\sqrt{2}G_F V_{us}} \left[\frac{(V_{us}y_{s\tau}^{S_1*} + V_{ub}y_{b\tau}^{S_1*})y_{s\tau}^{S_1}}{m_{S_1}^2} - \frac{(V_{us}y_{s\tau}^{S_3*} + V_{ub}y_{b\tau}^{S_3*})y_{b\tau}^{S_3}}{m_{S_3}^2} \right]. \quad (\text{E.22})$$

Constructing the ratio between the tau and the muon we have

$$\frac{r_K^{\tau/\mu}}{(r_K^{\tau/\mu})_{\text{SM}}} = \frac{|1 + g_{V_L}^{us\tau\nu_\tau}|^2}{|1 + g_{V_L}^{us\mu\nu_\mu}|^2}. \quad (\text{E.23})$$

We use the experimental values from Ref. [152] obtaining

$$\frac{r_K^{e/\mu}}{(r_K^{e/\mu})_{\text{SM}}} = 1.004 \pm 0.004 \quad \text{and} \quad \frac{r_K^{\tau/\mu}}{(r_K^{\tau/\mu})_{\text{SM}}} = 0.972 \pm 0.015 \quad (\text{E.24})$$

E.7 $D_s \rightarrow \ell \nu_\ell$ with $\ell = \mu, \tau$

Analogously to other charged meson decays to leptons, we can construct the effective Hamiltonian as

$$\mathcal{H}_{\text{eff}}^{cs\ell\nu_\ell} = -2\sqrt{2}G_F V_{cs}(1 + g_{V_L}^{cs\ell\nu_\ell})(\bar{s}\gamma_\mu P_L c)(\bar{\ell}\gamma^\mu P_L \nu_\ell) + \text{h.c.}, \quad (\text{E.25})$$

with

$$g_{V_L}^{cs\ell\nu_\ell} = \frac{1}{4\sqrt{2}G_F V_{cs}} \left[\frac{(V_{cs}y_{s\ell}^{S_1^*} + V_{cb}y_{b\ell}^{S_1^*})y_{s\ell}^{S_1}}{m_{S_1}^2} - \frac{(V_{cs}y_{s\ell}^{S_3^*} + V_{cb}y_{b\ell}^{S_3^*})y_{b\ell}^{S_3}}{m_{S_3}^2} \right], \quad (\text{E.26})$$

for both tau and muon. For the experimental value we use the branching ratios in [152] finding $\text{Br}(D_s \rightarrow \mu\nu_\mu)^{\text{exp}} = (0.550 \pm 0.023)10^{-2}$ and $\text{Br}(D_s \rightarrow \tau\nu_\tau)^{\text{exp}} = (5.48 \pm 0.23)10^{-2}$.

E.8 $B \rightarrow \tau\nu_\tau$

In this B decay, we proceed in the same manner as other meson decays but with b and u quarks. The relevant effective Hamiltonian is

$$\mathcal{H}_{\text{eff}}^{ub\ell\nu_\ell} = -2\sqrt{2}G_F V_{cs}(1 + g_{V_L}^{ub\tau\nu_\tau})(\bar{b}\gamma_\mu P_L u)(\bar{\tau}\gamma^\mu P_L \nu_\tau) + \text{h.c.}, \quad (\text{E.27})$$

with

$$g_{V_L}^{ub\tau\nu_\tau} = \frac{1}{4\sqrt{2}G_F V_{ub}} \left[\frac{(V_{us}y_{s\tau}^{S_1^*} + V_{ub}y_{b\tau}^{S_1^*})y_{s\tau}^{S_1}}{m_{S_1}^2} - \frac{(V_{us}y_{s\tau}^{S_3^*} + V_{ub}y_{b\tau}^{S_3^*})y_{b\tau}^{S_3}}{m_{S_3}^2} \right], \quad (\text{E.28})$$

and using the experimental value from the PDG [152] $\text{Br}(B \rightarrow \tau\nu_\tau)^{\text{exp}} = (1.06 \pm 0.19)10^{-4}$.

E.9 $B \rightarrow K\mu\tau$

This decay is very similar to the one giving R_K but in this case we can explore the possibility of LFV. The effective Hamiltonian is

$$\mathcal{H}_{\text{eff}} = C_9^{\mu\tau} \mathcal{O}_9^{\mu\tau} + C_9^{\tau\mu} \mathcal{O}_9^{\tau\mu} + C_{10}^{\mu\tau} \mathcal{O}_{10}^{\mu\tau} + C_{10}^{\tau\mu} \mathcal{O}_{10}^{\tau\mu} + \text{h.c.}, \quad (\text{E.29})$$

where

$$\mathcal{O}_9^{\ell\ell'} = \frac{\alpha_{\text{EM}}}{4\pi} (\bar{s}\gamma_\mu P_L b)(\bar{\ell}\gamma^\mu \ell'), \quad \mathcal{O}_{10} = \frac{\alpha_{\text{EM}}}{4\pi} (\bar{s}\gamma_\mu P_L b)(\bar{\ell}\gamma^\mu \gamma_5 \ell'). \quad (\text{E.30})$$

The leading contribution to this process in our model is obtained via S_3 exchange at tree-level, with the $C_9 = -C_{10}$ pattern, having different couplings for $\mu\tau$ and $\tau\mu$ combination

$$C_9^{\mu\tau} = \frac{\pi}{\sqrt{2}G_F V_{ts}^* V_{tb} \alpha_{\text{em}}} \frac{y_{s\tau}^{S_3^*} y_{b\mu}^{S_3}}{m_{S_3}^2} \quad C_9^{\tau\mu} = \frac{\pi}{\sqrt{2}G_F V_{ts}^* V_{tb} \alpha_{\text{em}}} \frac{y_{s\mu}^{S_3^*} y_{b\tau}^{S_3}}{m_{S_3}^2}, \quad (\text{E.31})$$

We use the branching fraction as observable with

$$\text{Br}(B \rightarrow K\mu\tau) = 10^{-9} (a_9 |C_9^{\mu\tau} + C_9^{\tau\mu}| + a_{10} |C_{10}^{\mu\tau} + C_{10}^{\tau\mu}|^2) \quad (\text{E.32})$$

where we take $a_9 = 9.6$ and $a_{10} = 10$ from Ref. [110]. The experimental value we take it to be $\text{Br}(B \rightarrow K\mu\tau) < 4.8 \times 10^{-5}$ [152].

E.10 χ^2 Tables

In this section we list the tables with the χ^2 value for each observable. The χ^2 for an observable X with an error σ is defined as¹

$$\chi^2 = \frac{(X_{\text{th}} - X_{\text{exp}})^2}{\sigma_{\text{th}}^2 + \sigma_{\text{exp}}^2}. \quad (\text{E.33})$$

In the following tables we list 16 observables. The first table has the numbers assuming the Yukawas in Eq. 5.53, the second table refers to the Yukawas in Eq. 5.59, and the last table is obtained using the ones in Eq. 5.60. The last column in each table indicates the χ^2 value for each observable in the SM, while in the intermediate columns we list the χ^2 value for each observable in the best fit point, where in each column the fit is performed with the numbers without the mark \otimes only. In this way, we can assess if a certain value of any observable is spoiled (respect to its experimental value) if it is included or not in the fit.

¹For upper-bounded experimental values we assume $X_{\text{exp}} = 0$ and we take σ_{exp} as the value of the upper-bound.

Scenario 1 Eq. 5.53	SM values			
$R_{D^{(*)}}$	0.02	3.06	3.11	15.1
$b \rightarrow s\mu\mu$	0.00	0.00	0.01	16.0
ΔM_s	\otimes 101	0.84	0.94	0.38
$Z \rightarrow \mu\mu$	0.01	0.00	0.00	0.01
$Z \rightarrow \tau\tau$	0.41	0.60	0.55	0.47
$Z \rightarrow \nu\nu$	4.29	4.15	4.09	3.81
$b \rightarrow s\nu\nu$	0.12	0.81	0.79	0.14
$R_D^{\mu/e}$	0.00	0.01	0.02	0.00
$\tau \rightarrow \mu\gamma$	\otimes 0.00	\otimes 0.00	0.00	0.00
$\tau \rightarrow \mu\phi$	\otimes 0.07	\otimes 0.00	0.00	0.00
$r_K^{e/\mu}$	\otimes 1.20	\otimes 1.21	1.22	1.20
$r_K^{\tau/\mu}$	\otimes 3.42	\otimes 3.38	3.29	3.54
$D_s \rightarrow \mu\nu$	\otimes 0.38	\otimes 0.38	0.38	0.38
$D_s \rightarrow \tau\nu$	\otimes 1.18	\otimes 1.20	1.21	1.17
$B^+ \rightarrow \tau\nu$	\otimes 0.00	\otimes 0.00	0.00	0.24
$B \rightarrow K\mu\tau$	\otimes 0.00	\otimes 0.00	0.00	0.00
TOTAL	112	15.6	15.6	42.4

Table E.1: χ^2 values for each observables in different left-handed fits with the Yukawa pattern in (5.53) and SM. The \otimes mark indicates which observable is not considered in the fit. To obtain the plot in Fig. 5.6 we include all the observables in the fit.

Scenario 2 Eq. 5.59	SM values			
$R_{D^{(*)}}$	5.03	5.04	5.03	15.1
$b \rightarrow s\mu\mu$	0.00	0.00	0.00	16.0
ΔM_s	1.15	1.14	1.15	0.38
$Z \rightarrow \mu\mu$	\otimes 0.01	0.01	0.01	0.01
$Z \rightarrow \tau\tau$	\otimes 0.41	0.45	0.43	0.47
$Z \rightarrow \nu\nu$	\otimes 4.00	3.89	3.94	3.81
$b \rightarrow s\nu\nu$	0.20	0.20	0.21	0.14
$R_D^{\mu/e}$	\otimes 0.00	\otimes 0.00	0.00	0.00
$\tau \rightarrow \mu\gamma$	0.00	0.00	0.00	0.00
$\tau \rightarrow \mu\phi$	\otimes 0.01	\otimes 5.86	0.02	0.00
$r_K^{e/\mu}$	\otimes 1.20	\otimes 1.20	1.20	1.20
$r_K^{\tau/\mu}$	\otimes 3.55	\otimes 3.55	3.55	3.54
$D_s \rightarrow \mu\nu$	\otimes 0.38	\otimes 0.38	0.38	0.38
$D_s \rightarrow \tau\nu$	\otimes 1.17	\otimes 1.17	1.17	1.17
$B^+ \rightarrow \tau\nu$	\otimes 0.02	\otimes 0.02	0.02	0.24
$B \rightarrow K\mu\tau$	0.00	0.00	0.00	0.00
TOTAL	17.11	22.88	17.03	42.43

Table E.2: χ^2 values for each observables in different left-handed fits with the Yukawa pattern in (5.59) and SM. The \otimes mark indicates which observable is not considered in the fit. To obtain the plot in Fig. 5.6 we include all the observables in the fit.

Scenario 3 Eq. 5.60	SM values				
$R_{D^{(*)}}$	2.40	1.74	0.02	1.57	15.1
$b \rightarrow s\mu\mu$	0.01	0.01	0.01	0.00	16.0
ΔM_s	0.68	0.54	\otimes 100	0.81	0.38
$Z \rightarrow \mu\mu$	0.01	\otimes 0.01	0.01	0.01	0.01
$Z \rightarrow \tau\tau$	0.95	\otimes 2.26	0.42	0.74	0.47
$Z \rightarrow \nu\nu$	3.93	\otimes 4.03	3.90	3.82	3.81
$b \rightarrow s\nu\nu$	0.88	0.79	0.32	\otimes 10.7	0.14
$R_D^{\mu/e}$	0.00	0.00	0.00	\otimes 0.00	0.00
$\tau \rightarrow \mu\gamma$	0.00	0.00	0.00	\otimes 2.08	0.00
$\tau \rightarrow \mu\phi$	0.21	0.22	0.22	\otimes 10^5	0.00
$r_K^{e/\mu}$	1.19	1.19	1.19	\otimes 42.9	1.20
$r_K^{\tau/\mu}$	0.92	0.82	0.65	\otimes 12.9	3.54
$D_s \rightarrow \mu\nu$	0.38	0.38	0.38	\otimes 1.73	0.38
$D_s \rightarrow \tau\nu$	1.93	1.98	2.07	\otimes 1.45	1.17
$B^+ \rightarrow \tau\nu$	0.00	0.00	0.00	\otimes 0.00	0.24
$B \rightarrow K\mu\tau$	0.02	0.02	0.05	\otimes 0.73	0.00
TOTAL	13.51	13.98	109	10^5	42.43

Table E.3: χ^2 values for each observables in different left-handed fits with the Yukawa pattern in (5.60) and SM. The \otimes mark indicates which observable is not considered in the fit. To obtain the plot in Fig. 5.6 we include all the observables in the fit.

Appendix F

Two Higgs Doublet Model

F.1 Hadronic Matrix Elements

For completeness we give the definitions of the decay constant (f_{B_s}) and of the form factors [$f_{+,0,T}(q^2)$], quantities which parametrize the hadronic matrix elements relevant to the processes discussed in this paper:

$$\begin{aligned}\langle 0 | \bar{b} \gamma_\mu \gamma_5 s | B_s(p) \rangle &= i p_\mu f_{B_s}, \\ \langle \bar{K}(k) | \bar{s} \gamma_\mu b | \bar{B}(p) \rangle &= \left[(p+k)_\mu - \frac{m_B^2 - m_K^2}{q^2} q_\mu \right] f_+(q^2) + \frac{m_B^2 - m_K^2}{q^2} q_\mu f_0(q^2), \\ \langle \bar{K}(k) | \bar{s} b | \bar{B}(p) \rangle &= \frac{1}{m_b - m_s} q^\mu \langle \bar{K}(k) | \bar{s} \gamma_\mu b | \bar{B}(p) \rangle = \frac{m_B^2 - m_K^2}{m_b - m_s} f_0(q^2), \\ \langle \bar{K}(k) | \bar{s} \sigma_{\mu\nu} b | \bar{B}(p) \rangle &= -i (p_\mu k_\nu - p_\nu k_\mu) \frac{2f_T(q^2, \mu)}{m_B + m_K},\end{aligned}\tag{F.1}$$

where for $B \rightarrow K \ell^+ \ell^-$ the kinematically accessible q^2 values lie in the interval $4m_\ell^2 \leq q^2 \leq (m_B - m_K)^2$. Notice that we do not write explicitly the scale dependence of the quark masses, nor of the scalar and tensor densities and of the form factor $f_T(q^2)$. In the actual computations the $\overline{\text{MS}}$ values of these quantities are taken at $\mu = m_b$.

F.2 Scalar penguins and Auxiliary Functions

In this Appendix we give the expressions for the Wilson coefficients generated by each diagram shown in Fig. 6.5. We also give the expressions for the auxiliary functions (f_i and g_i) used in

Chap. 6.

The penguins arising from coupling to $\varphi_i^0 \in \{h, H, A\}$ contribute to the effective coefficient $C_{S,P}$ and can be generically written as

$$C_S^{\text{NP},\varphi_i^0} = \frac{\sqrt{x_b x_\ell}}{\sin^2 \theta_W} \sum_{k=1}^{18} \frac{m_t^2}{m_{\varphi_i^0}} \text{Re} \left(\xi_\ell^{\varphi_i^0} \right) \widehat{C}^{k,\varphi_i^0}, \quad (\text{F.2})$$

$$C_P^{\text{NP},\varphi_i^0} = \frac{\sqrt{x_b x_\ell}}{\sin^2 \theta_W} \sum_{k=1}^{18} \frac{m_t^2}{m_{\varphi_i^0}} i \text{Im} \left(\xi_\ell^{\varphi_i^0} \right) \widehat{C}^{k,\varphi_i^0}, \quad (\text{F.3})$$

where $\widehat{C}^{k,\varphi_i^0}$ is a common coefficient generated by the diagram k , with $k = 1, \dots, 18$. Since, in our framework, $\zeta_\ell^h, \zeta_\ell^H \in \mathbb{R}$ and $\zeta_\ell^A \in i \times \mathbb{R}$, it is clear that the CP-even scalars h and H contribute only to C_S , whereas the CP-odd Higgs A contributes only to C_P , as expected from the assumption of CP conservation. We obtain in the unitary gauge,

$$\begin{aligned} \widehat{C}^{1,\varphi_i^0} = & \frac{\xi_u^{\varphi_i^0}}{4} \left\{ \zeta_d \zeta_u^* \frac{x_t}{x_{H^\pm} - x_t} \left[1 - \frac{x_{H^\pm}}{x_{H^\pm} - x_t} \log \left(\frac{x_{H^\pm}}{x_t} \right) \right] \right. \\ & + |\zeta_u|^2 \frac{x_t}{2(x_{H^\pm} - x_t)^2} \left[\frac{3x_t - x_{H^\pm}}{2} + \frac{x_{H^\pm}(x_{H^\pm} - 2x_t)}{x_{H^\pm} - x_t} \log \left(\frac{x_{H^\pm}}{x_t} \right) \right] \left. \right\} \\ & + \frac{\xi_u^{\varphi_i^0*}}{4} \left\{ \zeta_d \zeta_u^* \left[\Lambda - \frac{x_t}{x_{H^\pm} - x_t} - \frac{x_{H^\pm}^2}{(x_{H^\pm} - x_t)^2} \log x_{H^\pm} + \frac{x_t(2x_{H^\pm} - x_t)}{(x_{H^\pm} - x_t)^2} \log x_t \right] \right. \\ & + |\zeta_u|^2 \frac{x_t}{2(x_{H^\pm} - x_t)^2} \left[\frac{3x_{H^\pm} - x_t}{2} - \frac{x_{H^\pm}^2}{x_{H^\pm} - x_t} \log \left(\frac{x_{H^\pm}}{x_t} \right) \right] \left. \right\}, \end{aligned} \quad (\text{F.4})$$

$$\begin{aligned} \widehat{C}^{2,\varphi_i^0} = & -\varepsilon_{\varphi_i^0} \frac{\sin^2 \theta_W \lambda_{H^+ H^-}^{\varphi_i^0}}{4\pi\alpha(x_{H^\pm} - x_t)} \left\{ \zeta_d \zeta_u^* \left[\frac{x_t}{x_{H^\pm} - x_t} \log \left(\frac{x_{H^\pm}}{x_t} \right) - 1 \right] \right. \\ & + |\zeta_u|^2 \left[\frac{x_t^2}{2(x_{H^\pm} - x_t)^2} \log \left(\frac{x_{H^\pm}}{x_t} \right) + \frac{x_{H^\pm} - 3x_t}{4(x_{H^\pm} - x_t)} \right] \left. \right\}, \end{aligned} \quad (\text{F.5})$$

$$\widehat{C}^{3,\varphi_i^0} = \frac{\xi_d^{\varphi_i^0}}{4} \zeta_d \zeta_u^* \left[-\Lambda + \frac{x_{H^\pm}}{x_{H^\pm} - x_t} \log x_{H^\pm} - \frac{x_t}{x_{H^\pm} - x_t} \log x_t \right], \quad (\text{F.6})$$

$$\widehat{C}^{4,\varphi_i^0} = 0, \quad (\text{F.7})$$

$$\begin{aligned} \widehat{C}^{5,\varphi_i^0} = \frac{1}{4} \left\{ \xi_u^{\varphi_i^0*} \left[\Lambda - \frac{5x_t^2 - 13x_t - 2}{4(x_t - 1)^2} - \frac{2x_t^3 - 6x_t^2 + 9x_t - 2}{2(x_t - 1)^3} \log x_t \right] \right. \\ \left. + \xi_u^{\varphi_i^0} \left[\frac{\Lambda}{2} - \frac{2x_t^2 - x_t - 7}{4(x_t - 1)^2} - \frac{x_t^3 - 3x_t^2 + 3x_t + 2}{2(x_t - 1)^2} \log x_t \right] \right\}, \end{aligned} \quad (\text{F.8})$$

$$\widehat{C}^{6,\varphi_i^0} = \varepsilon_{\varphi_i^0} \frac{\lambda_{W^+W^-}^{\varphi_i^0}}{8} \left[-3\Lambda + \frac{x_t^2 - 2x_t - 11}{2(x_t - 1)^2} + \frac{3x_t(x_t^2 - 3x_t + 4)}{(x_t - 1)^3} \log x_t \right], \quad (\text{F.9})$$

$$\widehat{C}^{7,\varphi_i^0} = \widehat{C}^{8,\varphi_i^0} = 0, \quad (\text{F.10})$$

$$\widehat{C}^{9,\varphi_i^0} = \frac{\lambda_{H^+W^-}^{\varphi_i^0}}{8} \zeta_u^* \left[\frac{1}{2} - \Lambda + \frac{x_{H^\pm}(x_{H^\pm} + 2) \log x_{H^\pm}}{(x_{H^\pm} - 1)(x_{H^\pm} - x_t)} - \frac{x_t(x_t + 2) \log x_t}{(x_t - 1)(x_{H^\pm} - x_t)} \right], \quad (\text{F.11})$$

$$\begin{aligned} \widehat{C}^{10,\varphi_i^0} = \frac{\lambda_{H^+W^-}^{\varphi_i^0*}}{4} \left\{ -\frac{\zeta_u}{2} \left[\frac{x_t(x_{H^\pm}x_t - 4x_{H^\pm} + 3x_t)}{(x_t - 1)(x_{H^\pm} - x_t)^2} \log x_t - \frac{x_{H^\pm}(x_{H^\pm}x_t - 3x_{H^\pm} + 2x_t)}{(x_t - 1)(x_{H^\pm} - x_t)^2} \log x_{H^\pm} \right. \right. \\ \left. \left. + \frac{x_{H^\pm}}{x_{H^\pm} - x_t} \right] + \zeta_d \left[-\Lambda + \frac{x_{H^\pm} \log x_{H^\pm}}{x_{H^\pm} - x_t} - \frac{x_t \log x_t}{x_{H^\pm} - x_t} \right] \right\}, \end{aligned} \quad (\text{F.12})$$

where the couplings $\lambda_{W^+W^-}^{\varphi_i^0}$ and $\lambda_{H^\pm W^\mp}^{\varphi_i^0}$ are defined below Eq. (F.34) and Eq. (F.36), respectively. The coefficient $\varepsilon_{\varphi_i^0} = -1$ for $\varphi_i^0 = A$, and $+1$ otherwise. Moreover, $\Lambda = -\frac{2\mu^{D-4}}{D-4} - \gamma_E + \log 4\pi - \log\left(\frac{m_W^2}{\mu^2}\right) + 1$ contains an ultraviolet divergence which cancels out after summing up all the diagrams. The diagrams (9.11)–(9.18) do not contribute in our computation, owing to the fact that we work in the unitary gauge. To make sure that our resulting (total) expressions are gauge independent we performed the computation in the Feynman gauge too. In comparison with Ref. [238], we only disagree with one of the signs in the expression for $\widehat{C}^{5,\varphi_i^0}$, which we believe is a typo.

The auxiliary functions $g_{0,1,2}$ used in Eq. (6.43) are defined by

$$\begin{aligned} g_0 = \frac{1}{4(x_{H^\pm} - x_t)} \left\{ \zeta_d \zeta_u^* \left[\frac{x_t}{x_{H^\pm} - x_t} \log\left(\frac{x_{H^\pm}}{x_t}\right) - 1 \right] \right. \\ \left. + |\zeta_u|^2 \left[\frac{x_t^2}{2(x_{H^\pm} - x_t)^2} \log\left(\frac{x_{H^\pm}}{x_t}\right) + \frac{x_{H^\pm} - 3x_t}{4(x_{H^\pm} - x_t)} \right] \right\} \end{aligned} \quad (\text{F.13})$$

$$g_1 = -\frac{3}{4} + \zeta_d \zeta_u^* \frac{x_t}{x_{H^\pm} - x_t} \left[1 - \frac{x_{H^\pm}}{x_{H^\pm} - x_t} \log \left(\frac{x_{H^\pm}}{x_t} \right) \right] \quad (\text{F.14})$$

$$+ |\zeta_u|^2 \frac{x_t}{2(x_{H^\pm} - x_t)^2} \left[\frac{x_{H^\pm} + x_t}{2} - \frac{x_{H^\pm} x_t}{x_{H^\pm} - x_t} \log \left(\frac{x_{H^\pm}}{x_t} \right) \right],$$

$$g_2 = \zeta_d (\zeta_d \zeta_u^* + 1) f_1(x_t, x_{H^\pm}) + \zeta_d (\zeta_u^*)^2 f_2(x_t, x_{H^\pm}) + \zeta_d |\zeta_u|^2 f_3(x_t, x_{H^\pm})$$

$$+ \zeta_u |\zeta_u|^2 f_4(x_t, x_{H^\pm}) - \zeta_u^* |\zeta_u|^2 f_5(x_t, x_{H^\pm}) + \zeta_u f_6(x_t, x_{H^\pm}) - \zeta_u^* f_7(x_t, x_{H^\pm}), \quad (\text{F.15})$$

with

$$f_1(x_t, x_{H^\pm}) = \frac{1}{2(x_{H^\pm} - x_t)} [-x_{H^\pm} + x_t + x_{H^\pm} \log x_{H^\pm} - x_t \log x_t], \quad (\text{F.16})$$

$$f_2(x_t, x_{H^\pm}) = \frac{1}{2(x_{H^\pm} - x_t)} \left[x_t - \frac{x_{H^\pm} x_t}{x_{H^\pm} - x_t} \log \left(\frac{x_{H^\pm}}{x_t} \right) \right], \quad (\text{F.17})$$

$$f_3(x_t, x_{H^\pm}) = \frac{1}{2(x_{H^\pm} - x_t)} \left[x_{H^\pm} - \frac{x_{H^\pm}^2 \log x_{H^\pm}}{x_{H^\pm} - x_t} + \frac{x_t(2x_{H^\pm} - x_t) \log x_t}{x_{H^\pm} - x_t} \right], \quad (\text{F.18})$$

$$f_4(x_t, x_{H^\pm}) = \frac{1}{4(x_{H^\pm} - x_t)^2} \left[\frac{x_t(3x_{H^\pm} - x_t)}{2} - \frac{x_{H^\pm}^2 x_t}{x_{H^\pm} - x_t} \log \left(\frac{x_{H^\pm}}{x_t} \right) \right], \quad (\text{F.19})$$

$$f_5(x_t, x_{H^\pm}) = \frac{1}{4(x_{H^\pm} - x_t)^2} \left[\frac{x_t(x_{H^\pm} - 3x_t)}{2} - \frac{x_{H^\pm} x_t (x_{H^\pm} - 2x_t)}{x_{H^\pm} - x_t} \log \left(\frac{x_{H^\pm}}{x_t} \right) \right], \quad (\text{F.20})$$

$$f_6(x_t, x_{H^\pm}) = \frac{1}{2(x_{H^\pm} - x_t)} \left[\frac{x_t(x_t^2 - 3x_{H^\pm} x_t + 9x_{H^\pm} - 5x_t - 2)}{4(x_t - 1)^2} \right] \quad (\text{F.21})$$

$$+ \frac{x_{H^\pm}(x_{H^\pm} x_t - 3x_{H^\pm} + 2x_t) \log x_{H^\pm}}{2(x_{H^\pm} - 1)(x_{H^\pm} - x_t)}$$

$$+ \frac{x_{H^\pm}^2 (-2x_t^3 + 6x_t^2 - 9x_t + 2)}{2(x_t - 1)^3 (x_{H^\pm} - x_t)} \log x_t$$

$$+ \left. \frac{3x_{H^\pm} x_t^2 (x_t^2 - 2x_t + 3) - x_t^2 (2x_t^3 - 3x_t^2 + 3x_t + 1)}{2(x_t - 1)^3 (x_{H^\pm} - x_t)} \log x_t \right], \quad (\text{F.22})$$

$$f_7(x_t, x_{H^\pm}) = \frac{1}{2(x_{H^\pm} - x_t)} \left[\frac{(x_t^2 + x_t - 8)(x_{H^\pm} - x_t)}{4(x_t - 1)^2} - \frac{x_{H^\pm}(x_{H^\pm} + 2)}{2(x_{H^\pm} - 1)} \log x_{H^\pm} \right] \quad (\text{F.23})$$

$$+ \frac{x_{H^\pm}(x_t^3 - 3x_t^2 + 3x_t + 2) + 3(x_t - 2)x_t^2 \log x_t}{2(x_t - 1)^3}.$$

Notice that in the above expressions we assumed the couplings $\zeta_f \in \mathbb{C}$ in order to keep our formulas as general as possible, although in the body of the paper we consistently used $\zeta_f \in \mathbb{R}$.

Wilson Coefficients for the Derivative Operators

In this subsection we present the explicit expressions for the Wilson coefficients relevant to the derivative operators given in Eq. (6.46). From the Z -penguins we obtain,

$$C_{RR}^{\mathcal{T}q} = |\zeta_u|^2 \frac{\sqrt{x_b x_t}}{72} \left\{ \frac{3(x_{H^\pm}^2 - 5x_{H^\pm} x_t - 2x_t^2)}{(x_{H^\pm} - x_t)^3} + \frac{18x_{H^\pm} x_t^2}{(x_{H^\pm} - x_t)^4} \log \left(\frac{x_{H^\pm}}{x_t} \right) \right. \quad (\text{F.24})$$

$$\left. - 2 \sin^2 \theta_W \left[\frac{7x_{H^\pm}^2 - 5x_{H^\pm} x_t - 8x_t^2}{(x_{H^\pm} - x_t)^3} - \frac{6x_{H^\pm} x_t (2x_{H^\pm} - 3x_t)}{(x_{H^\pm} - x_t)^4} \log \left(\frac{x_{H^\pm}}{x_t} \right) \right] \right\} \quad (\text{F.25})$$

$$+ \zeta_u^* \zeta_d \frac{\sqrt{x_b x_t}}{24} \left\{ \frac{3(x_{H^\pm} - 3x_t)}{(x_{H^\pm} - x_t)^2} - \frac{6x_{H^\pm} (x_{H^\pm} - 2x_t)}{x_{H^\pm} - x_t} \log \left(\frac{x_{H^\pm}}{x_t} \right) \right. \quad (\text{F.26})$$

$$\left. + 4 \sin^2 \theta_W \left[\frac{5x_t - 3x_{H^\pm}}{(x_{H^\pm} - x_t)^2} + \frac{2x_{H^\pm} (2x_{H^\pm} - 3x_t)}{(x_{H^\pm} - x_t)^3} \log \left(\frac{x_{H^\pm}}{x_t} \right) \right] \right\}, \quad (\text{F.27})$$

$$\text{and } C_{RL}^{\mathcal{T}q} = C_{RR}^{\mathcal{T}q} \left(1 - \frac{1}{2 \sin^2 \theta_W} \right).$$

Similarly, from the box diagrams we get

$$C_{LL}^{\mathcal{T}\ell} = -\zeta_u \zeta_\ell^* \frac{\sqrt{x_\ell x_t}}{4(x_{H^\pm} - x_t) \sin^2 \theta_W} \left[-\frac{1}{(x_{H^\pm} - 1)} + \frac{x_{H^\pm} (1 - x_{H^\pm}) \log x_t}{(x_{H^\pm} - x_t)(x_t - 1)(x_{H^\pm} - 1)} \right. \quad (\text{F.28})$$

$$\left. - \frac{x_{H^\pm} (x_t + 1 - 2x_{H^\pm}) \log x_{H^\pm}}{(x_{H^\pm} - x_t)(x_{H^\pm} - 1)^2} \right], \quad (\text{F.29})$$

$$\text{and } C_{LL}^{\mathcal{T}\ell} = (C_{LR}^{\mathcal{T}\ell})^*.$$

Wilson Coefficients Suppressed by m_ℓ

In addition to the Wilson coefficients given in Section 6.1, in the computation of the box diagrams one gets contributions suppressed by the lepton mass. For completeness, we give these

contributions here. We obtain:

$$C_{T(5)}^{\text{NP, box}} = \zeta_u^* \zeta_\ell \frac{\sqrt{x_b x_\ell x_t}}{32(x_{H^\pm} - x_t) \sin^2 \theta_W} \times \quad (\text{F.30})$$

$$\left[\frac{x_t \log x_t}{(x_t - 1)(x_{H^\pm} - x_t)} - \frac{x_{H^\pm} \log x_{H^\pm}}{(x_{H^\pm} - 1)(x_{H^\pm} - x_t)} + \frac{x_t - \log x_t - 1}{(x_t - 1)^2} \right], \quad (\text{F.31})$$

and

$$C_9^{\text{NP, box}} = \frac{x_\ell x_t}{16 \sin^2 \theta_W} \left\{ |\zeta_u|^2 |\zeta_\ell|^2 \left[-\frac{1}{x_{H^\pm} - x_t} + \frac{x_t}{(x_{H^\pm} - x_t)^2} \log \left(\frac{x_{H^\pm}}{x_t} \right) \right] \right. \quad (\text{F.32})$$

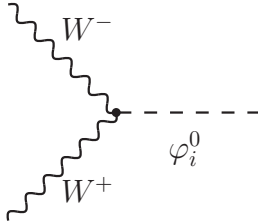
$$\left. + 2\text{Re}[\zeta_u \zeta_\ell^*] \left[\frac{(x_t + 2) \log x_t}{(x_{H^\pm} - x_t)(x_t - 1)} - \frac{(x_{H^\pm} + 2) \log x_{H^\pm}}{(x_{H^\pm} - x_t)(x_{H^\pm} - 1)} \right] \right\} + 2\sqrt{x_\ell} \text{Re}(C_{LL}^{\mathcal{T}\ell}),$$

$$C_{10}^{\text{NP, box}} = \frac{x_\ell x_t}{16 \sin^2 \theta_W} \left\{ |\zeta_u|^2 |\zeta_\ell|^2 \left[-\frac{1}{x_{H^\pm} - x_t} + \frac{x_t}{(x_{H^\pm} - x_t)^2} \log \left(\frac{x_{H^\pm}}{x_t} \right) \right] \right. \quad (\text{F.33})$$

$$\left. + 2\text{Re}[\zeta_u \zeta_\ell^*] \left[\frac{(x_t - 2) \log x_t}{(x_{H^\pm} - x_t)(x_t - 1)} - \frac{(x_{H^\pm} - 2) \log x_{H^\pm}}{(x_{H^\pm} - x_t)(x_{H^\pm} - 1)} \right] \right\}.$$

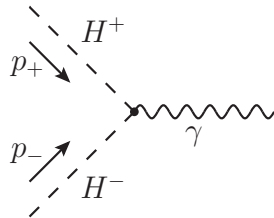
F.3 Feynman Rules

In this section we collect the Feynman rules used in our computation. For the couplings between the gauge bosons and the scalars we have

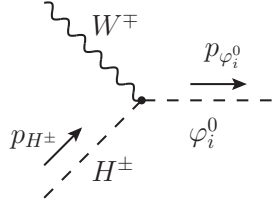


$$igm_W \lambda_{W+W-}^{\varphi_i^0} g^{\mu\nu}, \quad (\text{F.34})$$

where $\lambda_{W+W-}^h = \sin(\beta - \alpha)$, $\lambda_{W+W-}^H = \cos(\beta - \alpha)$ and $\lambda_{W+W-}^A = 0$. Similarly, we also have

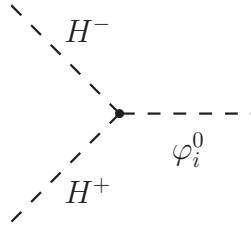


$$ie(p_- - p_+)^{\mu}, \quad (\text{F.35})$$



$$\pm \frac{ig}{2} \lambda_{H^\pm W^\mp}^{\varphi_i^0} (p_{H^\pm} + p_{\varphi_i^0})^\mu, \quad (\text{F.36})$$

where $\lambda_{H^\pm W^\mp}^h = \cos(\beta - \alpha)$, $\lambda_{H^\pm W^\mp}^H = -\sin(\beta - \alpha)$, and $\lambda_{H^\pm W^\mp}^A = \mp i$, depending on the charges of the initial particles. For the trilinear scalar interactions, we have



$$iv \lambda_{H^+ H^-}^{\varphi_i^0} \quad (\text{F.37})$$

where the trilinear couplings read

$$\begin{aligned} \lambda_{H^+ H^-}^h &= -\frac{m_h^2 [3 \cos(\alpha + \beta) + \cos(\alpha - 3\beta)] + 4 \sin(2\beta) \sin(\beta - \alpha) m_{H^\pm}^2 - 4M^2 \cos(\alpha + \beta)}{2v^2 \sin(2\beta)}, \\ \lambda_{H^+ H^-}^H &= -\frac{m_H^2 [3 \sin(\alpha + \beta) + \sin(\alpha - 3\beta)] + 4 \sin(2\beta) \cos(\beta - \alpha) m_{H^\pm}^2 - 4M^2 \sin(\alpha + \beta)}{2v^2 \sin(2\beta)}, \\ \lambda_{H^+ H^-}^A &= 0. \end{aligned} \quad (\text{F.38})$$

These results agree with the ones given in Refs. [238, 271] after the appropriate change of basis and/or conventions.¹

¹Notice that our λ is $-\lambda$ of Ref. [238].

Bibliography

- [1] Georges Aad et al. “Observation of a new particle in the search for the Standard Model Higgs boson with the ATLAS detector at the LHC”. In: *Phys.Lett.* B716 (2012), pp. 1–29. DOI: [10.1016/j.physletb.2012.08.020](https://doi.org/10.1016/j.physletb.2012.08.020). arXiv: [1207.7214](https://arxiv.org/abs/1207.7214) [hep-ex].
- [2] Serguei Chatrchyan et al. “Observation of a new boson at a mass of 125 GeV with the CMS experiment at the LHC”. In: *Phys.Lett.* B716 (2012), pp. 30–61. DOI: [10.1016/j.physletb.2012.08.021](https://doi.org/10.1016/j.physletb.2012.08.021). arXiv: [1207.7235](https://arxiv.org/abs/1207.7235) [hep-ex].
- [3] R.Sekhar Chivukula and Howard Georgi. “Composite Technicolor Standard Model”. In: *Phys. Lett. B* 188 (1987), pp. 99–104. DOI: [10.1016/0370-2693\(87\)90713-1](https://doi.org/10.1016/0370-2693(87)90713-1).
- [4] J. Hisano et al. “Lepton flavor violation via right-handed neutrino Yukawa couplings in supersymmetric standard model”. In: *Phys. Rev. D* 53 (1996), pp. 2442–2459. DOI: [10.1103/PhysRevD.53.2442](https://doi.org/10.1103/PhysRevD.53.2442). arXiv: [hep-ph/9510309](https://arxiv.org/abs/hep-ph/9510309).
- [5] G. D’Ambrosio et al. “Minimal flavor violation: An Effective field theory approach”. In: *Nucl. Phys. B* 645 (2002), pp. 155–187. DOI: [10.1016/S0550-3213\(02\)00836-2](https://doi.org/10.1016/S0550-3213(02)00836-2). arXiv: [hep-ph/0207036](https://arxiv.org/abs/hep-ph/0207036).
- [6] Vincenzo Cirigliano et al. “Minimal flavor violation in the lepton sector”. In: *Nucl. Phys. B* 728 (2005), pp. 121–134. DOI: [10.1016/j.nuclphysb.2005.08.037](https://doi.org/10.1016/j.nuclphysb.2005.08.037). arXiv: [hep-ph/0507001](https://arxiv.org/abs/hep-ph/0507001).
- [7] Rodrigo Alonso, Benjamín Grinstein, and Jorge Martin Camalich. “Lepton universality violation and lepton flavor conservation in B -meson decays”. In: *JHEP* 10 (2015), p. 184. DOI: [10.1007/JHEP10\(2015\)184](https://doi.org/10.1007/JHEP10(2015)184). arXiv: [1505.05164](https://arxiv.org/abs/1505.05164) [hep-ph].
- [8] Roel Aaij et al. “Test of lepton universality using $B^+ \rightarrow K^+ \ell^+ \ell^-$ decays”. In: *Phys.Rev.Lett.* 113.15 (2014), p. 151601. DOI: [10.1103/PhysRevLett.113.151601](https://doi.org/10.1103/PhysRevLett.113.151601). arXiv: [1406.6482](https://arxiv.org/abs/1406.6482) [hep-ex].
- [9] Roel Aaij et al. “Angular analysis of the $B^0 \rightarrow K^{*0} \mu^+ \mu^-$ decay using 3 fb^{-1} of integrated luminosity”. In: *JHEP* 02 (2016), p. 104. DOI: [10.1007/JHEP02\(2016\)104](https://doi.org/10.1007/JHEP02(2016)104). arXiv: [1512.04442](https://arxiv.org/abs/1512.04442) [hep-ex].
- [10] R. Aaij et al. “Test of lepton universality with $B^0 \rightarrow K^{*0} \ell^+ \ell^-$ decays”. In: *JHEP* 08 (2017), p. 055. DOI: [10.1007/JHEP08\(2017\)055](https://doi.org/10.1007/JHEP08(2017)055). arXiv: [1705.05802](https://arxiv.org/abs/1705.05802) [hep-ex].
- [11] Roel Aaij et al. “Search for lepton-universality violation in $B^+ \rightarrow K^+ \ell^+ \ell^-$ decays”. In: (2019). arXiv: [1903.09252](https://arxiv.org/abs/1903.09252) [hep-ex].

- [12] M. Huschle et al. “Measurement of the branching ratio of $\bar{B} \rightarrow D^{(*)}\tau^-\bar{\nu}_\tau$ relative to $\bar{B} \rightarrow D^{(*)}\ell^-\bar{\nu}_\ell$ decays with hadronic tagging at Belle”. In: *Phys. Rev. D* 92.7 (2015), p. 072014. DOI: [10.1103/PhysRevD.92.072014](https://doi.org/10.1103/PhysRevD.92.072014). arXiv: [1507.03233](https://arxiv.org/abs/1507.03233) [hep-ex].
- [13] G. Caria et al. “Measurement of $\mathcal{R}(D)$ and $\mathcal{R}(D^*)$ with a semileptonic tagging method”. In: (Oct. 2019). arXiv: [1910.05864](https://arxiv.org/abs/1910.05864) [hep-ex].
- [14] E. Fermi. “An attempt of a theory of beta radiation. 1.” In: *Z. Phys.* 88 (1934), pp. 161–177. DOI: [10.1007/BF01351864](https://doi.org/10.1007/BF01351864).
- [15] Andrzej J. Buras. “Weak Hamiltonian, CP violation and rare decays”. In: *Probing the standard model of particle interactions. Proceedings, Summer School in Theoretical Physics, NATO Advanced Study Institute, 68th session, Les Houches, France, July 28-September 5, 1997. Pt. 1, 2.* 1998, pp. 281–539. arXiv: [hep-ph/9806471](https://arxiv.org/abs/hep-ph/9806471) [hep-ph].
- [16] Roel Aaij et al. “Measurements of the S-wave fraction in $B^0 \rightarrow K^+\pi^-\mu^+\mu^-$ decays and the $B^0 \rightarrow K^{*(892)^0}\mu^+\mu^-$ differential branching fraction”. In: *JHEP* 11 (2016), p. 047. DOI: [10.1007/JHEP11\(2016\)047](https://doi.org/10.1007/JHEP11(2016)047). arXiv: [1606.04731](https://arxiv.org/abs/1606.04731) [hep-ex].
- [17] Roel Aaij et al. “Angular analysis and differential branching fraction of the decay $B_s^0 \rightarrow \phi\mu^+\mu^-$ ”. In: *JHEP* 09 (2015), p. 179. DOI: [10.1007/JHEP09\(2015\)179](https://doi.org/10.1007/JHEP09(2015)179). arXiv: [1506.08777](https://arxiv.org/abs/1506.08777) [hep-ex].
- [18] A. Abdesselam et al. “Test of lepton flavor universality in $B \rightarrow K^*\ell^+\ell^-$ decays at Belle”. In: (2019). arXiv: [1904.02440](https://arxiv.org/abs/1904.02440) [hep-ex].
- [19] Bernat Capdevila et al. “Patterns of New Physics in $b \rightarrow s\ell^+\ell^-$ transitions in the light of recent data”. In: *JHEP* 01 (2018), p. 093. DOI: [10.1007/JHEP01\(2018\)093](https://doi.org/10.1007/JHEP01(2018)093). arXiv: [1704.05340](https://arxiv.org/abs/1704.05340) [hep-ph].
- [20] Wolfgang Altmannshofer, Peter Stangl, and David M. Straub. “Interpreting Hints for Lepton Flavor Universality Violation”. In: *Phys. Rev. D* 96.5 (2017), p. 055008. DOI: [10.1103/PhysRevD.96.055008](https://doi.org/10.1103/PhysRevD.96.055008). arXiv: [1704.05435](https://arxiv.org/abs/1704.05435) [hep-ph].
- [21] Guido D’Amico et al. “Flavour anomalies after the R_{K^*} measurement”. In: *JHEP* 09 (2017), p. 010. DOI: [10.1007/JHEP09\(2017\)010](https://doi.org/10.1007/JHEP09(2017)010). arXiv: [1704.05438](https://arxiv.org/abs/1704.05438) [hep-ph].
- [22] Gudrun Hiller and Ivan Nisandzic. “ R_K and R_{K^*} beyond the standard model”. In: *Phys. Rev. D* 96.3 (2017), p. 035003. DOI: [10.1103/PhysRevD.96.035003](https://doi.org/10.1103/PhysRevD.96.035003). arXiv: [1704.05444](https://arxiv.org/abs/1704.05444) [hep-ph].
- [23] Li-Sheng Geng et al. “Towards the discovery of new physics with lepton-universality ratios of $b \rightarrow s\ell\ell$ decays”. In: *Phys. Rev. D* 96.9 (2017), p. 093006. DOI: [10.1103/PhysRevD.96.093006](https://doi.org/10.1103/PhysRevD.96.093006). arXiv: [1704.05446](https://arxiv.org/abs/1704.05446) [hep-ph].
- [24] Marco Ciuchini et al. “On Flavourful Easter eggs for New Physics hunger and Lepton Flavour Universality violation”. In: *Eur. Phys. J. C* 77.10 (2017), p. 688. DOI: [10.1140/epjc/s10052-017-5270-2](https://doi.org/10.1140/epjc/s10052-017-5270-2). arXiv: [1704.05447](https://arxiv.org/abs/1704.05447) [hep-ph].
- [25] Ashutosh Kumar Alok et al. “New Physics in $b \rightarrow s\mu^+\mu^-$ after the Measurement of R_{K^*} ”. In: *Phys. Rev. D* 96.9 (2017), p. 095009. DOI: [10.1103/PhysRevD.96.095009](https://doi.org/10.1103/PhysRevD.96.095009). arXiv: [1704.07397](https://arxiv.org/abs/1704.07397) [hep-ph].

- [26] T. Hurth et al. “Lepton nonuniversality in exclusive $b \rightarrow s\ell\ell$ decays”. In: *Phys. Rev. D* 96.9 (2017), p. 095034. DOI: [10.1103/PhysRevD.96.095034](https://doi.org/10.1103/PhysRevD.96.095034). arXiv: [1705.06274](https://arxiv.org/abs/1705.06274) [hep-ph].
- [27] Marcel Algueró et al. “Are we overlooking Lepton Flavour Universal New Physics in $b \rightarrow s\ell\ell$?” In: (2018). arXiv: [1809.08447](https://arxiv.org/abs/1809.08447) [hep-ph].
- [28] Marcel Algueró et al. “Addendum: ”Patterns of New Physics in $b \rightarrow s\ell^+\ell^-$ transitions in the light of recent data” and ”Are we overlooking Lepton Flavour Universal New Physics in $b \rightarrow s\ell\ell$?””. In: (2019). arXiv: [1903.09578](https://arxiv.org/abs/1903.09578) [hep-ph].
- [29] Ashutosh Kumar Alok et al. “Continuing search for new physics in $b \rightarrow s\mu\mu$ decays: two operators at a time”. In: (2019). arXiv: [1903.09617](https://arxiv.org/abs/1903.09617) [hep-ph].
- [30] Marco Ciuchini et al. “New Physics in $b \rightarrow s\ell^+\ell^-$ confronts new data on Lepton Universality”. In: (2019). arXiv: [1903.09632](https://arxiv.org/abs/1903.09632) [hep-ph].
- [31] Jason Aebischer et al. “B-decay discrepancies after Moriond 2019”. In: (2019). arXiv: [1903.10434](https://arxiv.org/abs/1903.10434) [hep-ph].
- [32] Kamila Kowalska, Dinesh Kumar, and Enrico Maria Sessolo. “Implications for New Physics in $b \rightarrow s\mu\mu$ transitions after recent measurements by Belle and LHCb”. In: (2019). arXiv: [1903.10932](https://arxiv.org/abs/1903.10932) [hep-ph].
- [33] J. P. Lees et al. “Evidence for an excess of $\bar{B} \rightarrow D^{(*)}\tau^-\bar{\nu}_\tau$ decays”. In: *Phys. Rev. Lett.* 109 (2012), p. 101802. DOI: [10.1103/PhysRevLett.109.101802](https://doi.org/10.1103/PhysRevLett.109.101802). arXiv: [1205.5442](https://arxiv.org/abs/1205.5442) [hep-ex].
- [34] Y. Sato et al. “Measurement of the branching ratio of $\bar{B}^0 \rightarrow D^{*+}\tau^-\bar{\nu}_\tau$ relative to $\bar{B}^0 \rightarrow D^{*+}\ell^-\bar{\nu}_\ell$ decays with a semileptonic tagging method”. In: *Phys. Rev. D* 94.7 (2016), p. 072007. DOI: [10.1103/PhysRevD.94.072007](https://doi.org/10.1103/PhysRevD.94.072007). arXiv: [1607.07923](https://arxiv.org/abs/1607.07923) [hep-ex].
- [35] R. Aaij et al. “Measurement of the ratio of the $B^0 \rightarrow D^{*-}\tau^+\nu_\tau$ and $B^0 \rightarrow D^{*-}\mu^+\nu_\mu$ branching fractions using three-prong τ -lepton decays”. In: *Phys. Rev. Lett.* 120.17 (2018), p. 171802. DOI: [10.1103/PhysRevLett.120.171802](https://doi.org/10.1103/PhysRevLett.120.171802). arXiv: [1708.08856](https://arxiv.org/abs/1708.08856) [hep-ex].
- [36] R. Aaij et al. “Test of Lepton Flavor Universality by the measurement of the $B^0 \rightarrow D^{*-}\tau^+\nu_\tau$ branching fraction using three-prong τ decays”. In: *Phys. Rev. D* 97.7 (2018), p. 072013. DOI: [10.1103/PhysRevD.97.072013](https://doi.org/10.1103/PhysRevD.97.072013). arXiv: [1711.02505](https://arxiv.org/abs/1711.02505) [hep-ex].
- [37] Peter W. Higgs. “Broken Symmetries and the Masses of Gauge Bosons”. In: *Phys. Rev. Lett.* 13 (1964), pp. 508–509. DOI: [10.1103/PhysRevLett.13.508](https://doi.org/10.1103/PhysRevLett.13.508).
- [38] Gudrun Hiller and Frank Kruger. “More model independent analysis of $b \rightarrow s$ processes”. In: *Phys. Rev. D* 69 (2004), p. 074020. DOI: [10.1103/PhysRevD.69.074020](https://doi.org/10.1103/PhysRevD.69.074020). arXiv: [hep-ph/0310219](https://arxiv.org/abs/hep-ph/0310219) [hep-ph].
- [39] Marzia Bordone, Gino Isidori, and Andrea Pattori. “On the Standard Model predictions for R_K and R_{K^*} ”. In: *Eur. Phys. J. C* 76.8 (2016), p. 440. DOI: [10.1140/epjc/s10052-016-4274-7](https://doi.org/10.1140/epjc/s10052-016-4274-7). arXiv: [1605.07633](https://arxiv.org/abs/1605.07633) [hep-ph].

- [40] A. Abdesselam et al. “Angular analysis of $B^0 \rightarrow K^*(892)^0 \ell^+ \ell^-$ ”. In: *LHCski 2016 Obergurgl, Tyrol, Austria, April 10-15, 2016*. 2016. arXiv: [1604.04042 \[hep-ex\]](https://arxiv.org/abs/1604.04042). URL: <http://inspirehep.net/record/1446979/files/arXiv:1604.04042.pdf>.
- [41] S. Wehle et al. “Lepton-Flavor-Dependent Angular Analysis of $B \rightarrow K^* \ell^+ \ell^-$ ”. In: *Phys. Rev. Lett.* 118.11 (2017), p. 111801. DOI: [10.1103/PhysRevLett.118.111801](https://doi.org/10.1103/PhysRevLett.118.111801). arXiv: [1612.05014 \[hep-ex\]](https://arxiv.org/abs/1612.05014).
- [42] Sebastien Descotes-Genon et al. “Optimizing the basis of $B \rightarrow K^* \ell^+ \ell^-$ observables in the full kinematic range”. In: *JHEP* 1305 (2013), p. 137. DOI: [10.1007/JHEP05\(2013\)137](https://doi.org/10.1007/JHEP05(2013)137). arXiv: [1303.5794 \[hep-ph\]](https://arxiv.org/abs/1303.5794).
- [43] Joaquim Matias et al. “Complete Anatomy of $\bar{B}_d \rightarrow \bar{K}^{*0} (- \rightarrow K\pi) l^+ l^-$ and its angular distribution”. In: *JHEP* 04 (2012), p. 104. DOI: [10.1007/JHEP04\(2012\)104](https://doi.org/10.1007/JHEP04(2012)104). arXiv: [1202.4266 \[hep-ph\]](https://arxiv.org/abs/1202.4266).
- [44] Sébastien Descotes-Genon et al. “On the impact of power corrections in the prediction of $B \rightarrow K \mu^+ \mu^-$ observables”. In: *JHEP* 1412 (2014), p. 125. DOI: [10.1007/JHEP12\(2014\)125](https://doi.org/10.1007/JHEP12(2014)125). arXiv: [1407.8526 \[hep-ph\]](https://arxiv.org/abs/1407.8526).
- [45] Yasmine Sara Amhis et al. “Averages of b -hadron, c -hadron, and τ -lepton properties as of 2018”. In: (2019). arXiv: [1909.12524 \[hep-ex\]](https://arxiv.org/abs/1909.12524).
- [46] Martin Beneke, Christoph Bobeth, and Robert Szafron. “Enhanced electromagnetic correction to the rare B -meson decay $B_{s,d} \rightarrow \mu^+ \mu^-$ ”. In: *Phys. Rev. Lett.* 120.1 (2018), p. 011801. DOI: [10.1103/PhysRevLett.120.011801](https://doi.org/10.1103/PhysRevLett.120.011801). arXiv: [1708.09152 \[hep-ph\]](https://arxiv.org/abs/1708.09152).
- [47] Roel Aaij et al. “Test of lepton universality with $\Lambda_b^0 \rightarrow p K^- \ell^+ \ell^-$ decays”. In: (Dec. 2019). arXiv: [1912.08139 \[hep-ex\]](https://arxiv.org/abs/1912.08139).
- [48] S. Aoki et al. “FLAG Review 2019”. In: (2019). arXiv: [1902.08191 \[hep-lat\]](https://arxiv.org/abs/1902.08191).
- [49] R. Aaij et al. “Measurement of the ratio of branching fractions $\mathcal{B}(B_c^+ \rightarrow J/\psi \tau^+ \nu_\tau) / \mathcal{B}(B_c^+ \rightarrow J/\psi \mu^+ \nu_\mu)$ ”. In: *Phys. Rev. Lett.* 120.12 (2018), p. 121801. DOI: [10.1103/PhysRevLett.120.121801](https://doi.org/10.1103/PhysRevLett.120.121801). arXiv: [1711.05623 \[hep-ex\]](https://arxiv.org/abs/1711.05623).
- [50] Ryoutaro Watanabe. “New Physics effect on $B_c \rightarrow J/\psi \tau \bar{\nu}$ in relation to the $R_{D^{(*)}}$ anomaly”. In: *Phys. Lett.* B776 (2018), pp. 5–9. DOI: [10.1016/j.physletb.2017.11.016](https://doi.org/10.1016/j.physletb.2017.11.016). arXiv: [1709.08644 \[hep-ph\]](https://arxiv.org/abs/1709.08644).
- [51] Damir Bečirević et al. “Lepton Flavor Universality tests through angular observables of $\bar{B} \rightarrow D^{(*)} \ell \bar{\nu}$ decay modes”. In: (July 2019). arXiv: [1907.02257 \[hep-ph\]](https://arxiv.org/abs/1907.02257).
- [52] Rui-Xiang Shi et al. “Revisiting the new-physics interpretation of the $b \rightarrow c \tau \nu$ data”. In: *JHEP* 12 (2019), p. 065. DOI: [10.1007/JHEP12\(2019\)065](https://doi.org/10.1007/JHEP12(2019)065). arXiv: [1905.08498 \[hep-ph\]](https://arxiv.org/abs/1905.08498).
- [53] Monika Blanke et al. “Addendum to “Impact of polarization observables and $B_c \rightarrow \tau \nu$ on new physics explanations of the $b \rightarrow c \tau \nu$ anomaly””. In: (May 2019). [Addendum: *Phys.Rev.D* 100, 035035 (2019)]. DOI: [10.1103/PhysRevD.100.035035](https://doi.org/10.1103/PhysRevD.100.035035). arXiv: [1905.08253 \[hep-ph\]](https://arxiv.org/abs/1905.08253).
- [54] Clara Murgui et al. “Global fit to $b \rightarrow c \tau \nu$ transitions”. In: *JHEP* 09 (2019), p. 103. DOI: [10.1007/JHEP09\(2019\)103](https://doi.org/10.1007/JHEP09(2019)103). arXiv: [1904.09311 \[hep-ph\]](https://arxiv.org/abs/1904.09311).

- [55] Zhuo-Ran Huang et al. “Footprints of New Physics in $b \rightarrow c\tau\nu$ Transitions”. In: *Phys. Rev. D* 98.9 (2018), p. 095018. DOI: [10.1103/PhysRevD.98.095018](https://doi.org/10.1103/PhysRevD.98.095018). arXiv: [1808.03565](https://arxiv.org/abs/1808.03565) [hep-ph].
- [56] Damir Bečirević et al. “Scalar leptoquarks from grand unified theories to accommodate the B -physics anomalies”. In: *Phys. Rev. D* 98.5 (2018), p. 055003. DOI: [10.1103/PhysRevD.98.055003](https://doi.org/10.1103/PhysRevD.98.055003). arXiv: [1806.05689](https://arxiv.org/abs/1806.05689) [hep-ph].
- [57] Aleksandr Azatov et al. “Anatomy of $b \rightarrow c\tau\nu$ anomalies”. In: *JHEP* 11 (2018), p. 187. DOI: [10.1007/JHEP11\(2018\)187](https://doi.org/10.1007/JHEP11(2018)187). arXiv: [1805.03209](https://arxiv.org/abs/1805.03209) [hep-ph].
- [58] Martin Jung and David M. Straub. “Constraining new physics in $b \rightarrow c\ell\nu$ transitions”. In: *JHEP* 01 (2019), p. 009. DOI: [10.1007/JHEP01\(2019\)009](https://doi.org/10.1007/JHEP01(2019)009). arXiv: [1801.01112](https://arxiv.org/abs/1801.01112) [hep-ph].
- [59] Ben Gripaios, Marco Nardecchia, and S. A. Renner. “Composite leptoquarks and anomalies in B -meson decays”. In: *JHEP* 05 (2015), p. 006. DOI: [10.1007/JHEP05\(2015\)006](https://doi.org/10.1007/JHEP05(2015)006). arXiv: [1412.1791](https://arxiv.org/abs/1412.1791) [hep-ph].
- [60] Damir Bečirević, Svjetlana Fajfer, and Nejc Konik. “Lepton flavor nonuniversality in $b \rightarrow s\ell^+\ell^-$ processes”. In: *Phys. Rev. D* 92.1 (2015), p. 014016. DOI: [10.1103/PhysRevD.92.014016](https://doi.org/10.1103/PhysRevD.92.014016). arXiv: [1503.09024](https://arxiv.org/abs/1503.09024) [hep-ph].
- [61] Ivo de Medeiros Varzielas and Gudrun Hiller. “Clues for flavor from rare lepton and quark decays”. In: *JHEP* 06 (2015), p. 072. DOI: [10.1007/JHEP06\(2015\)072](https://doi.org/10.1007/JHEP06(2015)072). arXiv: [1503.01084](https://arxiv.org/abs/1503.01084) [hep-ph].
- [62] Lorenzo Calibbi, Andreas Crivellin, and Toshihiko Ota. “Effective field theory approach to $b \rightarrow s\ell\ell^{(\prime)}$, $B \rightarrow K^{(*)}\nu\bar{\nu}$ and $B \rightarrow D^{(*)}\tau\nu$ with third generation couplings”. In: *Phys. Rev. Lett.* 115.18 (2015), p. 181801. DOI: [10.1103/PhysRevLett.115.181801](https://doi.org/10.1103/PhysRevLett.115.181801). arXiv: [1506.02661](https://arxiv.org/abs/1506.02661) [hep-ph].
- [63] Geneviève Bélanger, Cédric Delaunay, and Susanne Westhoff. “A Dark Matter Relic From Muon Anomalies”. In: *Phys. Rev. D* 92 (2015), p. 055021. DOI: [10.1103/PhysRevD.92.055021](https://doi.org/10.1103/PhysRevD.92.055021). arXiv: [1507.06660](https://arxiv.org/abs/1507.06660) [hep-ph].
- [64] Riccardo Barbieri et al. “Anomalies in B -decays and $U(2)$ flavour symmetry”. In: (2015). arXiv: [1512.01560](https://arxiv.org/abs/1512.01560) [hep-ph].
- [65] Damir Bečirević et al. “Palatable Leptoquark Scenarios for Lepton Flavor Violation in Exclusive $b \rightarrow s\ell_1\ell_2$ modes”. In: *JHEP* 11 (2016), p. 035. DOI: [10.1007/JHEP11\(2016\)035](https://doi.org/10.1007/JHEP11(2016)035). arXiv: [1608.07583](https://arxiv.org/abs/1608.07583) [hep-ph].
- [66] Damir Bečirević et al. “Leptoquark model to explain the B -physics anomalies, R_K and R_D ”. In: *Phys. Rev. D* 94.11 (2016), p. 115021. DOI: [10.1103/PhysRevD.94.115021](https://doi.org/10.1103/PhysRevD.94.115021). arXiv: [1608.08501](https://arxiv.org/abs/1608.08501) [hep-ph].
- [67] Suchismita Sahoo, Rukmani Mohanta, and Anjan K. Giri. “Explaining the R_K and $R_{D^{(*)}}$ anomalies with vector leptoquarks”. In: *Phys. Rev. D* 95.3 (2017), p. 035027. DOI: [10.1103/PhysRevD.95.035027](https://doi.org/10.1103/PhysRevD.95.035027). arXiv: [1609.04367](https://arxiv.org/abs/1609.04367) [hep-ph].
- [68] Gudrun Hiller, Dennis Loose, and Kay Schönwald. “Leptoquark Flavor Patterns & B Decay Anomalies”. In: *JHEP* 12 (2016), p. 027. DOI: [10.1007/JHEP12\(2016\)027](https://doi.org/10.1007/JHEP12(2016)027). arXiv: [1609.08895](https://arxiv.org/abs/1609.08895) [hep-ph].

- [69] Estefania Coluccio Leskow et al. “ $(g - 2)_\mu$, lepton flavor violation, and Z decays with leptoquarks: Correlations and future prospects”. In: *Phys. Rev. D* 95.5 (2017), p. 055018. DOI: [10.1103/PhysRevD.95.055018](https://doi.org/10.1103/PhysRevD.95.055018). arXiv: [1612.06858](https://arxiv.org/abs/1612.06858) [hep-ph].
- [70] Peter Cox et al. “SU(5) Unification with TeV-scale Leptoquarks”. In: *JHEP* 03 (2017), p. 035. DOI: [10.1007/JHEP03\(2017\)035](https://doi.org/10.1007/JHEP03(2017)035). arXiv: [1612.03923](https://arxiv.org/abs/1612.03923) [hep-ph].
- [71] Andreas Crivellin, Dario Müller, and Toshihiko Ota. “Simultaneous explanation of $R(D^{(*)})$ and $b \rightarrow s\mu^+\mu^-$: the last scalar leptoquarks standing”. In: *JHEP* 09 (2017), p. 040. DOI: [10.1007/JHEP09\(2017\)040](https://doi.org/10.1007/JHEP09(2017)040). arXiv: [1703.09226](https://arxiv.org/abs/1703.09226) [hep-ph].
- [72] Yi Cai et al. “Reconsidering the One Leptoquark solution: flavor anomalies and neutrino mass”. In: *JHEP* 10 (2017), p. 047. DOI: [10.1007/JHEP10\(2017\)047](https://doi.org/10.1007/JHEP10(2017)047). arXiv: [1704.05849](https://arxiv.org/abs/1704.05849) [hep-ph].
- [73] Ilja Doršner et al. “The role of the S_3 GUT leptoquark in flavor universality and collider searches”. In: (2017). [*JHEP*10,188(2017)]. DOI: [10.1007/JHEP10\(2017\)188](https://doi.org/10.1007/JHEP10(2017)188). arXiv: [1706.07779](https://arxiv.org/abs/1706.07779) [hep-ph].
- [74] Dario Buttazzo et al. “B-physics anomalies: a guide to combined explanations”. In: *JHEP* 11 (2017), p. 044. DOI: [10.1007/JHEP11\(2017\)044](https://doi.org/10.1007/JHEP11(2017)044). arXiv: [1706.07808](https://arxiv.org/abs/1706.07808) [hep-ph].
- [75] Nima Assad, Bartosz Fornal, and Benjamin Grinstein. “Baryon Number and Lepton Universality Violation in Leptoquark and Diquark Models”. In: *Phys. Lett. B* 777 (2018), pp. 324–331. DOI: [10.1016/j.physletb.2017.12.042](https://doi.org/10.1016/j.physletb.2017.12.042). arXiv: [1708.06350](https://arxiv.org/abs/1708.06350) [hep-ph].
- [76] Luca Di Luzio, Admir Greljo, and Marco Nardecchia. “Gauge leptoquark as the origin of B-physics anomalies”. In: *Phys. Rev. D* 96.11 (2017), p. 115011. DOI: [10.1103/PhysRevD.96.115011](https://doi.org/10.1103/PhysRevD.96.115011). arXiv: [1708.08450](https://arxiv.org/abs/1708.08450) [hep-ph].
- [77] Lorenzo Calibbi, Andreas Crivellin, and Tianjun Li. “Model of vector leptoquarks in view of the B -physics anomalies”. In: *Phys. Rev. D* 98.11 (2018), p. 115002. DOI: [10.1103/PhysRevD.98.115002](https://doi.org/10.1103/PhysRevD.98.115002). arXiv: [1709.00692](https://arxiv.org/abs/1709.00692) [hep-ph].
- [78] Marzia Bordone et al. “A three-site gauge model for flavor hierarchies and flavor anomalies”. In: *Phys. Lett. B* 779 (2018), pp. 317–323. DOI: [10.1016/j.physletb.2018.02.011](https://doi.org/10.1016/j.physletb.2018.02.011). arXiv: [1712.01368](https://arxiv.org/abs/1712.01368) [hep-ph].
- [79] Monika Blanke and Andreas Crivellin. “ B Meson Anomalies in a Pati-Salam Model within the Randall-Sundrum Background”. In: *Phys. Rev. Lett.* 121.1 (2018), p. 011801. DOI: [10.1103/PhysRevLett.121.011801](https://doi.org/10.1103/PhysRevLett.121.011801). arXiv: [1801.07256](https://arxiv.org/abs/1801.07256) [hep-ph].
- [80] David Marzocca. “Addressing the B-physics anomalies in a fundamental Composite Higgs Model”. In: *JHEP* 07 (2018), p. 121. DOI: [10.1007/JHEP07\(2018\)121](https://doi.org/10.1007/JHEP07(2018)121). arXiv: [1803.10972](https://arxiv.org/abs/1803.10972) [hep-ph].
- [81] Marzia Bordone et al. “Low-energy signatures of the PS^3 model: from B -physics anomalies to LFV”. In: *JHEP* 10 (2018), p. 148. DOI: [10.1007/JHEP10\(2018\)148](https://doi.org/10.1007/JHEP10(2018)148). arXiv: [1805.09328](https://arxiv.org/abs/1805.09328) [hep-ph].
- [82] Andreas Crivellin et al. “Importance of Loop Effects in Explaining the Accumulated Evidence for New Physics in B Decays with a Vector Leptoquark”. In: *Phys. Rev. Lett.* 122.1 (2019), p. 011805. DOI: [10.1103/PhysRevLett.122.011805](https://doi.org/10.1103/PhysRevLett.122.011805). arXiv: [1807.02068](https://arxiv.org/abs/1807.02068) [hep-ph].

- [83] Ivo de Medeiros Varzielas and Stephen F. King. “ $R_{K^{(*)}}$ with leptoquarks and the origin of Yukawa couplings”. In: *JHEP* 11 (2018), p. 100. DOI: [10.1007/JHEP11\(2018\)100](https://doi.org/10.1007/JHEP11(2018)100). arXiv: [1807.06023](https://arxiv.org/abs/1807.06023) [hep-ph].
- [84] Luca Di Luzio et al. “Maximal Flavour Violation: a Cabibbo mechanism for leptoquarks”. In: *JHEP* 11 (2018), p. 081. DOI: [10.1007/JHEP11\(2018\)081](https://doi.org/10.1007/JHEP11(2018)081). arXiv: [1808.00942](https://arxiv.org/abs/1808.00942) [hep-ph].
- [85] T. Faber et al. “A unified leptoquark model confronted with lepton non-universality in B -meson decays”. In: *Phys. Lett. B* 787 (2018), pp. 159–166. DOI: [10.1016/j.physletb.2018.10.051](https://doi.org/10.1016/j.physletb.2018.10.051). arXiv: [1808.05511](https://arxiv.org/abs/1808.05511) [hep-ph].
- [86] Julian Heeck and Daniele Teresi. “Pati-Salam explanations of the B-meson anomalies”. In: *JHEP* 12 (2018), p. 103. DOI: [10.1007/JHEP12\(2018\)103](https://doi.org/10.1007/JHEP12(2018)103). arXiv: [1808.07492](https://arxiv.org/abs/1808.07492) [hep-ph].
- [87] A. Angelescu et al. “Closing the window on single leptoquark solutions to the B -physics anomalies”. In: *JHEP* 10 (2018), p. 183. DOI: [10.1007/JHEP10\(2018\)183](https://doi.org/10.1007/JHEP10(2018)183). arXiv: [1808.08179](https://arxiv.org/abs/1808.08179) [hep-ph].
- [88] Valerio Gherardi et al. “Rank-One Flavor Violation and B-meson anomalies”. In: (2019). arXiv: [1903.10954](https://arxiv.org/abs/1903.10954) [hep-ph].
- [89] Claudia Cornella, Javier Fuentes-Martin, and Gino Isidori. “Revisiting the vector leptoquark explanation of the B-physics anomalies”. In: (2019). arXiv: [1903.11517](https://arxiv.org/abs/1903.11517) [hep-ph].
- [90] Martin Bauer and Matthias Neubert. “Minimal Leptoquark Explanation for the $R_{D^{(*)}}$, R_K , and $(g-2)_g$ Anomalies”. In: *Phys. Rev. Lett.* 116.14 (2016), p. 141802. DOI: [10.1103/PhysRevLett.116.141802](https://doi.org/10.1103/PhysRevLett.116.141802). arXiv: [1511.01900](https://arxiv.org/abs/1511.01900) [hep-ph].
- [91] Damir Bečirević and Olcyr Sumensari. “A leptoquark model to accommodate $R_K^{\text{exp}} < R_K^{\text{SM}}$ and $R_{K^*}^{\text{exp}} < R_{K^*}^{\text{SM}}$ ”. In: *JHEP* 08 (2017), p. 104. DOI: [10.1007/JHEP08\(2017\)104](https://doi.org/10.1007/JHEP08(2017)104). arXiv: [1704.05835](https://arxiv.org/abs/1704.05835) [hep-ph].
- [92] Andreas Crivellin, Dario Müller, and Francesco Saturnino. “Flavor Phenomenology of the Leptoquark Singlet-Triplet Model”. In: (Dec. 2019). arXiv: [1912.04224](https://arxiv.org/abs/1912.04224) [hep-ph].
- [93] Ben Gripaios, M. Nardecchia, and S. A. Renner. “Linear flavour violation and anomalies in B physics”. In: *JHEP* 06 (2016), p. 083. DOI: [10.1007/JHEP06\(2016\)083](https://doi.org/10.1007/JHEP06(2016)083). arXiv: [1509.05020](https://arxiv.org/abs/1509.05020) [hep-ph].
- [94] Basabendu Barman et al. “Correlating the anomalous results in $b \rightarrow s$ decays with inert Higgs doublet dark matter and muon $(g-2)$ ”. In: (2018). arXiv: [1808.06639](https://arxiv.org/abs/1808.06639) [hep-ph].
- [95] B. Grinstein, S. Pokorski, and G. G. Ross. “Lepton non-universality in B decays and fermion mass structure”. In: *JHEP* 12 (2018). [JHEP18,079(2020)], p. 079. DOI: [10.1007/JHEP12\(2018\)079](https://doi.org/10.1007/JHEP12(2018)079). arXiv: [1809.01766](https://arxiv.org/abs/1809.01766) [hep-ph].
- [96] Shao-Ping Li et al. “ $R_{D^{(*)}}$, $R_{K^{(*)}}$ and neutrino mass in the 2HDM-III with right-handed neutrinos”. In: *JHEP* 09 (2018), p. 149. DOI: [10.1007/JHEP09\(2018\)149](https://doi.org/10.1007/JHEP09(2018)149). arXiv: [1807.08530](https://arxiv.org/abs/1807.08530) [hep-ph].
- [97] Carlo Marzo, Luca Marzola, and Martti Raidal. “Common explanation to the $R_{K^{(*)}}$, $R_{D^{(*)}}$ and e'/ϵ anomalies in a 3HDM+ ν_R and connections to neutrino physics”. In: (2019). arXiv: [1901.08290](https://arxiv.org/abs/1901.08290) [hep-ph].

Bibliography

- [98] Andreas Crivellin, Dario Müller, and Christoph Wiegand. “ $b \rightarrow s\ell^+\ell^-$ Transitions in Two-Higgs-Doublet Models”. In: (2019). arXiv: [1903.10440 \[hep-ph\]](#).
- [99] Sebastien Descotes-Genon, Joaquim Matias, and Javier Virto. “Understanding the $B \rightarrow K^*\mu^+\mu^-$ Anomaly”. In: *Phys.Rev.* D88.7 (2013), p. 074002. DOI: [10.1103/PhysRevD.88.074002](#). arXiv: [1307.5683 \[hep-ph\]](#).
- [100] Rhorry Gauld, Florian Goertz, and Ulrich Haisch. “An explicit Z' -boson explanation of the $B \rightarrow K^*\mu^+\mu^-$ anomaly”. In: *JHEP* 1401 (2014), p. 069. DOI: [10.1007/JHEP01\(2014\)069](#). arXiv: [1310.1082 \[hep-ph\]](#).
- [101] Andrzej J. Buras, Fulvia De Fazio, and Jennifer Girrbach. “331 models facing new $b \rightarrow s\mu^+\mu^-$ data”. In: *JHEP* 1402 (2014), p. 112. DOI: [10.1007/JHEP02\(2014\)112](#). arXiv: [1311.6729 \[hep-ph\]](#).
- [102] Wolfgang Altmannshofer et al. “Quark flavor transitions in $L_\mu - L_\tau$ models”. In: *Phys.Rev.* D89.9 (2014), p. 095033. DOI: [10.1103/PhysRevD.89.095033](#). arXiv: [1403.1269 \[hep-ph\]](#).
- [103] Andreas Crivellin, Giancarlo D’Ambrosio, and Julian Heeck. “Explaining $h \rightarrow \mu^\pm\tau^\mp$, $B \rightarrow K^*\mu^+\mu^-$ and $B \rightarrow K\mu^+\mu^-/B \rightarrow Ke^+e^-$ in a two-Higgs-doublet model with gauged $L_\mu - L_\tau$ ”. In: *Phys. Rev. Lett.* 114 (2015), p. 151801. DOI: [10.1103/PhysRevLett.114.151801](#). arXiv: [1501.00993 \[hep-ph\]](#).
- [104] Andreas Crivellin, Giancarlo D’Ambrosio, and Julian Heeck. “Addressing the LHC flavor anomalies with horizontal gauge symmetries”. In: *Phys. Rev.* D91.7 (2015), p. 075006. DOI: [10.1103/PhysRevD.91.075006](#). arXiv: [1503.03477 \[hep-ph\]](#).
- [105] Christoph Niehoff, Peter Stangl, and David M. Straub. “Violation of lepton flavour universality in composite Higgs models”. In: *Phys. Lett.* B747 (2015), pp. 182–186. DOI: [10.1016/j.physletb.2015.05.063](#). arXiv: [1503.03865 \[hep-ph\]](#).
- [106] D. Aristizabal Sierra, Florian Staub, and Avelino Vicente. “Shedding light on the $b \rightarrow s$ anomalies with a dark sector”. In: *Phys. Rev.* D92.1 (2015), p. 015001. DOI: [10.1103/PhysRevD.92.015001](#). arXiv: [1503.06077 \[hep-ph\]](#).
- [107] Andreas Crivellin et al. “Lepton-flavour violating B decays in generic Z' models”. In: *Phys. Rev.* D92.5 (2015), p. 054013. DOI: [10.1103/PhysRevD.92.054013](#). arXiv: [1504.07928 \[hep-ph\]](#).
- [108] Alejandro Celis et al. “Family nonuniversal Z' models with protected flavor-changing interactions”. In: *Phys. Rev.* D92.1 (2015), p. 015007. DOI: [10.1103/PhysRevD.92.015007](#). arXiv: [1505.03079 \[hep-ph\]](#).
- [109] Ben Allanach et al. “ Z' models for the LHCb and $g - 2$ muon anomalies”. In: *Phys. Rev.* D93.5 (2016), p. 055045. DOI: [10.1103/PhysRevD.93.055045](#). arXiv: [1511.07447 \[hep-ph\]](#).
- [110] Damir Bečirević, Olcyr Sumensari, and Renata Zukanovich Funchal. “Lepton flavor violation in exclusive $b \rightarrow s$ decays”. In: *Eur. Phys. J.* C76.3 (2016), p. 134. DOI: [10.1140/epjc/s10052-016-3985-0](#). arXiv: [1602.00881 \[hep-ph\]](#).

- [111] Alejandro Celis, Wan-Zhe Feng, and Martin Vollmann. “Dirac Dark Matter and $b \rightarrow s\ell^+\ell^-$ with $U(1)$ gauge symmetry”. In: (2016). arXiv: [1608.03894 \[hep-ph\]](#).
- [112] Sofiane M. Boucenna et al. “Non-abelian gauge extensions for B-decay anomalies”. In: *Phys. Lett.* B760 (2016), pp. 214–219. DOI: [10.1016/j.physletb.2016.06.067](#). arXiv: [1604.03088 \[hep-ph\]](#).
- [113] Sofiane M. Boucenna et al. “Phenomenology of an $SU(2) \times SU(2) \times U(1)$ model with lepton-flavour non-universality”. In: (2016). arXiv: [1608.01349 \[hep-ph\]](#).
- [114] Eugenio Megias et al. “A Natural origin for the LHCb anomalies”. In: (2016). arXiv: [1608.02362 \[hep-ph\]](#).
- [115] Wolfgang Altmannshofer et al. “Explaining dark matter and B decay anomalies with an $L_\mu - L_\tau$ model”. In: *JHEP* 12 (2016), p. 106. DOI: [10.1007/JHEP12\(2016\)106](#). arXiv: [1609.04026 \[hep-ph\]](#).
- [116] Andreas Crivellin et al. “Lepton Flavor Non-Universality in B decays from Dynamical Yukawas”. In: *Phys. Lett.* B766 (2017), pp. 77–85. DOI: [10.1016/j.physletb.2016.12.057](#). arXiv: [1611.02703 \[hep-ph\]](#).
- [117] Stefano Di Chiara et al. “Minimal flavor-changing Z' models and muon $g-2$ after the R_{K^*} measurement”. In: *Nucl. Phys.* B923 (2017), pp. 245–257. DOI: [10.1016/j.nuclphysb.2017.08.003](#). arXiv: [1704.06200 \[hep-ph\]](#).
- [118] Cheng-Wei Chiang et al. “ $R_{K^{(*)}}$ and related $b \rightarrow s\ell\bar{\ell}$ anomalies in minimal flavor violation framework with Z' boson”. In: *Phys. Rev.* D96.11 (2017), p. 115022. DOI: [10.1103/PhysRevD.96.115022](#). arXiv: [1706.02696 \[hep-ph\]](#).
- [119] Miguel Crispim Romao, Stephen F. King, and George K. Leontaris. “Non-universal Z' from fluxed GUTs”. In: *Phys. Lett.* B782 (2018), pp. 353–361. DOI: [10.1016/j.physletb.2018.05.057](#). arXiv: [1710.02349 \[hep-ph\]](#).
- [120] Ligong Bian, Hyun Min Lee, and Chan Beom Park. “ B -meson anomalies and Higgs physics in flavored $U(1)'$ model”. In: *Eur. Phys. J.* C78.4 (2018), p. 306. DOI: [10.1140/epjc/s10052-018-5777-1](#). arXiv: [1711.08930 \[hep-ph\]](#).
- [121] Adam Falkowski et al. “Flavourful Z' portal for vector-like neutrino Dark Matter and $R_{K^{(*)}}$ ”. In: *JHEP* 08 (2018), p. 061. DOI: [10.1007/JHEP08\(2018\)061](#). arXiv: [1803.04430 \[hep-ph\]](#).
- [122] Diego Guadagnoli, M  ril Rebound, and Olcyr Sumensari. “A gauged horizontal $SU(2)$ symmetry and $R_{K^{(*)}}$ ”. In: *JHEP* 11 (2018), p. 163. DOI: [10.1007/JHEP11\(2018\)163](#). arXiv: [1807.03285 \[hep-ph\]](#).
- [123] Paul Langacker. “The Physics of Heavy Z' Gauge Bosons”. In: *Rev.Mod.Phys.* 81 (2009), pp. 1199–1228. DOI: [10.1103/RevModPhys.81.1199](#). arXiv: [0801.1345 \[hep-ph\]](#).
- [124] Seungwon Baek et al. “Muon anomalous $g-2$ and gauged $L(\text{muon}) - L(\text{tau})$ models”. In: *Phys.Rev.* D64 (2001), p. 055006. DOI: [10.1103/PhysRevD.64.055006](#). arXiv: [hep-ph/0104141 \[hep-ph\]](#).

Bibliography

- [125] Ernest Ma, D.P. Roy, and Sourov Roy. “Gauged $L_\mu - L_\tau$ with large muon anomalous magnetic moment and the bimaximal mixing of neutrinos”. In: *Phys.Lett.* B525 (2002), pp. 101–106. DOI: [10.1016/S0370-2693\(01\)01428-9](https://doi.org/10.1016/S0370-2693(01)01428-9). arXiv: [hep-ph/0110146](https://arxiv.org/abs/hep-ph/0110146) [hep-ph].
- [126] S. N. Gninenko and N. V. Krasnikov. “The Muon anomalous magnetic moment and a new light gauge boson”. In: *Phys. Lett.* B513 (2001), p. 119. DOI: [10.1016/S0370-2693\(01\)00693-1](https://doi.org/10.1016/S0370-2693(01)00693-1). arXiv: [hep-ph/0102222](https://arxiv.org/abs/hep-ph/0102222) [hep-ph].
- [127] Maxim Pospelov. “Secluded U(1) below the weak scale”. In: *Phys. Rev.* D80 (2009), p. 095002. DOI: [10.1103/PhysRevD.80.095002](https://doi.org/10.1103/PhysRevD.80.095002). arXiv: [0811.1030](https://arxiv.org/abs/0811.1030) [hep-ph].
- [128] Julian Heeck and Werner Rodejohann. “Gauged $L_\mu - L_\tau$ Symmetry at the Electroweak Scale”. In: *Phys.Rev.* D84 (2011), p. 075007. DOI: [10.1103/PhysRevD.84.075007](https://doi.org/10.1103/PhysRevD.84.075007). arXiv: [1107.5238](https://arxiv.org/abs/1107.5238) [hep-ph].
- [129] Carla Biggio et al. “Massive vectors and loop observables: the $g - 2$ case”. In: (2016). arXiv: [1607.07621](https://arxiv.org/abs/1607.07621) [hep-ph].
- [130] Keisuke Harigaya et al. “Muon $g - 2$ and LHC phenomenology in the $L_\mu - L_\tau$ gauge symmetric model”. In: *JHEP* 1403 (2014), p. 105. DOI: [10.1007/JHEP03\(2014\)105](https://doi.org/10.1007/JHEP03(2014)105). arXiv: [1311.0870](https://arxiv.org/abs/1311.0870) [hep-ph].
- [131] Wolfgang Altmannshofer et al. “Neutrino Trident Production: A Powerful Probe of New Physics with Neutrino Beams”. In: *Phys.Rev.Lett.* 113 (2014), p. 091801. DOI: [10.1103/PhysRevLett.113.091801](https://doi.org/10.1103/PhysRevLett.113.091801). arXiv: [1406.2332](https://arxiv.org/abs/1406.2332) [hep-ph].
- [132] Wolfgang Altmannshofer et al. “Lepton flavor violating Z’ explanation of the muon anomalous magnetic moment”. In: (2016). arXiv: [1607.06832](https://arxiv.org/abs/1607.06832) [hep-ph].
- [133] Debrupa Chakraverty, Debajyoti Choudhury, and Anindya Datta. “A Nonsupersymmetric resolution of the anomalous muon magnetic moment”. In: *Phys. Lett.* B506 (2001), pp. 103–108. DOI: [10.1016/S0370-2693\(01\)00419-1](https://doi.org/10.1016/S0370-2693(01)00419-1). arXiv: [hep-ph/0102180](https://arxiv.org/abs/hep-ph/0102180) [hep-ph].
- [134] King-man Cheung. “Muon anomalous magnetic moment and leptoquark solutions”. In: *Phys. Rev.* D64 (2001), p. 033001. DOI: [10.1103/PhysRevD.64.033001](https://doi.org/10.1103/PhysRevD.64.033001). arXiv: [hep-ph/0102238](https://arxiv.org/abs/hep-ph/0102238) [hep-ph].
- [135] E. O. Iltan and H. Sundu. “Anomalous magnetic moment of muon in the general two Higgs doublet model”. In: *Acta Phys. Slov.* 53 (2003), p. 17. arXiv: [hep-ph/0103105](https://arxiv.org/abs/hep-ph/0103105) [hep-ph].
- [136] Yuji Omura, Eibun Senaha, and Kazuhiro Tobe. “Lepton-flavor-violating Higgs decay $h \rightarrow \mu\tau$ and muon anomalous magnetic moment in a general two Higgs doublet model”. In: (2015). arXiv: [1502.07824](https://arxiv.org/abs/1502.07824) [hep-ph].
- [137] Wolfgang Altmannshofer, Marcela Carena, and Andreas Crivellin. “A $L_\mu - L_\tau$ theory of Higgs flavor violation and $(g - 2)_\mu$ ”. In: (2016). arXiv: [1604.08221](https://arxiv.org/abs/1604.08221) [hep-ph].
- [138] Alessandro Broggio et al. “Limiting two-Higgs-doublet models”. In: *JHEP* 11 (2014), p. 058. DOI: [10.1007/JHEP11\(2014\)058](https://doi.org/10.1007/JHEP11(2014)058). arXiv: [1409.3199](https://arxiv.org/abs/1409.3199) [hep-ph].
- [139] Lei Wang and Xiao-Fang Han. “A light pseudoscalar of 2HDM confronted with muon $g-2$ and experimental constraints”. In: *JHEP* 05 (2015), p. 039. DOI: [10.1007/JHEP05\(2015\)039](https://doi.org/10.1007/JHEP05(2015)039). arXiv: [1412.4874](https://arxiv.org/abs/1412.4874) [hep-ph].

- [140] Tomohiro Abe, Ryosuke Sato, and Kei Yagyu. “Lepton-specific two Higgs doublet model as a solution of muon $g - 2$ anomaly”. In: *JHEP* 07 (2015), p. 064. DOI: [10.1007/JHEP07\(2015\)064](https://doi.org/10.1007/JHEP07(2015)064). arXiv: [1504.07059](https://arxiv.org/abs/1504.07059) [hep-ph].
- [141] Andreas Crivellin, Julian Heeck, and Peter Stoffer. “A perturbed lepton-specific two-Higgs-doublet model facing experimental hints for physics beyond the Standard Model”. In: *Phys. Rev. Lett.* 116.8 (2016), p. 081801. DOI: [10.1103/PhysRevLett.116.081801](https://doi.org/10.1103/PhysRevLett.116.081801). arXiv: [1507.07567](https://arxiv.org/abs/1507.07567) [hep-ph].
- [142] Brian Batell et al. “The Leptonic Higgs Portal”. In: (2016). arXiv: [1606.04943](https://arxiv.org/abs/1606.04943) [hep-ph].
- [143] Ayres Freitas et al. “Testing the Muon $g-2$ Anomaly at the LHC”. In: *JHEP* 05 (2014). [Erratum: *JHEP*09,155(2014)], p. 145. DOI: [10.1007/JHEP09\(2014\)155](https://doi.org/10.1007/JHEP09(2014)155), [10.1007/JHEP05\(2014\)145](https://doi.org/10.1007/JHEP05(2014)145). arXiv: [1402.7065](https://arxiv.org/abs/1402.7065) [hep-ph].
- [144] Florian Goertz et al. “Indirect Constraints on the Scalar Di-Photon Resonance at the LHC”. In: *JHEP* 05 (2016), p. 187. DOI: [10.1007/JHEP05\(2016\)187](https://doi.org/10.1007/JHEP05(2016)187). arXiv: [1512.08500](https://arxiv.org/abs/1512.08500) [hep-ph].
- [145] S. Bertolini et al. “Effects of supergravity induced electroweak breaking on rare B decays and mixings”. In: *Nucl. Phys. B* 353 (1991), pp. 591–649. DOI: [10.1016/0550-3213\(91\)90320-w](https://doi.org/10.1016/0550-3213(91)90320-w).
- [146] Andrzej J. Buras et al. “ $B \rightarrow K^{(*)}\nu\bar{\nu}$ decays in the Standard Model and beyond”. In: *JHEP* 02 (2015), p. 184. DOI: [10.1007/JHEP02\(2015\)184](https://doi.org/10.1007/JHEP02(2015)184). arXiv: [1409.4557](https://arxiv.org/abs/1409.4557) [hep-ph].
- [147] J. Grygier et al. “Search for $B \rightarrow h\nu\bar{\nu}$ decays with semileptonic tagging at Belle”. In: *Phys. Rev. D* 96.9 (2017). [Addendum: *Phys. Rev. D* 97, no. 9, 099902 (2018)], p. 091101. DOI: [10.1103/PhysRevD.97.099902](https://doi.org/10.1103/PhysRevD.97.099902), [10.1103/PhysRevD.96.091101](https://doi.org/10.1103/PhysRevD.96.091101). arXiv: [1702.03224](https://arxiv.org/abs/1702.03224) [hep-ex].
- [148] John S. Hagelin, S. Kelley, and Toshiaki Tanaka. “Supersymmetric flavor changing neutral currents: Exact amplitudes and phenomenological analysis”. In: *Nucl. Phys. B* 415 (1994), pp. 293–331. DOI: [10.1016/0550-3213\(94\)90113-9](https://doi.org/10.1016/0550-3213(94)90113-9).
- [149] Luca Di Luzio et al. “ ΔM_s theory precision confronts flavour anomalies”. In: *JHEP* 12 (2019), p. 009. DOI: [10.1007/JHEP12\(2019\)009](https://doi.org/10.1007/JHEP12(2019)009). arXiv: [1909.11087](https://arxiv.org/abs/1909.11087) [hep-ph].
- [150] R. J. Dowdall et al. “Neutral B-meson mixing from full lattice QCD at the physical point”. In: *Phys. Rev. D* 100.9 (2019), p. 094508. DOI: [10.1103/PhysRevD.100.094508](https://doi.org/10.1103/PhysRevD.100.094508). arXiv: [1907.01025](https://arxiv.org/abs/1907.01025) [hep-lat].
- [151] Daniel King, Alexander Lenz, and Thomas Rauh. “ B_s mixing observables and $-V_{td}/V_{ts}$ — from sum rules”. In: (2019). arXiv: [1904.00940](https://arxiv.org/abs/1904.00940) [hep-ph].
- [152] M. Tanabashi et al. “Review of Particle Physics”. In: *Phys. Rev. D* 98.3 (2018), p. 030001. DOI: [10.1103/PhysRevD.98.030001](https://doi.org/10.1103/PhysRevD.98.030001).
- [153] N. Carrasco et al. “B-physics from $N_f = 2$ tmQCD: the Standard Model and beyond”. In: *JHEP* 03 (2014), p. 016. DOI: [10.1007/JHEP03\(2014\)016](https://doi.org/10.1007/JHEP03(2014)016). arXiv: [1308.1851](https://arxiv.org/abs/1308.1851) [hep-lat].
- [154] Thomas Besmer, Christoph Greub, and Tobias Hurth. “Bounds on supersymmetric flavor violating parameters from $B \rightarrow X_s \gamma$ ”. In: *Nucl. Phys. B* 609 (2001), pp. 359–386. DOI: [10.1016/S0550-3213\(01\)00306-6](https://doi.org/10.1016/S0550-3213(01)00306-6). arXiv: [hep-ph/0105292](https://arxiv.org/abs/hep-ph/0105292) [hep-ph].

- [155] Christoph Bobeth, Mikolaj Misiak, and Joerg Urban. “Matching conditions for $b \rightarrow s\gamma$ and $b \rightarrow sgluon$ in extensions of the standard model”. In: *Nucl. Phys.* B567 (2000), pp. 153–185. DOI: [10.1016/S0550-3213\(99\)00688-4](https://doi.org/10.1016/S0550-3213(99)00688-4). arXiv: [hep-ph/9904413](https://arxiv.org/abs/hep-ph/9904413) [hep-ph].
- [156] Mikolaj Misiak, Abdur Rehman, and Matthias Steinhauser. “NNLO QCD counterterm contributions to $\bar{B} \rightarrow X_{s\gamma}$ for the physical value of m_c ”. In: *Phys. Lett.* B770 (2017), pp. 431–439. DOI: [10.1016/j.physletb.2017.05.008](https://doi.org/10.1016/j.physletb.2017.05.008). arXiv: [1702.07674](https://arxiv.org/abs/1702.07674) [hep-ph].
- [157] M. Misiak et al. “Updated NNLO QCD predictions for the weak radiative B-meson decays”. In: *Phys. Rev. Lett.* 114.22 (2015), p. 221801. DOI: [10.1103/PhysRevLett.114.221801](https://doi.org/10.1103/PhysRevLett.114.221801). arXiv: [1503.01789](https://arxiv.org/abs/1503.01789) [hep-ph].
- [158] A. Crivellin et al. “SUSY_FLAVOR v2: A Computational tool for FCNC and CP-violating processes in the MSSM”. In: *Comput. Phys. Commun.* 184 (2013), pp. 1004–1032. DOI: [10.1016/j.cpc.2012.11.007](https://doi.org/10.1016/j.cpc.2012.11.007). arXiv: [1203.5023](https://arxiv.org/abs/1203.5023) [hep-ph].
- [159] A. Djouadi et al. “(e b), (e t) TYPE LEPTOQUARKS AT e p COLLIDERS”. In: *Z. Phys.* C46 (1990), pp. 679–686. DOI: [10.1007/BF01560270](https://doi.org/10.1007/BF01560270).
- [160] Takeo Moroi. “The Muon anomalous magnetic dipole moment in the minimal supersymmetric standard model”. In: *Phys. Rev.* D53 (1996). [Erratum: *Phys. Rev.*D56,4424(1997)], pp. 6565–6575. DOI: [10.1103/PhysRevD.53.6565](https://doi.org/10.1103/PhysRevD.53.6565), [10.1103/PhysRevD.56.4424](https://doi.org/10.1103/PhysRevD.56.4424). arXiv: [hep-ph/9512396](https://arxiv.org/abs/hep-ph/9512396) [hep-ph].
- [161] G.W. Bennett et al. “Final Report of the Muon E821 Anomalous Magnetic Moment Measurement at BNL”. In: *Phys. Rev.* D73 (2006), p. 072003. DOI: [10.1103/PhysRevD.73.072003](https://doi.org/10.1103/PhysRevD.73.072003). arXiv: <http://arxiv.org/abs/hep-ex/0602035> [arXiv:hep-ex/0602035] [hep-ex].
- [162] J. Grange et al. “Muon (g-2) Technical Design Report”. In: (2015). arXiv: [1501.06858](https://arxiv.org/abs/1501.06858) [physics.ins-det].
- [163] Naohito Saito. “A novel precision measurement of muon g-2 and EDM at J-PARC”. In: *AIP Conf. Proc.* 1467 (2012), pp. 45–56. DOI: [10.1063/1.4742078](https://doi.org/10.1063/1.4742078).
- [164] T. P. Gorringer and D. W. Hertzog. “Precision Muon Physics”. In: *Prog. Part. Nucl. Phys.* 84 (2015), pp. 73–123. DOI: [10.1016/j.pnpnp.2015.06.001](https://doi.org/10.1016/j.pnpnp.2015.06.001). arXiv: [1506.01465](https://arxiv.org/abs/1506.01465) [hep-ex].
- [165] Andrzej Czarnecki, Bernd Krause, and William J. Marciano. “Electroweak Fermion loop contributions to the muon anomalous magnetic moment”. In: *Phys. Rev.* D52 (1995), R2619–R2623. DOI: [10.1103/PhysRevD.52.R2619](https://doi.org/10.1103/PhysRevD.52.R2619). arXiv: [hep-ph/9506256](https://arxiv.org/abs/hep-ph/9506256) [hep-ph].
- [166] Andrzej Czarnecki, Bernd Krause, and William J. Marciano. “Electroweak corrections to the muon anomalous magnetic moment”. In: *Phys. Rev. Lett.* 76 (1996), pp. 3267–3270. DOI: [10.1103/PhysRevLett.76.3267](https://doi.org/10.1103/PhysRevLett.76.3267). arXiv: [hep-ph/9512369](https://arxiv.org/abs/hep-ph/9512369) [hep-ph].
- [167] Fred Jegerlehner and Andreas Nyffeler. “The Muon g-2”. In: *Phys. Rept.* 477 (2009), pp. 1–110. DOI: [10.1016/j.physrep.2009.04.003](https://doi.org/10.1016/j.physrep.2009.04.003). arXiv: [0902.3360](https://arxiv.org/abs/0902.3360) [hep-ph].

- [168] Kaoru Hagiwara et al. “ $(g-2)_\mu$ and $\alpha(M_Z^2)$ re-evaluated using new precise data”. In: *J. Phys.* G38 (2011), p. 085003. DOI: [10.1088/0954-3899/38/8/085003](https://doi.org/10.1088/0954-3899/38/8/085003). arXiv: [1105.3149](https://arxiv.org/abs/1105.3149) [hep-ph].
- [169] Tatsumi Aoyama et al. “Complete Tenth-Order QED Contribution to the Muon $g-2$ ”. In: *Phys. Rev. Lett.* 109 (2012), p. 111808. DOI: [10.1103/PhysRevLett.109.111808](https://doi.org/10.1103/PhysRevLett.109.111808). arXiv: [1205.5370](https://arxiv.org/abs/1205.5370) [hep-ph].
- [170] C. Gnendiger, D. Stöckinger, and H. Stöckinger-Kim. “The electroweak contributions to $(g-2)_\mu$ after the Higgs boson mass measurement”. In: *Phys. Rev.* D88 (2013), p. 053005. DOI: [10.1103/PhysRevD.88.053005](https://doi.org/10.1103/PhysRevD.88.053005). arXiv: [1306.5546](https://arxiv.org/abs/1306.5546) [hep-ph].
- [171] Bipasha Chakraborty et al. “The hadronic vacuum polarization contribution to a_μ from full lattice QCD”. In: *Phys. Rev.* D96.3 (2017), p. 034516. DOI: [10.1103/PhysRevD.96.034516](https://doi.org/10.1103/PhysRevD.96.034516). arXiv: [1601.03071](https://arxiv.org/abs/1601.03071) [hep-lat].
- [172] Fred Jegerlehner. “Muon $g-2$ theory: The hadronic part”. In: *EPJ Web Conf.* 166 (2018), p. 00022. DOI: [10.1051/epjconf/201816600022](https://doi.org/10.1051/epjconf/201816600022). arXiv: [1705.00263](https://arxiv.org/abs/1705.00263) [hep-ph].
- [173] M. Della Morte et al. “The hadronic vacuum polarization contribution to the muon $g-2$ from lattice QCD”. In: *JHEP* 10 (2017), p. 020. DOI: [10.1007/JHEP10\(2017\)020](https://doi.org/10.1007/JHEP10(2017)020). arXiv: [1705.01775](https://arxiv.org/abs/1705.01775) [hep-lat].
- [174] Michel Davier et al. “Reevaluation of the hadronic vacuum polarisation contributions to the Standard Model predictions of the muon $g-2$ and $\alpha(m_Z^2)$ using newest hadronic cross-section data”. In: *Eur. Phys. J.* C77.12 (2017), p. 827. DOI: [10.1140/epjc/s10052-017-5161-6](https://doi.org/10.1140/epjc/s10052-017-5161-6). arXiv: [1706.09436](https://arxiv.org/abs/1706.09436) [hep-ph].
- [175] Sz. Borsanyi et al. “Hadronic vacuum polarization contribution to the anomalous magnetic moments of leptons from first principles”. In: *Phys. Rev. Lett.* 121.2 (2018), p. 022002. DOI: [10.1103/PhysRevLett.121.022002](https://doi.org/10.1103/PhysRevLett.121.022002). arXiv: [1711.04980](https://arxiv.org/abs/1711.04980) [hep-lat].
- [176] D. Giusti, F. Sanfilippo, and S. Simula. “Light-quark contribution to the leading hadronic vacuum polarization term of the muon $g-2$ from twisted-mass fermions”. In: *Phys. Rev.* D98.11 (2018), p. 114504. DOI: [10.1103/PhysRevD.98.114504](https://doi.org/10.1103/PhysRevD.98.114504). arXiv: [1808.00887](https://arxiv.org/abs/1808.00887) [hep-lat].
- [177] D. Giusti et al. “Electromagnetic and strong isospin-breaking corrections to the muon $g-2$ from Lattice QCD+QED”. In: (2019). arXiv: [1901.10462](https://arxiv.org/abs/1901.10462) [hep-lat].
- [178] T. Blum et al. “Calculation of the hadronic vacuum polarization contribution to the muon anomalous magnetic moment”. In: *Phys. Rev. Lett.* 121.2 (2018), p. 022003. DOI: [10.1103/PhysRevLett.121.022003](https://doi.org/10.1103/PhysRevLett.121.022003). arXiv: [1801.07224](https://arxiv.org/abs/1801.07224) [hep-lat].
- [179] Alexander Keshavarzi, Daisuke Nomura, and Thomas Teubner. “Muon $g-2$ and $\alpha(M_Z^2)$: a new data-based analysis”. In: *Phys. Rev.* D97.11 (2018), p. 114025. DOI: [10.1103/PhysRevD.97.114025](https://doi.org/10.1103/PhysRevD.97.114025). arXiv: [1802.02995](https://arxiv.org/abs/1802.02995) [hep-ph].
- [180] Gilberto Colangelo et al. “Dispersion relation for hadronic light-by-light scattering: theoretical foundations”. In: *JHEP* 09 (2015), p. 074. DOI: [10.1007/JHEP09\(2015\)074](https://doi.org/10.1007/JHEP09(2015)074). arXiv: [1506.01386](https://arxiv.org/abs/1506.01386) [hep-ph].

- [181] Jeremy Green et al. “Lattice QCD calculation of hadronic light-by-light scattering”. In: *Phys. Rev. Lett.* 115.22 (2015), p. 222003. DOI: [10.1103/PhysRevLett.115.222003](https://doi.org/10.1103/PhysRevLett.115.222003). arXiv: [1507.01577](https://arxiv.org/abs/1507.01577) [hep-lat].
- [182] Antoine Gérardin, Harvey B. Meyer, and Andreas Nyffeler. “Lattice calculation of the pion transition form factor $\pi^0 \rightarrow \gamma^* \gamma^*$ ”. In: *Phys. Rev. D* 94.7 (2016), p. 074507. DOI: [10.1103/PhysRevD.94.074507](https://doi.org/10.1103/PhysRevD.94.074507). arXiv: [1607.08174](https://arxiv.org/abs/1607.08174) [hep-lat].
- [183] Thomas Blum et al. “Connected and Leading Disconnected Hadronic Light-by-Light Contribution to the Muon Anomalous Magnetic Moment with a Physical Pion Mass”. In: *Phys. Rev. Lett.* 118.2 (2017), p. 022005. DOI: [10.1103/PhysRevLett.118.022005](https://doi.org/10.1103/PhysRevLett.118.022005). arXiv: [1610.04603](https://arxiv.org/abs/1610.04603) [hep-lat].
- [184] Gilberto Colangelo et al. “Rescattering effects in the hadronic-light-by-light contribution to the anomalous magnetic moment of the muon”. In: *Phys. Rev. Lett.* 118.23 (2017), p. 232001. DOI: [10.1103/PhysRevLett.118.232001](https://doi.org/10.1103/PhysRevLett.118.232001). arXiv: [1701.06554](https://arxiv.org/abs/1701.06554) [hep-ph].
- [185] Thomas Blum et al. “Using infinite volume, continuum QED and lattice QCD for the hadronic light-by-light contribution to the muon anomalous magnetic moment”. In: *Phys. Rev. D* 96.3 (2017), p. 034515. DOI: [10.1103/PhysRevD.96.034515](https://doi.org/10.1103/PhysRevD.96.034515). arXiv: [1705.01067](https://arxiv.org/abs/1705.01067) [hep-lat].
- [186] Martin Hoferichter et al. “Pion-pole contribution to hadronic light-by-light scattering in the anomalous magnetic moment of the muon”. In: *Phys. Rev. Lett.* 121.11 (2018), p. 112002. DOI: [10.1103/PhysRevLett.121.112002](https://doi.org/10.1103/PhysRevLett.121.112002). arXiv: [1805.01471](https://arxiv.org/abs/1805.01471) [hep-ph].
- [187] Alexander Kurz et al. “Hadronic contribution to the muon anomalous magnetic moment to next-to-next-to-leading order”. In: *Phys. Lett. B* 734 (2014), pp. 144–147. DOI: [10.1016/j.physletb.2014.05.043](https://doi.org/10.1016/j.physletb.2014.05.043). arXiv: [1403.6400](https://arxiv.org/abs/1403.6400) [hep-ph].
- [188] Gilberto Colangelo et al. “Remarks on higher-order hadronic corrections to the muon $g-2$ ”. In: *Phys. Lett. B* 735 (2014), pp. 90–91. DOI: [10.1016/j.physletb.2014.06.012](https://doi.org/10.1016/j.physletb.2014.06.012). arXiv: [1403.7512](https://arxiv.org/abs/1403.7512) [hep-ph].
- [189] Sz. Borsanyi et al. “Leading-order hadronic vacuum polarization contribution to the muon magnetic moment from lattice QCD”. In: (2020). arXiv: [2002.12347](https://arxiv.org/abs/2002.12347) [hep-lat].
- [190] Wolfgang Altmannshofer and David M. Straub. “New physics in $b \rightarrow s$ transitions after LHC run 1”. In: *Eur. Phys. J. C* 75.8 (2015), p. 382. DOI: [10.1140/epjc/s10052-015-3602-7](https://doi.org/10.1140/epjc/s10052-015-3602-7). arXiv: [1411.3161](https://arxiv.org/abs/1411.3161) [hep-ph].
- [191] Sébastien Descotes-Genon et al. “Global analysis of $b \rightarrow s \ell \ell$ anomalies”. In: *JHEP* 06 (2016), p. 092. DOI: [10.1007/JHEP06\(2016\)092](https://doi.org/10.1007/JHEP06(2016)092). arXiv: [1510.04239](https://arxiv.org/abs/1510.04239) [hep-ph].
- [192] A. M. Baldini et al. “Search for the lepton flavour violating decay $\mu^+ \rightarrow e^+ \gamma$ with the full dataset of the MEG experiment”. In: *Eur. Phys. J. C* 76.8 (2016), p. 434. DOI: [10.1140/epjc/s10052-016-4271-x](https://doi.org/10.1140/epjc/s10052-016-4271-x). arXiv: [1605.05081](https://arxiv.org/abs/1605.05081) [hep-ex].
- [193] S. Schael et al. “Precision electroweak measurements on the Z resonance”. In: *Phys. Rept.* 427 (2006), pp. 257–454. DOI: [10.1016/j.physrep.2005.12.006](https://doi.org/10.1016/j.physrep.2005.12.006). arXiv: [hep-ex/0509008](https://arxiv.org/abs/hep-ex/0509008).

- [194] Morad Aaboud et al. “Search for bottom squark pair production in proton–proton collisions at $\sqrt{s} = 13$ TeV with the ATLAS detector”. In: *Eur. Phys. J. C* 76.10 (2016), p. 547. DOI: [10.1140/epjc/s10052-016-4382-4](https://doi.org/10.1140/epjc/s10052-016-4382-4). arXiv: [1606.08772](https://arxiv.org/abs/1606.08772) [hep-ex].
- [195] Vardan Khachatryan et al. “Search for new physics in same-sign dilepton events in proton–proton collisions at $\sqrt{s} = 13$ TeV”. In: *Eur. Phys. J. C* 76.8 (2016), p. 439. DOI: [10.1140/epjc/s10052-016-4261-z](https://doi.org/10.1140/epjc/s10052-016-4261-z). arXiv: [1605.03171](https://arxiv.org/abs/1605.03171) [hep-ex].
- [196] Marie E. Machacek and Michael T. Vaughn. “Two Loop Renormalization Group Equations in a General Quantum Field Theory. 2. Yukawa Couplings”. In: *Nucl. Phys.* B236 (1984), pp. 221–232. DOI: [10.1016/0550-3213\(84\)90533-9](https://doi.org/10.1016/0550-3213(84)90533-9).
- [197] Ming-xing Luo, Hua-wen Wang, and Yong Xiao. “Two loop renormalization group equations in general gauge field theories”. In: *Phys. Rev.* D67 (2003), p. 065019. DOI: [10.1103/PhysRevD.67.065019](https://doi.org/10.1103/PhysRevD.67.065019). arXiv: [hep-ph/0211440](https://arxiv.org/abs/hep-ph/0211440) [hep-ph].
- [198] Florian Staub et al. “Precision tools and models to narrow in on the 750 GeV diphoton resonance”. In: *Eur. Phys. J. C* 76.9 (2016), p. 516. DOI: [10.1140/epjc/s10052-016-4349-5](https://doi.org/10.1140/epjc/s10052-016-4349-5). arXiv: [1602.05581](https://arxiv.org/abs/1602.05581) [hep-ph].
- [199] Zijie Poh and Stuart Raby. “Vectorlike leptons: Muon g-2 anomaly, lepton flavor violation, Higgs boson decays, and lepton nonuniversality”. In: *Phys. Rev.* D96.1 (2017), p. 015032. DOI: [10.1103/PhysRevD.96.015032](https://doi.org/10.1103/PhysRevD.96.015032). arXiv: [1705.07007](https://arxiv.org/abs/1705.07007) [hep-ph].
- [200] Stuart Raby and Andreas Trautner. “Vectorlike chiral fourth family to explain muon anomalies”. In: *Phys. Rev.* D97.9 (2018), p. 095006. DOI: [10.1103/PhysRevD.97.095006](https://doi.org/10.1103/PhysRevD.97.095006). arXiv: [1712.09360](https://arxiv.org/abs/1712.09360) [hep-ph].
- [201] G. C. Branco and L. Lavoura. “On the Addition of Vector Like Quarks to the Standard Model”. In: *Nucl. Phys.* B278 (1986), pp. 738–754. DOI: [10.1016/0550-3213\(86\)90060-X](https://doi.org/10.1016/0550-3213(86)90060-X).
- [202] F. del Aguila et al. “Vector Like Fermion and Standard Higgs Production at Hadron Colliders”. In: *Nucl. Phys.* B334 (1990), pp. 1–23. DOI: [10.1016/0550-3213\(90\)90655-W](https://doi.org/10.1016/0550-3213(90)90655-W).
- [203] Paul Langacker and David London. “Mixing Between Ordinary and Exotic Fermions”. In: *Phys. Rev.* D38 (1988), p. 886. DOI: [10.1103/PhysRevD.38.886](https://doi.org/10.1103/PhysRevD.38.886).
- [204] F. del Aguila, J. A. Aguilar-Saavedra, and G. C. Branco. “CP violation from new quarks in the chiral limit”. In: *Nucl. Phys.* B510 (1998), pp. 39–60. DOI: [10.1016/S0550-3213\(97\)00708-6](https://doi.org/10.1016/S0550-3213(97)00708-6), [10.1016/S0550-3213\(98\)81003-1](https://doi.org/10.1016/S0550-3213(98)81003-1). arXiv: [hep-ph/9703410](https://arxiv.org/abs/hep-ph/9703410) [hep-ph].
- [205] F. Gabbiani et al. “A Complete analysis of FCNC and CP constraints in general SUSY extensions of the standard model”. In: *Nucl. Phys.* B477 (1996), pp. 321–352. DOI: [10.1016/0550-3213\(96\)00390-2](https://doi.org/10.1016/0550-3213(96)00390-2). arXiv: [hep-ph/9604387](https://arxiv.org/abs/hep-ph/9604387) [hep-ph].
- [206] Jonathan A. Bagger, Konstantin T. Matchev, and Ren-Jie Zhang. “QCD corrections to flavor changing neutral currents in the supersymmetric standard model”. In: *Phys. Lett.* B412 (1997), pp. 77–85. DOI: [10.1016/S0370-2693\(97\)00920-9](https://doi.org/10.1016/S0370-2693(97)00920-9). arXiv: [hep-ph/9707225](https://arxiv.org/abs/hep-ph/9707225) [hep-ph].

- [207] Joachim Brod and Martin Gorbahn. “The Z Penguin in Generic Extensions of the Standard Model”. In: (2019). arXiv: [1903.05116 \[hep-ph\]](#).
- [208] A. Dedes et al. “Feynman rules for the Standard Model Effective Field Theory in R_ξ -gauges”. In: *JHEP* 06 (2017), p. 143. DOI: [10.1007/JHEP06\(2017\)143](#). arXiv: [1704.03888 \[hep-ph\]](#).
- [209] R Aaij et al. “Measurement of the ratio of branching fractions $BR(B_0 \rightarrow K^{*0}\gamma)/BR(B_{s0} \rightarrow \phi\gamma)$ and the direct CP asymmetry in $B_0 \rightarrow K^{*0}\gamma$ ”. In: *Nucl. Phys.* B867 (2013), pp. 1–18. DOI: [10.1016/j.nuclphysb.2012.09.013](#). arXiv: [1209.0313 \[hep-ex\]](#).
- [210] Roel Aaij et al. “Angular analysis of the $B^0 \rightarrow K^{*0} e^+ e^-$ decay in the low- q^2 region”. In: *JHEP* 04 (2015), p. 064. DOI: [10.1007/JHEP04\(2015\)064](#). arXiv: [1501.03038 \[hep-ex\]](#).
- [211] Morad Aaboud et al. “Angular analysis of $B_d^0 \rightarrow K^{*0}\mu^+\mu^-$ decays in pp collisions at $\sqrt{s} = 8$ TeV with the ATLAS detector”. In: *JHEP* 10 (2018), p. 047. DOI: [10.1007/JHEP10\(2018\)047](#). arXiv: [1805.04000 \[hep-ex\]](#).
- [212] Vardan Khachatryan et al. “Angular analysis of the decay $B^0 \rightarrow K^{*0}\mu^+\mu^-$ from pp collisions at $\sqrt{s} = 8$ TeV”. In: *Phys. Lett.* B753 (2016), pp. 424–448. DOI: [10.1016/j.physletb.2015.12.020](#). arXiv: [1507.08126 \[hep-ex\]](#).
- [213] Albert M Sirunyan et al. “Measurement of angular parameters from the decay $B^0 \rightarrow K^{*0}\mu^+\mu^-$ in proton-proton collisions at $\sqrt{s} = 8$ TeV”. In: *Phys. Lett.* B781 (2018), pp. 517–541. DOI: [10.1016/j.physletb.2018.04.030](#). arXiv: [1710.02846 \[hep-ex\]](#).
- [214] Wolfgang Altmannshofer et al. “Symmetries and Asymmetries of $B \rightarrow K^*\mu^+\mu^-$ Decays in the Standard Model and Beyond”. In: *JHEP* 01 (2009), p. 019. DOI: [10.1088/1126-6708/2009/01/019](#). arXiv: [0811.1214 \[hep-ph\]](#).
- [215] Wolfgang Altmannshofer, Christoph Niehoff, and David M. Straub. “ $B_s \rightarrow \mu^+\mu^-$ as current and future probe of new physics”. In: *JHEP* 05 (2017), p. 076. DOI: [10.1007/JHEP05\(2017\)076](#). arXiv: [1702.05498 \[hep-ph\]](#).
- [216] Tobias Hurth, Enrico Lunghi, and Werner Porod. “Untagged $\bar{B} \rightarrow X_{s+d}\gamma$ CP asymmetry as a probe for new physics”. In: *Nucl. Phys.* B704 (2005), pp. 56–74. DOI: [10.1016/j.nuclphysb.2004.10.024](#). arXiv: [hep-ph/0312260 \[hep-ph\]](#).
- [217] D. Bečirević et al. “ $B_d - \bar{B}_d$ mixing and the $B_d \rightarrow J/\psi K_s$ asymmetry in general SUSY models”. In: *Nucl. Phys.* B634 (2002), pp. 105–119. DOI: [10.1016/S0550-3213\(02\)00291-2](#). arXiv: [hep-ph/0112303 \[hep-ph\]](#).
- [218] A. Bazavov et al. “ $B_{(s)}^0$ -mixing matrix elements from lattice QCD for the Standard Model and beyond”. In: *Phys. Rev.* D93.11 (2016), p. 113016. DOI: [10.1103/PhysRevD.93.113016](#). arXiv: [1602.03560 \[hep-lat\]](#).
- [219] Luca Di Luzio, Matthew Kirk, and Alexander Lenz. “ B_s - \bar{B}_s mixing interplay with B anomalies”. In: *10th International Workshop on the CKM Unitarity Triangle (CKM 2018) Heidelberg, Germany, September 17-21, 2018*. 2018. arXiv: [1811.12884 \[hep-ph\]](#).

- [220] Luca Di Luzio, Matthew Kirk, and Alexander Lenz. “Updated B_s -mixing constraints on new physics models for $b \rightarrow s\ell^+\ell^-$ anomalies”. In: *Phys. Rev. D* 97.9 (2018), p. 095035. DOI: [10.1103/PhysRevD.97.095035](https://doi.org/10.1103/PhysRevD.97.095035). arXiv: [1712.06572](https://arxiv.org/abs/1712.06572) [hep-ph].
- [221] G. W. Bennett et al. “Final Report of the Muon E821 Anomalous Magnetic Moment Measurement at BNL”. In: *Phys. Rev. D* 73 (2006), p. 072003. DOI: [10.1103/PhysRevD.73.072003](https://doi.org/10.1103/PhysRevD.73.072003). arXiv: [hep-ex/0602035](https://arxiv.org/abs/hep-ex/0602035) [hep-ex].
- [222] *HEPfit, a tool to combine indirect and direct constraints on High Energy Physics*. <http://hepfit.roma1.infn.it/>.
- [223] Allen Caldwell, Daniel Kollar, and Kevin Kroninger. “BAT: The Bayesian Analysis Toolkit”. In: *Comput. Phys. Commun.* 180 (2009), pp. 2197–2209. DOI: [10.1016/j.cpc.2009.06.026](https://doi.org/10.1016/j.cpc.2009.06.026). arXiv: [0808.2552](https://arxiv.org/abs/0808.2552) [physics.data-an].
- [224] Morad Aaboud et al. “Search for supersymmetry in events with b -tagged jets and missing transverse momentum in pp collisions at $\sqrt{s} = 13$ TeV with the ATLAS detector”. In: *JHEP* 11 (2017), p. 195. DOI: [10.1007/JHEP11\(2017\)195](https://doi.org/10.1007/JHEP11(2017)195). arXiv: [1708.09266](https://arxiv.org/abs/1708.09266) [hep-ex].
- [225] Morad Aaboud et al. “Search for squarks and gluinos in final states with jets and missing transverse momentum using 36 fb^{-1} of $\sqrt{s} = 13$ TeV pp collision data with the ATLAS detector”. In: *Phys. Rev. D* 97.11 (2018), p. 112001. DOI: [10.1103/PhysRevD.97.112001](https://doi.org/10.1103/PhysRevD.97.112001). arXiv: [1712.02332](https://arxiv.org/abs/1712.02332) [hep-ex].
- [226] M. Aaboud et al. “Search for electroweak production of supersymmetric particles in final states with two or three leptons at $\sqrt{s} = 13$ TeV with the ATLAS detector”. In: *Eur. Phys. J. C* 78.12 (2018), p. 995. DOI: [10.1140/epjc/s10052-018-6423-7](https://doi.org/10.1140/epjc/s10052-018-6423-7). arXiv: [1803.02762](https://arxiv.org/abs/1803.02762) [hep-ex].
- [227] CMS Collaboration. “Search for new physics in events with two low momentum opposite-sign leptons and missing transverse energy at $\sqrt{s} = 13$ TeV”. In: (2017).
- [228] Kamila Kowalska and Enrico Maria Sessolo. “Expectations for the muon $g-2$ in simplified models with dark matter”. In: *JHEP* 09 (2017), p. 112. DOI: [10.1007/JHEP09\(2017\)112](https://doi.org/10.1007/JHEP09(2017)112). arXiv: [1707.00753](https://arxiv.org/abs/1707.00753) [hep-ph].
- [229] Lorenzo Calibbi, Robert Ziegler, and Jure Zupan. “Minimal models for dark matter and the muon $g-2$ anomaly”. In: *JHEP* 07 (2018), p. 046. DOI: [10.1007/JHEP07\(2018\)046](https://doi.org/10.1007/JHEP07(2018)046). arXiv: [1804.00009](https://arxiv.org/abs/1804.00009) [hep-ph].
- [230] I. Doršner et al. “Physics of leptoquarks in precision experiments and at particle colliders”. In: *Phys. Rept.* 641 (2016), pp. 1–68. DOI: [10.1016/j.physrep.2016.06.001](https://doi.org/10.1016/j.physrep.2016.06.001). arXiv: [1603.04993](https://arxiv.org/abs/1603.04993) [hep-ph].
- [231] Ferruccio Feruglio, Paride Paradisi, and Andrea Pattori. “Revisiting Lepton Flavor Universality in B Decays”. In: *Phys. Rev. Lett.* 118.1 (2017), p. 011801. DOI: [10.1103/PhysRevLett.118.011801](https://doi.org/10.1103/PhysRevLett.118.011801). arXiv: [1606.00524](https://arxiv.org/abs/1606.00524) [hep-ph].
- [232] Asmaa Abada et al. “Sterile neutrinos facing kaon physics experiments”. In: *Phys. Rev. D* 95.7 (2017), p. 075023. DOI: [10.1103/PhysRevD.95.075023](https://doi.org/10.1103/PhysRevD.95.075023). arXiv: [1612.04737](https://arxiv.org/abs/1612.04737) [hep-ph].

- [233] Vladimir A. Smirnov. “Asymptotic expansions in momenta and masses and calculation of Feynman diagrams”. In: *Mod. Phys. Lett. A* 10 (1995), pp. 1485–1500. DOI: [10.1142/S0217732395001617](https://doi.org/10.1142/S0217732395001617). arXiv: [hep-th/9412063](https://arxiv.org/abs/hep-th/9412063).
- [234] T. Hahn and M. Perez-Victoria. “Automatized one loop calculations in four-dimensions and D-dimensions”. In: *Comput. Phys. Commun.* 118 (1999), pp. 153–165. DOI: [10.1016/S0010-4655\(98\)00173-8](https://doi.org/10.1016/S0010-4655(98)00173-8). arXiv: [hep-ph/9807565](https://arxiv.org/abs/hep-ph/9807565).
- [235] Hiren H. Patel. “Package-X: A Mathematica package for the analytic calculation of one-loop integrals”. In: *Comput. Phys. Commun.* 197 (2015), pp. 276–290. DOI: [10.1016/j.cpc.2015.08.017](https://doi.org/10.1016/j.cpc.2015.08.017). arXiv: [1503.01469](https://arxiv.org/abs/1503.01469) [[hep-ph](https://arxiv.org/abs/hep-ph)].
- [236] G.C. Branco et al. “Theory and phenomenology of two-Higgs-doublet models”. In: *Phys. Rept.* 516 (2012), pp. 1–102. DOI: [10.1016/j.physrep.2012.02.002](https://doi.org/10.1016/j.physrep.2012.02.002). arXiv: [1106.0034](https://arxiv.org/abs/1106.0034) [[hep-ph](https://arxiv.org/abs/hep-ph)].
- [237] Alberto Filipuzzi, Jorge Portoles, and Martin Gonzalez-Alonso. “ $U(2)^5$ flavor symmetry and lepton universality violation in $W \rightarrow \tau\nu_\tau$ ”. In: *Phys. Rev. D* 85 (2012), p. 116010. DOI: [10.1103/PhysRevD.85.116010](https://doi.org/10.1103/PhysRevD.85.116010). arXiv: [1203.2092](https://arxiv.org/abs/1203.2092) [[hep-ph](https://arxiv.org/abs/hep-ph)].
- [238] Xin-Qiang Li, Jie Lu, and Antonio Pich. “ $B_{s,d}^0 \rightarrow \ell^+\ell^-$ Decays in the Aligned Two-Higgs-Doublet Model”. In: *JHEP* 06 (2014), p. 022. DOI: [10.1007/JHEP06\(2014\)022](https://doi.org/10.1007/JHEP06(2014)022). arXiv: [1404.5865](https://arxiv.org/abs/1404.5865) [[hep-ph](https://arxiv.org/abs/hep-ph)].
- [239] John F. Gunion and Howard E. Haber. “The CP conserving two Higgs doublet model: The Approach to the decoupling limit”. In: *Phys. Rev. D* 67 (2003), p. 075019. DOI: [10.1103/PhysRevD.67.075019](https://doi.org/10.1103/PhysRevD.67.075019). arXiv: [hep-ph/0207010](https://arxiv.org/abs/hep-ph/0207010).
- [240] A. Barroso et al. “Metastability bounds on the two Higgs doublet model”. In: *JHEP* 06 (2013), p. 045. DOI: [10.1007/JHEP06\(2013\)045](https://doi.org/10.1007/JHEP06(2013)045). arXiv: [1303.5098](https://arxiv.org/abs/1303.5098) [[hep-ph](https://arxiv.org/abs/hep-ph)].
- [241] Shinya Kanemura, Takahiro Kubota, and Eiichi Takasugi. “Lee-Quigg-Thacker bounds for Higgs boson masses in a two doublet model”. In: *Phys. Lett. B* 313 (1993), pp. 155–160. DOI: [10.1016/0370-2693\(93\)91205-2](https://doi.org/10.1016/0370-2693(93)91205-2). arXiv: [hep-ph/9303263](https://arxiv.org/abs/hep-ph/9303263).
- [242] Bogumił a Świeżewska. “Yukawa independent constraints for two-Higgs-doublet models with a 125 GeV Higgs boson”. In: *Phys. Rev. D* 88.5 (2013). [Erratum: *Phys.Rev.D* 88, 119903 (2013)], p. 055027. DOI: [10.1103/PhysRevD.88.055027](https://doi.org/10.1103/PhysRevD.88.055027). arXiv: [1209.5725](https://arxiv.org/abs/1209.5725) [[hep-ph](https://arxiv.org/abs/hep-ph)].
- [243] D. Bečirević et al. “Can the new resonance at LHC be a CP-Odd Higgs boson?” In: *Phys. Lett. B* 757 (2016), pp. 261–267. DOI: [10.1016/j.physletb.2016.03.073](https://doi.org/10.1016/j.physletb.2016.03.073). arXiv: [1512.05623](https://arxiv.org/abs/1512.05623) [[hep-ph](https://arxiv.org/abs/hep-ph)].
- [244] Riccardo Barbieri et al. “Supersymmetry without a Light Higgs Boson”. In: *Phys. Rev. D* 75 (2007), p. 035007. DOI: [10.1103/PhysRevD.75.035007](https://doi.org/10.1103/PhysRevD.75.035007). arXiv: [hep-ph/0607332](https://arxiv.org/abs/hep-ph/0607332).
- [245] M. Baak et al. “The global electroweak fit at NNLO and prospects for the LHC and ILC”. In: *Eur. Phys. J. C* 74 (2014), p. 3046. DOI: [10.1140/epjc/s10052-014-3046-5](https://doi.org/10.1140/epjc/s10052-014-3046-5). arXiv: [1407.3792](https://arxiv.org/abs/1407.3792) [[hep-ph](https://arxiv.org/abs/hep-ph)].

- [246] Tyler Corbett et al. “The Higgs Legacy of the LHC Run I”. In: *JHEP* 08 (2015), p. 156. DOI: [10.1007/JHEP08\(2015\)156](https://doi.org/10.1007/JHEP08(2015)156). arXiv: [1505.05516](https://arxiv.org/abs/1505.05516) [hep-ph].
- [247] Anke Biekötter, Tyler Corbett, and Tilman Plehn. “The Gauge-Higgs Legacy of the LHC Run II”. In: *SciPost Phys.* 6.6 (2019), p. 064. DOI: [10.21468/SciPostPhys.6.6.064](https://doi.org/10.21468/SciPostPhys.6.6.064). arXiv: [1812.07587](https://arxiv.org/abs/1812.07587) [hep-ph].
- [248] Vincenzo Cacchio et al. “Next-to-leading order unitarity fits in Two-Higgs-Doublet models with soft \mathbb{Z}_2 breaking”. In: *JHEP* 11 (2016), p. 026. DOI: [10.1007/JHEP11\(2016\)026](https://doi.org/10.1007/JHEP11(2016)026). arXiv: [1609.01290](https://arxiv.org/abs/1609.01290) [hep-ph].
- [249] Beranger Dumont et al. “Constraints on and future prospects for Two-Higgs-Doublet Models in light of the LHC Higgs signal”. In: *Phys. Rev. D* 90 (2014), p. 035021. DOI: [10.1103/PhysRevD.90.035021](https://doi.org/10.1103/PhysRevD.90.035021). arXiv: [1405.3584](https://arxiv.org/abs/1405.3584) [hep-ph].
- [250] Otto Eberhardt, Ulrich Nierste, and Martin Wiebusch. “Status of the two-Higgs-doublet model of type II”. In: *JHEP* 07 (2013), p. 118. DOI: [10.1007/JHEP07\(2013\)118](https://doi.org/10.1007/JHEP07(2013)118). arXiv: [1305.1649](https://arxiv.org/abs/1305.1649) [hep-ph].
- [251] Debtosh Chowdhury and Otto Eberhardt. “Global fits of the two-loop renormalized Two-Higgs-Doublet model with soft Z_2 breaking”. In: *JHEP* 11 (2015), p. 052. DOI: [10.1007/JHEP11\(2015\)052](https://doi.org/10.1007/JHEP11(2015)052). arXiv: [1503.08216](https://arxiv.org/abs/1503.08216) [hep-ph].
- [252] Christoph Bobeth, Mikolaj Misiak, and Jorg Urban. “Photonic penguins at two loops and m_t dependence of $BR[B \rightarrow X_s \ell^+ \ell^-]$ ”. In: *Nucl. Phys. B* 574 (2000), pp. 291–330. DOI: [10.1016/S0550-3213\(00\)00007-9](https://doi.org/10.1016/S0550-3213(00)00007-9). arXiv: [hep-ph/9910220](https://arxiv.org/abs/hep-ph/9910220).
- [253] Chao-Shang Huang et al. “ $B_s \rightarrow$ lepton + lepton - in a general 2 HDM and MSSM”. In: *Phys. Rev. D* 63 (2001). [Erratum: *Phys.Rev.D* 64, 059902 (2001)], p. 114021. DOI: [10.1103/PhysRevD.63.114021](https://doi.org/10.1103/PhysRevD.63.114021). arXiv: [hep-ph/0006250](https://arxiv.org/abs/hep-ph/0006250).
- [254] Heather E. Logan and Ulrich Nierste. “ $B_{s,d} \rightarrow \ell^+ \ell^-$ in a two Higgs doublet model”. In: *Nucl. Phys. B* 586 (2000), pp. 39–55. DOI: [10.1016/S0550-3213\(00\)00417-X](https://doi.org/10.1016/S0550-3213(00)00417-X). arXiv: [hep-ph/0004139](https://arxiv.org/abs/hep-ph/0004139).
- [255] C. Bobeth et al. “Analysis of neutral Higgs boson contributions to the decays $\bar{B}(s) \rightarrow \ell^+ \ell^-$ and $\bar{B} \rightarrow K \ell^+ \ell^-$ ”. In: *Phys. Rev. D* 64 (2001), p. 074014. DOI: [10.1103/PhysRevD.64.074014](https://doi.org/10.1103/PhysRevD.64.074014). arXiv: [hep-ph/0104284](https://arxiv.org/abs/hep-ph/0104284).
- [256] Gino Isidori and Alessandra Retico. “Scalar flavor changing neutral currents in the large tan beta limit”. In: *JHEP* 11 (2001), p. 001. DOI: [10.1088/1126-6708/2001/11/001](https://doi.org/10.1088/1126-6708/2001/11/001). arXiv: [hep-ph/0110121](https://arxiv.org/abs/hep-ph/0110121).
- [257] Piotr H. Chankowski and Lucja Slawianowska. “ $B_0(d,s) \rightarrow \mu^- \mu^+$ decay in the MSSM”. In: *Phys. Rev. D* 63 (2001), p. 054012. DOI: [10.1103/PhysRevD.63.054012](https://doi.org/10.1103/PhysRevD.63.054012). arXiv: [hep-ph/0008046](https://arxiv.org/abs/hep-ph/0008046).
- [258] Athanasios Dedes, Janusz Rosiek, and Philip Tanedo. “Complete One-Loop MSSM Predictions for $B \rightarrow \mu^+ \mu^-$ lepton lepton’ at the Tevatron and LHC”. In: *Phys. Rev. D* 79 (2009), p. 055006. DOI: [10.1103/PhysRevD.79.055006](https://doi.org/10.1103/PhysRevD.79.055006). arXiv: [0812.4320](https://arxiv.org/abs/0812.4320) [hep-ph].

- [259] Christoph Bobeth, Andrzej J. Buras, and Thorsten Ewerth. “Anti-B \rightarrow X(s) l+ l- in the MSSM at NNLO”. In: *Nucl. Phys. B* 713 (2005), pp. 522–554. DOI: [10.1016/j.nuclphysb.2005.02.011](https://doi.org/10.1016/j.nuclphysb.2005.02.011). arXiv: [hep-ph/0409293](https://arxiv.org/abs/hep-ph/0409293).
- [260] Marco Ciuchini et al. “Next-to-leading QCD corrections to $B \rightarrow X_s \gamma$: Standard model and two Higgs doublet model”. In: *Nucl. Phys. B* 527 (1998), pp. 21–43. DOI: [10.1016/S0550-3213\(98\)00244-2](https://doi.org/10.1016/S0550-3213(98)00244-2). arXiv: [hep-ph/9710335](https://arxiv.org/abs/hep-ph/9710335).
- [261] G. Degrandi, P. Gambino, and P. Slavich. “QCD corrections to radiative B decays in the MSSM with minimal flavor violation”. In: *Phys. Lett. B* 635 (2006), pp. 335–342. DOI: [10.1016/j.physletb.2006.02.067](https://doi.org/10.1016/j.physletb.2006.02.067). arXiv: [hep-ph/0601135](https://arxiv.org/abs/hep-ph/0601135).
- [262] Thomas Hermann, Mikolaj Misiak, and Matthias Steinhauser. “ $\bar{B} \rightarrow X_s \gamma$ in the Two Higgs Doublet Model up to Next-to-Next-to-Leading Order in QCD”. In: *JHEP* 11 (2012), p. 036. DOI: [10.1007/JHEP11\(2012\)036](https://doi.org/10.1007/JHEP11(2012)036). arXiv: [1208.2788 \[hep-ph\]](https://arxiv.org/abs/1208.2788).
- [263] R. Aaij et al. “Differential branching fractions and isospin asymmetries of $B \rightarrow K^{(*)} \mu^+ \mu^-$ decays”. In: *JHEP* 06 (2014), p. 133. DOI: [10.1007/JHEP06\(2014\)133](https://doi.org/10.1007/JHEP06(2014)133). arXiv: [1403.8044 \[hep-ex\]](https://arxiv.org/abs/1403.8044).
- [264] Chris Bouchard et al. “Rare decay $B \rightarrow K \ell^+ \ell^-$ form factors from lattice QCD”. In: *Phys. Rev. D* 88.5 (2013). [Erratum: *Phys.Rev.D* 88, 079901 (2013)], p. 054509. DOI: [10.1103/PhysRevD.88.054509](https://doi.org/10.1103/PhysRevD.88.054509). arXiv: [1306.2384 \[hep-lat\]](https://arxiv.org/abs/1306.2384).
- [265] Jon A. Bailey et al. “ $B \rightarrow K \ell^+ \ell^-$ Decay Form Factors from Three-Flavor Lattice QCD”. In: *Phys. Rev. D* 93.2 (2016), p. 025026. DOI: [10.1103/PhysRevD.93.025026](https://doi.org/10.1103/PhysRevD.93.025026). arXiv: [1509.06235 \[hep-lat\]](https://arxiv.org/abs/1509.06235).
- [266] M. Beylich, G. Buchalla, and T. Feldmann. “Theory of $B \rightarrow K^{(*)} \ell^+ \ell^-$ decays at high q^2 : OPE and quark-hadron duality”. In: *Eur. Phys. J. C* 71 (2011), p. 1635. DOI: [10.1140/epjc/s10052-011-1635-0](https://doi.org/10.1140/epjc/s10052-011-1635-0). arXiv: [1101.5118 \[hep-ph\]](https://arxiv.org/abs/1101.5118).
- [267] Mikolaj Misiak and Matthias Steinhauser. “Weak radiative decays of the B meson and bounds on M_{H^\pm} in the Two-Higgs-Doublet Model”. In: *Eur. Phys. J. C* 77.3 (2017), p. 201. DOI: [10.1140/epjc/s10052-017-4776-y](https://doi.org/10.1140/epjc/s10052-017-4776-y). arXiv: [1702.04571 \[hep-ph\]](https://arxiv.org/abs/1702.04571).
- [268] Patricia Ball and Roman Zwicky. “ $B_{d,s} \rightarrow \rho, \omega, K^*, \phi$ decay form-factors from light-cone sum rules revisited”. In: *Phys. Rev. D* 71 (2005), p. 014029. DOI: [10.1103/PhysRevD.71.014029](https://doi.org/10.1103/PhysRevD.71.014029). arXiv: [hep-ph/0412079 \[hep-ph\]](https://arxiv.org/abs/hep-ph/0412079).
- [269] Ferruccio Feruglio, Paride Paradisi, and Olcyr Sumensari. “Implications of scalar and tensor explanations of $R_{D^{(*)}}$ ”. In: *JHEP* 11 (2018), p. 191. DOI: [10.1007/JHEP11\(2018\)191](https://doi.org/10.1007/JHEP11(2018)191). arXiv: [1806.10155 \[hep-ph\]](https://arxiv.org/abs/1806.10155).
- [270] R. Glattauer et al. “Measurement of the decay $B \rightarrow D \ell \nu_\ell$ in fully reconstructed events and determination of the Cabibbo-Kobayashi-Maskawa matrix element $|V_{cb}|$ ”. In: *Phys. Rev. D* 93.3 (2016), p. 032006. DOI: [10.1103/PhysRevD.93.032006](https://doi.org/10.1103/PhysRevD.93.032006). arXiv: [1510.03657 \[hep-ex\]](https://arxiv.org/abs/1510.03657).
- [271] Shinya Kanemura et al. “Higgs coupling constants as a probe of new physics”. In: *Phys. Rev. D* 70 (2004), p. 115002. DOI: [10.1103/PhysRevD.70.115002](https://doi.org/10.1103/PhysRevD.70.115002). arXiv: [hep-ph/0408364](https://arxiv.org/abs/hep-ph/0408364).